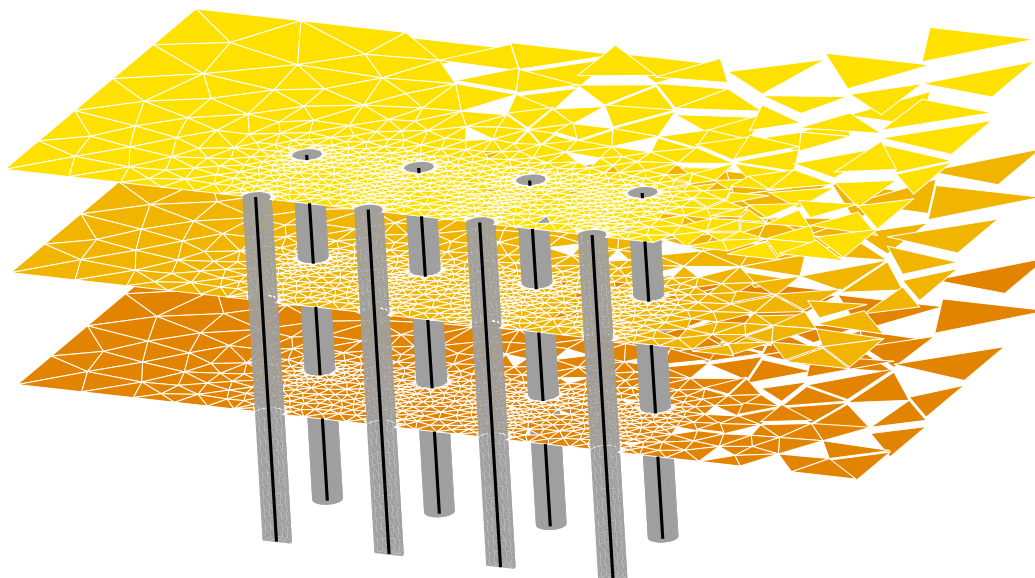


DOCTORAL DISSERTATION

Dynamic response of piled structures. Implementation of a model based on the integral formulation of the problem and the use of a fundamental solution for the layered half space



Guillermo Manuel Álamo Meneses

Continuum Mechanics and Structures Division

Las Palmas de Gran Canaria • July 2018



Programa de Doctorado: Tecnologías de Telecomunicación e Ingeniería Computacional



UNIVERSIDAD DE LAS PALMAS
DE GRAN CANARIA



INSTITUTO UNIVERSITARIO
SIANI
INGENIERIA COMPUTACIONAL

Dynamic response of piled structures. Implementation of a model based on the integral formulation of the problem and the use of a fundamental solution for the layered half space

Guillermo Manuel Álamo Meneses

Programa de doctorado

Tecnologías de Telecomunicación e Ingeniería Computacional

Director:

Juan José Aznárez González

Las Palmas de Gran Canaria, July 2018

*To Ale,
for being the smile that
always lights up my soul.*

*“We can only see a short distance ahead,
but we can see plenty there that needs to be done.”*

Alan Turin, Computing machinery and intelligence

Acknowledgements

I could not start these acknowledgements without giving my most sincere and deep thanks to my supervisor Prof. Juan José Aznárez. Thank you for guiding me during these years, and for being such an inspiring source of knowledge, expertise and support. Honestly, this work would have not been possible without you. Also, I would like to extend my gratitude to Prof. Orlando Maeso and Prof. Luis Alberto Padrón. The three of you have been the (better than piled) foundation of my research career, and for that I will be always be grateful.

I would also like to thank the rest of members of the Continuum Mechanics and Structures Division for being such a marvellous group to work with. Starting with Prof. Francisco Chirino, Prof. José María Emperador and Prof. Fidel García; and continuing with Cristina Medina, Rayco Toledo, Ariel Santana, Jacob Rodríguez, Lorenzo Baños, Francisco Pérez, María Castro, Juan Carlos Galván, and Román Quevedo.

I wish to thank all the people involved in the University Institute SIANI for providing such a nice place to work in. To Juan Ignacio González for having the solution for any technical issue. And, especially, to my dear friend Adriel Sosa.

I am really indebted to Prof. Rafael Gallego and Prof. Alejandro Martínez Castro for raising the seed of this work. Without their experience in the use of advanced fundamental solutions, it would have turned into an extremely arduous task.

I would like to thank Prof. Masato Saitoh and Prof. Chandra Shekhar Goit for receiving me at Saitama University and giving me the opportunity to work with them. Your guidance and assistance, together with the kindness of the rest of the Lab colleges, helped me to feel like home in (almost literally) the other side of the world.

I would like to thank Prof. Geert Lombaert for allowing me to work alongside him and his research team in KU Leuven, and for his guidance and interesting discussions. Also, to Prof. Guido De Roeck, Prof. Mario Solís (University of Sevilla) and Manthos Papadopoulos for all their experience and support shared with me regarding the work about the Palmas Altas bridge. I would like to thank all the members of the Department and, especially, the “ALMA team” for cheering up all the lunch times.

Last, but never least, I wish to express warm thanks to my family for always being there for me. Especially to my parents, my brother, and my grandparents for making me the person who I am today. I kept my last lines for Ale, without your love and support I couldn't have reached this point. Thank you.

The author was recipient of a predoctoral fellowship from the Program of the Universidad de Las Palmas de Gran Canaria from July 2014 until September 2015, and he is currently recipient of the research fellowship FPU14/06115 from the Ministerio de Educación, Cultura y Deporte of Spain, which also provided the author with the two research short stay grants EST15/00597 and EST16/00617.

This work was supported by the Ministerio de Economía, Industria y Competitividad (MINECO) and the Agencia Estatal de Investigación (AEI) of Spain and FEDER through research Projects BIA2014-57640-R and BIA2017-88770-R.

Las Palmas de Gran Canaria, July 2018
Guillermo Manuel Álamo Meneses

An abstract graphic on the left side of the page. It features a vertical solid grey line. To its left, several concentric dashed grey arcs are visible. Below these, a dashed line forms a jagged, irregular shape. Further down, another dashed arc is present. The word 'CONTENTS' is centered within a dark blue rectangular box that overlaps the vertical line and the dashed shapes.

CONTENTS





Contents	iii
List of Figures	vii
List of Tables	xiii
1 Introduction and background	3
1.1 Introduction	3
1.2 Aims and objectives	6
1.3 Framework. Research Project BIA2014-57640-R	7
1.4 Published works derived from the Ph. D. Thesis	8
1.4.1 Contributions in JCR journals	9
1.4.2 Conference contributions	9
1.4.3 Book Chapter contributions	10
1.5 Structure of the dissertation	11
2 Integral model for the analysis of pile foundations	15
2.1 Introduction and general hypotheses	15
2.2 Pile finite element equations	16
2.2.1 Pile elements	16
2.2.2 External forces	20
2.2.3 Inclined piles	21
2.2.4 Pile union through a rigid cap	23
2.3 Soil equations	24
2.3.1 Pak and Guzina's Green's functions for the layered half space	25
2.3.2 Soil base equations	25
2.4 Seismic excitation	30
2.5 Excitation at the soil surface	32
2.6 Pile-soil coupling	33
2.7 Displacements at internal points of the soil	34
2.8 Influence of the omitted tangential tractions	35
3 Impedance functions for inclined piles	41
3.1 Introduction	41
3.2 Verification results	42
3.3 Problem definition	44
3.4 Impedance functions	47
3.4.1 Inclined single pile impedance functions	47
3.4.2 Inclined 3×3 pile group impedance functions	48
3.5 Conclusions	53
4 Seismic response of pile foundations	57
4.1 Introduction	57
4.2 Verification results	58
4.3 Problem definition	59



4.4	Foundation kinematic interaction factors	64
4.4.1	Translational kinematic interaction factors (I_u)	67
4.4.2	Rotational kinematic interaction factors (I_ϕ)	69
4.4.3	Kinematic interaction factors for soil type C	74
4.5	Structural maximum accelerations	75
4.6	Influence of the pile head condition on the foundation seismic input factors	80
4.7	Pile kinematic bending moments	90
4.8	Conclusions	96
5	Pile barriers as ground vibration mitigation measure	101
5.1	Introduction	101
5.2	Problem definition	102
5.3	Validation of the proposed model	103
5.4	Results	108
5.5	Conclusions	117
6	Dynamic characterization of monopiled OWT	121
6.1	Introduction	121
6.2	Problem definition	124
6.3	Reduced substructuring methodology	128
6.3.1	Foundation modelling	128
6.3.2	FE model for the dynamic characterization of the superstructure on fixed base	129
6.3.3	Reduced substructuring model	130
6.4	Analysis of the properties of the set of OWTs	133
6.5	Dynamic characterization of OWT including SSI	136
6.5.1	Influence of the superstructure properties	137
6.5.2	Influence of the soil profile	140
6.5.3	Influence of the monopile dimensions	143
6.6	Conclusions	144
7	Summary, conclusions and future research directions	149
7.1	Summary and conclusions	149
7.2	Future research directions	150
A	Formulation of the incident field for oblique waves in layered soils based on TRM	157
A.1	Problem definition	157
A.2	Incident SH waves (out-of-plane problem)	158
A.3	Incident SV-P waves (in-plane problem)	165
A.4	Generic incident waves	170
A.5	Numerical aspects	170
A.5.1	Vertical incidence	170



A.5.2	Routine pseudo-algorithm	171
B	Savings in the computational time due to the reuse of influence sub-matrices	175
C	Winkler model for the evaluation of the influence of the tangential tractions on the pile seismic response	181
C.1	Introduction	181
C.2	Problem definition	181
C.3	Loads acting over the soil-pile interface	182
C.4	Formulation of the Winkler model	183
D	Resumen en castellano	191
D.1	Objetivos	191
D.2	Modelo integral	192
D.3	Problemas estudiados	194
D.3.1	Efecto de la variabilidad del perfil en las impedancias de pilotes inclinados	194
D.3.2	Efecto de la variabilidad del perfil en la respuesta sísmica de cimentaciones pilotadas	194
D.3.3	Efecto de la estratigrafía en la eficacia de barreras de pilotes	195
D.3.4	Efecto de la variabilidad del perfil en la caracterización dinámica de estructuras de aerogeneradores monopilotados	196
D.4	Conclusiones y desarrollos futuros	196
	Bibliography	201



List of Figures

1.1	Evolution of the numerical models used by the Research Group for the analysis of pile foundations. Adapted from [32].	5
1.2	Typical foundations for offshore wind turbines in shallow (left), moderately deep waters (centre) and deep waters (right). Adapted from [41].	8
2.1	Simplification of the pile geometry. Treatment of the pile deformed shape (left) and the soil-pile interaction tractions (right).	15
2.2	Pile element degrees-of-freedom.	17
2.3	External forces acting on the pile head and tip (left). Nodal forces for each pile element (centre). Nodal values of the pile-soil distributed tractions acting over each element of the pile (right).	20
2.4	Typical inclined piles configurations (left). Definition of the local and global pile coordinate systems (right).	22
2.5	Sketch of the pile union through a rigid cap. Definition of the cap degrees of freedom.	23
2.6	Non-nodal collocation strategies. (a) Due to integrating in the same load line than the collocation point. (b) Due to pile inclination. (c) Due to discontinuities in the soil-pile interaction tractions.	27
2.7	Equivalent collocation-observation pile pairs. (a) Definition of relative distances and rotation angle. (b) Additional conditions for inclined piles.	29
2.8	Example of equivalent collocation-observation pile pairs. 3×3 pile group with vertical piles.	30
2.9	Decomposition of the total field into the incident and the scattered ones.	31
2.10	Discretization of external forces acting over the free-surface. Point (left), line (centre) and surface (right) loads. Only the vertical component is presented.	32
2.11	Structure of the coefficient matrix \mathcal{A} .	34
2.12	Influence of the tangential tractions on the envelopes of maximum shear forces and bending moments for a single pile under seismic excitation. Results obtained through different models and contact conditions.	37
3.1	Horizontal, rocking and vertical impedances of a vertical 2×2 pile group. Comparison with the solution presented by Miura et al. [85].	43
3.2	Horizontal, rocking and vertical impedances of 2×2 pile group with piles inclined in the direction of the horizontal excitation. Comparison with the solution presented by Medina et al. [30].	44
3.3	Sketch of the impedance problem.	45
3.4	Soil profiles in terms of shear wave velocity	47
3.5	Impedance functions for a single inclined pile in different non-homogeneous media	49



LIST OF FIGURES

3.6	Horizontal impedance functions for a 3×3 group in different non-homogeneous media	50
3.7	Torsional impedance functions for a 3×3 group in different non-homogeneous media	50
3.8	Vertical impedance functions for a 3×3 group in different non-homogeneous media	51
3.9	Rocking impedance functions for a 3×3 group in different non-homogeneous media	51
3.10	Horizontal-rocking coupling impedance functions for a 3×3 group in different non-homogeneous media	52
4.1	Lateral displacements of the foundation for different soil profiles. Comparison with Kaynia and Kausel [84].	59
4.2	Sketch of the seismic problem.	59
4.3	Shear wave velocity of the studied profiles.	62
4.4	Time evolution of the real accelerograms used in the seismic analyses.	63
4.5	Translational kinematic interaction factors for free-head single piles. Representative configurations highlighted in light-gray. (Imaginary components presented by dashed lines).	65
4.6	Rotational kinematic interaction factors for free-head single piles. Representative configurations highlighted in light-gray. (Imaginary components presented by dashed lines).	66
4.7	Translational kinematic interaction factors for single piles. (Imaginary components presented by dashed lines).	67
4.8	Translational kinematic interaction factors for 2×2 pile groups. (Imaginary components presented by dashed lines).	68
4.9	Translational kinematic interaction factors for 3×3 pile groups. (Imaginary components presented by dashed lines).	70
4.10	Rotational kinematic interaction factors for single piles. (Imaginary components presented by dashed lines).	71
4.11	Rotational kinematic interaction factors for 2×2 pile groups. (Imaginary components presented by dashed lines).	72
4.12	Rotational kinematic interaction factors for 3×3 pile groups. (Imaginary components presented by dashed lines).	73
4.13	Kinematic interaction factors for 3×3 pile groups embedded in soil type C. (Imaginary components presented by dashed lines).	74
4.14	Elastic response spectra (PSA) and differences between results of the equivalent homogeneous and non-homogeneous profiles (Δ_{PSA}). Single pile, configuration $L30d1.5$.	76
4.15	Differences between the elastic response spectra of the equivalent homogeneous and non-homogeneous profiles (Δ_{PSA}). 3×3 pile group, configuration $L30d1.5$.	77
4.16	Influence of head condition on the translational kinematic interaction factors of single piles. (Imaginary components presented by dashed lines).	80



4.17 Influence of head condition on the translational kinematic interaction factors of 3×3 pile groups. (Imaginary components presented by dashed lines).	82
4.18 Influence of head condition on the rotational kinematic interaction factors of 3×3 pile groups. (Imaginary components presented by dashed lines).	83
4.19 Differences between the elastic response spectra of the free and fixed-rotation pile head condition ($\Delta_{PSA}^{h.c.}$). Single pile, configuration $L30d1.5$.	84
4.20 Differences between the elastic response spectra of the hinged and fixed pile-cap union condition ($\Delta_{PSA}^{h.c.}$). 3×3 pile group, configuration $L30d1.5$. Soil Type D.	85
4.21 Differences between the elastic response spectra of the hinged and fixed pile-cap union condition ($\Delta_{PSA}^{h.c.}$). 3×3 pile group, configuration $L30d1.5$. Soil Type E.	90
4.22 Influence of the variability of the soil profile on the pile envelope of maximum bending moments. Fixed-rotation at head single piles.	91
4.23 Influence of the variability of the soil profile on the pile envelope of maximum bending moments. Free-head single pile.	92
4.24 Influence of the group configuration on the pile envelope of maximum bending moments. Fixed pile-cap union condition.	93
4.25 Influence of the group configuration on the pile envelope of maximum bending moments. Hinged pile-cap union condition.	94
4.26 Influence of the pile position in the group on the envelope of maximum bending moments. 3×3 pile group ($s/d = 2$) with fixed pile-cap union condition.	95
4.27 Envelopes of maximum bending moments for a large pile foundation.	96
5.1 Sketch of the pile barrier problem.	102
5.2 Examples of the meshes used for the BE (left) and integral (right) models.	105
5.3 Distribution of the differences Δ_{A_r} between the integral and BE models.	106
5.4 Range of applicability of the integral model. (a): Expected difference $\Delta_{A_r}^*$ between the integral and BE models. (b): Maximum dimensionless frequency in which $\Delta_{A_r}^* < 0.1$ as function of the pile separation distance s/d .	106
5.5 Comparison between amplitude reduction ratios obtained by the integral and BE models. $\nu_s = 0.485$, $L/d = 20$. Observation points located at the centre of the barrier ($y_o/d = 0$).	107
5.6 Comparison between amplitude reduction ratios obtained by the integral and BE models. $\nu_s = 0.485$, $L/d = 20$. Observation points located at the centre of the barrier ($y_o/d = 0$). Rigid bedrock located at the pile tip depth.	108
5.7 Case A. Average amplitude reduction factor. Influence of the pile aspect ratio and presence of a rigid bedrock. $E_p/E_s = 250$.	110
5.8 Case A. Vertical displacements and amplitude reduction ratio at specific observation points located at the central line ($y_o/d = 0$) behind the barrier. Pile aspect ratio $L/d = 20$. $E_p/E_s = 250$.	111



LIST OF FIGURES

5.9	Case A. Average amplitude reduction ratio. Influence of the pile-soil stiffness ratio.	112
5.10	Case B. Average amplitude reduction ratio. Influence of the layer thickness and pile tip boundary condition.	113
5.11	Case C. Average amplitude reduction ratio. Influence of the position of the source.	114
5.12	Case D. Average amplitude reduction ratio. Influence of the flexibility of the bedrock.	114
5.13	Case E. Average amplitude reduction ratio. Influence of the profile of the soil layer.	115
5.14	Pile barrier configurations analysed in Case F.	116
5.15	Case F. Average amplitude reduction ratio. Influence of the pile separation and pile disposition.	116
6.1	Representation of a generic OWT and identification of geometrical and material parameters.	125
6.2	Soil profiles used in the study. Evolution of the shear wave velocity with depth.	127
6.3	Stages of the substructuring methodology. (a): System real geometry. (b): Superstructure representation through modal parameters. (c): Foundation stiffness representation through impedance functions. (d): Simplified substructuring model.	128
6.4	Modal parameters for the studied set of OWT (crosses). Polynomial regressions of the modal height (a, solid lines) or mass (b, solid lines) as a function of the fixed-base fundamental frequency. Relation between the modal mass and modal height obtained by using the regressed expressions (c, dashed lines).	133
6.5	Pile diameter (a) and pile length (b) with respect to superstructure modal parameters for the studied OWT systems (crosses). Polynomial regressions of the pile diameter as a function of the fixed-base fundamental frequency (a, solid lines). Relations between the pile diameter and modal height or mass obtained by using the regressed expressions (a, dashed lines). Polynomial regressions of the pile embedded length as a functions of the fixed-base fundamental frequency (b, solid lines).	136
6.6	Effective-to-fixed-base natural frequency and effective-to-structural damping ratios. Comparison between the results of the regressed (lines) and real (crosses) modal parameters and pile dimensions. Results for the Nelson Field soil profile. Pile length $L_p = 25$ m for the regressed dimensions.	137
6.7	Influence of the modal parameters on the fundamental frequency and damping variations. Pile diameter $D_p = 4$ m and length $L_p = 25$ m. Results for the Nelson Field soil profile.	139
6.8	Influence of the fixed-base structural modal damping on the damping variations. Pile length $L_p = 25$ m. Results for the Nelson Field soil profile.	139



6.9	Influence of the soil profile on the effective-to-fixed-base natural frequency ratio and effective-to-structural damping ratio. Pile length $L_p = 25$ m.	141
6.10	Influence of the soil profile on the effective-to-fixed-base natural frequency ratio and effective-to-structural damping ratio. Comparison between soft (solid) and hard (dashed) soils and between homogeneous (blue) and variable-with-depth (black) profiles with identical $c_{s,30}$. Pile length $L_p = 25$ m.	142
6.11	Influence of the soil Poisson's ratio on the effective-to-fixed-base natural frequency ratio and effective-to-structural damping ratio. Pile length $L_p = 25$ m. Results for the Nelson Field soil profile.	142
6.12	Influence of pile diameter and pile length on the effective-to-fixed-base natural frequency ratio and effective-to-structural damping ratio. Linear fitting. $L_p = 15$ m (solid lines) and $L_p = 25$ m (dashed lines).	143
7.1	Sketch of the enhanced integral model with finite element structures.	151
7.2	Regularization of the fundamental solution for the layered half space.	152
A.1	Definition of the soil stratification.	157
A.2	Definition of the waves travelling through each layer. Incident SH waves.	158
A.3	Interpretation of the transmission and reflection matrices for layer interface j .	162
A.4	Definition of the waves travelling through each layer. Incident SV-P waves.	165
B.1	Cases considered for the analysis of the savings in the computational time due to the reuse of influence sub-matrices.	175
B.2	Computational time required to obtain the response of the foundation at the considered frequency. Regular pile groups.	177
C.1	(a) Problem under study. (b) Tangential tractions due to the incident field. (c) Normal and tangential tractions due to a horizontal displacement of the pile cross-section. (d) Tangential tractions due to a rotation of the pile cross-section.	181
C.2	(a) Forces and moments acting over a differential element of the beam. (b) BDWF model for a pile embedded in a soil layer. (c) Winkler's soil impedance terms for different deformation modes.	184
D.1	Grados de libertad de los elementos empleados para los pilotes.	194
D.2	Representación del problema sísmico.	195
D.3	Representación del problema de barreras de pilotes.	195



List of Tables

2.1	Reduction in the number of collocation-integration pairs for the evaluation of the influence matrix integrals through the reuse of equivalent submatrices. Regular groups with vertical piles.	30
2.2	Description of the BE and Winkler model variations used in this study.	36
4.1	Soil profiles used for the seismic analyses.	61
4.2	Real accelerograms used in the seismic analyses. Source: PEER NGA-West2 Database [123].	62
4.3	Differences between the PSA of the equivalent homogeneous and non-homogeneous profiles Δ_{PSA} (units in a_g). Minimum values (unsafe homogeneous assumption) for different period ranges. Soil type D.	78
4.4	Differences between the PSA of the equivalent homogeneous and non-homogeneous profiles Δ_{PSA} (units in a_g). Minimum values (unsafe homogeneous assumption) for different period ranges. Soil type E.	79
4.5	Differences between the PSA of the fixed and hinged head conditions $\Delta_{PSA}^{h.c.}$ (units in a_g). Minimum values (higher response for hinged condition) for different period ranges. Soil type D.	86
4.6	Differences between the PSA of the fixed and hinged head conditions $\Delta_{PSA}^{h.c.}$ (units in a_g). Maximum values (higher response for fixed condition) for different period ranges. Soil type D.	87
4.7	Differences between the PSA of the fixed and hinged head conditions $\Delta_{PSA}^{h.c.}$ (units in a_g). Minimum values (higher response for hinged condition) for different period ranges. Soil type E.	88
4.8	Differences between the PSA of the fixed and hinged head conditions $\Delta_{PSA}^{h.c.}$ (units in a_g). Maximum values (higher response for fixed condition) for different period ranges. Soil type E.	89
5.1	Definition of the cases of study.	109
5.2	Dimensionless properties assumed for all of the cases of study.	109
6.1	Definition of the set of existent OWTs used in the study.	126
6.2	Validation of the proposed three-step formulation against the FEM model. Flexible-base fundamental frequency for the OWT systems. Results for the Nelson Field soil profile.	132
6.3	Modal parameters for the studied OWT systems.	134
B.1	Times required to obtain the response of the foundation at the considered frequency. Regular pile groups.	176



1. Introduction and background

- 1.1 Introduction
- 1.2 Aims and objectives
- 1.3 Framework. Research Project BIA2014-57640-R
- 1.4 Published works derived from the Ph. D. Thesis
- 1.5 Structure of the dissertation





1.1 Introduction

Pile foundations are usually selected as the structural supporting system employed to transmit the structural loads to the surrounding soil. Normally, this type of foundation is used when the soil has a poor bearing capacity, when rocks or more rigid strata are found at deeper levels of the terrain, or when the supported construction is subjected to large horizontal loads or upwards vertical loads. An additional benefit of the use of pile foundations is that they can improve the structural seismic response. The deeply-buried elements generally filter the seismic motion imposed by the ground and also increase the damping of the foundation-structure system. For these reasons, this type of foundation is normally chosen for large tall buildings, bridge piers and for marine structures or platforms that need to cover significant water depths. Regarding this last typology, it is important to highlight that foundations using a single monopile or several groups of piles are the most common solution for supporting the structures of offshore wind turbines.

There exist numerous expressions and approximate computational methods that can be used for the design and study of piles. Despite in the past most of these strategies were limited to the static behaviour of the foundations, during the last decades a large number of studies have focused on the analysis and modelling of the dynamic behaviour of pile foundations. However, there is still a lack of understanding in some of the phenomena that are involved in the dynamic behaviour of this foundation type. Also, more parametric studies of how the response of the piles are affected by some properties of the soil-foundation system, such as the soil profile and its features, need to be conducted. Furthermore, the study of the changes in the dynamic characteristics and behaviour of piled structures that are produced by the flexibility of the foundation (referred to as soil-structure interaction) is also a rising research direction inside the structural field.

The objective of the present Ph. D. Thesis is to develop an efficient numerical model for the dynamic analysis of pile foundations in non-homogeneous soils. The soil non-homogeneity is considered in terms of a horizontally layered domain. The formulation of the proposed model is based on the same integral approach that results in the Boundary Element Method in order to take advantage of its benefits for representing the physics of the problem. Specifically, the chosen strategy is to incorporate a fundamental solution for the layered half space into a previous Boundary Element - Finite Element (BE-FE) coupling formulation. In this previous model, the soil, considered as an infinite medium, is discretized through standard boundary elements. On the other hand, the piles are modelled as classic beam finite elements. In order to directly solve the coupled problem, additional coupling equations are introduced between the piles and soil, and between the piles and the pile caps. These equations are obtained from compatibility and equilibrium conditions in terms of the representative degrees of freedom, with a meaning that is more or less direct depending on the methodology (BE or FE) used to represent the behaviour of the studied regions.

In order to improve the abilities and versatility of the previous model, advanced fundamental solutions for the layered half space are introduced in the formulation that represents the soil dynamic behaviour. This way, it would be possible to avoid any meshing of the free-surface or layer interface boundaries. Thus, the size of the problem is drastically reduced. Also, the uncertainties related to the surface meshes, such as setting the size of the elements

or the quantity of soil that needs to be discretized, are also avoided.

Regarding the proposed model, it should not be referred to as a boundary element formulation as:

- The strategy used for the pile-soil coupling (which is identical to the one of the previous model) does not imply any boundary variable of the soil. No discretization of the interface between the pile and the soil is made, but the interaction forces are treated as body forces acting inside the soil domain.
- In the case that a pile cap is considered, it is assumed not to be in contact with the soil.
- The boundary conditions at each layer interface and at the free-surface are already satisfied by the new fundamental solution, so there is no need to discretize these regions.

Therefore, the developed tool should be better referred to in terms of a collocation methodology based on the integral formulation of the soil problem. In this integral model, only the piles are discretized through beam finite elements and the degrees of freedom of the problem are limited to pile displacements and soil-pile tractions representing the interaction between these two media. Thus, all of the variables of the integral model are defined along the pile axes.

As mentioned before, this new model is an incremental step inside the work direction followed by the Research Group of the Continuum Mechanics and Structures Division of the SIANI Institute of the University of Las Palmas de Gran Canaria. This group has been developing models for solving wave equations in continuum media for more than 30 years. The key methodology is the Boundary Element Method. The research line started from the works of Alarcón y Domínguez from the University of Sevilla [1–5]. The close collaboration between the groups of the two universities resulted in the development of a boundary element code for solving three-dimensional problems in the frequency domain [6–8]. This multi-region model was further developed [9], including the possibility of including poroelastic regions as well as viscoelastic media. This advance in the numeric tool allowed the study of the influence of the presence of porous sediments on the dynamic behaviour of arch dams [10–12], as well as the effects derived from the spatial nature of the excitation found in the seismic response of this dam type [13, 14]. Regarding the analysis of pile foundations, the boundary element model was also used to obtain the impedance functions of single piles and pile groups both in viscoelastic and poroelastic soils [15, 16]. In order to study this problem, the discretization of the interface between the pile and soil regions introduced a large number of degrees of freedom, limiting the application of the model only to the analysis of small pile configurations.

With the intention to have more efficient numeric tools to tackle the problem of the dynamic analysis of pile foundations, in the Ph. D. Thesis work of Padrón [17] a coupled boundary element - finite element (BE-FE) model was formulated and implemented. Based on the idea presented in the static model of Mendonça et al. [18–20], the interaction between soil and pile was reduced to a set of tractions acting over a load line inside the soil domain, while the flexibility of piles was taken into account through their modelling with finite elements. This way, as mentioned before, the treatment of piles as dimensionless load lines



avoids the discretization of the interfaces between them and the soil. This BE-FE coupling model also had the possibility of considering structures supported by the pile foundations. The efficiency and versatility of that tool allowed numerous studies related to the dynamic behaviour of pile foundations and piled structures [21–30].

As the reader figures out, this BE-FE model is, precisely, the starting point of the present Ph. D. Thesis work. Despite the treatment of piles as dimensionless load lines implies a huge saving in the variables corresponding to the soil-pile interfaces, the BE-FE model still needs to discretize the soil free-surface and, in case of considering soil profiles with several strata, the layer interfaces. Therefore, the application of the former model to treat soils with non-uniform properties is limited to profiles with a reduced number of different layers. As mentioned before, the model developed in the present document is aimed to solve this limitation. For this purpose, the fundamental solution for the unbounded viscoelastic medium used by Padrón's BE-FE model is substituted with an advance fundamental solution for the layered half space that already satisfies the boundary conditions of these soils. As result, a formulation only in terms of the pile variables is obtained. This evolution of the Research Group models for the study of pile foundations is depicted in Fig. 1.1.

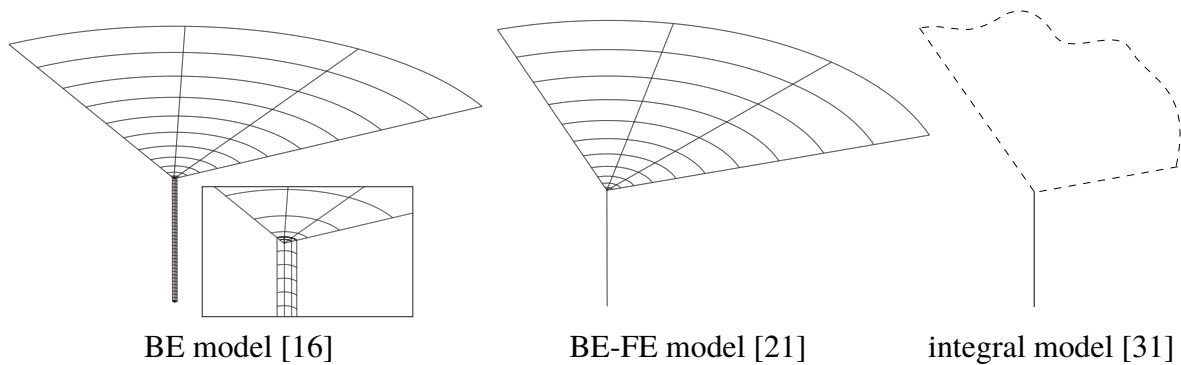


Figure 1.1: Evolution of the numerical models used by the Research Group for the analysis of pile foundations. Adapted from [32].

At this point, it is important to highlight that the current Ph. D. Thesis work has been developed with a close collaboration with Prof. R. Gallego and Prof. A.E. Martínez-Castro from the University of Granada (Spain). This way, it has been possible to incorporate their large experience in the development of fundamental solutions for the viscoelastic layered media [33,34] into the developed work.

Finally, it is worthy to comment that in parallel to the work developed within the field of pile foundations, the Research Group of the Continuum Mechanics and Structures Division continues to develop several numerical model for the study of wave propagation problems that are of high interest in the engineering field. Optimization of noise barriers by combining Genetic Algorithms and boundary element codes [35–37], or the study of buried shell structures through the coupling of boundary and finite elements [38–40] are some of these applications based on hypersingular or dual boundary element formulations.

1.2 Aims and objectives

The aim of the present research is to develop and implement a numerical model based on the integral formulation of the elastic problem and the use of an advance fundamental solution for the layered half space, and its application to the dynamic analysis of pile foundations and piled structures.

The half space (in general, layered) is modelled through a numerical collocation strategy, while the piles are treated as beam finite elements. The developed software will significantly reduce the computational requirements, allowing the study of problems that cannot be handled with the previous tools available for the Research Group.

In order to fulfil this main objective, the following partial objectives have to be considered:

Formulation and implementation:

- Study of the theoretical framework and formulation of the advanced fundamental solution for the layered half space. Familiarization with the code modules that compute this type of fundamental solutions.
- Formulation and implementation of a numerical model that includes the new fundamental solution. This formulation will be based on the same ideas and strategies that were used in the previous BE-FE code.
- Validation of the model. Study the applicability range of the model and the numerical technique (problems related with the behaviour of the fundamental solution, or with the discretization of continuously varying soil profiles). Comparison with available results corresponding to different problems and configurations.
- Formulation and implementation of numerical strategies aimed at optimizing the performance and computational requirements of the developed code.

Application of the developed model:

- Characterization of the dynamic properties of pile foundations in terms of their stiffness and damping impedance functions in the frequency domain. Study of the influence of the variability of the soil profile on these variables.
- Study of the kinematic interaction factors of pile configurations. Analysis of the influence of the variability of the soil profile.
- Study of kinematic bending moments for single piles and pile groups embedded in stratified soils and subjected to seismic waves.
- Study of the soil-structure interaction effects on the dynamic characterization of structures for offshore wind turbines by using substructuring techniques.
- Analysis of the performance of pile barriers as ground vibration mitigation measures.

**Research communications:**

- Diffusion of the obtained results to the scientific community through publications in referred journals and international conferences.

1.3 Framework. Research Project BIA2014-57640-R¹

The present Ph. D. Thesis was part of the Research Project BIA2014-57640-R supported by the Subdirección General de Proyectos de Investigación of the Ministerio de Economía y Competitividad (MINECO) of Spain and the European Regional Development Fund (ERDF) or, in Spanish, Fondo Europeo de Desarrollo Regional (FEDER). The project is entitled “Advances in the development of numerical models for the dynamic characterisation of wind turbines”.

The support structures for wind turbines should be designed keeping away the natural frequencies of the system from the frequency content of the principal dynamic loads to which they are subjected: unbalance loads from the rotor, shadowing effects from the passing blades and the spectra of wind and, for offshore wind turbines, wave loads. One of the sub-system that involves great uncertainties and simplifications in its analyses is the soil-foundation system, especially in the case of deep foundations. On the other hand, as the number of land-based and offshore wind farms increases, it is becoming more frequent to install new farms in sites where the soil has poorer characteristics, requiring the use of deep foundations such as piles and suction caissons (also referred to as buckets). This situation is completely generalized for the case of offshore wind turbines, being foundations based on monopiles or groups of piles or buckets the standard technical solutions. As an example, Fig. 1.2 shows some of the more common types of foundations for offshore wind turbines depending on the water depth.

The facts stated before explain the need to develop computational models able to estimate the dynamic properties of the afore-mentioned foundation types in a more efficient and accurate way than it is done with the current design tools. This will contribute to the design of optimal and safer wind turbine structures with longer service lifetimes (due to lower fatigue loading), helping to reduce the cost per unit of energy and to improve the profitability of this technology.

In order to contribute in this direction, the objective of the Research Project is to develop two computational models that will allow more accurate dynamic analyses of the two types of foundations mentioned above:

- **Objective 1.** A model for the dynamic analysis of pile foundations in layered soils, through the development and implementation of a collocation methodology based on the integral formulation of the problem for the soil and making use of an advanced

¹Adapted from the abstract of the Scientific Report for the application of the Research Project. Accepted on 27/07/2015 by Secretaría de Estado de Investigación, Desarrollo e Innovación del Ministerio de Economía y Competitividad (Spain). Project duration: 3 years (2015-2017).

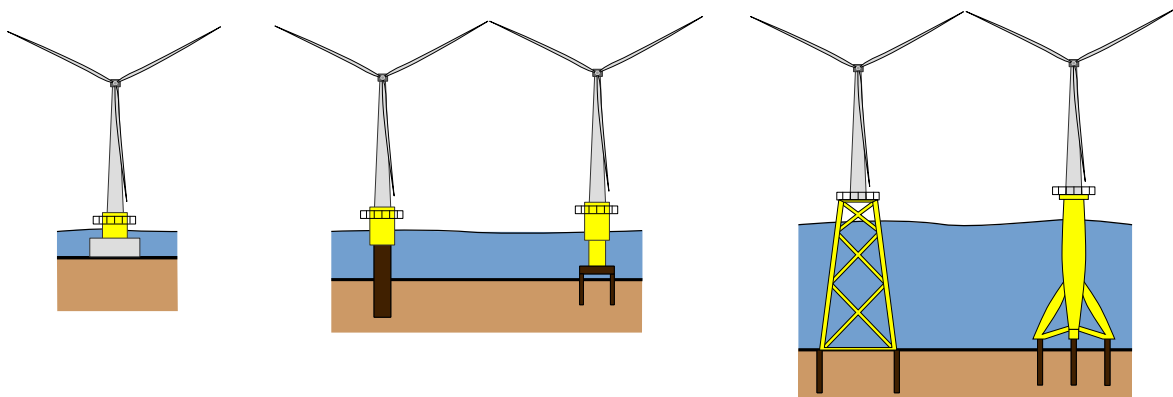


Figure 1.2: Typical foundations for offshore wind turbines in shallow (left), moderately deep waters (centre) and deep waters (right). Adapted from [41].

three-dimensional fundamental solution for the layered half space. (Present Ph. D. Thesis)

- **Objective 2.** A model for the dynamic analysis of buried thin laminar flexible structures such as suction caissons, through the development and implementation of a dual formulation of the Boundary Element Method coupled to shell finite elements. (J.D.R. Bordón's Ph. D. Thesis [41]).

Both goals imply developments related to the Boundary Element Method, which is especially suitable for the study of unbounded media such as the soil. The achievement of the first goal allows the study of piled foundations in stratified soils without requiring any meshing of the surrounding soil boundaries or domains, in such a way that only the piles will be discretized by using beam finite elements. This will allow tackling problems with complex stratigraphies that are computationally unapproachable using the formulations and codes developed so far by the research team. The second goal implies the formulation and implementation of boundary element codes that make use of a dual formulation, combining the standard singular boundary integral equation for viscoelastic and poroelastic media, with its hypersingular form. This allows the numerical treatment of problems involving thin inclusions with reduced computational costs and high accuracy.

The two developed models will be used to contribute to the scientific knowledge related to the dynamic characterization of wind turbine foundations, both land based and offshore in shallow and moderately deep waters.

1.4 Published works derived from the Ph. D. Thesis

Some of the work conducted during the realization of the present Ph. D. Thesis have contributed to different publications and communications. This section lists these contributions.



1.4.1 Contributions in JCR journals

- G. M. Álamo, L. A. Padrón, J. J. Aznárez and O. Maeso. Structure-soil-structure interaction effects on the dynamic response of piled structures under obliquely incident seismic shear waves. *Soil Dynamics and Earthquake Engineering*, 78:142–153, 2015
- G. M. Álamo, A. E. Martínez-Castro, L. A. Padrón, J. J. Aznárez, R. Gallego and O. Maeso. Efficient numerical model for the computation of impedance functions of inclined pile groups in layered soils. *Engineering Structures*, 126:379–390, 2016
- M. Faghihnia Torshizi, M. Saitoh, G. M. Álamo, C. S. Goit and L. A. Padrón. Influence of pile radius on the pile head kinematic bending strains of end-bearing pile groups. *Soil Dynamics and Earthquake Engineering*, 105:184–203, 2018
- G. M. Álamo, J. D. Bordón, J. J. Aznárez and O. Maeso. Relevance of soil-pile tangential tractions for the estimation of kinematic seismic forces: Formulation and setting of a Winkler approach. *Applied Mathematical Modelling*, 59:1–19, 2018
- G. M. Álamo, J. J. Aznárez, L. A. Padrón, A. E. Martínez-Castro, R. Gallego and O. Maeso. Dynamic soil-structure interaction in offshore wind turbines on monopiles in layered seabed based on real data. *Ocean Engineering*, 156:14–24, 2018
- G. M. Álamo, J. J. Aznárez, L. A. Padrón, A. E. Martínez-Castro and O. Maeso. Importance of using accurate soil profiles for the estimation of pile kinematic input factors. *Journal of Geotechnical and Geoenvironmental Engineering*, (under review), submitted on Dec 2017
- C. Medina, G. M. Álamo, J. J. Aznárez, L. A. Padrón and O. Maeso. Variations in the dynamic properties of structures founded on piles induced by obliquely incident SV waves. *Earthquake Engineering & Structural Dynamics*, (under review), submitted on May 2018

1.4.2 Conference contributions

- F. García, G. M. Álamo, L. A. Padrón, J. J. Aznárez and O. Maeso. Rigidez dinámica de cimentaciones tripilote para aerogeneradores marinos. In *Congress of Numerical Method in Engineering (CMN 2015)*. Lisbon, Portugal, 29 June – 2 July 2015
- L. A. Padrón, C. Medina, G. M. Álamo, J. J. Aznárez, A. Santana, O. Maeso, F. García and F. Chirino. Pilotes inclinados: situación normativa y ventajas e inconvenientes de su uso en proyectos de edificación en zonas con riesgo sísmico. In *19th International Congress on Project Management and Engineering*. Granada, Spain, 15–17 July 2015
- G. M. Álamo, J. D. R. Bordón, F. García, J. J. Aznárez, L. A. Padrón, F. Chirino and O. Maeso. Revisión de modelos numéricos para el estudio del comportamiento dinámico de cimentaciones profundas para el diseño y proyecto de aerogeneradores. In *20th International Congress on Project Management and Engineering*. Cartagena, Spain, 13–15 July 2016



- G. M. Álamo, J. J. Aznárez, L. A. Padrón, A. E. Martínez-Castro, R. Gallego and O. Maeso. Dynamic response of real offshore wind turbines on monopiles in stratified seabed. In *VII European Congress on Computational Methods in Applied Sciences and Engineering (ECCOMAS 2016)*. Crete, Greece, 5–10 June 2016
- F. García, G. M. Álamo, L. A. Padrón, J. J. Aznárez and O. Maeso. Influencia del comportamiento poroelástico del fondo marino en la rigidez dinámica de cimentaciones pilotadas para aerogeneradores offshore. In *XXI Congreso Nacional de Ingeniería Mecánica (CNIM)*. Elche, Spain, 9–11 November 2016
- G. M. Álamo, M. Saitoh, C. S. Goit, L. A. Padrón, J. J. Aznárez and O. Maeso. Pile-to-pile kinematic interaction factors for vertically-incident shear waves. In *2nd Global Conference on Applied Computing in Science and Engineering (ACSE2)*. Las Palmas de Gran Canaria, Spain, 26–28 July 2017
- G. M. Álamo, J. J. Aznárez, L. A. Padrón, A. E. Martínez-Castro, R. Gallego and O. Maeso. Integral model for the analysis of pile foundations in stratified soils. In *2nd Global Conference on Applied Computing in Science and Engineering (ACSE2)*. Las Palmas de Gran Canaria, Spain, 26–28 July 2017
- M. Castro, J. D. R. Bordón, G. M. Álamo and J. J. Aznárez. Formulation and calibration of a pasternak model for seismic analysis of pile foundations. In *2nd Global Conference on Applied Computing in Science and Engineering (ACSE2)*. Las Palmas de Gran Canaria, Spain, 26–28 July 2017
- R. Quevedo, G. M. Álamo, J. J. Aznárez, L. A. Padrón and O. Maeso. Simplified model to calculate the envelopes of bending moments along offshore wind turbines on monopiles. In *2nd Global Conference on Applied Computing in Science and Engineering (ACSE2)*. Las Palmas de Gran Canaria, Spain, 26–28 July 2017
- G. M. Álamo, A. E. Martínez-Castro, L. A. Padrón, J. J. Aznárez, R. Gallego and O. Maeso. A proposal for normalized impedance functions of inclined piles in non-homogeneous media. In *X International Conference on Structural Dynamics (EURO-DYN 2017)*. Rome, Italy, 10–13 September 2017
- G. M. Álamo, J. J. Aznárez, L. A. Padrón, A. E. Martínez-Castro, R. Gallego and O. Maeso. Direct model for the dynamic analysis of piled structures on non-homogeneous media. In *1st Conference on Structural Dynamics (DinEst 2018)*. Madrid, Spain, 20–21 June 2018

1.4.3 Book Chapter contributions

- G. M. Álamo, J. D. R. Bordón, F. García, J. J. Aznárez, L. A. Padrón, F. Chirino and O. Maeso. Review of numerical models for studying the dynamic response of deep foundations for the design and project of wind turbines. In J. L. Ayuso, J. L. Yagüe and S. F. Capuz-Rizo, editors, *Project Management and Engineering Research. AEIPRO 2016, In Press*. Springer International Publishing, 2018



1.5 Structure of the dissertation

The present document is divided into 7 chapters, starting with the current introduction and ending with a summary of the main conclusions and future directions drawn from this piece of research. Because along the dissertation several problems of different nature will be handled, specific state-of-the-art revisions are presented at the beginning of each chapter instead of a single one at the beginning of the document. Following the introduction, the formulation of the proposed model is presented in the second chapter. Then, the developed tool is applied in the rest of the chapters to study several problems of engineering interest related to the dynamic behaviour of pile foundations and piled structures. After the main text, several appendices are presented with complementary information and results that enrich the research work. The last of these appendices is a summary of the work in Spanish. In the following, the contents of each chapter are briefly detailed.

The core of the developed work is presented in Chapter 2. This chapter starts with the main hypotheses that are assumed in the proposed numerical formulation. Then, the beam elements used for the discretization of the piles are presented together with their finite element equilibrium equations. Also, the additional equations that are used in order to couple the pile heads to a rigid cap are given. Then, the soil formulation is presented, explaining the benefits of using the particular fundamental solution for the layered half space. Regarding the computation of the soil equations, some numerical aspects are highlighted, including the details of the particular strategy used in the developed code to significantly speed up the computational time. Then, the modifications of these soil equations that are required in order to introduce either the presence of an incident wavefield or external loads acting over the free-surface are detailed. Finally, the formulation is closed by introducing the coupling between the pile and soil equations. At the end of this chapter, a validation of the developed tool is presented and its limitations are discussed. For this purpose, a comparison in terms of maximum seismic bending moments and shear forces is made against a boundary element model and a Winkler model specifically developed for this purpose. Despite presenting there this validation, other verification problems are conducted in Chapters 3, 4 and 5, which are adapted to the contents of each one of these chapters.

In Chapter 3 the impedance problem of reduced pile groups with inclined elements is tackled. The chapter is aimed at studying the influence of the variability of the soil profile on the stiffness and damping functions of the foundation. For this purpose, the results corresponding to the homogeneous half space profile are compared with the ones obtained for different soils whose shear wave velocity varies with depth following a power law. The results are presented through dimensionless graphs.

Following a similar direction that the previous chapter, Chapter 4 studies the influence of the variability of the soil profile on the seismic response of pile foundations. In this chapter, typical physical dimensions of piles are considered together with variable soil profiles that are representative to actual sites. The results obtained for these real soils are compared with the ones corresponding to a homogeneous medium with the mean properties recommended by several codes. The influence of the variability of the soil profile is studied both in terms of kinematic interaction factors and the maximum response spectra that a single degree of freedom oscillator atop of the foundation would present. Also, it is also analysed whether

these equivalent mean soil properties can be used to estimate the maximum kinematic bending moments of the piles.

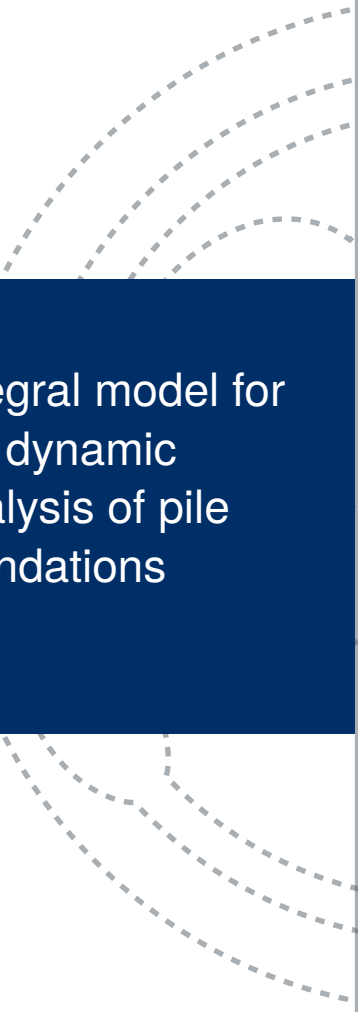
Chapter 5 introduces a problem that is relatively different from the ones studied before, but with high interest and application in civil engineering. In this chapter, instead of using the piles as a foundation system, they are arranged in the soil as a measure to mitigate the propagation of ground vibrations. Particularly, and taking advantage of the characteristics of the developed model, the study is focused on how the performance of the pile barrier is affected by the presence of a rigid stratum at certain depth inside the soil.

The last application chapter is closely related to the Research Project in which this Ph. D. Thesis is developed. In this Chapter 6, the problem of the dynamic characterization of monopiled offshore wind turbines is tackled. The integral model is used to compute the impedance functions of the monopiles and then, through a substructuring methodology, the changes in the fundamental frequency and damping ratio of the pile-structure system due to the flexibility of the foundation are quantified. Properties of several soil profiles and structural dimensions of offshore wind turbines that can be found in the literature are used in order to define the studied systems.

The main body of the document ends with Chapter 7, where a brief summary and the main conclusions drawn from this work are presented. Also, some future research directions based on the work conducted during these years are proposed.

After these chapters, several appendices are presented with supplementary results or complementary formulations that enrich the content of the Ph. D. Thesis. It is important to highlight the last Appendix D, which gives a brief summary in Spanish of the principal aspects of the work.

The document ends with the list of bibliographical references ordered by their appearance in the text.

A series of four dashed, curved lines in a light gray color, starting from the left edge and curving towards the right, positioned behind the main title box and extending across the page.

2. Integral model for the dynamic analysis of pile foundations

- 2.1 Introduction and general hypotheses
- 2.2 Pile finite element equations
- 2.3 Soil equations
- 2.4 Seismic excitation
- 2.5 Excitation at the soil surface
- 2.6 Pile-soil coupling
- 2.7 Displacements at internal points of the soil
- 2.8 Influence of the omitted tangential tractions



2.1 Introduction and general hypotheses

This chapter presents the formulation of the integral model that is developed for the analysis of pile foundations in layered soils. Before presenting the formulation corresponding to piles and soil, this section introduces the main hypothesis and ideas on which the proposed model is based.

The developed model is formulated in the frequency-domain and, therefore, within the scope of linear elasticity. The soil behaviour is modelled by using the integral expression of the reciprocity theorem in elastodynamics and specific Green's functions for the layered half space. Thus, the soil is considered to be formed by a finite number of zoned homogeneous, isotropic, hysteretic layers overlying a semi-infinite half space (unbounded domain).

Following the idea of Mendonça et al. [18–20] and the previous BE-FE model [17], piles are reduced to one-dimensional beam elements. The interaction between the soil and each pile is represented by three distributed tractions acting over the load lines that correspond to the piles. These distributed forces, henceforth referred to as soil-pile interaction tractions, will represent the resultants of the tractions that are acting over the actual interface surface that exists between the pile and the surrounding media (see Fig. 2.1). The integration of these tractions implies that some interaction phenomena cannot be reproduced by the simplified model, such as the local effect of the vertical tangential tractions that results in a distributed moment action over the pile. Note that as the soil-pile interaction tractions represent a global distributed force, it cannot be directly compared to the stress tensor of the internal points of the soil. On contrary, in the integral expression of the reciprocity theorem, the soil-pile interaction tractions are considered as body forces acting along the load lines inside the soil domain. It is important to highlight that the loss of dimension of the piles also implies that no geometrical diffraction effects can be captured by the proposed formulation.

On the other hand, the pile mid-line displacements that define the deformation of the beam can be directly compared to the displacements of the corresponding points of the soil (see Fig. 2.1). Welded conditions are assumed for the pile-soil contact, so these mid-line displacements of the beam section completely coincide with the soil displacements. On the

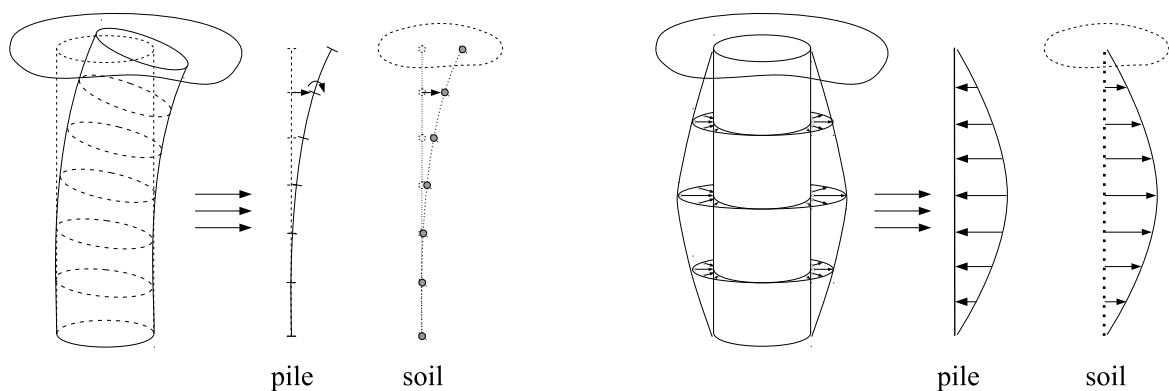


Figure 2.1: Simplification of the pile geometry. Treatment of the pile deformed shape (left) and the soil-pile interaction tractions (right).

other hand, there is no direct relation between the rotations of the pile cross-section and any soil variable.

The additional stiffness and mass introduced by the piles into the soil system are taken into account by considering their beam finite element equilibrium equations, in which the action of the soil-pile interaction tractions is also included. These equations couple the bending rotations of the piles with the lateral displacements and forces and, therefore, the pile-soil interaction will be affected by them. However, for the pile torsional motion the developed model does not include any interaction mechanism between the pile and the soil. Therefore, the pile torsional mode is neglected in the proposed formulation.

Finally, pile groups can be formed by connecting the pile heads through a rigid cap. In this case, no contact is assumed between the cap and the soil, so all the foundation-soil interaction is limited to the one produced along the piles.

In the following, the detailed equations corresponding to the modelling of piles and soil are obtained. After this process, and at the end of the chapter, a validation of the developed model is presented in order to discuss up to what point the simplifications made affect the capability of the integral model to analyse the pile dynamic behaviour.

2.2 Pile finite element equations

As mentioned before, piles are modelled through finite elements as one-dimensional beam elements. This way, the rigidity effects of the piles and their response to the loads transmitted by the soil are obtained by solving the classical finite element equilibrium equation. Assuming harmonic displacements and forces, and hysteretic material damping for the beam elements, the pile system of equations results in:

$$(\mathbf{K} (1 + 2i\beta_p) - \omega^2 \mathbf{M}) \mathbf{u} = \mathbf{F} \quad (2.1)$$

where \mathbf{K} and \mathbf{M} are the stiffness and mass matrices obtained from the assembly of the elemental ones, \mathbf{u} is the vector containing the complex amplitude of the degrees of freedom that determine the motion of the beam (nodal displacements and rotations), \mathbf{F} is the vector containing the complex amplitude of nodal external forces acting over the beams, β_p is the pile hysteretic damping coefficient, ω is the angular frequency of the excitation, and i is the imaginary unit. Note that in this expression, and in the rest of the document, the term $e^{i\omega t}$ is omitted for simplicity's sake.

2.2.1 Pile elements

Piles are discretized into 2-noded elements whose motion is determined through 10 degrees-of-freedom, which are depicted in Fig. 2.2. As mentioned in Section 2.1, the pile torsion is not considered in the proposed formulation because no mechanism of interaction with the soil is contemplated for this vibration mode.

The lateral displacements and rotations along each element of the pile are modelled through cubic ψ_u and quadratic ψ_θ shape functions, respectively. These shape functions are chosen

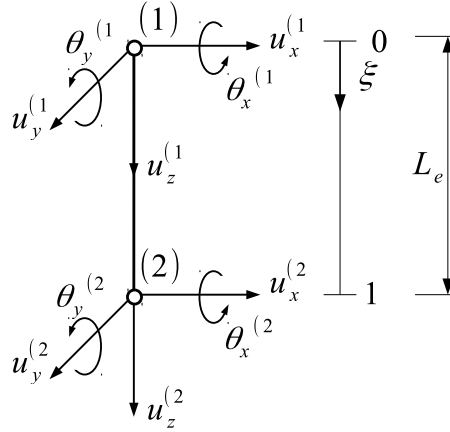


Figure 2.2: Pile element degrees-of-freedom.

in order to satisfy the static equation of the Timoshenko's Beam [59] and can be expressed in terms of the dimensionless axial coordinate $\xi = z/L_e$ as:

$$\psi_{u_1}(\xi) = \frac{1}{(1+\phi)} (2\xi^3 - 3\xi^2 - \phi\xi + (1+\phi)) \quad (2.2a)$$

$$\psi_{u_2}(\xi) = \frac{L_e}{(1+\phi)} \left(\xi^3 - (2 + \frac{\phi}{2})\xi^2 + (1 + \frac{\phi}{2})\xi \right) \quad (2.2b)$$

$$\psi_{u_3}(\xi) = \frac{-1}{(1+\phi)} (2\xi^3 - 3\xi^2 - \phi\xi) \quad (2.2c)$$

$$\psi_{u_4}(\xi) = \frac{L_e}{(1+\phi)} \left(\xi^3 - (1 - \frac{\phi}{2})\xi^2 - \frac{\phi}{2}\xi \right) \quad (2.2d)$$

$$\psi_{\theta_1}(\xi) = \frac{6}{(1+\phi)L_e} (\xi^2 - \xi) \quad (2.3a)$$

$$\psi_{\theta_2}(\xi) = \frac{1}{(1+\phi)} (3\xi^2 - (4+\phi)\xi + (1+\phi)) \quad (2.3b)$$

$$\psi_{\theta_3}(\xi) = \frac{-6}{(1+\phi)L_e} (\xi^2 - \xi) \quad (2.3c)$$

$$\psi_{\theta_4}(\xi) = \frac{1}{(1+\phi)} (3\xi^2 - (2-\phi)\xi) \quad (2.3d)$$

So the lateral displacements and rotations inside each pile element are defined in terms of the nodal values $u_i^{(n)}, \theta_i^{(n)}$ ($i = x, y$ and $n = 1, 2$) as:

$$u_x(\xi) = \psi_{u_1}(\xi) u_x^{(1)} + \psi_{u_2}(\xi) \theta_y^{(1)} + \psi_{u_3}(\xi) u_x^{(2)} + \psi_{u_4}(\xi) \theta_y^{(2)} \quad (2.4a)$$

$$u_y(\xi) = \psi_{u_1}(\xi) u_y^{(1)} - \psi_{u_2}(\xi) \theta_x^{(1)} + \psi_{u_3}(\xi) u_y^{(2)} - \psi_{u_4}(\xi) \theta_x^{(2)} \quad (2.4b)$$



$$\theta_x(\xi) = -\psi_{\theta_1}(\xi) u_x^{(1)} + \psi_{\theta_2}(\xi) \theta_y^{(1)} - \psi_{\theta_3}(\xi) u_x^{(2)} + \psi_{\theta_4}(\xi) \theta_y^{(2)} \quad (2.5a)$$

$$\theta_y(\xi) = \psi_{\theta_1}(\xi) u_y^{(1)} + \psi_{\theta_2}(\xi) \theta_x^{(1)} + \psi_{\theta_3}(\xi) u_y^{(2)} + \psi_{\theta_4}(\xi) \theta_x^{(2)} \quad (2.5b)$$

In the previous expressions, L_e is the length of the element and ϕ is the ratio between the flexural and shear stiffness of the beam that is defined as:

$$\phi = \frac{12E_p I_p}{L_e^2 \alpha G_p A_p} = \frac{24I_p}{L_e^2 \alpha A_p} (1 + \nu_p) \quad (2.6)$$

where E_p , G_p and ν_p are the Young's modulus, Shear modulus and Poisson's ratio of the pile material, I_p and A_p are the pile moment of inertia and area of the pile cross-section, and α is shear coefficient of the pile cross-section (Timoshenko's beam theory). It is important to highlight that this formulation collapses into the Bernoulli's beam theory if $\phi \rightarrow 0$.

On the other hand, the axial displacements of the pile element are approximated through lineal shape functions φ :

$$\varphi_1(\xi) = 1 - \xi \quad (2.7a)$$

$$\varphi_2(\xi) = \xi \quad (2.7b)$$

And the expression of the axial displacements inside each element is obtained in terms of the nodal values $u_z^{(n)}$ ($n = 1, 2$) as:

$$u_z(\xi) = \varphi_1(\xi) u_z^{(1)} + \varphi_2(\xi) u_z^{(2)} \quad (2.8)$$

Once the shape functions of the displacements and rotations are defined, the pile elemental stiffness and mass matrices are directly obtained through the application of the Principle of Virtual Displacements or the Hamilton's principle (see [59]).

Elemental stiffness matrices

The terms of the elemental stiffness sub-matrix for the axial behaviour of the pile are obtained from:

$$K_{e_{ij}}^a = \int_0^{L_e} \varphi_i' E_p A_p \varphi_j' dz \quad i = 1, 2 \quad (2.9)$$

where \square' denotes derivation with respect to z .

On the other hand, the terms of the lateral stiffness sub-matrix are obtained through:

$$K_{e_{ij}}^l = \int_0^{L_e} \psi_{\theta_i}' E_p I_p \psi_{\theta_j}' + (\psi_{u_i}' - \psi_{\theta_i}) \alpha G_p A_p (\psi_{u_j}' - \psi_{\theta_j}) dz \quad i = 1 - 4 \quad (2.10)$$

Substituting the expressions of the shape functions, the elemental axial \mathbf{K}_e^a and lateral \mathbf{K}_e^l stiffness sub-matrices for the pile beam elements are obtained as:

$$\mathbf{K}_e^a = \frac{E_p A_p}{L_e} \begin{bmatrix} 1 & -1 \\ -1 & 1 \end{bmatrix} \quad (2.11)$$



$$\mathbf{K}_e^l = \frac{E_p I_p}{(1 + \phi)L_e^3} \begin{bmatrix} 12 & 6L_e & -12 & 6L_e \\ & (4 + \phi)L_e^2 & -6L_e & (2 - \phi)L_e^2 \\ & & 12 & -6L_e \\ \text{symmetric} & & & (4 + \phi)L_e^2 \end{bmatrix} \quad (2.12)$$

Note that the sign criteria used for the lateral stiffness sub-matrix corresponds to the one of the $x - z$ plane. For the $y - z$ plane, the signs of some terms should be properly changed according to the criteria used for the rotations around the x axis. As commented before, the lateral formulation collapses into the one of a Bernoulli's beam if $\phi \rightarrow 0$.

Elemental mass matrices

The terms of the elemental axial mass sub-matrix are obtained through:

$$M_{te_{ij}}^a = \int_0^{L_e} \varphi_i \rho_p A_p \varphi_j dz \quad (2.13)$$

where ρ_p is the density of the pile material.

For the lateral behaviour, the contribution of both the translational and rotatory inertia effects are considered. The terms of the elemental mass sub-matrices are obtained from:

$$M_{te_{ij}}^l = \int_0^{L_e} \psi_{u_i} \rho_p A_p \psi_{u_j} dz ; \quad M_{re_{ij}}^l = \int_0^{L_e} \psi_{\theta_i} \rho_p I_p \psi_{\theta_j} dz \quad (2.14)$$

Note that, as the torsional mode of the pile is not included in the proposed model, the only contribution to the rotatory inertia of the pile element corresponds to the one of its lateral deformation.

By substituting the corresponding shape functions, the elemental axial mass sub-matrix \mathbf{M}_{te}^a and the elemental lateral mass sub-matrix $\mathbf{M}_e^l = \mathbf{M}_{te}^l + \mathbf{M}_{re}^l$ are obtained as:

$$\mathbf{M}_{te}^a = \frac{\rho_p A_p L_e}{6} \begin{bmatrix} 2 & 1 \\ 1 & 2 \end{bmatrix} \quad (2.15)$$

$$\mathbf{M}_{te}^l = \frac{\rho_p A_p L_e}{840(1 + \phi)^2} \begin{bmatrix} 4(70\phi^2 + 147\phi + 78) & L_e(35\phi^2 + 77\phi + 44) & 4(35\phi^2 + 63\phi + 27) & -L_e(35\phi^2 + 63\phi + 26) \\ & L_e^2(7\phi^2 + 14\phi + 8) & 4L_e(35\phi^2 + 63\phi + 26) & -L_e^2(7\phi^2 + 14\phi + 6) \\ & & 4(70\phi^2 + 147\phi + 78) & -L_e(35\phi^2 + 77\phi + 44) \\ \text{symmetric} & & & L_e^2(7\phi^2 + 14\phi + 8) \end{bmatrix} \quad (2.16)$$

$$\mathbf{M}_{re}^l = \frac{\rho_p I_p}{30(1 + \phi)^2 L_e} \begin{bmatrix} 36 & -L_e(15\phi - 3) & -36 & -L_e(15\phi - 3) \\ L_e^2(10\phi^2 + 5\phi + 4) & L_e(15\phi - 3) & L_e^2(5\phi^2 - 5\phi - 1) & \\ & 36 & L_e(15\phi - 3) & \\ \text{symmetric} & & L_e^2(10\phi^2 + 5\phi + 4) & \end{bmatrix} \quad (2.17)$$

Again, the sign criteria for the lateral sub-matrices correspond to the motion in the $x - z$ plane and should be properly changed for the $y - z$ plane.

2.2.2 External forces

The external loads acting over the pile can be divided into three components:

$$\mathbf{F} = \mathbf{F}^{\text{head}} + \mathbf{F}^{\text{tip}} + \mathbf{F}^q \quad (2.18)$$

being \mathbf{F}^q the forces produced due to the pile-soil interaction tractions acting along the pile length; \mathbf{F}^{head} the forces acting on the pile head that can correspond either to imposed external loads or to the forces arising due to the pile coupling with a rigid cap; and \mathbf{F}^{tip} the forces acting on the pile tip due to the imposition of fixed or hinged tip boundary conditions (for piles that reach a rigid stratum). For floating piles, always free-tip conditions are assumed.

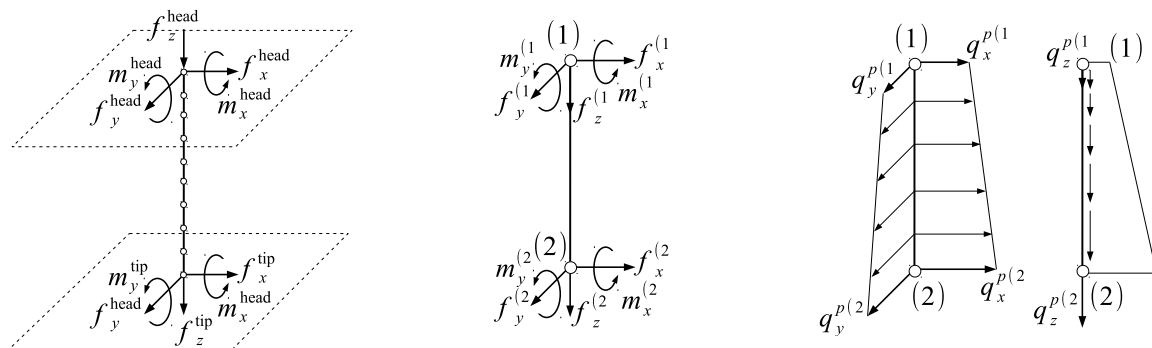


Figure 2.3: External forces acting on the pile head and tip (left). Nodal forces for each pile element (centre). Nodal values of the pile-soil distributed tractions acting over each element of the pile (right).

The pile-soil interaction is modelled through a lineal distribution of tractions acting in the three directions of the space, as depicted in Fig. 2.3. These distributed tractions are defined for each element through their nodal values $q_i^{p(n)}$ ($i = x, y, z$ and $n = 1, 2$) and the linear shape functions φ (Eqs. 2.7) as:

$$q_x^p(\xi) = \varphi_1(\xi) q_x^{p(1)} + \varphi_2(\xi) q_x^{p(2)} \quad (2.19a)$$

$$q_y^p(\xi) = \varphi_1(\xi) q_y^{p(1)} + \varphi_2(\xi) q_y^{p(2)} \quad (2.19b)$$

$$q_z^p(\xi) = \varphi_1(\xi) q_z^{p(1)} + \varphi_2(\xi) q_z^{p(2)} \quad (2.19c)$$



The nodal forces that these distributed interaction tractions produce over the pile are computed as:

$$\mathbf{F}^q = \mathbf{Q}\mathbf{q}^p \quad (2.20)$$

where \mathbf{Q} is the global matrix that transforms the distributed loads into equivalent nodal ones and \mathbf{q}^p is the vector containing the complex amplitudes of the pile-soil interaction tractions at each node of the pile.

By using the Principle of Virtual Displacements (see, e.g., [60]), the coefficients of the elemental sub-matrices \mathbf{Q}_e^l , \mathbf{Q}_e^a related to the lateral or axial deformations of the pile can be computed as:

$$Q_{eij}^l = \int_0^{L_e} \psi_{u_i} \varphi_j \, dz \quad (2.21)$$

$$Q_{eij}^a = \int_0^{L_e} \varphi_i \varphi_j \, dz \quad (2.22)$$

Resulting both sub-matrices in:

$$\mathbf{Q}_e^l = \frac{L_e}{(1 + \phi)} \begin{bmatrix} \left(\frac{7}{20} + \frac{\phi}{3}\right) & \left(\frac{3}{20} + \frac{\phi}{6}\right) \\ L_e\left(\frac{1}{20} + \frac{\phi}{24}\right) & L_e\left(\frac{1}{30} + \frac{\phi}{24}\right) \\ \left(\frac{3}{20} + \frac{\phi}{6}\right) & \left(\frac{7}{20} + \frac{\phi}{3}\right) \\ -L_e\left(\frac{1}{30} + \frac{\phi}{24}\right) & -L_e\left(\frac{1}{20} + \frac{\phi}{24}\right) \end{bmatrix} \quad (2.23)$$

$$\mathbf{Q}_e^a = \frac{L_e}{6} \begin{bmatrix} 2 & 1 \\ 1 & 2 \end{bmatrix} \quad (2.24)$$

note again that the signs of the coefficients of the lateral sub-matrix correspond to the ones of the $x - z$ plane.

With these considerations, the system of equations corresponding to the finite element formulation of the piles can be written as:

$$(\mathbf{K} (1 + 2i\beta_p) - \omega^2 \mathbf{M}) \mathbf{u} - \mathbf{Q}\mathbf{q}^p = \mathbf{F}^{\text{head}} + \mathbf{F}^{\text{tip}} \quad (2.25)$$

2.2.3 Inclined piles

In the previous section, the formulation has been obtained considering the case of vertical piles and, therefore, no distinction has been made between the local and global coordinate systems. However, when dealing with configurations of inclined piles, the afore-mentioned expressions are only valid for the pile local coordinate system. Thus, proper rotation matrices are needed in order to transform the inclined piles elemental matrices into the global reference system in order to conduct the assembly process.

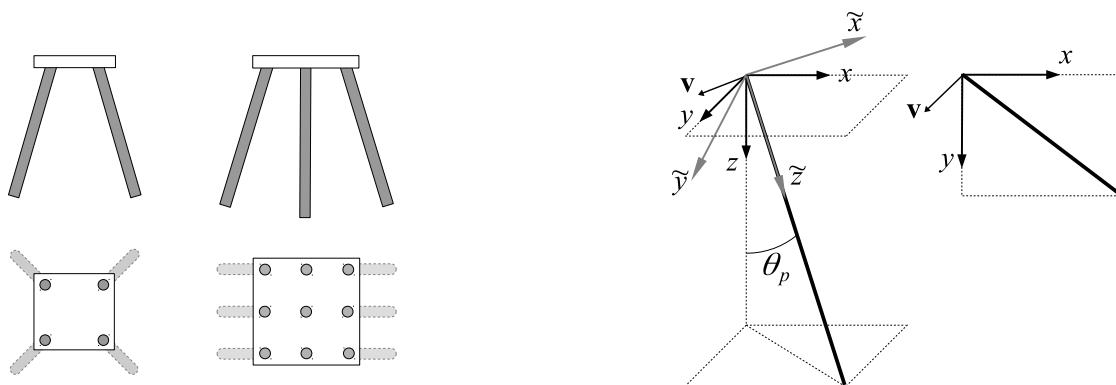


Figure 2.4: Typical inclined piles configurations (left). Definition of the local and global pile coordinate systems (right).

Considering typical pile configurations (see Fig. 2.4), pile inclination can be defined by a rotation angle θ_p around an axis contained in the $x - y$ plane given by the direction vector $\mathbf{v} = \{v_x, v_y, 0\}^T$. By applying Rodrigues' rotation formula, the rotation matrix \mathbf{R}_u that transform the local axes $\tilde{x}\tilde{y}\tilde{z}$ into the global xyz reference system is obtained as:

$$\mathbf{R}_u = \begin{bmatrix} \cos \theta_p + v_x^2(1 - \cos \theta_p) & v_x v_y(1 - \cos \theta_p) & v_y \sin \theta_p \\ v_x v_y(1 - \cos \theta_p) & \cos \theta_p + v_y^2(1 - \cos \theta_p) & -v_x \sin \theta_p \\ -v_y \sin \theta_p & v_x \sin \theta_p & \cos \theta_p \end{bmatrix} \quad (2.26)$$

In order to transform the rotations and moments of the inclined beam elements, the rotation matrix is modified in order to take into account the zero value condition around the \tilde{z} axis:

$$\mathbf{R}_\theta = \begin{bmatrix} R_{u11} - R_{u13} \frac{R_{u31}}{R_{u33}} & R_{u21} - R_{u23} \frac{R_{u31}}{R_{u33}} \\ R_{u12} - R_{u13} \frac{R_{u32}}{R_{u33}} & R_{u22} - R_{u23} \frac{R_{u32}}{R_{u33}} \end{bmatrix} \quad (2.27)$$

Now, by using these rotation matrices, the elemental stiffness and mass matrices in the global coordinate system ($\mathbf{K}_e, \mathbf{M}_e$) can be computed from the elemental stiffness and mass matrices in the pile local system of reference ($\tilde{\mathbf{K}}_e, \tilde{\mathbf{M}}_e$) through:

$$\mathbf{K}_e = \mathbf{R}_K^{-1} \tilde{\mathbf{K}}_e \mathbf{R}_K \quad (2.28)$$

$$\mathbf{M}_e = \mathbf{R}_K^{-1} \tilde{\mathbf{M}}_e \mathbf{R}_K \quad (2.29)$$

with

$$\mathbf{R}_K = \begin{bmatrix} \mathbf{R}_u & \emptyset & \emptyset & \emptyset \\ & \mathbf{R}_\theta & \emptyset & \emptyset \\ & & \mathbf{R}_u & \emptyset \\ \text{symmetric} & & & \mathbf{R}_\theta \end{bmatrix} \quad (2.30)$$

On the other hand, considering that the soil-pile interaction tractions act over the three directions of the space, but do not contain any component regarding distributed moments, the rotation of the local elemental matrix $\tilde{\mathbf{Q}}_e$ to the global one \mathbf{Q}_e is conducted through:

$$\mathbf{Q}_e = \mathbf{R}_K^{-1} \tilde{\mathbf{Q}}_e \mathbf{R}_q \quad (2.31)$$

with

$$\mathbf{R}_q = \begin{bmatrix} \mathbf{R}_u & \mathbf{\emptyset} \\ \mathbf{\emptyset} & \mathbf{R}_u \end{bmatrix} \quad (2.32)$$

2.2.4 Pile union through a rigid cap

Pile foundations with only one pile member are rarely found in engineering applications. Normally, a group of piles are joined together by using a pile cap in order to have a wider and stiffer foundation. For this reason, the coupling of a set of piles through a rigid cap can be considered in the proposed model.

The pile cap is assumed to be infinitely rigid, with a mass m^c and moments of inertia with respect to the three coordinate axes I_i^c ($i = x, y, z$). The thickness of the cap is neglected (i.e., the cap centre of gravity and all pile heads are assumed to be located at the same level), as well as the contact between the cap and the soil (i.e., the foundation-soil interaction is produced only along the piles). For simplicity's sake, the formulation corresponding to a fixed pile-cap union is first presented. Then, the modifications needed in order to consider a hinged pile-cap union are commented at the end of the section.

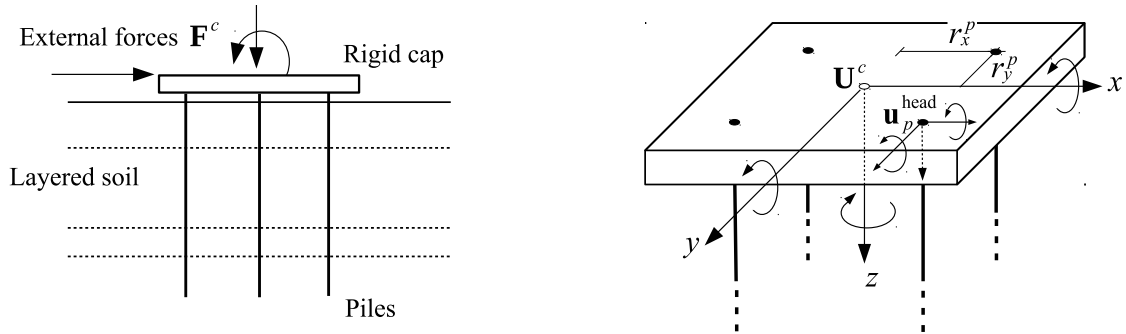


Figure 2.5: Sketch of the pile union through a rigid cap. Definition of the cap degrees of freedom.

By considering the rigid body motion of the cap, the displacements and rotations $\mathbf{u}_p^{\text{head}} = \{u_{x_p}^{\text{head}}, u_{y_p}^{\text{head}}, u_{z_p}^{\text{head}}, \theta_{x_p}^{\text{head}}, \theta_{y_p}^{\text{head}}\}^T$ at the head of each pile p fixedly connected to it can be obtained in terms of the three displacements and three rotations of the centre of gravity of the cap $\mathbf{U}^c = \{U_x^c, U_y^c, U_z^c, \Theta_x^c, \Theta_y^c, \Theta_z^c\}^T$ as:

$$\mathbf{u}_p^{\text{head}} = \mathbf{T}_p^c \mathbf{U}^c \quad (2.33)$$



with

$$\mathbf{T}_p^c = \begin{bmatrix} 1 & 0 & 0 & 0 & 0 & -r_y^p \\ 0 & 1 & 0 & 0 & 0 & r_x^p \\ 0 & 0 & 1 & r_y^p & -r_x^p & 0 \\ 0 & 0 & 0 & 1 & 0 & 0 \\ 0 & 0 & 0 & 0 & 1 & 0 \end{bmatrix} \quad (2.34)$$

where r_i^p is the relative distance of the head of pile p with respect to the centre of gravity of the cap in the i direction ($i = x, y$), see Fig 2.5.

On the other hand, equilibrium conditions are imposed at the pile cap between external forces, inertial forces and pile-cap reactions. These equilibrium equations can be written at the centre of gravity of the pile cap as:

$$\mathbf{F}^c - \sum_{p=1}^{N^c} (\mathbf{T}_p^c)^T \mathbf{F}_p^{\text{head}} + \omega^2 \mathbf{M}^c \mathbf{U}^c = \mathbf{0} \quad (2.35)$$

where $\mathbf{F}^c = \{F_x^c, F_y^c, F_z^c, M_x^c, M_y^c, M_z^c\}^T$ is the vector of external forces and torques acting over the cap's centre of gravity; N^c is the number of piles that are connected to the cap; $\mathbf{F}_p^{\text{head}} = \{f_{x_p}^{\text{head}}, f_{y_p}^{\text{head}}, f_{z_p}^{\text{head}}, m_{x_p}^{\text{head}}, m_{y_p}^{\text{head}}\}^T$ is the vector containing the pile-cap reaction forces and moments acting over each pile p ; and $\mathbf{M}^c = \text{diag}(m^c, m^c, m^c, I_x^c, I_y^c, I_z^c)$ is the diagonal mass matrix of the cap.

The fixed pile-cap union can be modified to a hinged union just by substituting the compatibility equations between the pile and cap rotations in the two last rows of Eq. (2.33) with the zero pile-cap moment reaction condition imposed by the hinged union:

$$\begin{aligned} \theta_{x_p}^{\text{head}} = \Theta_x^c & \rightarrow m_{x_p}^{\text{head}} = 0 \\ \theta_{y_p}^{\text{head}} = \Theta_y^c & \rightarrow m_{y_p}^{\text{head}} = 0 \end{aligned} \quad (2.36)$$

2.3 Soil equations

Let $\mathcal{S}(\mathbf{u}, \boldsymbol{\sigma}, \mathbf{b}; \omega, \Omega)$ and $\mathcal{S}^*(\mathbf{u}^*, \boldsymbol{\sigma}^*, \mathbf{b}^*; \omega, \Omega)$ be two different elastodynamic states that satisfy the Navier equations in the domain Ω . These two states can be related by applying the reciprocal theorem in elastodynamics [61]. Assuming harmonic conditions and zero initial values, the integral expression of the reciprocity theorem can be written as:

$$\int_{\Gamma} \mathbf{p}^* \mathbf{u} \, d\Gamma + \int_{\Omega} \mathbf{b}^* \mathbf{u} \, d\Omega = \int_{\Gamma} \mathbf{p} \mathbf{u}^* \, d\Gamma + \int_{\Omega} \mathbf{b} \mathbf{u}^* \, d\Omega \quad (2.37)$$

being \mathbf{u}, \mathbf{u}^* the displacements at any point of the domain Ω ; \mathbf{p}, \mathbf{p}^* the tractions acting over the boundary $\Gamma = \partial\Omega$ compatible with the stress tensors $\boldsymbol{\sigma}, \boldsymbol{\sigma}^*$; and \mathbf{b}, \mathbf{b}^* the body forces acting inside the domain.

In the previous expression, \mathcal{S}^* is a known state usually referred to as fundamental solution or Green's functions. The choose of a proper fundamental solution can significantly simplify the formulation of the problem. In this work, the Green's functions developed by Pak and Guzina [62] for the layered half space are considered as fundamental solution.



2.3.1 Pak and Guzina's Green's functions for the layered half space

The fundamental solution used in the proposed model represents the response of any point of a horizontally layered half space Ω (unbounded domain) when an unitary load is applied at point $\mathbf{\kappa}$ (collocation point) in each direction of the space. Mathematically, each component of the body forces that represent this point load can be expressed as:

$$b_k^* = \delta(\mathbf{\kappa})\delta_{lk} \quad (2.38)$$

being l the direction of the applied load, δ_{lk} the Kronecker's delta, and $\delta(\mathbf{\kappa})$ the Dirac's delta defined as:

$$\int_{\Omega} \delta(\mathbf{\kappa}) d\Omega = \begin{cases} 1 & \text{if } \mathbf{\kappa} \in \Omega \\ 0 & \text{if } \mathbf{\kappa} \notin \Omega \end{cases} \quad (2.39)$$

In their work, Pak and Guzina [62] addressed this problem by expressing the solution of the Navier's equations in terms of displacement potentials [63] in the cylindrical coordinate system. The angular dependence was handled through a Fourier decomposition, while a radial Hankel transform was used in order to obtain explicit expressions of the displacements and stresses at any point of the domain in the transformed space. In addition to this, propagation matrices relating the displacements and tractions at the boundaries of each layer with the ones of the surrounding strata were used in order to model the behaviour of the layered half space. Finally, a particular integration procedure [62, 64, 65] is required in order to evaluate the inverse Hankel transform and obtain the desired displacements and tractions. This integration procedure has been modified for low-frequencies based on the single layer solution problem by Martínez-Castro and Gallego [34].

The main benefit of these Green's functions is the fact that they use particular propagation matrices, which do not include any unbounded exponential terms. Thus, any possible numerical instabilities are avoided, yielding an accurate model with fast convergence. Furthermore, as the fundamental solution includes the layered half space domain as part of its hypotheses, the boundary conditions of the free-surface and layer interfaces are intrinsically satisfied.

2.3.2 Soil base equations

Once the fundamental solution is known, the reciprocity theorem can be used in order to compute the unknown state \mathcal{S} in the domain Ω corresponding to a horizontally layered half space (agreeing with the domain assumed for the computation of the Green's functions). Taking into account the definition of the body forces of the fundamental solution state, the domain integral of the left-side of Eq. (2.37) is reduced to:

$$\int_{\Omega} \mathbf{b}^* \mathbf{u} d\Omega = \int_{\Omega} \delta(\mathbf{\kappa}) \mathbf{u} d\Omega = \mathbf{u}^{\kappa} \quad (2.40)$$

On the other hand, the fundamental solution satisfies the free-surface boundary condition ($\mathbf{p}^* = 0$ at Γ), so the contour integral of the left-side of Eq. (2.37) vanishes:

$$\int_{\Gamma} \mathbf{p}^* \mathbf{u} d\Gamma = \mathbf{0} \quad (2.41)$$

As an initial approximation, no external forces acting over the free-surface will be considered in the unknown state \mathcal{S} (i.e., $\mathbf{p} = 0$ at Γ), so the contour integral of the right-side of the reciprocity theorem also vanishes:

$$\int_{\Gamma} \mathbf{p} \mathbf{u}^* d\Gamma = \mathbf{0} \quad (2.42)$$

Finally, the body forces of the elastodynamic state \mathcal{S} correspond to the pile-soil interaction tractions \mathbf{q}_p^s that act over the soil along the load lines Γ_p representing the piles. Thus, the domain integral of the right-side of the reciprocity theorem (2.37) is transformed into the following line contour integral:

$$\int_{\Omega} \mathbf{b} \mathbf{u}^* d\Omega = \int_{\Gamma_p} \mathbf{u}^* \mathbf{q}_p^s d\Gamma_p \quad (2.43)$$

With these considerations, the reduced integral expression of the reciprocity theorem can be written as:

$$\mathbf{u}^{\kappa} = \int_{\Gamma_p} \mathbf{u}^* \mathbf{q}_p^s d\Gamma_p \quad (2.44)$$

Note that this expression represents three equations corresponding to each Cartesian direction of the space. Thus, \mathbf{u}^{κ} is a vector containing the three displacements of the collocation point κ , \mathbf{u}^* is a tensor containing the three displacements for each direction of the punctual load, and \mathbf{q}_p^s is a vector containing the three components of the soil-pile interaction tractions.

Considering now the pile discretization, the evaluation of the integral in Eq. (2.44) can be handled as the superposition of the contribution of each element Γ_e . As done for the piles (Eq. 2.19), a linear variation of the soil-pile interaction tractions inside each element is assumed. Including these considerations, Eq. (2.44) can be evaluated as:

$$\mathbf{u}^{\kappa} = \sum_{e=1}^{N_e} \int_{\Gamma_e} \mathbf{u}^* (\varphi_1 \mathbf{q}_e^{s(1)} + \varphi_2 \mathbf{q}_e^{s(2)}) d\Gamma_e \quad (2.45)$$

being N_e the total number of pile elements; and $\mathbf{q}_e^{s(n)}$ the vector containing the three amplitudes of the interaction tractions at the node n ($n = 1, 2$) of the element e .

This equation can be expressed in matrix form as:

$$\mathbf{u}^{\kappa} = \mathbf{G}^{\kappa} \mathbf{q}^s \quad (2.46)$$

being \mathbf{q}^s the vector containing the nodal values of the interaction tractions acting over the soil, and \mathbf{G}^{κ} the influence sub-matrix obtained from the assembly of the elemental ones that are defined as:

$$\mathbf{G}_e^{\kappa} = \begin{bmatrix} \int_{\Gamma_e} \mathbf{u}^* \varphi_1 d\Gamma_e & \int_{\Gamma_e} \mathbf{u}^* \varphi_2 d\Gamma_e \end{bmatrix} \quad (2.47)$$

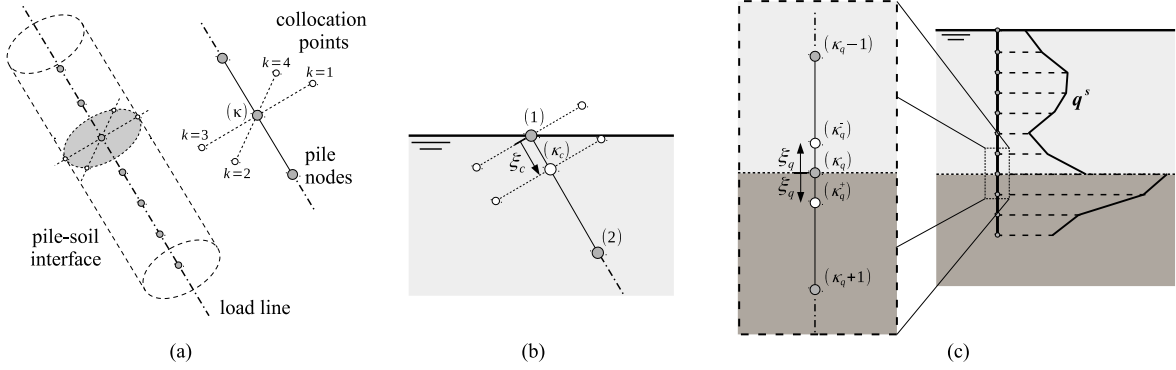


Figure 2.6: Non-nodal collocation strategies. (a) Due to integrating in the same load line than the collocation point. (b) Due to pile inclination. (c) Due to discontinuities in the soil-pile interaction tractions.

As the fundamental solution has no explicit expressions (but is obtained through a numerical iterative procedure), these integrals must be evaluated numerically through a standard Gaussian quadrature rule.

By applying Eq. (2.46) to all pile nodes, the following system of equations is obtained:

$$\mathbf{u}^s = \mathbf{G}\mathbf{q}^s \quad (2.48)$$

being \mathbf{u}^s the vector containing the three displacements at the points of the soil that correspond to the pile nodes, and \mathbf{G} the influence matrix.

2.3.2.1 Numerical aspects: non-nodal collocation strategies

The integral that needs to be evaluated in order to compute the terms of the influence matrix (Eq. 2.47) becomes singular when the collocation point belongs to the integration element due to the characteristics of the fundamental solution. In order to avoid this singularity, a non-nodal collocation strategy is followed as depicted in Fig. 2.6(a). This strategy coincides with the one proposed by Padrón et al. [21]. Four collocation points κ_k are used around the central node κ in order not to break the symmetry of the problem. These points are located at the soil-pile interface and their displacements can be expressed in terms of the ones of the central node by using the motion equations of the pile section. By adding the contribution of each collocation point κ_k , the influence matrix for an element e belonging to the same load line than the central collocation point κ results in:

$$\mathbf{G}_e^\kappa = \frac{1}{4} \sum_{k=1}^4 \mathbf{G}_e^{\kappa_k} \quad (2.49)$$

For computing the rest of terms of the influence matrices, the collocation point is assumed to be the node κ .

However, this non-nodal collocation strategy presents an issue when collocating around the first node of an inclined pile. As depicted in Fig. 2.6(b), at least one of the collocation

points κ_k will be located outside the half space domain and, therefore, the hypothesis of the used Green's functions will be not satisfied (the collocation point no longer belongs to the domain). To overcome this limitation, the central point of the collocation is displaced inside the element a quantity ξ_c that guarantees that all of the four additional collocation points stay inside the soil. By using Eqs. (2.4) and (2.8), the displacements of the new central collocation point κ_c can be expressed in terms of the ones corresponding to the two nodes of the first element. Thus, the soil equations of the first node of an inclined pile result in:

$$\mathbf{u}^{\kappa_c} = \Psi(\xi_c) \begin{bmatrix} \mathbf{u}^{(1)} \\ \mathbf{u}^{(2)} \end{bmatrix} = \mathbf{G}^{\kappa_c} \mathbf{q}^s \quad (2.50)$$

where:

$$\Psi(\xi_c) = \begin{bmatrix} \psi_{u_1}(\xi_c) & 0 & 0 & 0 & \psi_{u_2}(\xi_c) & \psi_{u_3}(\xi_c) & 0 & 0 & 0 & \psi_{u_4}(\xi_c) \\ 0 & \psi_{u_1}(\xi_c) & 0 & -\psi_{u_2}(\xi_c) & 0 & 0 & \psi_{u_3}(\xi_c) & 0 & -\psi_{u_4}(\xi_c) & 0 \\ 0 & 0 & \varphi_1(\xi_c) & 0 & 0 & 0 & 0 & \varphi_2(\xi_c) & 0 & 0 \end{bmatrix} \quad (2.51)$$

A similar situation is found at the points of the soil at which a discontinuity in the soil-pile interaction tractions is assumed. This assumption is usually made when a strong variation between the properties of two consecutive soil layers is produced. In this case, as depicted in Fig. 2.6(c), the equations corresponding to the node κ_q with duplicity of \mathbf{q}^s are written two times by displacing the collocation point a quantity ξ_q inside the two elements to which this point belongs. As done before, the displacements of the new collocation points are expressed in terms of the nodal ones by using the proper shape functions:

$$\begin{bmatrix} \mathbf{u}^{\kappa_q^-} \\ \mathbf{u}^{\kappa_q^+} \end{bmatrix} = \begin{bmatrix} \Psi(1 - \xi_q) & \emptyset \\ \emptyset & \Psi(\xi_q) \end{bmatrix} \begin{bmatrix} \mathbf{u}^{(\kappa_q-1)} \\ \mathbf{u}^{(\kappa_q)} \\ \mathbf{u}^{(\kappa_q+1)} \end{bmatrix} = \mathbf{G}^{\kappa_q} \mathbf{q}^s \quad (2.52)$$

2.3.2.2 Numerical aspects: reuse of influence sub-matrices

The computation of the influence matrix is the sub-process of the model that consumes the main part of the computational time. This happens because of the fact that the evaluation of the Green's functions required for the integration is relatively slow due to the complexity and iterative nature of the fundamental solution. This issue is magnified when increasing the number or discretization of the piles (i.e., greater number of collocation-observation points), being the computational time of the model of order $\mathcal{O}(N_e^2)$, being N_e the number of pile elements. Besides, the evaluation of the fundamental solution demands more time for higher frequencies and for problems with large distances between the observation and collocation points or with a high number of layers.

However, as pile configurations generally present a regular disposition, a high number of the terms of the influence matrix \mathbf{G} coincide or, at least, are equivalent through a simple in-plane rotation. By identifying these equivalent sub-matrices, a significant portion of the computational time can be saved because the integrals will be computed once and then assembled in all the corresponding positions.

Attending to the characteristics of the fundamental solution, it is known that the tensor \mathbf{u}^* only depends on the relative distance between the collocation and observation points, and

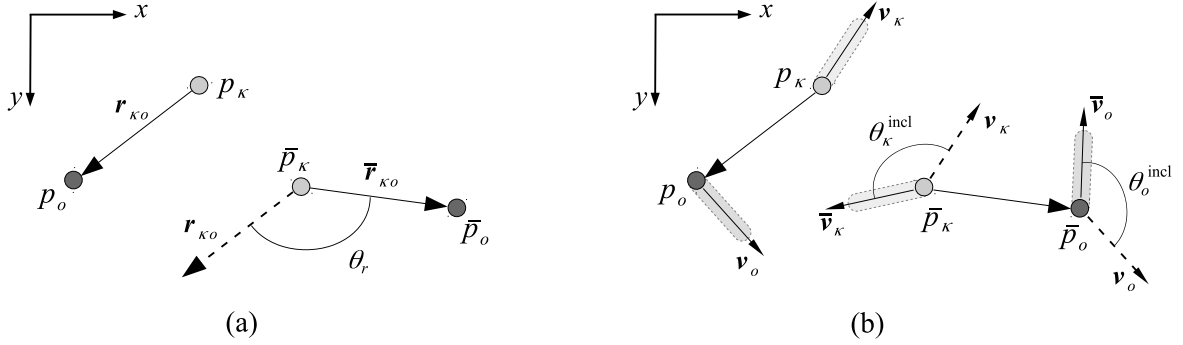


Figure 2.7: Equivalent collocation-observation pile pairs. (a) Definition of relative distances and rotation angle. (b) Additional conditions for inclined piles.

on the distances of these points to the free-surface. Taking into account this last aspect, and noting that all nodes of the same pile are located at different depths, the reuse of the influence sub-matrices is contemplated at a pile scale.

Let p_o and p_κ be the observation and collocation piles, respectively. Let $\mathbf{G}_{p_o}^{p_\kappa}$ be the sub-matrix of \mathbf{G} that corresponds to the terms of the soil equations in which the collocation is done at the nodes of pile p_κ , and the integration is done along the elements of pile p_o . Then, two pairs of collocation-observation piles $\{p_\kappa, p_o\}$ and $\{\bar{p}_\kappa, \bar{p}_o\}$ are said to be equivalent in terms of the computation of their influence sub-matrices if the following conditions are met:

1. The geometry and discretization of pile p_κ coincide with the ones of pile \bar{p}_κ , and the geometry and discretization of pile p_o coincide with the ones of pile \bar{p}_o .
2. The radial distance $|\mathbf{r}_{\kappa o}|$ between piles p_κ and p_o coincide with the radial distance $|\bar{\mathbf{r}}_{\kappa o}|$ between piles \bar{p}_κ and \bar{p}_o . The angle between the two distance vectors is denoted as θ_r , see Fig. 2.7(a).
3. For inclined piles, it is also necessary that the angle θ_κ^{incl} between the projections in the plane $x - y$ of the direction vectors of piles p_κ and \bar{p}_κ and the angle θ_o^{incl} between the ones of piles p_o and \bar{p}_o coincide with the angle θ_r , see Fig. 2.7(b).

If these conditions are satisfied, the influence sub-matrix corresponding to the pair $\{p_\kappa, p_o\}$ can be obtained from the one of the equivalent reference pair $\{\bar{p}_\kappa, \bar{p}_o\}$ as:

$$\mathbf{G}_{p_o}^{p_\kappa} = \mathbf{R}^T \mathbf{G}_{\bar{p}_o}^{\bar{p}_\kappa} \mathbf{R} \quad (2.53)$$

where the rotation matrix \mathbf{R} is a band matrix formed by the simple in-plane rotation matrix:

$$\mathbf{R}_z = \begin{bmatrix} \cos \theta_r & \sin \theta_r & 0 \\ -\sin \theta_r & \cos \theta_r & 0 \\ 0 & 0 & 1 \end{bmatrix} \quad (2.54)$$

Fig. 2.8 illustrates the different equivalent collocation-observation pile pairs corresponding to the case of a regular 3×3 pile group with identical vertical piles. Note that only six

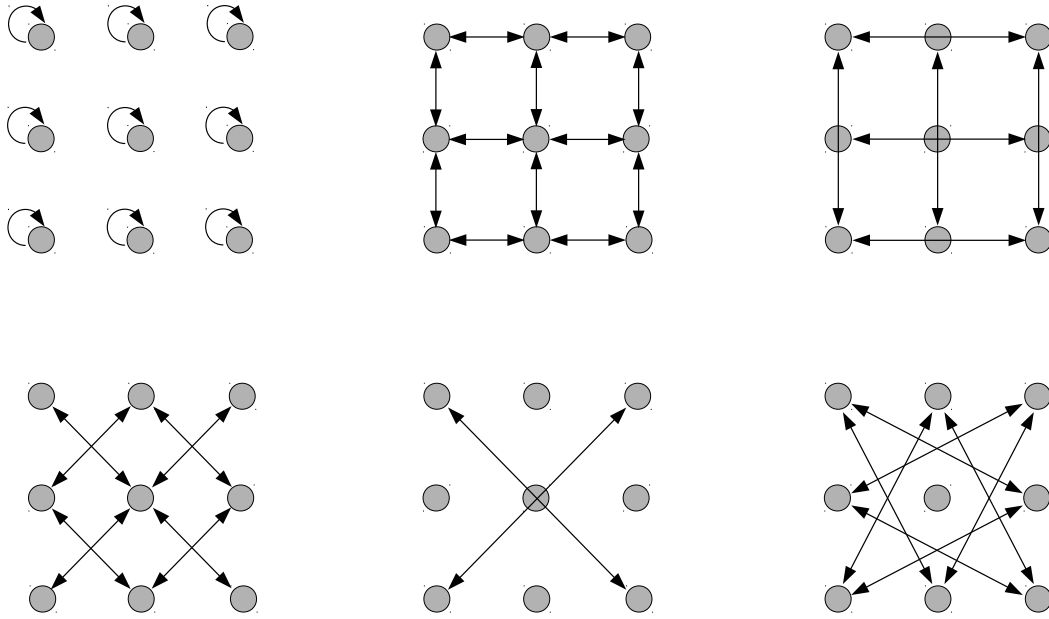


Figure 2.8: Example of equivalent collocation-observation pile pairs. 3×3 pile group with vertical piles.

Group	single	2×2	3×3	4×4	5×5	8×8	10×10	20×20
No. piles	1	4	9	16	25	64	100	400
No. possible p_k, p_o pairs	1	16	81	256	625	4096	10000	160000
No. equivalent p_k, p_o pairs	1	4	6	10	15	34	51	180

Table 2.1: Reduction in the number of collocation-integration pairs for the evaluation of the influence matrix integrals through the reuse of equivalent sub-matrices. Regular groups with vertical piles.

non-equivalent sets of p_k, p_o pairs exist within the 81 possible combinations of pile pairs in the group. In order to give a better insight into the reduction in the number of times that each different influence sub-matrix needs to be evaluated, Table 2.1 presents the number of equivalent collocation-observation pile pairs with respect to all possible pair combinations for regular square configurations of vertical piles. It can be easily found that the order of pairs is reduced from $\mathcal{O}(N^2)$ to $\mathcal{O}(N)$, being N the number of piles of the configuration. In Appendix B an example case about the savings in computational time that the proposed reuse of influence sub-matrices is presented.

2.4 Seismic excitation

The seismic excitation can be modelled as travelling wavefronts propagating through the soil that impose an incident field of displacements and stresses at each point of the half space

domain. The presence of the pile foundation originates reflection and refraction phenomena which produce an additional wave field that interacts with the original incident field. Therefore, for the analysis of the seismic excitation, the total field is assumed to be obtained as the sum of the incident field plus the scattered field [22, 66], as sketched by Fig. 2.9.

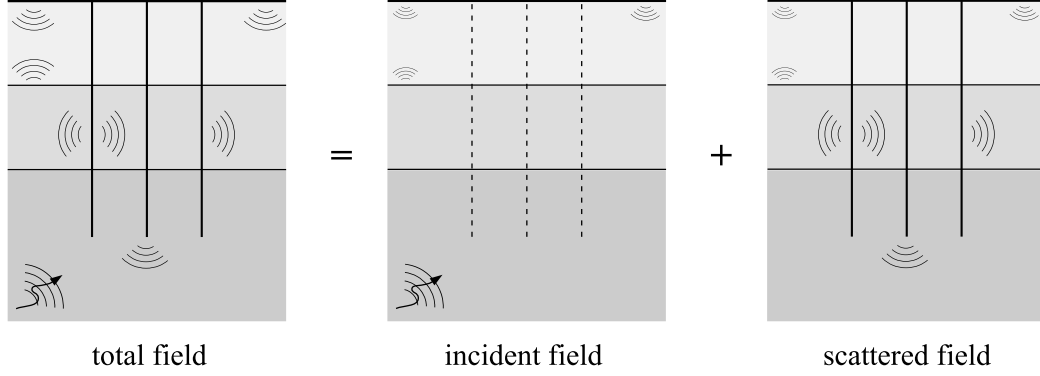


Figure 2.9: Decomposition of the total field into the incident and the scattered ones.

As mentioned before, the incident field is a displacement and stress field imposed by a wave front generated by a far source. Analytical expressions of these displacements and stresses can be obtained through the analysis of the wave propagation problems assuming different wave types. In Appendix A, the formulation of the incident field corresponding to body waves with a generic direction of propagation through the layered half space is obtained through a TRM (Transmission-Reflection Matrix) methodology.

On the other hand, the scattered field arises from the presence of the piles in the soil. The different stiffness of the piles makes them to oppose to the motion of the soil, creating an additional field of displacements and stresses that propagates from the piles to the surrounding media. Taking into account that the soil-pile interaction tractions can only be found in this scattered field, the integral equation of the soil (2.44) should be interpreted in terms of the variables of the scattered field.

$$\mathbf{u}_{\text{scattered}}^{\kappa} = \int_{\Gamma_p} \mathbf{u}^* \mathbf{q}_p^s d\Gamma_p \quad (2.55)$$

However, as the total displacement field is obtained from the superposition of the scattered and incident fields (e.g., $\mathbf{u}^{\kappa} = \mathbf{u}_{\text{scattered}}^{\kappa} + \mathbf{u}_I^{\kappa}$), this equation can be easily rewritten in order to introduce the total displacement field as:

$$\mathbf{u}^{\kappa} = \int_{\Gamma_p} \mathbf{u}^* \mathbf{q}_p^s d\Gamma_p + \mathbf{u}_I^{\kappa} \quad (2.56)$$

where \mathbf{u}_I^{κ} is the vector containing the displacements along the three directions of the space of the incident field evaluated at the collocation point κ .

This equation can be rewritten in matrix form as:

$$\mathbf{u}^{\kappa} = \mathbf{G}^{\kappa} \mathbf{q}^s + \mathbf{u}_I^{\kappa} \quad (2.57)$$

Finally, applying Eq. (2.57) to all pile nodes, the soil system of equations (2.48) including the seismic excitation results in:

$$\mathbf{u}^s = \mathbf{G}\mathbf{q}^s + \mathbf{u}_I^s \quad (2.58)$$

where \mathbf{u}_I^s is the vector containing the displacements of the incident field evaluated at all of the soil collocation points.

2.5 Excitation at the soil surface

The proposed model allows the assumption of additional loads acting over the free surface of the soil. Different load types (such as point, line and surface loads) can be considered. These forces could be used to represent different sources of excitation of the soil-pile system, such as near machines, construction operations or even the passing of vehicles.

Let \mathbf{p}_s be the load vector acting over a part Γ_s of the soil boundary Γ (free-surface). As this load vector is not zero, the contour integral of the right-side of the reciprocity theorem (2.37) does not longer vanishes, but is reduced to:

$$\int_{\Gamma} \mathbf{p}\mathbf{u}^* d\Gamma = \int_{\Gamma_s} \mathbf{p}_s \mathbf{u}^* d\Gamma_s \quad (2.59)$$

Then, the integral soil equation (2.44) including the action of external loads at the free-surface results in:

$$\mathbf{u}^k = \int_{\Gamma_p} \mathbf{u}^* \mathbf{q}_p^s d\Gamma_p + \int_{\Gamma_s} \mathbf{p}_s \mathbf{u}^* d\Gamma_s \quad (2.60)$$

In order to numerically evaluate the integral over the contour Γ_s , it is necessary to define the elements that discretize the external load. Obviously, the case of a point load is completely determined by setting the value of each one of its three components, but for the distributed loads different element types can be selected. As a first approach in this work, classical two- and four-noded elements are used to represent the line and surface loads, respectively. These elements are depicted in Fig. 2.10 and are chosen due to their simplicity and versatility to represent different configurations of loads by using a suitable amount of them. However, different line or surface elements could be employed in order to rigorously represent more

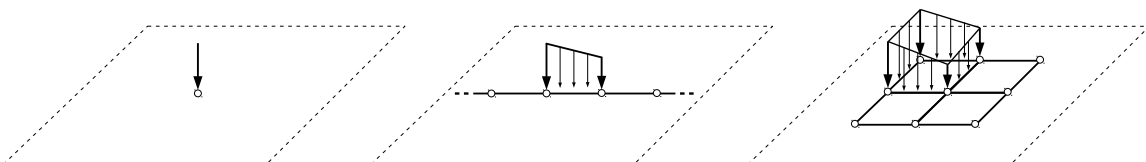


Figure 2.10: Discretization of external forces acting over the free-surface. Point (left), line (centre) and surface (right) loads. Only the vertical component is presented.



complex load shapes corresponding to specific excitation types. For this reason, in the following, the formulation is presented in general terms, without assuming any particular element type for the load discretization.

Once the external load is discretized through the corresponding elements, the previous integral equation, Eq. (2.60), can be written in matrix form as:

$$\mathbf{u}^\kappa = \mathbf{G}^\kappa \mathbf{q}^s + \mathbf{G}_s^\kappa \mathbf{p}^s \quad (2.61)$$

where \mathbf{p}^s is the vector containing the nodal values that define the external load, and \mathbf{G}_s^κ is the load influence sub-matrix corresponding to the collocation point κ that is obtained by integrating the displacement fundamental solution times the proper shape functions.

If a point load is considered, the influence sub-matrix \mathbf{G}_s^κ is directly obtained as the tensor containing the displacement fundamental solution evaluated at the point where the external force is applied:

$$\mathbf{G}_s^\kappa = \mathbf{u}^* \quad (2.62)$$

On the other hand, when a distributed load is assumed, its influence sub-matrix \mathbf{G}_s^κ is obtained through the assembly of the elemental ones $\mathbf{G}_{s_e}^\kappa$. Considering that inside each element Γ_{s_e} the external load is determined by its nodal values and general shape functions $\Phi = \{\Phi_1, \dots, \Phi_m\}$, the elemental sub-matrix is defined as:

$$\mathbf{G}_{s_e}^\kappa = \begin{bmatrix} \int_{\Gamma_{s_e}} \mathbf{u}^* \Phi_1 d\Gamma_{s_e} & \dots & \int_{\Gamma_{s_e}} \mathbf{u}^* \Phi_m d\Gamma_{s_e} \end{bmatrix} \quad (2.63)$$

where Γ_{s_e} can represent either a line or surface element depending on the load type.

Finally, applying Eq. (2.61) to all pile nodes, the soil system of equations (2.48) with the inclusion of the superficial external loads results in:

$$\mathbf{u}^s = \mathbf{G} \mathbf{q}^s + \mathbf{G}_s \mathbf{p}^s \quad (2.64)$$

2.6 Pile-soil coupling

In the previous sections, the systems of equations corresponding to the piles and the soil have been introduced independently from each other. However, in order to solve them and obtain the response of the soil-foundation system, a unique system of linear equation is required. This system of equations is obtained by imposing compatibility and equilibrium conditions in the soil-pile variables.

As welded soil-pile contact conditions are assumed, the compatibility conditions imply that the displacements at the points of the soil corresponding to the load lines \mathbf{u}^s are equal to the translations contained in the beam kinematic degrees of freedom \mathbf{u} . On the other hand, the equilibrium conditions at the soil-pile interface impose that the interaction tractions acting over the soil are equal, but with opposite sign, to the ones acting over the piles, i.e. $\mathbf{q}^s = -\mathbf{q}^p$.



	\mathbf{q}^s	\mathbf{u}	\mathbf{F}^{head}	\mathbf{U}^c
Soil Equations (2.48) / (2.58) / (2.64)				
Pile FE Equations (2.25)				
Cap Equilibrium (2.35)				
Cap Restrictions (2.33)				

Figure 2.11: Structure of the coefficient matrix \mathcal{A} .

With these considerations, Eqs. (2.25), (2.33), (2.35), (2.48), (2.58), and (2.64) can be grouped together into a system of linear equations which, in the general scenario, has the form:

$$\mathcal{A} \{ \mathbf{u}, \mathbf{q}^p, \mathbf{F}^{\text{head}}, \mathbf{F}^{\text{tip}}, \mathbf{U}^c \}^T = \mathcal{B} \quad (2.65)$$

where \mathcal{A} is the square matrix of coefficients obtained from the application of the aforementioned equations that presents the form depicted in Fig. 2.11, and \mathcal{B} is the right-hand side vector of known coefficients that contains the boundary conditions at the pile head or tip, the external forces acting over the foundation, as well as, the terms associated to the seismic excitation and loads acting over the soil surface. It is important to remark that the obtained system is written exclusively in terms of pile (and cap) variables.

2.7 Displacements at internal points of the soil

Once the model system of equations (2.65) is solved, the displacements at any point of the soil domain can be computed in a post-processing stage through the application of Eqs. (2.46), (2.57), or (2.59) (depending on the system excitation).

Assuming the case in which both a seismic excitation and an external action over the soil surface coexist, the equation that allows the computation of the displacement vector \mathbf{u}^i at an internal point i belonging to the soil domain is:

$$\mathbf{u}^i = -\mathbf{G}^i \mathbf{q}^p + \mathbf{G}_s^i \mathbf{p}^s + \mathbf{u}_I^i \quad (2.66)$$



2.8 Influence of the omitted tangential tractions

Models that take into account the actual geometry of the piles, such as BE models, can capture all interaction phenomena (i.e. interaction tractions) between the soil and the piles. On the other side, the proposed model (or the previous BE-FE model) is not able to completely capture these interaction effects. As piles are reduced to load lines, only the resultant of the tractions around the pile cross-section is considered by the simplified models, but not the effects that arise due to a local variation of these tractions.

In order to analyse the importance of the omitted tractions, different boundary conditions between the soil and the pile can be directly employed in BE models. By assuming smooth contact conditions, instead of welded contact conditions, the effects of the tangential tractions of the soil-pile interface vanish. However, this approach does not allow to identify the different components that contribute to the problem. To overcome this limitation, a Winkler model that explicitly incorporate each component involved in the problem is used. The formulation of this Winkler model is detailed in Appendix C.

For example, for seismic excitations, the spatial variability of the incident field generates tangential tractions around the soil-pile interface that produce the effect of a distributed moment over the pile shaft (see Appendix C). This kind of excitation, as deduced from the formulation presented in this chapter, cannot be captured by the proposed model.

The objective of this section is to determine which response variables are affected by the simplification of the soil-pile interaction made in the proposed model. In previous works (see, e.g. [23,28]) it has been verified that the simplified BE-FE model accurately reproduces the global response of the foundation (impedance functions, kinematic interaction factors...) that is obtained by a rigorous BE model. Thus, this section is aimed at studying the influence of the pile simplification upon more local response variables, specifically the pile kinematic bending moments and shear forces.

For this purpose, the problem of a single pile embedded in a homogeneous half space and subjected to vertically-incident shear waves is considered. The rotation of the pile head is assumed to be restrained. The pile dimensions and material properties are: diameter $d = 0.6$ m, length $L = 12$ m, Young's modulus $E_p = 30$ GPa, density $\rho_p = 2500$ kg/m³ and Poisson's ratio $\nu_p = 0.25$. The pile cross-section is assumed to be solid and no material damping is considered for the pile. On the other hand, several soil domains are studied with the following material properties: shear wave propagation velocity $c_s = 110, 250$, and 350 m/s (corresponding to pile-soil Young's modulus ratio $E_p/E_s = 50, 100$ and 500), soil density $\rho_s = 1750$ kg/m³, soil Poisson's ratio $\nu_s = 0.4$ and soil hysteretic damping ratio $\beta_s = 5\%$. The pile response is presented in terms of envelopes of maximum shear forces and bending moments which are obtained by computing the time response through the standard frequency-domain method [67]. For this purpose, one synthetic accelerogram compatible with the Type 2 response spectrum for Ground Type C [68] with a maximum acceleration equal to 0.375 g is used as excitation input.

Fig. 2.12 presents the envelopes of maximum shear forces (top row) and bending moments (bottom row) obtained for the three different pile-soil stiffness ratios. The results corresponding to the BE model (B1 and B3) are plotted with solid lines, the ones obtained by



Model	Description
B1	BE model. Smooth contact condition on the pile shaft. Free pile tip.
B3	BE model. Welded contact condition on the pile shaft and tip.
W1	Winkler model. Horizontal soil stiffness. Free pile tip.
W2	Winkler model. Horizontal and rocking soil stiffness. Free pile tip.
W3	Winkler model. Horizontal and rocking soil stiffness. m_I included. Loaded pile tip.

Table 2.2: Description of the BE and Winkler model variations used in this study.

the Winkler model (W1, W2 and W3) are shown with dashed lines, and the results of the proposed integral model are represented by red crosses. The descriptions of the different variations of the BE and Winkler models are listed in Table 2.2.

Attending to the results in terms of the envelopes of bending moments, it is found that the influence of the tangential tractions in this variable is limited. Virtually the same results are obtained for the different models, including the proposed integral one. Only some differences are seen close to the pile tip, especially for the stiff soils. For these cases, the results of the integral model are closer to the ones obtained by the BE model with smooth contact condition (B1), i.e. the one that does not include the tangential tractions.

On the other hand, a great influence of the tangential tractions on the pile maximum shear forces is found. Larger forces are obtained for the BE model that includes these tractions (B3) with respect to the one with smooth contact conditions (B1). Regarding the Winkler models, it is found that the model that does not take into account the effects of the tangential tractions (W1) produces very similar shear forces to the corresponding BE model. On the other hand, in order to match the results of the continuous model with welded contact conditions, the Winkler model must incorporate both the effects of the tangential tractions produced by the soil as reaction to the pile rotation as well as the ones produced by the action of the incident field (W3). If only the contribution of the tractions arising due to the pile rotation are considered (W2) the maximum shear forces are significantly reduced with respect to the reference ones (BE model). As expected, the envelopes of maximum shear forces obtained by the integral model coincide with the ones of the formulations that do not incorporate the effects of any tangential tractions, matching almost perfectly the results obtained by the BE model.

The main conclusion extracted from this study is that the simplification of the soil-pile interaction assumed by the proposed model is only relevant to the analysis of the pile shear forces. The developed model accurately reproduces the response of the foundation in terms of bending moments and global foundation variables. Despite the comparisons made in this section and in the cited BE-FE works, additional verification results, adapted to each particular problem, are briefly presented at the beginning of the following chapters.

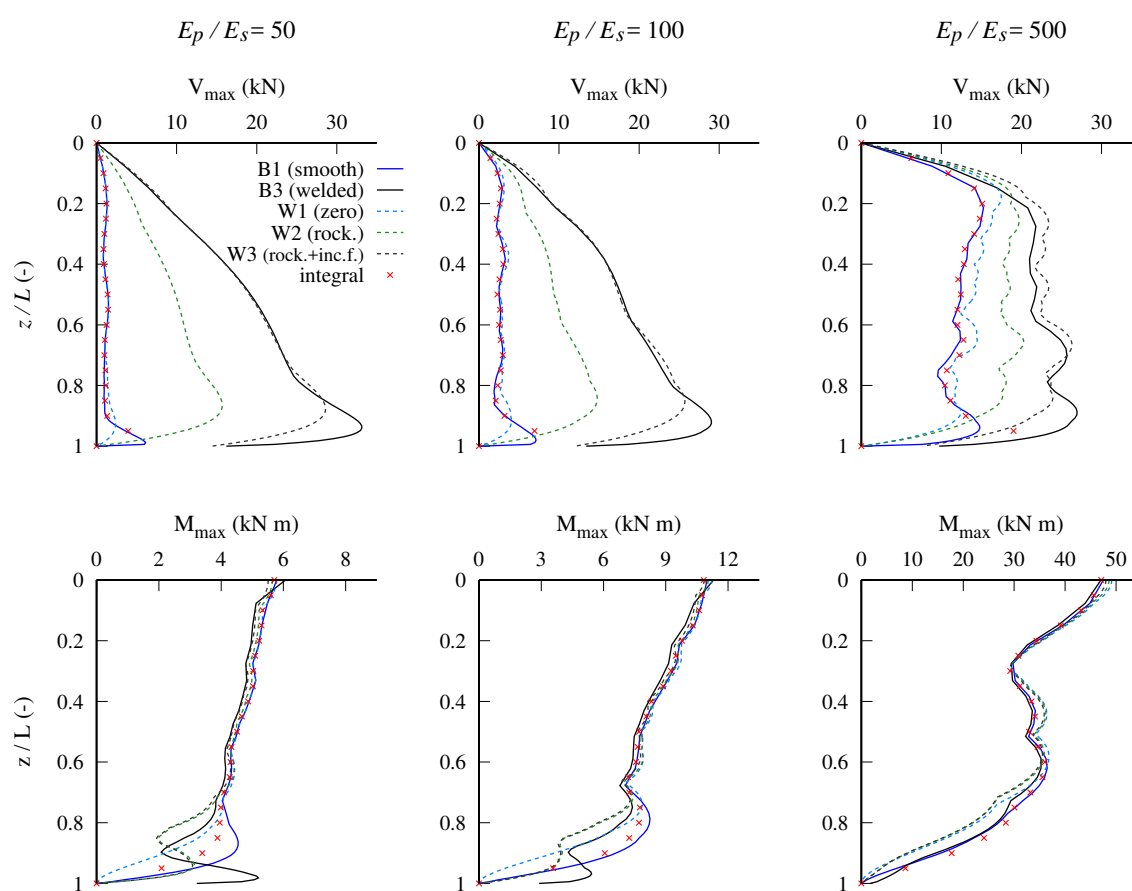
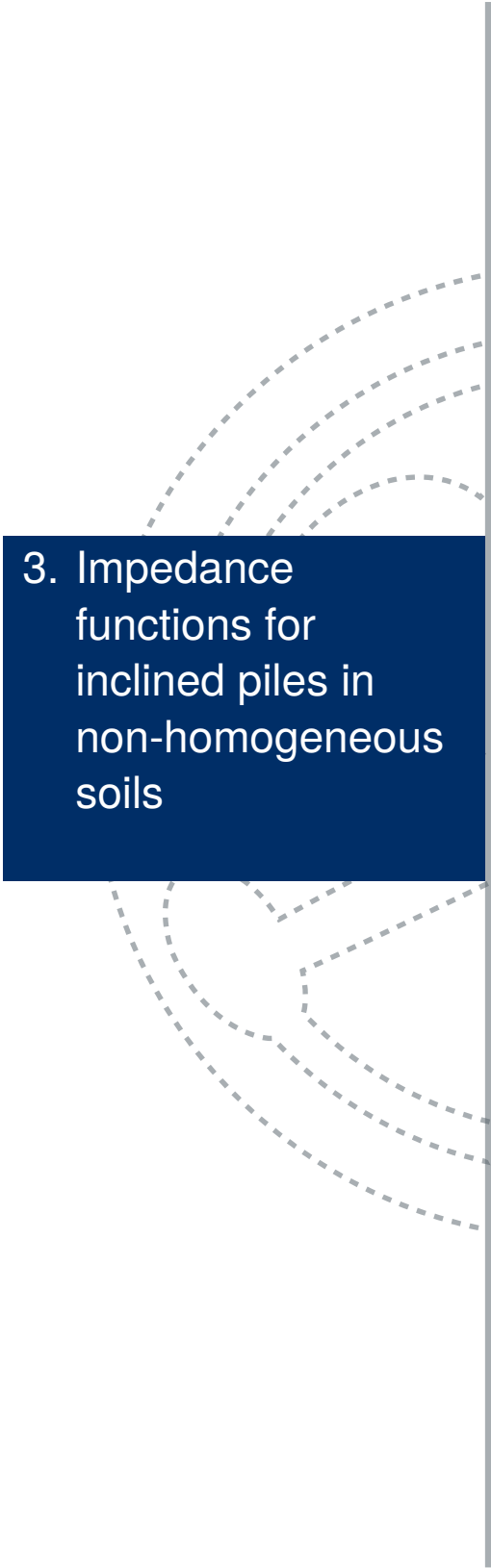


Figure 2.12: Influence of the tangential tractions on the envelopes of maximum shear forces and bending moments for a single pile under seismic excitation. Results obtained through different models and contact conditions.

A vertical grey line runs down the page. To its left, several sets of concentric dashed grey arcs are drawn, resembling wave fronts or field lines emanating from a point on the left.

3. Impedance functions for inclined piles in non-homogeneous soils

- 3.1 Introduction
- 3.2 Verification results
- 3.3 Problem definition
- 3.4 Impedance functions
- 3.5 Conclusions





3.1 Introduction

In situations where loads with great horizontal components are present inclined piles are used in combination with vertical piles to increase the foundation lateral stiffness. For the last decades, the use of inclined piles in seismic events have been strongly discouraged by several codes [68,69] due to the bad performance observed in various earthquakes during the 90's. Nevertheless, in the last years the use of inclined piles has increased again and some studies have revealed that they might have a beneficial effect not only for the foundation, but for the superstructure too [70–73]. However, further study is needed in order to achieve a better understanding of the dynamic behaviour of raked pile foundations.

Despite the fact that seismic response of inclined piles has been the object of analysis for different studies [28, 72–76], the impedance problem of this type of pile foundation has received little attention. Impedance functions for specific configurations of inclined pile groups were studied by Mamoon et al. [77] for a 3×3 pile group with a rake angle of $\theta = 15^\circ$. Padrón et al. presented a complete set of impedance functions for configurations of single piles and pile groups embedded in a homogeneous half space [23] and in a soil layer resting on a bedrock [25]. A strong dependence on the configuration and rake angle was found for the group impedances, specially in the rocking and cross horizontal-rocking ones. Model tests on a single battered pile [78] and a 2×2 group [79] in dry cohesionless soil were carried out by Goit and Saitoh. In the first study, a comparison with a FEM numerical model was made, while in the latter the effects of soil non-linearity were analysed. Carbonari et al. [80] proposed an analytical Winkler-type model for the analysis of impedance functions of inclined piles. Dezi et al. [81] introduced a numerical model for the analysis of pile foundations in layered soil deposits and presented impedance functions for 2×2 inclined pile groups embedded in a homogeneous soil deposit and in a two-layered soil deposit over a rigid bedrock.

In the aforementioned papers only homogeneous half spaces or up to two-layered soil deposits were considered. However, real soils can present properties that vary with depth and the assumption of soil homogeneity can lead to misleading predictions of the foundation behaviour in the actual profile. Up to the author's knowledge, only Giannakou et al. [82] have presented dynamic impedances for a single inclined pile in a soil profile whose properties vary continuously with depth.

For vertical pile foundations in non-homogeneous soils, the impedance problem has been studied by several authors with different methodologies. Velez et al. [83] employed a FEM formulation to obtain the lateral impedance of a single end-bearing pile in a non-homogeneous soil deposit overlaying a rigid bedrock. The results for the non-homogeneous media were compared against the ones corresponding to an 'statically equivalent' homogeneous deposit, showing that the static equivalence does not guarantee identical pile response under dynamic loads. Kaynia and Kausel [84], followed by Miura et al. [85], used a three-dimensional formulation based on Green's functions of cylindrical loads in layered semi-infinite media and presented a wide set of results for single piles and pile groups embedded in different soil profiles. Their results revealed that the horizontal impedance is more affected by near-surface soil properties than the vertical one, and that the interaction effects between the group piles are more pronounced in the non-homogeneous medium. Mylonakis and Gazetas [86,87] presented a Winkler model to solve this problem. For pile groups, the pile-soil-pile effects were

considered through interaction factors [88, 89] which relate the response of a ‘receiver’ pile to the oscillation of a near (‘source’) pile. The behaviour of the non-homogeneous media was represented by a transfer-matrix formulation [90, 91]. The same methodology has been used by other authors to handle the impedance problem in non-homogeneous media [92–94]. In their recent work, Rovithis et al. [94] studied the lateral impedance of a single pile in a soil profile with properties varying according to a power law. Their results showed that lateral damping is overestimated when using the homogeneous assumption, leading to an un-conservative evaluation of the lateral pile deflections at high frequencies. This conclusion agrees with the results obtained by Giannakou et al. [82] for a lineal-varying non-homogeneous soil with a FEM model.

In this chapter, impedance functions for single inclined piles and small pile groups with inclined elements embedded in soils whose properties vary with depth are obtained. The intention of the work presented in this chapter is to take advantage of the capabilities of the developed model to analyse the influence that the variability of the soil profile has on the stiffness of the foundation. First, the use of the proposed formulation to tackle the impedance problem is verified in Section 3.2. Then, the foundation geometry and soil profiles are defined in Section 3.3. Finally, the impedance functions for several configurations are presented in Section 3.4, followed by the main conclusion that are drawn from them in Section 3.5.

3.2 Verification results

The impedance functions (K_{ij}) are defined as the ratios between the steady-state force (or moment) applied at the pile cap and the resulting displacement (or rotation). In order to compute them, a unitary harmonic displacement (or rotation) is imposed to the group cap so the dynamic stiffness can be calculated by applying equilibrium with the forces at the pile heads. The impedance function is generally expressed through two frequency dependent coefficients representing the stiffness (k_{ij}) and damping (c_{ij}) components:

$$K_{ij} = k_{ij} + c_{ij}a_o i \quad (3.1)$$

where a_o is the dimensionless frequency corresponding to each particular case.

In this section, the ability of the proposed formulation to address the impedance problem is verified. First, results for configurations of vertical piles in non-homogeneous media are reproduced in order to verify the capability of the integral model to tackle a varying soil profile. Then, the implementation of the pile inclination is tested by comparing with previous impedance results for a foundation with battered elements.

Vertical piles in non-homogeneous media

In order to verify the ability of the presented formulation to address the impedance problem in non-homogeneous media, the results obtained for vertical elements by Miura et al. [85] of the horizontal, rocking and vertical impedances of a single vertical pile and 2×2 and 4×4 vertical pile groups in different soil types are reproduced.

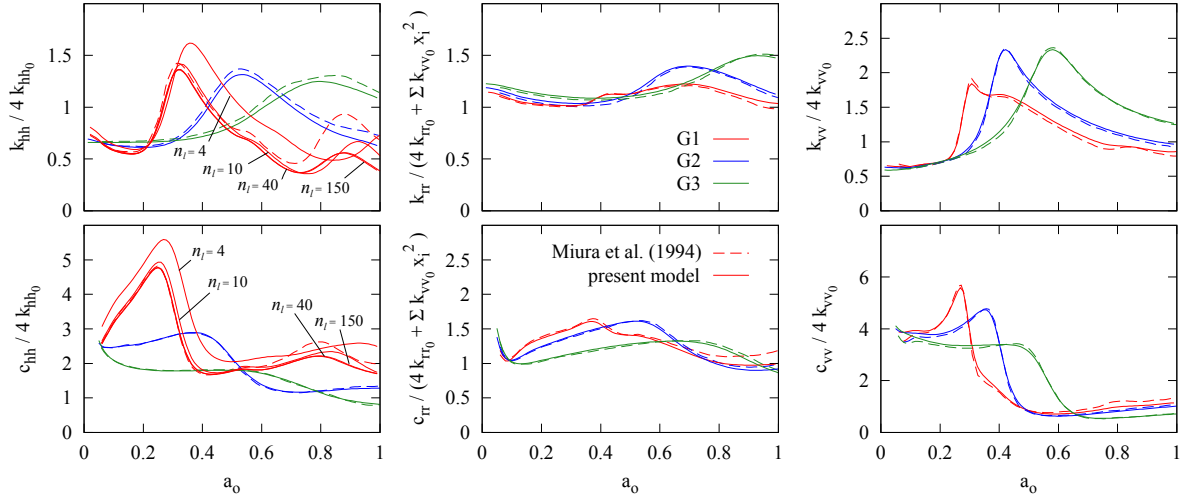


Figure 3.1: Horizontal, rocking and vertical impedances of a vertical 2×2 pile group. Comparison with the solution presented by Miura et al. [85].

The parameters that define the properties of the soil and piles are: Young's modulus ratio $E_p/E_s^L = 100$, density ratio $\rho_s/\rho_p = 0.7$, Poisson's coefficient $\nu_s = 0.4$ for the soil and $\nu_p = 0.25$ for the piles and soil damping coefficient $\beta = 0.05$. The pile group geometry is defined by: piles aspect ratio $L/d = 20$ and distance ratio between adjacent pile centres $s/d = 5$. Three soil types are used (G1, G2 and G3 following the notation used by Miura et al.): two non-homogeneous soils with a linear variation of the Young's modulus value along the pile length (following the notation presented in Section 3.3: $n = 0.5$ with a value of $b = 0.1$ for G1 and $b = 0.4$ for G2) and a homogeneous soil (G3). All soil types keep the Young's modulus value constant and equal to E_s^L below the pile tip.

For simplicity's sake, only the comparison corresponding to the 2×2 group is shown in Fig. 3.1, where the stiffness and damping coefficients are presented against the dimensionless frequency $a_0 = \omega d/c_s^L$. For the vertical and horizontal impedance problems, the coefficients are normalized by the pile static stiffness value k_{ij0} times the number of piles. A different case is the one regarding the rocking impedances, where the contribution of the vertical static stiffness times the square of the distance to the rotation axis x_i is also included for this purpose. Note that this normalization is used only in this section in order to reproduce the results of Miura et al. A good agreement between the two methods can be seen for all soil types. The largest differences take place for the soil type G1 (the one with the highest properties variation), particularly for horizontal impedances.

The problems under study consider non-homogeneous soils whose properties vary continuously with depth; while the Green's functions used by the integral model assume a finite number of zoned-homogeneous horizontal layers. Thus, the number of layers needed to model the continuously-varying soil must be assessed. Fig. 3.1 also presents the horizontal impedance functions obtained for different number of layers ($n_l = 4, 10, 40$ and 150), showing that, once a certain number of layer is reached, increasing the soil subdivision does not have any perceptible effect on the obtained results. The number of layers needed to achieve

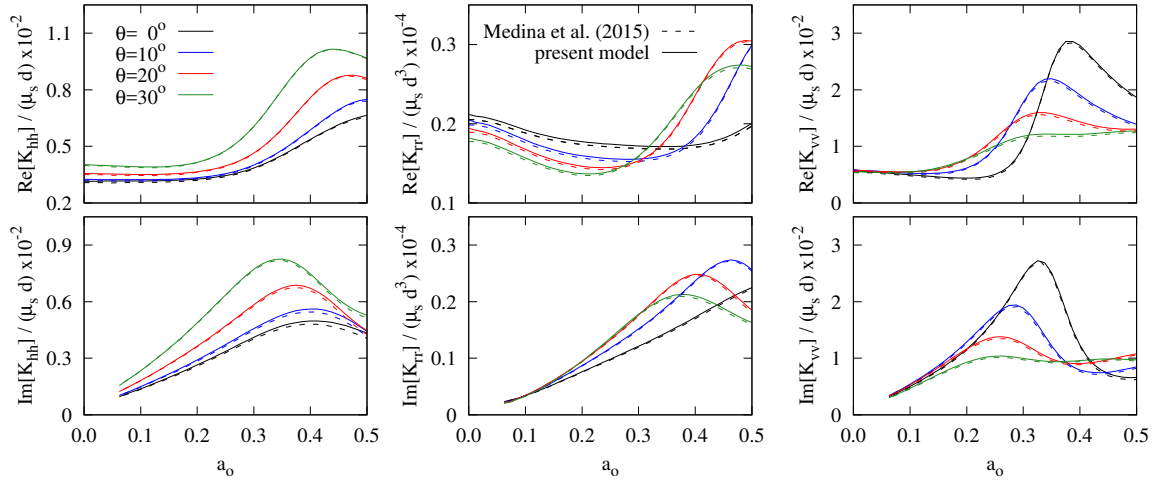


Figure 3.2: Horizontal, rocking and vertical impedances of 2×2 pile group with piles inclined in the direction of the horizontal excitation. Comparison with the solution presented by Medina et al. [30].

convergence depends on soil type, frequency range and problem type. In general, capturing adequately the impedance functions that involve horizontal components (i.e. horizontal, torsional and horizontal-rocking coupling ones) requires a larger number of layers: e.g. 30 layers were needed for the accurate computation of these impedances versus the 10 layers needed for the vertical and rocking problems.

Inclined piles in homogeneous media

On the other hand, in order to verify the implementation in case of the inclined piles, the impedance functions of a 2×2 pile group with inclined members presented by Medina et al. [30] are reproduced in Fig. 3.2, where the real and imaginary parts of the normalized impedances functions are plotted against the dimensionless frequency $a_0 = \omega d/c_s$. The curves correspond to a foundation with $L/d = 15$ and $s/d = 7.5$ with the piles inclined θ degrees with respect to the vertical axis in the direction of the horizontal excitation. Pile-soil Young's modulus $E_p/E_s = 1000$ and density $\rho_s/\rho_p = 0.7$ ratios, soil $\nu_s = 0.4$ and pile $\nu_p = 0.25$ Poisson's ratios and soil hysteretic damping coefficient $\beta = 0.05$ are assumed. The results obtained by the proposed formulation agree very well with the ones obtained by Medina et al. using the previous BE-FE model.

3.3 Problem definition

The problem studied in this chapter is sketched in Fig. 3.3. The foundations consist of one or more piles of equal length L , diameter d and material properties. In the group configurations,



the space between two adjacent pile centres at cap level is defined by s . The rake angle θ measures the angle between the pile axis and the vertical.

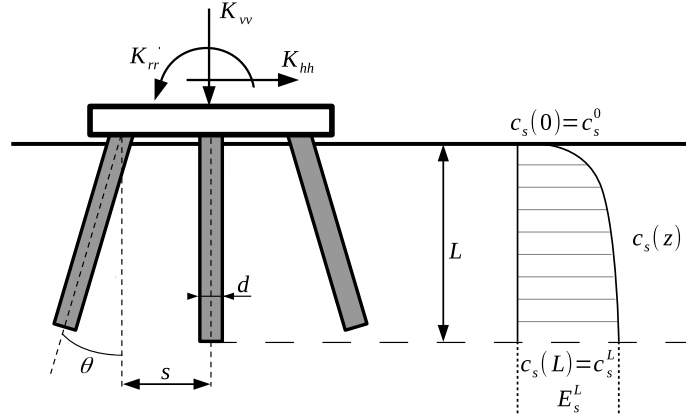


Figure 3.3: Sketch of the impedance problem.

The configurations studied correspond to the following properties: hysteretic damping coefficients $\beta_s = 0.05$ for soil and $\beta_p = 0$ for piles; Poisson's ratios $\nu_s = 0.4$ for soil and $\nu_p = 0.25$ for piles; soil-pile density ratio $\rho_s/\rho_p = 0.7$ and pile aspect ratio $L/d = 15$. Two values of pile-soil modulus ratio $E_p/E_s^L = 10^3$ and 10^2 are studied in order to represent soft and stiff soils.

Results for the rake angles $\theta = 0^\circ, 10^\circ, 20^\circ$ and 30° are presented. The pile orientation can be parallel or perpendicular to the direction of excitation or along the cap diagonal (as indicated in each figure). For pile groups, separations between piles of $s/d = 5$ and 10 are considered.

Soil profiles

The soil profile is modelled as a viscoelastic unbounded region with constant density ρ_s , constant Poisson's ratio ν_s , constant hysteretic damping coefficient β_s and a varying shear wave velocity that increases continuously with depth along the pile length following the generalized power law function [95]:

$$c_s(z) = c_s^r \left(b + q \frac{z}{z^r} \right)^n \quad (3.2)$$

where b, q, n are dimensionless parameters that determine the soil non-homogeneity and z^r, c_s^r are the depth and shear wave velocity at the reference point. In the present study, the reference point is located at the pile tip ($z^r = L$) as assumed by several authors when treating non-homogeneity (e.g., [84,85,94]). However, some other researchers (e.g., [82,83]) consider the reference point at a depth equal to the pile diameter ($z^r = d$). These assumptions are equally valid but have to be carefully considered when comparing results.



Following Rovithis et al. [95], the general expression (3.2) can be rewritten in order to include the shear wave velocity at the surface (c_s^0) as:

$$c_s(z) = c_s^L \left[b + (1 - b) \frac{z}{L} \right]^n \quad \text{with} \quad b = \left(\frac{c_s^0}{c_s^L} \right)^{1/n} \quad (3.3)$$

Using this expression, the soil profile depends upon two parameters: the ratio between the shear wave velocity at the surface and at the pile tip (c_s^0/c_s^L) and the non-homogeneity factor n . This factor is usually considered between 0 and 1, resulting in a homogeneous media when $n \rightarrow 0$ and in a linear variation of the shear velocity when $n \rightarrow 1$.

The shear wave velocity is kept constant for depths below the pile tip. As the soil density and Poisson's ratio are kept constant for the whole half space, the profile can be also expressed in terms of the soil Young's modulus as:

$$E_s(z) = \begin{cases} E_s^L \left[b + (1 - b) \frac{z}{L} \right]^{2n} & \text{if } 0 \leq z \leq L \\ E_s^L & \text{if } z > L \end{cases} \quad (3.4)$$

where E_s^L corresponds to the soil Young's modulus at the reference point (i.e. the pile tip). Note that for a non-homogeneity factor $n = 0.5$, a linear variation with depth of the soil Young's modulus is obtained (Gibson soil).

In order to study a wide set of non-homogeneous media, four values of the ratio between shear wave velocity at surface and pile tip ($c_s^0/c_s^L = 0.7, 0.5, 0.25$ and 0.1) are combined with three values of the non-homogeneity factor ($n = 0.3, 0.5$ and 0.9) resulting in 12 different soil profiles. In addition, impedances for the homogeneous soil are also computed so they can be used as reference values.

As the number of soil profiles is relatively large, and some of them yield similar results, four representative soils are chosen after having computed and compared all impedance functions. For this purpose, soil profiles that present similar impedance curves are grouped together, and the representative profile is selected as the closest to the group mean value. For this clustering process all of the pile configurations introduced before are considered. Fig. 3.4 shows the final soil clusters and their respective representative profiles (black solid lines). The variation of the shear wave velocity along the pile length is presented. The soil groups are arranged from left to right in ascending order of non-homogeneity.

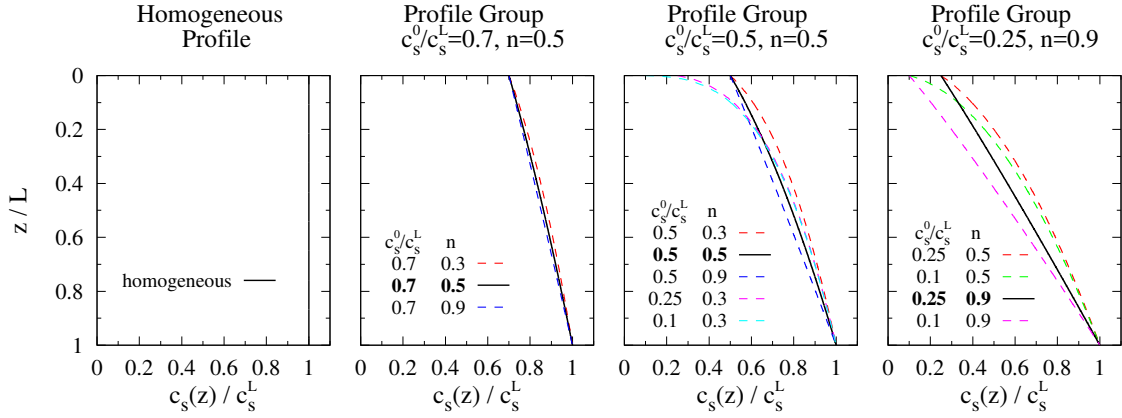


Figure 3.4: Soil profiles in terms of shear wave velocity. Each subplot presents all profiles yielding very similar impedance functions for the considered pile configurations. The profile chosen as representative in each case is shown in black solid line.

3.4 Impedance functions

In the following, normalized horizontal $K_{hh}/\bar{E}_s d$, rocking $K_{rr}/\bar{E}_s d^3$, vertical $K_{vv}/\bar{E}_s d$, torsional $K_{tt}/\bar{E}_s d^3$ and horizontal-rocking coupling $K_{hr}/\bar{E}_s d^2$ impedance functions are presented as functions of the dimensionless frequency $\bar{\omega}_o = \omega d/\bar{c}_s$. The mean shear wave velocity along the pile length \bar{c}_s is used in order to handle the depth-varying profiles:

$$\bar{c}_s = \frac{1}{L} \int_0^L c_s(z) dz \quad (3.5)$$

In coherence with the normalization of the frequency, the mean value of the soil Young's modulus along the pile length \bar{E}_s is used to obtain a dimensionless expression of the impedance functions:

$$\bar{E}_s = \frac{1}{L} \int_0^L E_s(z) dz \quad (3.6)$$

In order to clarify the analysis, only a few of the obtained results are displayed along this chapter. Thus, from the configurations defined in Section 3.3, only impedance functions for single inclined piles and 3×3 inclined pile groups oriented both parallel and perpendicular to the horizontal component with a separation distance of $s/d = 5$ are presented for the representative soil profiles defined before. The 3×3 group is selected as its results clearly illustrate the effects of the soil non-homogeneity on the dynamic impedances of the pile groups. On the other hand, the case with inclination along the cap diagonal is omitted as its results can be extrapolated from the results corresponding to the two configurations shown.

3.4.1 Inclined single pile impedance functions

Fig. 3.5 presents the impedance functions for a single pile inclined in the direction of the horizontal excitation. Note that for the rocking and horizontal-rocking cross impedances only

the curves corresponding to vertical piles are presented as they are virtually insensitive to the rake angle.

The definition of the dimensionless frequency in terms of the mean shear wave velocity causes that the curves of the different soil profiles present similar evolutions with frequency, only scaling its value depending on the profile. For the horizontal impedance term, lower stiffness values are found as the soil non-homogeneity (as defined above) increases. The opposite effect is seen for the vertical, rocking and coupled terms, for which the normalized stiffness is higher for the non-homogeneous profiles.

The damping coefficients, on the other hand, present slightly smaller values as the soil non-homogeneity increases. This imply that, for non-homogeneous soils, the damping term is lower than the one corresponding to the homogeneous assumption, agreeing with the findings of previous works [82, 94]. This effect is manifested for all the angles of inclination. The only exception is found for the rocking and cross horizontal-rocking impedance functions, for which the damping component strongly increases depending on the soil non-homogeneity in the same sense as the stiffness term.

Regarding the effects of the rake angle: the horizontal impedance increases as the pile inclination augments due to the participation of the pile axial stiffness. This also explains why the vertical impedance decreases as the rake angle augments. This coupling between the horizontal and vertical components produces a horizontal-vertical cross impedance term arising for inclined piles. Contrary to what is found for the rest of impedance terms, the evolution with the frequency of the stiffness component of the vertical and horizontal-vertical cross impedances follows different trends depending on the soil stiffness: for soft soils ($E_p/E_s^L = 1000$), a reduction of the stiffness is seen as the frequency increases; while for stiff soils ($E_p/E_s^L = 100$), those stiffness terms augment continuously with this parameter.

3.4.2 Inclined 3 × 3 pile group impedance functions

Figs. 3.6 to 3.10 show the normalized impedance functions for the 3×3 pile groups with inclined elements for the studied soil profile sets. In general, the effects of the soil profile are the same for all of the group impedance functions: an average reduction in the stiffness and damping components and an increase in their dependence on the frequency as the soil non-homogeneity increases. These trends are the same for the curves corresponding to stiff (dashed lines) and soft soil configurations (solid lines).

The peaks on the impedances curves, produced due to resonance in the interaction between near piles, take place at smaller frequencies as the soil non-homogeneity increases. This effect make sense considering that if the wave velocity is reduced in the upper layers, the frequency at which resonance takes place should be reduced too. This effect is magnified with the increase in the rake angle as the distance between piles augments and, consequently, the frequency must be further reduced. Related to this effect, sharper peaks in the damping component at these frequencies can be seen as the non-homogeneity increases. This behaviour produces large differences at high frequencies between the damping component of the homogeneous media and the ones corresponding to the non-homogeneous profiles, even when a mean shear velocity is used for the definition of the dimensionless frequency.

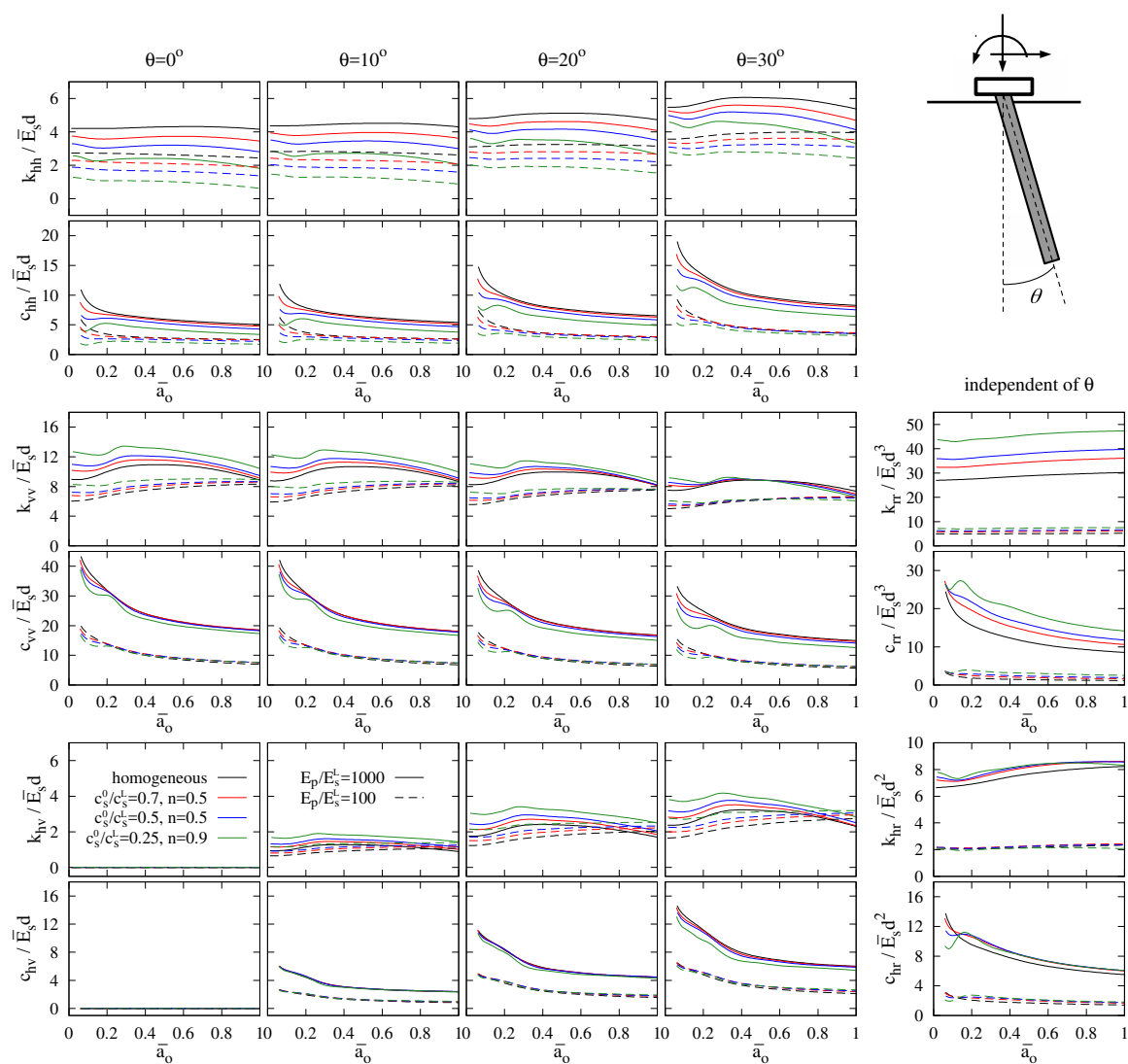


Figure 3.5: Impedance functions for a single inclined pile in different non-homogeneous media

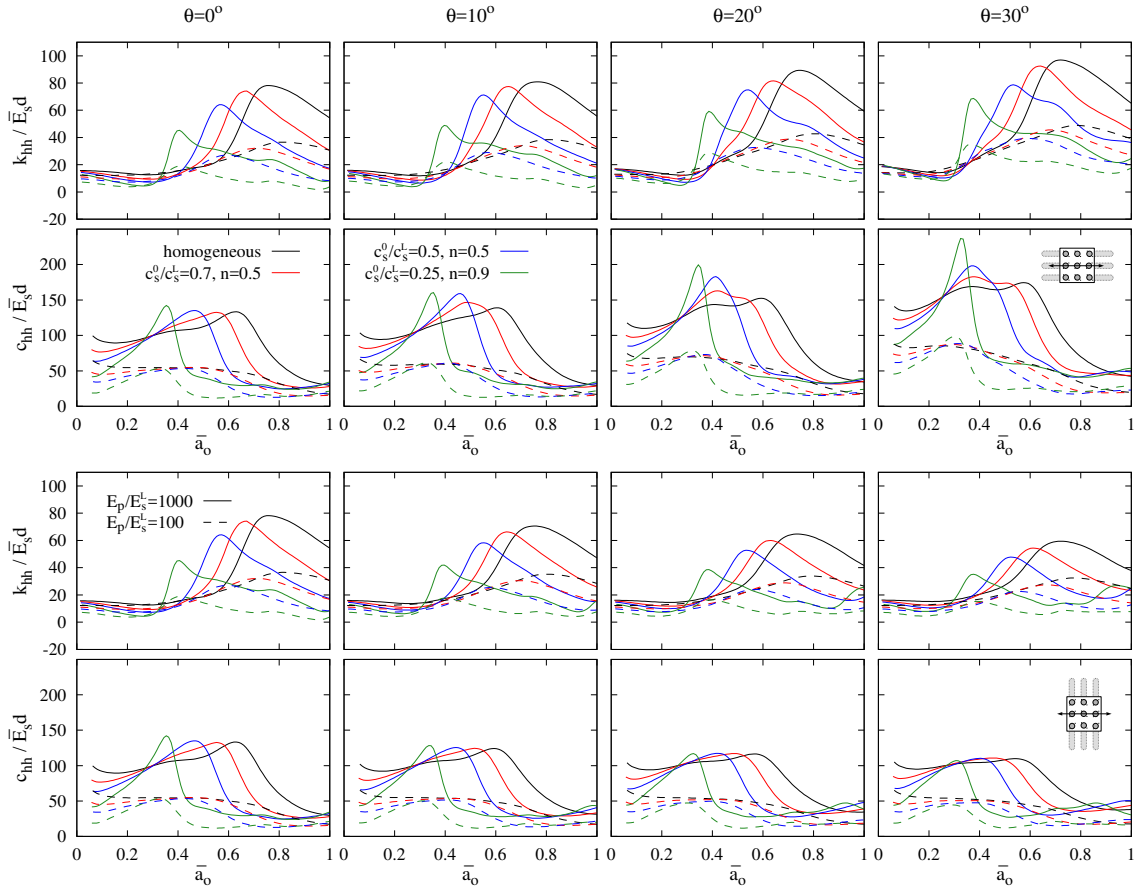


Figure 3.6: Horizontal impedance functions for a 3×3 group in different non-homogeneous media

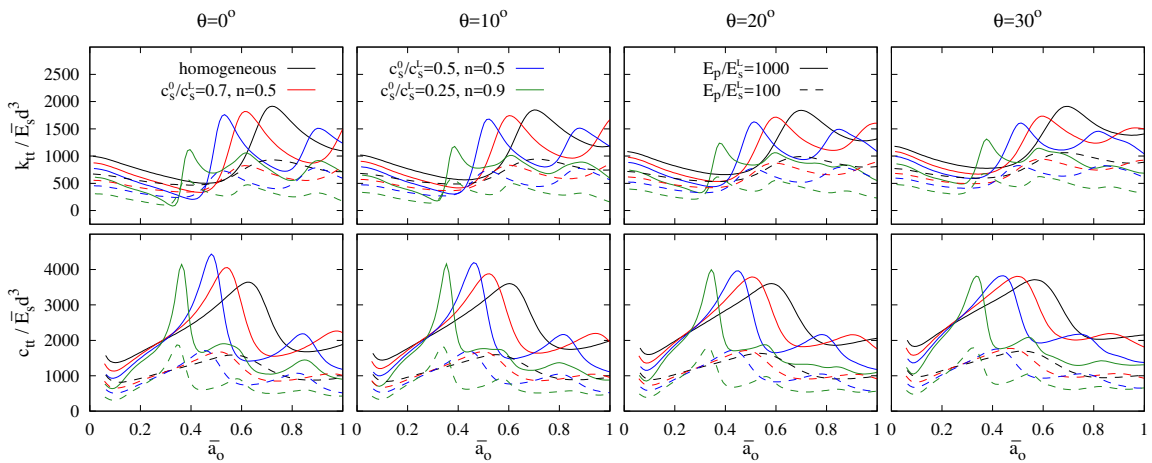


Figure 3.7: Torsional impedance functions for a 3×3 group in different non-homogeneous media

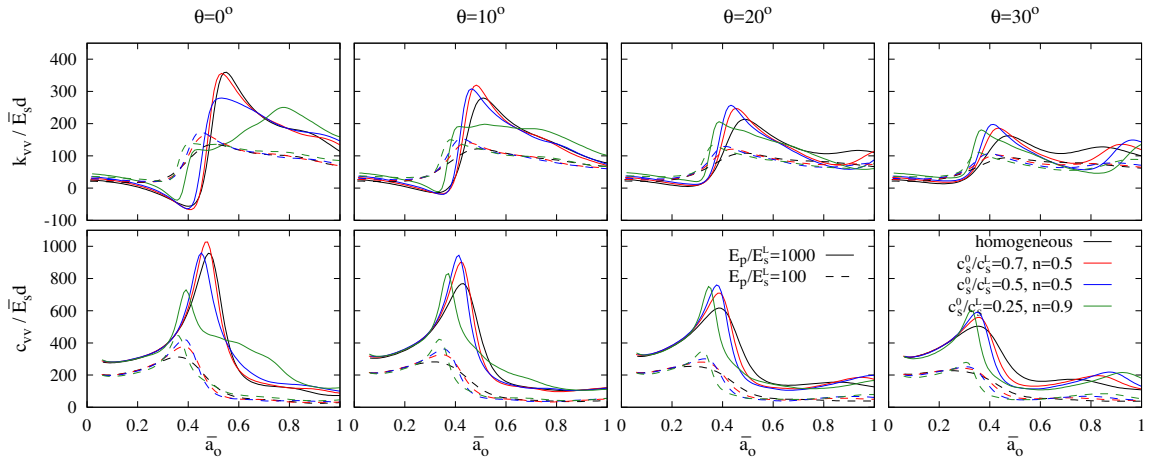


Figure 3.8: Vertical impedance functions for a 3×3 group in different non-homogeneous media

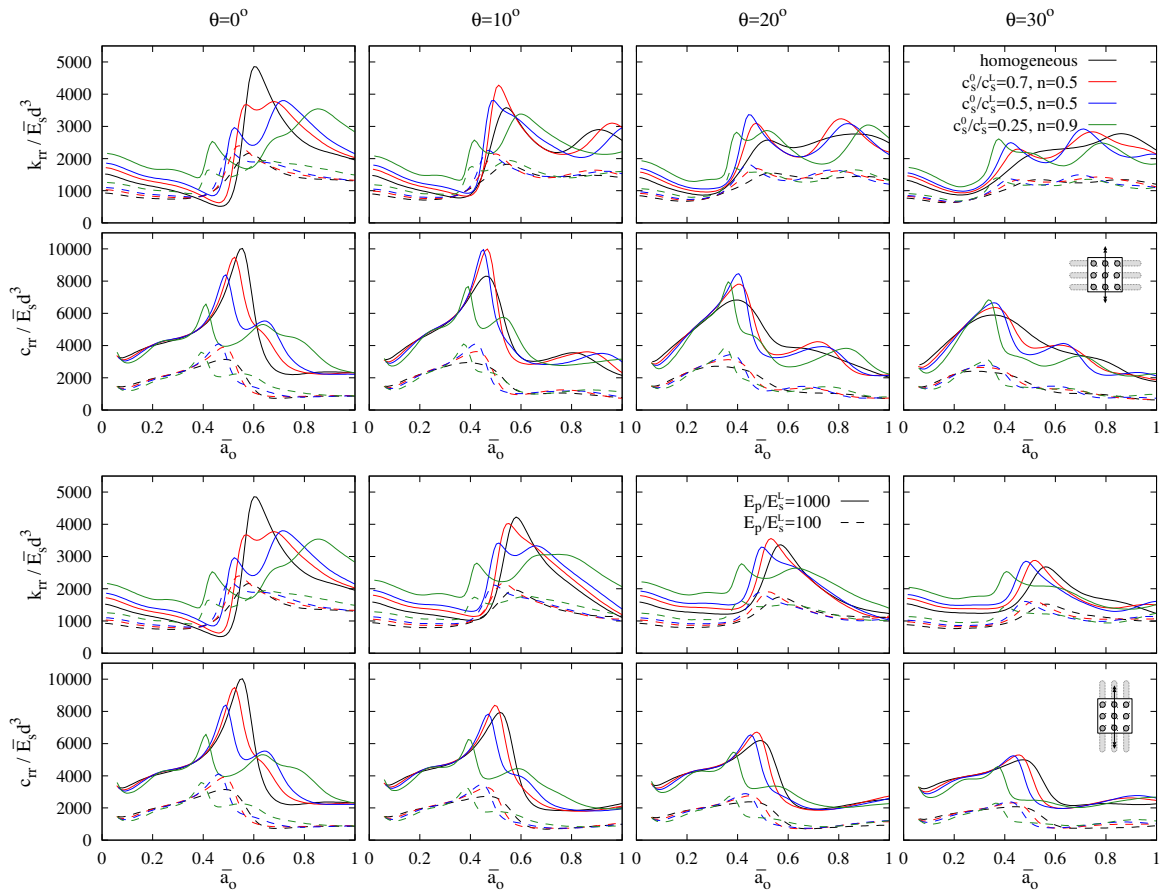


Figure 3.9: Rocking impedance functions for a 3×3 group in different non-homogeneous media

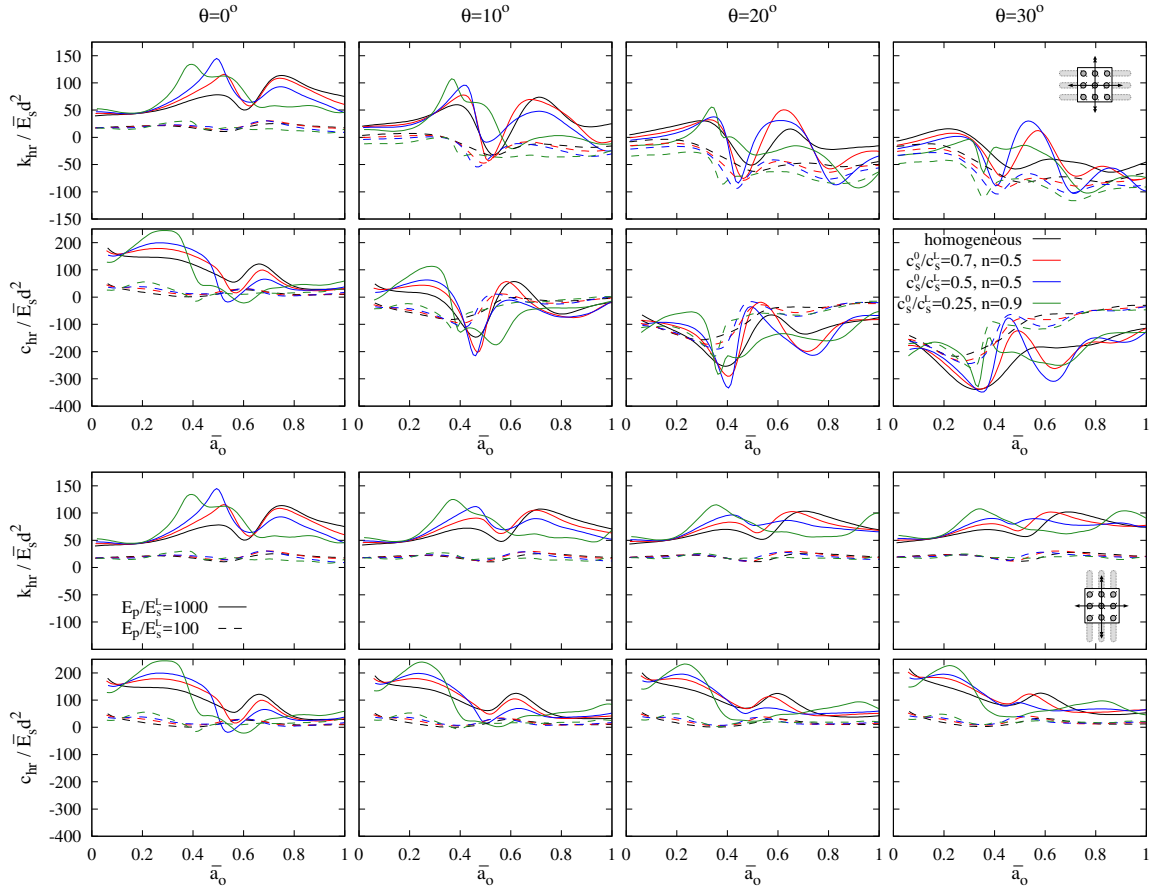


Figure 3.10: Horizontal-rocking coupling impedance functions for a 3×3 group in different non-homogeneous media

However, the magnitude of the shift in the frequency at which those peaks appear is much larger for horizontal (Fig. 3.6) impedances than for the vertical (Fig. 3.8) modes, for which the peaks take place almost at the same dimensionless frequency regardless of the soil profile. Following [85], this can be explained assuming that the horizontal impedance is more affected by the superficial properties than the vertical one, which present a higher contribution of deeper soil properties.

Similar behaviour, in terms of frequencies at which the peaks are produced and the effects of the soil non-homogeneity, is seen between the vertical (Fig. 3.8) and rocking (Fig. 3.9) curves owing to the contribution of the former in the latter. This also happens between the horizontal (Fig. 3.6) and torsional (Fig. 3.7) impedance functions. In all of the mentioned curves, as the rake angle and the soil non-homogeneity increase, the interaction between distant piles becomes more important producing that new peaks arise.

Attending to the horizontal impedance curves (Fig. 3.6), different effects are seen depending on the direction of the pile inclination. When the piles are inclined perpendicular to the horizontal excitation, the stiffness and damping components slightly decrease with respect to the vertical pile configuration. On the other hand, if the piles are inclined parallel to



the excitation, an increment in the impedance functions is found as the rake angle augments. Furthermore, the inclination of the piles parallel to the horizontal excitation intensifies the differences in the curve shapes between the studied profiles. Thus, the variability in the damping functions is highest for $\theta = 30^\circ$. Contrary to what happened for the single pile impedances, the soil profiles with depth-varying properties produce similar or even higher values of the maximum damping coefficient; while their stiffness component is significantly lower when compared to the homogeneous profile. Thus, for pile groups, the homogeneous assumption does not imply higher damping-stiffness ratios. This effect can also be seen for the torsional impedance functions, but not for the rest of terms. Noteworthy is the fact that these conclusions are obtained based on the normalization used: if the values of \bar{E}_s and \bar{c}_s used to normalize the frequency and the impedance components change, the stiffness component will vary in a greater extent than the damping one due to its definition (Eq. 3.1).

Fig. 3.8 shows that, with the normalization employed, the vertical impedance functions for the homogeneous and $n = 0.5$ soil profiles are very close to each other, although their maxima do not appear at exactly the same dimensionless frequency. Both stiffness and damping functions for the most non-homogeneous profile ($n = 0.9$) converge to the results for the rest of profiles only for large rake angles ($\theta \geq 20^\circ$).

Owing to the great contribution of the vertical component to the rocking impedance functions, the effects of the normalization on the similarity of the curves described in the previous paragraph can also be seen in Fig. 3.9. However, these effects are manifested in a lower extent than for the vertical impedance curves. The rocking impedance curves strongly depend on the soil profile, presenting more peaks as the soil non-homogeneity increases. This influence of the soil profile is stronger for piles with lower angles of inclination. Contrary to what was found for the horizontal impedance functions, an increase in the rake angle always produces a reduction in the rocking impedance value regardless of the direction of inclination. However, different curves are obtained depending on whether the piles are inclined parallel or perpendicular to the horizontal motion direction.

Regarding the cross horizontal-rocking component (Fig. 3.10), again different situations are seen depending on the direction of pile inclination. If the piles are inclined perpendicular to the excitation (bottom figures), the rake angle has virtually no influence on this impedance component. On the contrary, if the pile inclination is parallel to the excitation direction (top figures), the magnitude of the impedance values and its sign change as the angle increases, going from positive values for vertical piles to negative ones for higher inclination angles. This effect is produced for all the studied profiles.

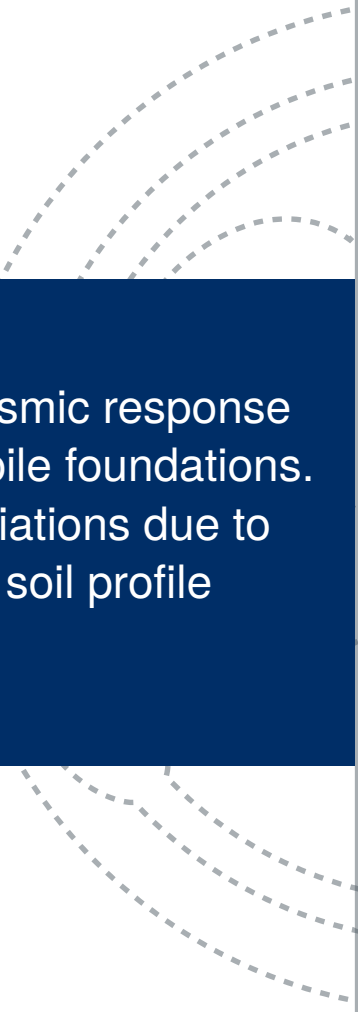
3.5 Conclusions

In this chapter, the proposed integral model is used for the analysis of the impedance functions for foundations with inclined piles in non-homogeneous media. For studying the influence of the soil profile on the foundation response, configurations of single piles and 2×2 and 3×3 pile groups with inclined elements embedded in different soil profiles whose shear wave velocity varies along the pile length following a generalized power law are considered. Attending to the computed results, three soils profiles are selected as representative of the



twelve studied media and their corresponding impedance functions are compared with the ones of the homogeneous soil. From the analysis of these results the following conclusions are drawn:

- The impedance functions are found to strongly depend on the soil profile, which highlights the importance of estimating the ground real profile and the need of using it to accurately analyse the dynamic response of the foundation.
- Evidently, the magnitude of the stiffness functions tends to decrease when the mean shear wave velocity of the soil profile decreases, with the exception of the vertical mode, for which normalized impedance functions are largely independent of the soil profile, in the cases studied herein.
- The damping functions present, in general, the same behaviour than the stiffness functions.
- The magnitude of the stiffness function peaks and the frequencies at which they appear, decrease significantly when the non-homogeneity of the soil increases, with the exception, again, of the vertical mode.
- The magnitude of the differences among the results corresponding to the different profiles diminishes for large pile rake angles.
- The equivalent homogeneous assumption can lead to impedance values that are significantly away from the ones that correspond to the actual soil profile depending on the frequency range of interest.



4. Seismic response of pile foundations. Variations due to the soil profile

- 4.1 Introduction
- 4.2 Verification results
- 4.3 Problem definition
- 4.4 Foundation kinematic interaction factors
- 4.5 Structural maximum accelerations
- 4.6 Influence of the pile head condition on the foundation seismic input factors
- 4.7 Pile kinematic bending moments
- 4.8 Conclusions





4.1 Introduction

The seismic response of pile foundations is a demanding object of study within the soil-structure interaction field. Depending on the focus of the study, the seismic response of the foundation can be measured in terms of: 1. the kinematic interaction factors of the foundation, or 2. the kinematic internal forces of the piles.

Regarding the study of kinematic interaction factors, numerous research works have tackled this problem during the last decades [96–100]. These factors represent how the foundation filters the seismic motion of the soil and are generally used as part of substructuring methodologies (see e.g. [26]) in order to study the structural response.

Different studies have analysed the influence of different variables on the kinematic interaction factors of pile foundations. Mamoon and co-workers [101, 102], followed by Kaynia and Novak [103] and Makris and Badoni [104], highlighted the importance of the wave type and its direction of propagation when computing the foundation seismic motion. More recent works [28, 74] presented kinematic interaction factors for configurations with battered elements, showing the influence of the pile rake angle on the foundation response.

However, the effects of the variability of the soil profile on the kinematic interaction factors of pile foundations demand more study, specially for the case of pile group configurations. Up to the author's knowledge, only in the work of Rovithis et al. [94], the interaction factors for a single pile embedded in different soils with depth-varying properties were thoroughly analysed based on a Beam-on-dynamic-Winkler approach. Previous to his work, a brief overview of the higher filtering effects of non-homogeneous soils was also presented by Kaynia and Kausel [84] for the particular cases of a single pile and a 3×3 pile group in a linearly-variable profile.

Regarding the pile seismic internal forces and based on field evidences and experimental tests [105–108], it has been concluded that those kinematic forces can be as significant as the ones produced by the vibration of the supported structure (inertial forces) in the pile failure. The influence of the soil profile on the behaviour of the pile kinematic bending moments have received great attention during the last years. Particularly, numerous research works [109–118] have studied the critical bending moments that arise at the interface between two soil layers with sharply differing stiffness. Some of these works [113–117] facilitate design-orientated expressions to estimate these maximum kinematic bending moments, as well as the ones produced atop of the piles with a head-rotation restrain. Dezi and Poulos [118] also proposed correction factors that can be used for including group effects in those expressions. Regarding soils presenting a continuous non-homogeneity, few documents are available in the literature. Di Laora and Rovithis [119] studied the kinematic bending of a single pile embedded in various continuously non-homogeneous soils through a Winkler approach.

In order to contribute to the scope of continuously non-homogeneous media, the effects of the variability of the soil profile on the seismic response of pile foundations are analysed in this chapter. First, Section 4.2 presents complementary results that verify the applicability of the developed model to reproduce the seismic response of pile foundations in non-homogeneous media. After the verification process, the problem under study is defined in Section 4.3. Then, the effects of the variability of the soil profile on the foundation kinematic response are analysed in Section 4.4; while Section 4.5 extends how these results affect the

supported structure maximum response. Section 4.6 studies how the kinematic response of the foundation both in homogeneous and non-homogeneous media is influenced by the pile head conditions. Finally, in Section 4.7 the use of equivalent homogeneous properties to estimate the maximum kinematic bending moments of pile foundations embedded in variable soil profiles is discussed. At the end of the chapter, the main conclusions drawn from these studies are listed in Section 4.8.

4.2 Verification results

The capability of the proposed formulation to estimate the internal forces of a pile subjected to a seismic excitation was discussed in Section 2.8. It was found that, due to the omission of the tangential tractions in the integral formulation, the shear forces of the pile cannot be completely reproduced as the contributions of both the distributed moment produced by the action of the incident field and the one produced as reaction of the surrounding soil against the pile rotation are neglected. On the other hand, the seismic bending moments of the pile are accurately estimated by the proposed model due to the small influence of those tangential tractions on them.

In order to complete the verification of the proposed formulation for the seismic problem, and to check its ability to reproduce the seismic response of the foundation in terms of displacements, the results presented by Kaynia and Kausel [84] are reproduced in this section. The methodology employed by those authors was based on the use of Green's functions of cylindrical loads in a layered media obtained through a layer stiffness approach [91].

The problem under study consists of a single pile or a 3×3 pile group embedded in two different soils: a homogeneous viscoelastic half space ($E_p/E_s = 100$) and a semi-infinite medium in which the elastic modulus linearly increases from zero at the ground surface level to $E_p/E_s = 100$ at a depth equal to the pile length and remains constant for the underlying half space. The rest of the soil properties, which are assumed to be the same for the two profiles, are: soil-pile density ratio $\rho_s/\rho_p = 0.7$, soil hysteretic damping ratio $\beta_s = 5\%$ and soil Poisson's ratio $\nu_s = 0.4$. On the other side, the pile properties are: pile hysteretic damping ratio $\beta_p = 0\%$, pile Poisson's ratio $\nu_p = 0.25$, pile aspect ratio $L/d = 20$ and, for the group configuration, centre-to-centre pile separation distance $s/d = 5$. The excitation of the system corresponds to vertically-incident S-waves.

Fig 4.1 shows the absolute value of the ratio between the foundation lateral displacement (u) and the free-field displacement (u_{ff}) as function of the dimensionless frequency $a_o = \omega d/c_s$, being c_s the shear wave velocity in the soil (for the non-homogeneous profile, the value corresponding at the pile tip level is assumed). The results of the integral model (solid lines) are compared with the ones presented by Kaynia and Kausel (points), while the different colours distinguish the two soil profiles. A good agreement is found between the two different methodologies for both the homogeneous and variable soil media and the two pile configurations. Note that in order to accurately reproduce the behaviour of the non-homogeneous profile with the proposed formulation, a high enough number of piecewise homogeneous layers is required. After a convergence analysis, 160 layers were used in order to obtain the presented results.

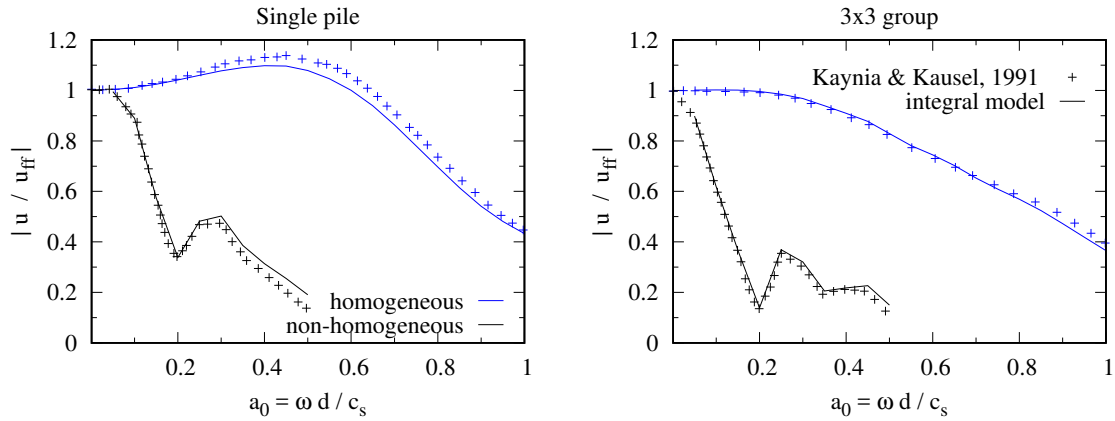


Figure 4.1: Lateral displacements of the foundation for different soil profiles. Comparison with Kaynia and Kausel [84].

4.3 Problem definition

The problem addressed in this chapter consists in a vertical pile foundation subjected to a vertically incident S-wave front. Special attention is given to the influence of considering the actual variability of the soil profile by comparing with an equivalent homogeneous half space in terms of mean properties. Also, the effects of the union condition between the piles and the rigid cap on the foundation seismic response is analysed. A schematic representation of the problem is depicted in Fig. 4.2.

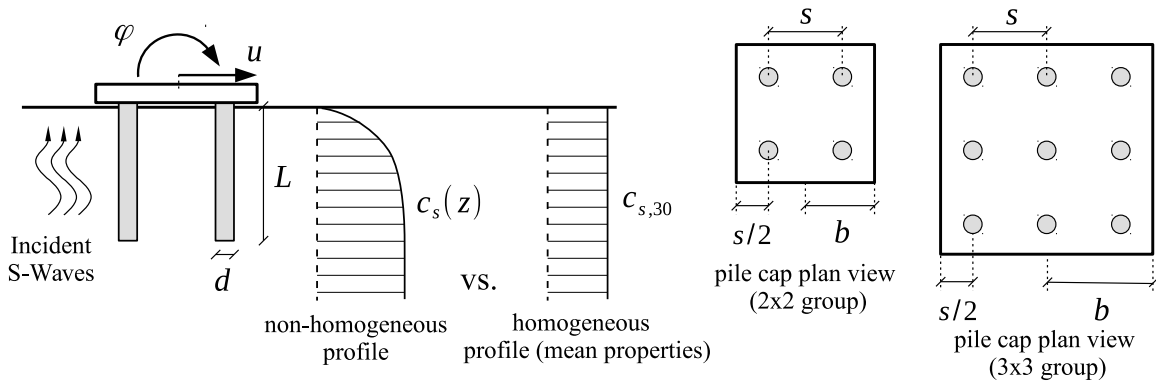


Figure 4.2: Sketch of the seismic problem.

In order to obtain results with practical interest, a set of different pile configurations and soil profiles are defined in the following through physical properties based on typical dimensions and data obtained from real case scenarios.

Foundation properties

Configurations of a single pile and 2×2 and 3×3 pile groups are considered. The results of the selected pile groups allow extracting the trend of the behaviour of larger configurations. Different geometries are assumed by combining the following parameters:

- pile length $L = 10$ m, 30 m and 50 m.
- pile diameter $d = 0.5$ m and 1.5 m.
- pile separation ratio $s/d = 2$ and 5.

In addition to these parameters, the foundation half-width b is defined in order to normalize some of the results, being its value equal to d , s or $3s/2$ for the single, 2×2 and 3×3 configurations, respectively. For the pile groups, all piles are assumed to be identical and can be connected to the rigid cap through a fixed union (default case) or by a hinged union (only if stated in the results). On the other hand, the default boundary condition for the single pile foundation corresponds to a completely free-head pile, but also the fixed-rotation condition at the pile head is considered for comparison purposes.

Regarding the material properties of the piles, a Young's modulus $E_p = 30$ GPa, a pile density $\rho_p = 2500$ kg/m³ and a Poisson's ratio $\nu_p = 0.2$ are assumed as representative to solid cross-section concrete piles and hollow steel piles (through equivalent solid cross-section properties). The shear correction factor of the Timoshenko's beam theory corresponding to solid cross-sections ($\alpha = 0.9$) is assumed. However, the results are virtually insensitive to changing its value to the one corresponding to the hollow sections ($\alpha = 0.5$). No material damping is considered for the piles.

Soil properties

Variable-with-depth profiles are selected based on the regressed expressions proposed by Wang and Wang [120]. In their work, they analysed two different databases with information of real boreholes from California and Japan sites and applied a fitting procedure in order to obtain linear and power-law expressions for the evolution of the shear wave velocity with depth depending on the soil type classification [121, 122].

For the analyses, the profiles corresponding to the California sites are chosen as these soils are representative to other seismically active areas (e.g. the Mediterranean area). Also, the power-law expressions are chosen over the linear ones because the former resulted in a better fitting of the real data. Table 4.1 shows the formulas obtained by Wang and Wang for the evolution of the shear wave velocity as functions of the depth z for the three soil types considered (corresponding to the softest soil types).

In order to measure the influence of assuming the variability of the soil profile, the results of the selected media are compared with the ones obtained by considering an equivalent homogeneous half space in terms of the average shear wave velocity $c_{s,30}$ [68, 121]. This average velocity is defined in such a way that the time needed for the shear wave to travel along the first 30 superficial meters is the same for both the variable and homogeneous profiles. For



Site Class clasification (ASCE)			Regressed expressions from empirical profiles [120]		
Type	$c_{s,30}^{\min}$	$c_{s,30}^{\max}$	$c_s(z)$	$c_{s,30}$	$E_p/E_s(c_{s,30})$
C	360	760	$242 z^{0.271}$	443.4	≈ 30
D	180	360	$126 z^{0.317}$	253.0	≈ 95
E	-	180	$80.9 z^{0.297}$	156.2	≈ 256

[†] Shear wave velocities in m/s

Table 4.1: Soil profiles used for the seismic analyses.

a discrete profile with N_{30} layers above the first 30 m, each layer i with a thickness h_i and a shear wave velocity c_{s_i} , the average shear wave velocity is defined as:

$$c_{s,30} = \frac{30}{\sum_{i=1}^{N_{30}} \frac{h_i}{c_{s_i}}} \quad (4.1)$$

While for a continuously varying profile, the definition of the average shear wave velocity can be adapted to:

$$c_{s,30} = \frac{30}{\int_0^{30} (c_s(z))^{-1} dz} \quad (4.2)$$

The remaining soil properties are assumed to be constant with depth and equal to the homogeneous and variable profiles: soil density $\rho_s = 1750 \text{ kg/m}^3$, soil Poisson's ratio $\nu_s = 0.4$ and soil hysteretic material damping coefficient $\beta_s = 5\%$.

The behaviour of the continuously-varying profiles is simulated with the integral model by discretizing the profile into piecewise homogeneous layers with a height of $h_l = 0.125 \text{ m}$ along the first 50 m of the soil profile. Below this depth, a constant shear wave velocity is assumed for the underlying half space. These values are obtained from a convergence study, and neither increasing the discretization nor the maximum depth alters the presented results. The evolution with depth of the shear wave velocity of the selected profiles together with the homogeneous half spaces used in the analyses are depicted in Fig. 4.3 for the three considered soil types.

Time excitation

The computation of the time response of the pile foundations requires the definition of the time evolution of the excitation. For this purpose, three real accelerograms per soil type are used as seismic input. Those accelerograms are extracted from the PEER Ground Motion Database [123]. The information of the excitation signals is presented in Table 4.2, while their time evolution is shown in Fig. 4.4.

In coherence with the definition of the variable soil profiles, the accelerograms correspond to earthquake events produced in the California area with magnitudes between 6-7 and measured in stations located over soils of type D or E. The accelerations are scaled, so all signals present the same value of the ground maximum acceleration a_g .

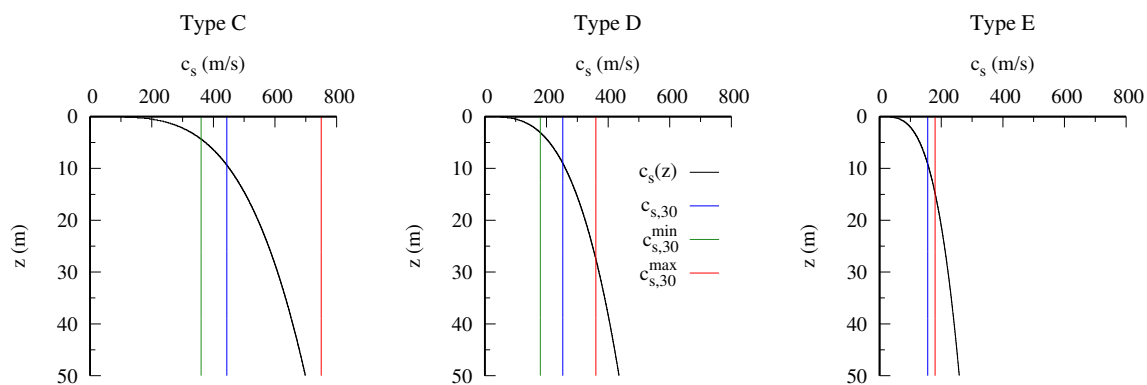


Figure 4.3: Shear wave velocity of the studied profiles.

RSN [†]	Event Name	Year	Station Name	$c_{s,30}$ (m/s)
322	Coalinga-01	1983	Cantua Creek School	275 (Type D)
766	Loma Prieta	1989	Gilroy Array #2	271 (Type D)
988	Northridge-01	1994	LA - Century City CC North	278 (Type D)
178	Imperial Valley-06	1979	El Centro Array #3	163 (Type E)
718	Superstition Hills-01	1987	Imperial Valley Wildlife Liquefaction Array	179 (Type E)
729	Superstition Hills-02	1987	Imperial Valley Wildlife Liquefaction Array	179 (Type E)

[†] Record Sequence Number of the database.

Table 4.2: Real accelerograms used in the seismic analyses. Source: PEER NGA-West2 Database [123].

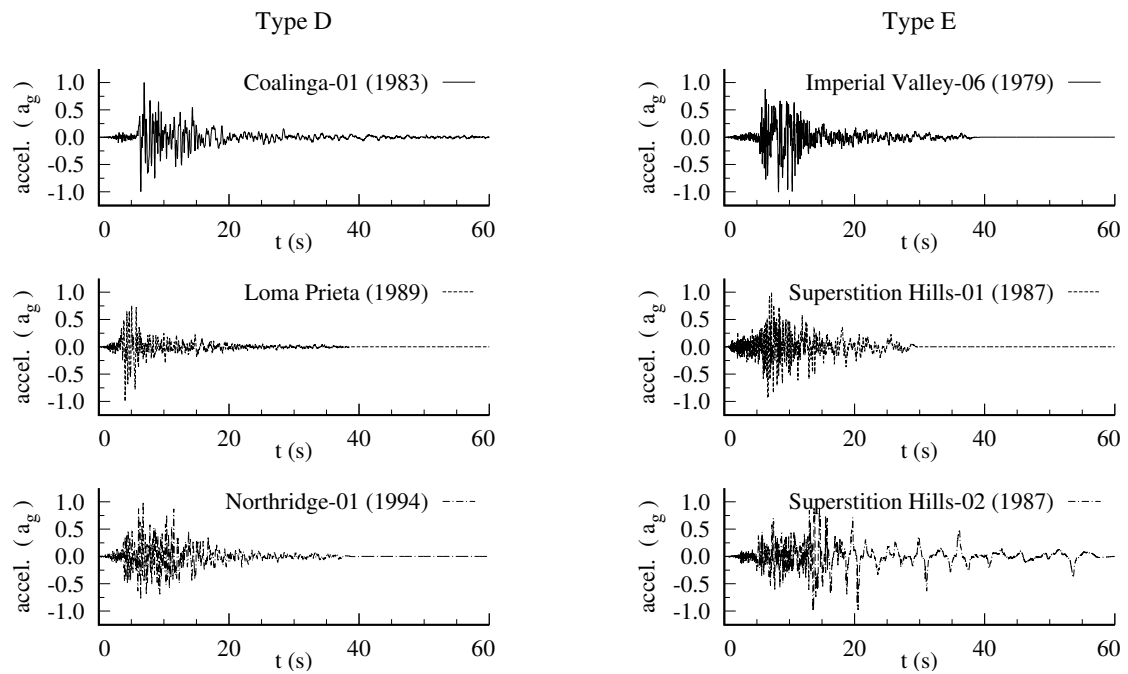


Figure 4.4: Time evolution of the real accelerograms used in the seismic analyses.

4.4 Foundation kinematic interaction factors

The translational and rotational kinematic interaction factors are defined as $I_u = u/u_{ff}$ and $I_\varphi = \varphi b/u_{ff}$, respectively, being u and φ the lateral displacement and rotation at the centre of the foundation, and u_{ff} the free field displacement at surface level, as depicted in Fig. 4.2. These kinematic interaction factors are complex-valued and frequency-dependent terms that indicate how the soil seismic motion is transmitted to the supported structure by the foundation.

In the following, a frequency range between 0 and 160 rad/s is considered, as the energy content of typical earthquakes lies within this range. Furthermore, this range coincide with the frequencies that a sampling of 50 Hz can capture, being that sampling frequency the one of most of the considered earthquake signals.

The influence of the variability of the soil profile on the kinematic interaction factors is analysed by comparing the results of the non-homogeneous profiles (black lines) with respect to the ones of their equivalent homogeneous half space in terms of $c_{s,30}$ (blue lines). Also the results for the stiffest ($c_{s,30}^{\max}$, red lines) and softest ($c_{s,30}^{\min}$, green lines) homogeneous profiles for each soil type are presented in order to enrich the comparison. Thus, the results presented along this section give an insight into the importance of considering the actual soil profile in the estimation of the foundation seismic motion.

As an example, Figs. 4.5 and 4.6 present the translational and rotational kinematic interaction factors, respectively, for a free-head single pile embedded in the three studied soil profiles. The results of the six sets of pile dimensions are presented in different rows. The real part of the kinematic interaction factors is presented with a solid line, while the imaginary component is displayed with a dashed line.

Attending to these results, it is found that the responses of the three pile geometries with the smallest diameter ($d = 0.5$ m) are nearly identical. In the same way, the two configurations of diameter $d = 1.5$ m and slender piles ($L/d \geq 20$) also exhibit virtually the same behaviour. For that reason, and in order to present the obtained results in the most compact way, only the kinematic interaction factors corresponding to the representative configurations are displayed in the following. Thus, the results of the configuration $L = 30$ m, $d = 0.5$ m (labelled as $L30d0.5$) also represent the ones of configurations $L = 10$ m, $d = 0.5$ m and $L = 50$ m, $d = 0.5$ m; while the results corresponding to the configuration $L = 30$ m, $d = 1.5$ m (labelled as $L30d1.5$) also describes the ones of configuration $L = 50$ m, $d = 1.5$ m. These representative configurations are highlighted in Figs. 4.5 and 4.6 and are found to be also valid for the results of the pile groups.

In the following sections, the kinematic interaction factors obtained for the representative configurations of free-head single piles and pile groups with fixed cap-pile union embedded in soils of type D and E are thoroughly analysed. These two soil types correspond to soft soils in which the use of pile foundations is typically required in order to safely support constructions. Nevertheless, in Section 4.4.3 the effects of the soil variability on the kinematic interaction factors for a soil type C are briefly described.

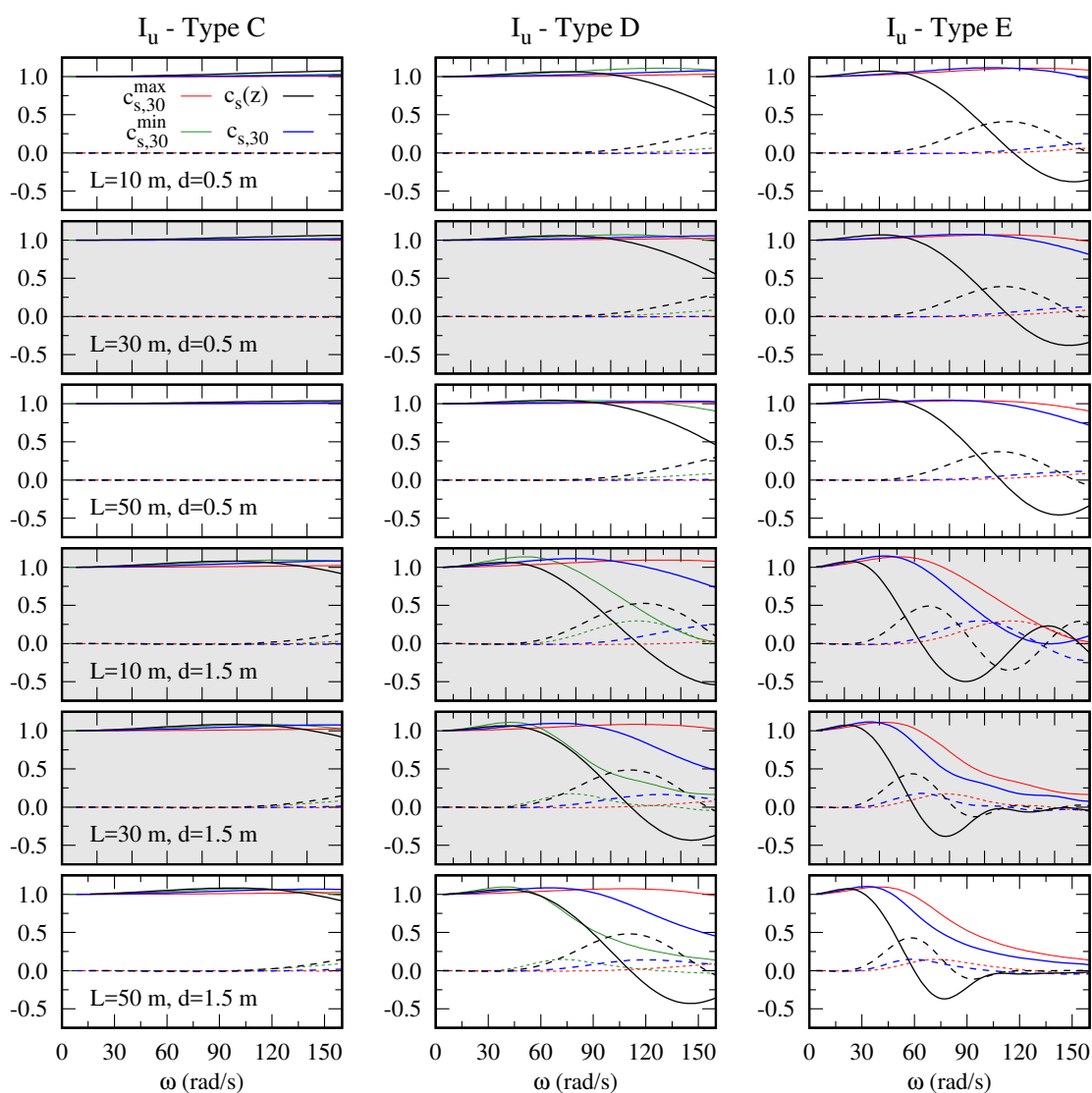


Figure 4.5: Translational kinematic interaction factors for free-head single piles. Representative configurations highlighted in light-gray. (Imaginary components presented by dashed lines).

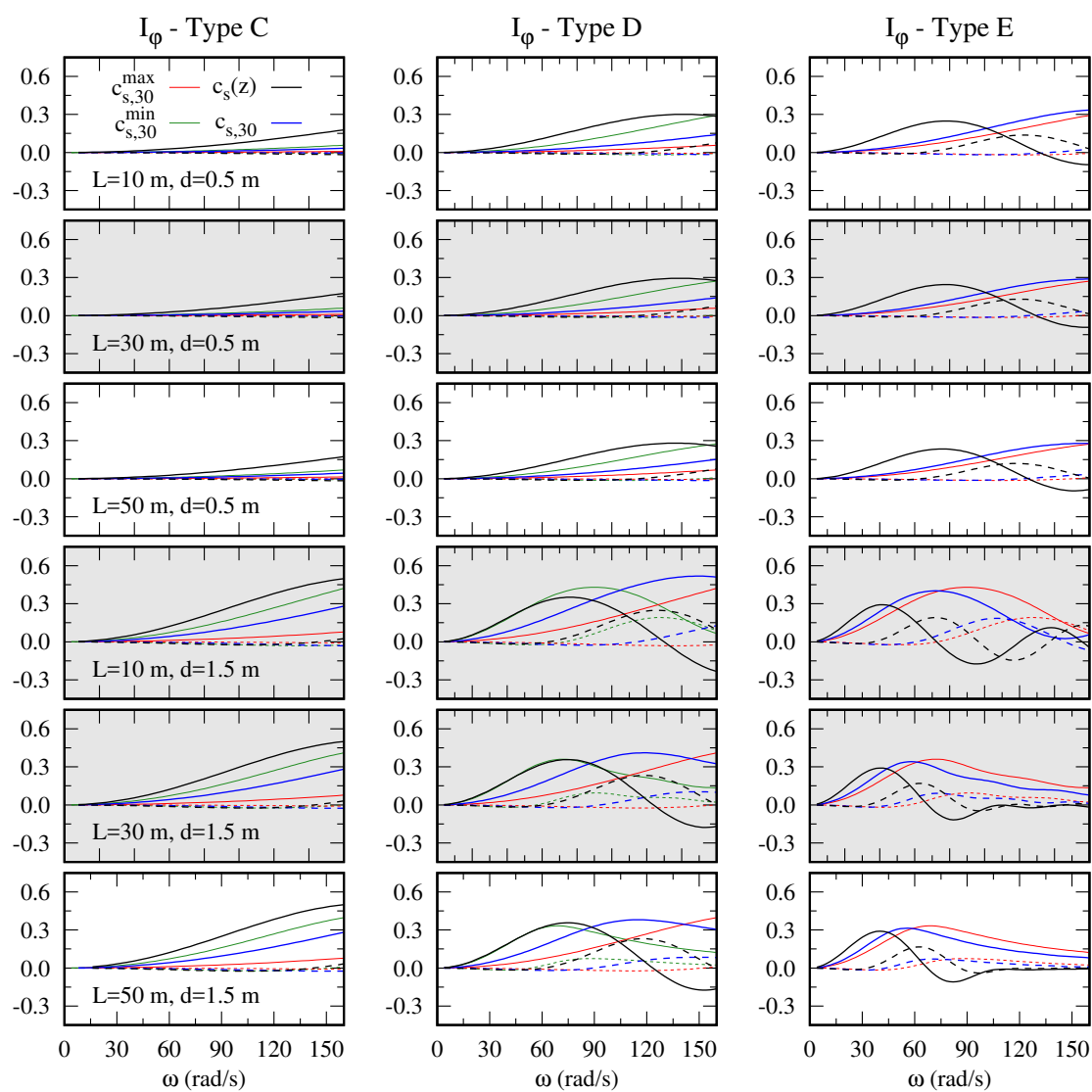


Figure 4.6: Rotational kinematic interaction factors for free-head single piles. Representative configurations highlighted in light-gray. (Imaginary components presented by dashed lines).

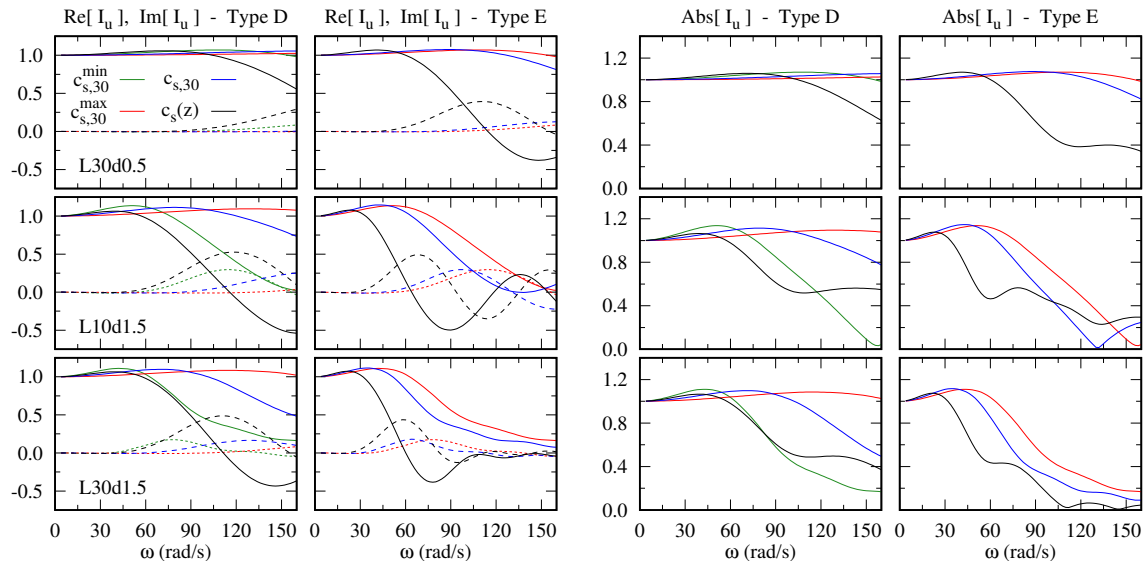


Figure 4.7: Translational kinematic interaction factors for single piles. (Imaginary components presented by dashed lines).

4.4.1 Translational kinematic interaction factors (I_u)

Fig. 4.7 presents the translational kinematic interaction factors for free-head single pile foundations embedded in soils of type D and E. The results of the representative configurations are displayed along the three rows. The first column shows the real (solid lines) and imaginary (dashed lines) components of the kinematic interaction factors for soil type D, while their absolute value is presented in the second column. On the other hand, the third and fourth columns present the real/imaginary and absolute values of the kinematic interaction factor for soil type E, respectively.

Attending to the results of soil D, it is found that the real component of I_u decays to a greater extent for the variable profile rather than for its equivalent homogeneous soil (or even for the homogeneous soil with minimum shear velocity). The effect of the variability of the soil profile is also seen for the imaginary component with a higher increment of its value as the frequency augments. Comparing the absolute value of the interaction factors for the non-homogeneous and its equivalent-homogeneous profiles for this soil type, it is found that in the low-frequency range both profiles present nearly the same values (the ones of the varying profile are slightly higher), while for larger frequencies the varying profile filters the ground motion to a greater extent with respect to its homogeneous equivalent profile. These results agree with the findings of previous works [84,94]. Attending to the classical representation of the interaction factors against the dimensionless frequency, it can be understood that, owing to its higher diameter (and, consequently, higher a_o for the same range of ω), the configurations with $d = 1.5$ m present lower values of $|I_u|$ at smaller frequencies than the foundations with $d = 0.5$ m.

On the other hand, for the soil type E, the effects of the variability of the profile commented above are intensified. The absolute value of the kinematic interaction factor for the

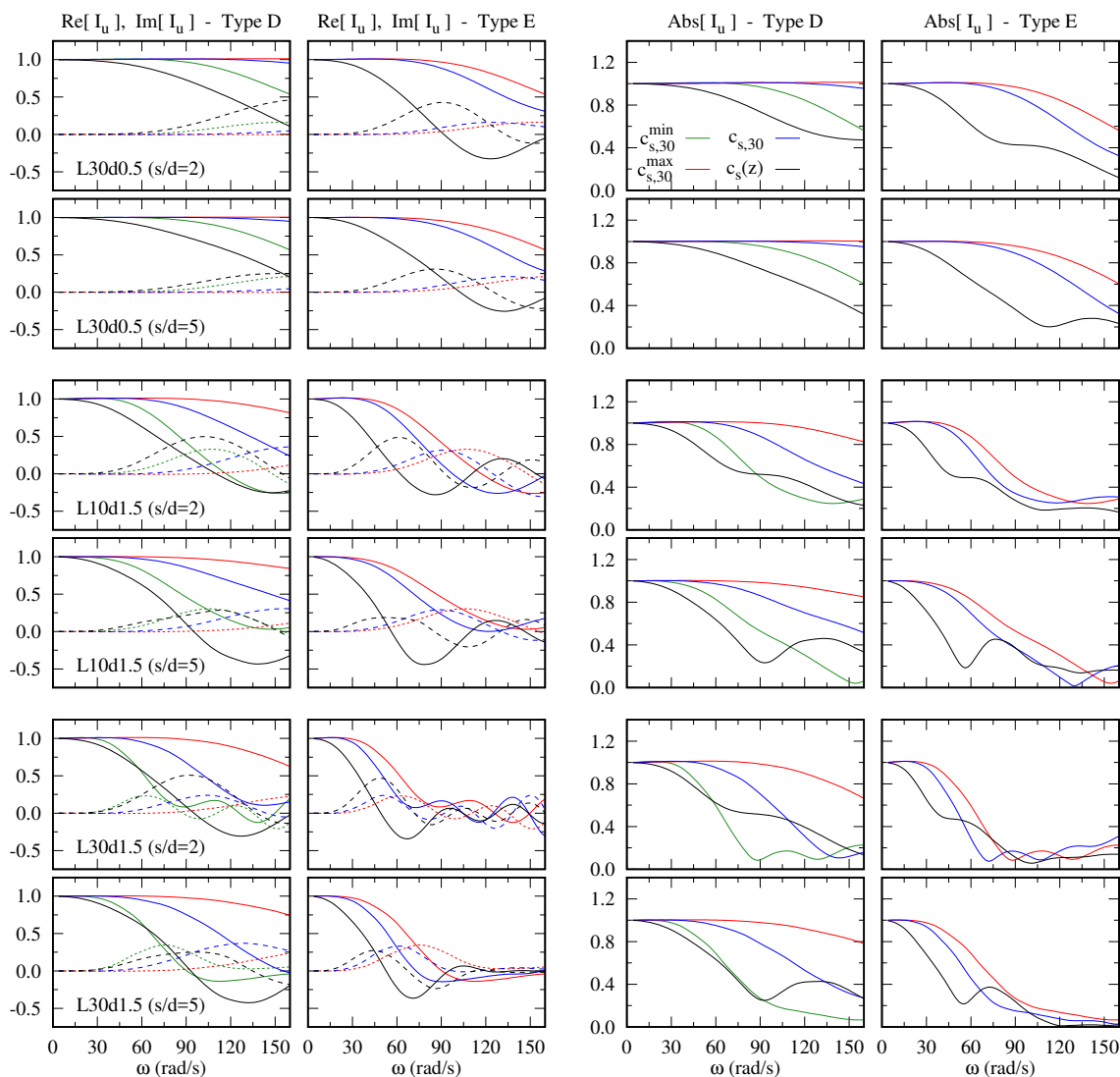


Figure 4.8: Translational kinematic interaction factors for 2×2 pile groups. (Imaginary components presented by dashed lines).

configuration $L30d1.5$ even vanishes for frequencies higher than 110 rad/s only for the non-homogeneous profile. A singular situation is found in this soil type for the configuration $L10d1.5$ (corresponding to the shortest pile), as for high frequencies the variable profile presents higher $|I_u|$ than its equivalent homogeneous one.

Fig. 4.8 presents the translational kinematic interaction factors for the 2×2 pile groups under study. The disposition of the results is the same as the one presented in Fig. 4.7, with the exception that now two rows per configuration are displayed in order to show the results for the two studied separation distances s/d . In general terms, it is found that for pile groups the effects of the variability of the soil profile can be observed at frequencies lower than those for the single pile. Furthermore, since for group configurations the absolute value of the translational kinematic interaction factor is always below unity, the results corresponding to the



non-homogeneous profiles are always smaller than the ones of their equivalent homogeneous soil in the low-frequency range.

The absolute values corresponding to the smallest distance between piles ($s/d = 2$) show that, for the $L30d0.5$ and $L10d1.5$ configurations, the varying profiles filter the seismic excitation to a greater extent than their $c_{s,30}$ homogeneous profiles along all the studied frequency range. On the other hand, for configuration $L30d1.5$ there is an interval of frequencies (100-160 rad/s for soil D, and 45-90 rad/s for type E) in which the non-homogeneous profiles present higher values of $|I_u|$ than their homogeneous equivalent ones. This effect is mainly produced due to the larger values of the imaginary component of the results for the variable profile, in addition to the fact that their real component reaches more negative values at smaller frequencies for this profile. Also, for this specific configuration ($L30d1.5$ and $s/d = 2$), it is important to highlight the large oscillations with the frequency that can be found in the real and imaginary components of the I_u in the high-frequency range. These oscillations occur both for the variable and the homogeneous profiles.

Regarding the influence of increasing the separation distance between the piles in the group, it has a minor effect on the $L30d0.5$ configuration, just slightly increasing the higher filtering effect of the varying profile in the medium-high-frequency range. On the contrary, for the configurations represented by $L30d1.5$, increasing the distance between the piles significantly diminishes the above-mentioned high oscillations of the real and imaginary components of the I_u at large frequencies. This phenomenon may indicate that this oscillatory behaviour is produced by the pile-to-pile interaction between the elements of the group, which is reduced as the distance between piles increases.

Fig. 4.9 shows now the results for the 3×3 configurations. The translational kinematic interaction factors and the effects of the soil profile variability and pile separation obtained for these pile groups are analogous to the ones corresponding to the 2×2 groups. Attending to the results of $L30d1.5$, increasing the number of piles in the group is found to augment the oscillations of the real and imaginary components at high frequencies for all soil profiles due to the higher number of piles that can interact with each other.

4.4.2 Rotational kinematic interaction factors (I_ϕ)

Fig. 4.10 shows the rotational kinematic interaction factors for the monopile configurations embedded in soil types D and E following the same distribution that was used for the translational factors in the previous section. In general terms, two zones with different behaviours can be distinguished in the obtained results. In the low-frequency range, the variable profiles present larger rotations at the pile head than their equivalent homogeneous soils. On the other hand, in the medium-high-frequency zone the real and imaginary components of the variable profiles decrease their values, changing their signs for large frequencies. This significant sign change is not produced for any of the homogeneous profiles in the studied frequency range. The two different zones can be also recognized in the absolute value of the rotational kinematic interaction factors. In the low-frequency range the $|I_\phi|$ of the varying profiles exceed the ones of the $c_{s,30}$ homogeneous profile; while, in the medium-high range, the non-homogeneous profiles present smaller rotations than the uniform soils. The frequencies that separate the two different zones depend on the diameter of the configuration and the

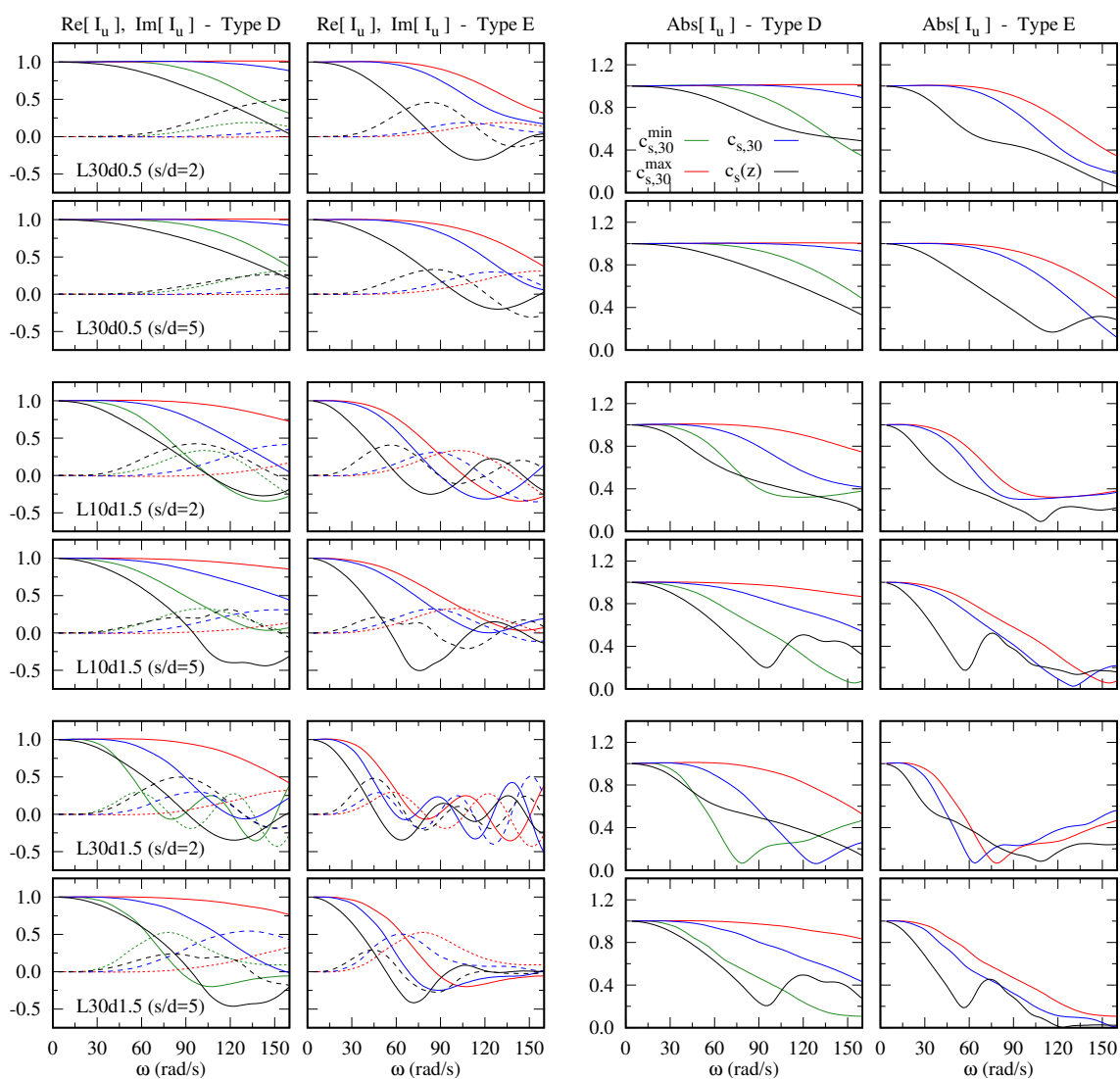


Figure 4.9: Translational kinematic interaction factors for 3×3 pile groups. (Imaginary components presented by dashed lines).

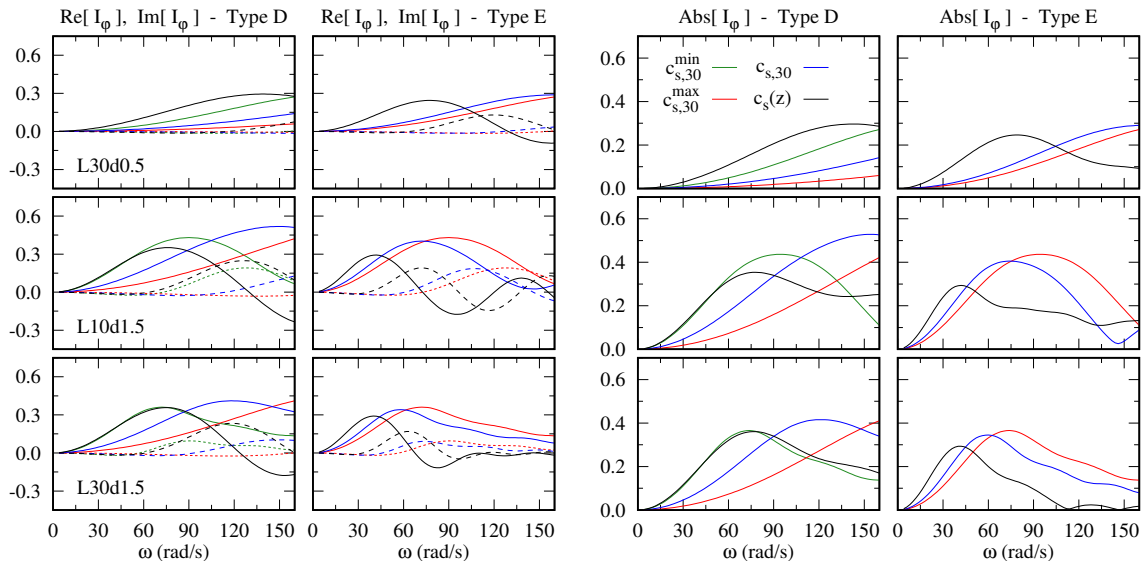


Figure 4.10: Rotational kinematic interaction factors for single piles. (Imaginary components presented by dashed lines).

soil type: approximately being 100 rad/s for $d = 0.5$ m and Soil E, and 90 or 42 rad/s for $d = 1.5$ m and Soil D or E, respectively.

For soil type E, and coinciding with what was found for the translational interaction factors, the $|I_\phi|$ vanishes at frequencies over 110 rad/s for the $L30d1.5$ configurations. Also, the singular behaviour of the $L10d1.5$ configuration of presenting a higher response for the varying profile than for the equivalent homogeneous at high frequencies is also seen in the rotational factors.

The results for the 2×2 configurations are presented in Fig. 4.11. A significant reduction of the rotational kinematic interaction factors is found for the pile group, despite the value of b that is used for the normalization augments with respect to the one of the single pile. This reduction is a well-known effect, which is produced by the vertical stiffness of the piles that restricts the rotation of the cap. Only the configuration $L10d1.5$ (shortest piles) presents results on the order of the ones of the single pile. Note that the same range is kept for all the figures that display the same variable in order to ease the comparison between them. Nevertheless, the results for the group configuration exhibit analogous behaviours as the ones of the single pile, also presenting the two frequency zones that were commented above.

Regarding the results corresponding to the foundations with closer piles ($s/d = 2$), the rotational interaction factors of the $L30d1.5$ configuration again present an oscillatory behaviour in its real and imaginary components at large frequencies for soil type E. These oscillations are likewise found in the absolute values of the homogeneous soils, but not for the $|I_\phi|$ of the variable profile. On the other hand, for soil type D this configuration ($L30d1.5$ $s/d = 2$) presents nearly the same rotational interaction factors for the non-homogeneous and the equivalent homogeneous soils in terms of the absolute value, despite important differences can be observed between their real and imaginary components.

Attending to the effects of the distance between piles, increasing their separation slightly

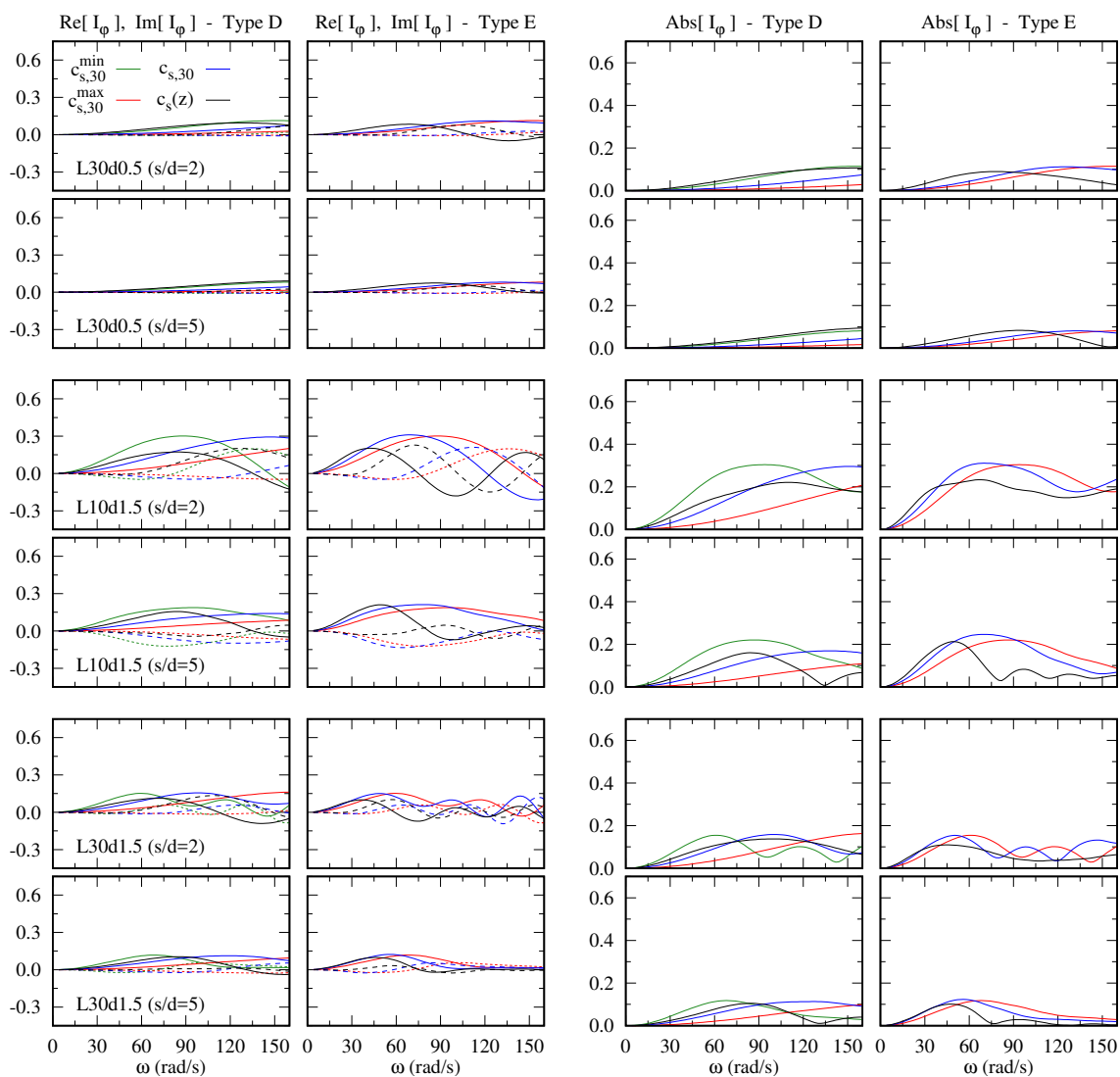


Figure 4.11: Rotational kinematic interaction factors for 2×2 pile groups. (Imaginary components presented by dashed lines).

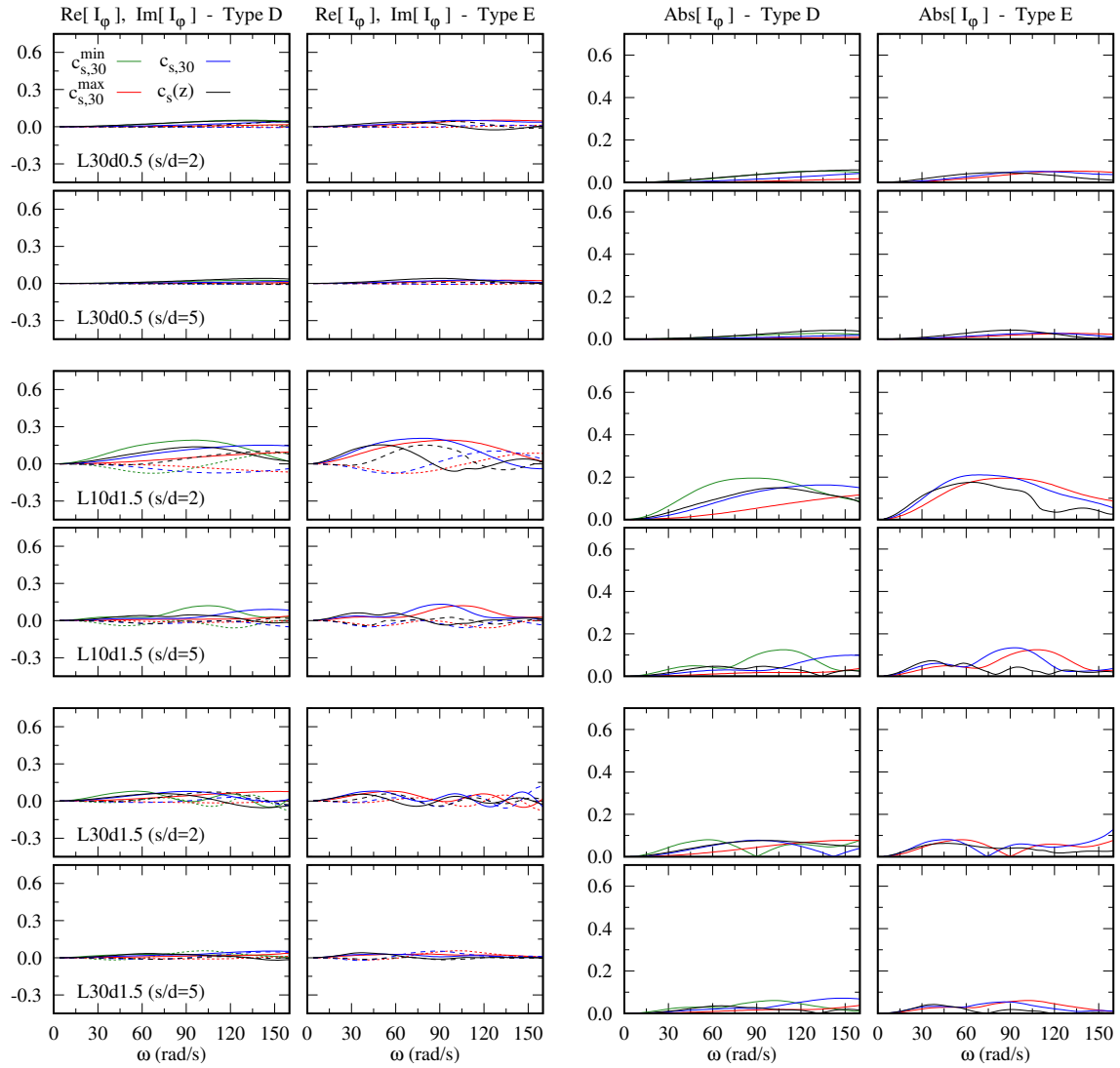


Figure 4.12: Rotational kinematic interaction factors for 3×3 pile groups. (Imaginary components presented by dashed lines).

reduces the rotation of the group. The most noticeable difference between the results of the two s/d values are found for the $d = 1.5$ m configurations: when the distance between the piles increases, the two frequency zones of different behaviours are appreciated in a clearer way, being the $|I_\phi|$ values of the varying profiles lower than the ones of the equivalent homogeneous soil at large frequencies. In addition to this, and coinciding with what was found for the translational factors, the increment of the separation between the piles removes the high-frequency oscillations in the rotational interaction factors for the configurations $L30d1.5$ in soil E.

Finally, Fig. 4.12 displays the rotational kinematic interaction factors for the configurations of 3×3 pile groups. As found in the previous results, the increment in the number of piles drastically reduces the rotation of the cap. The shape of the interaction factors of the

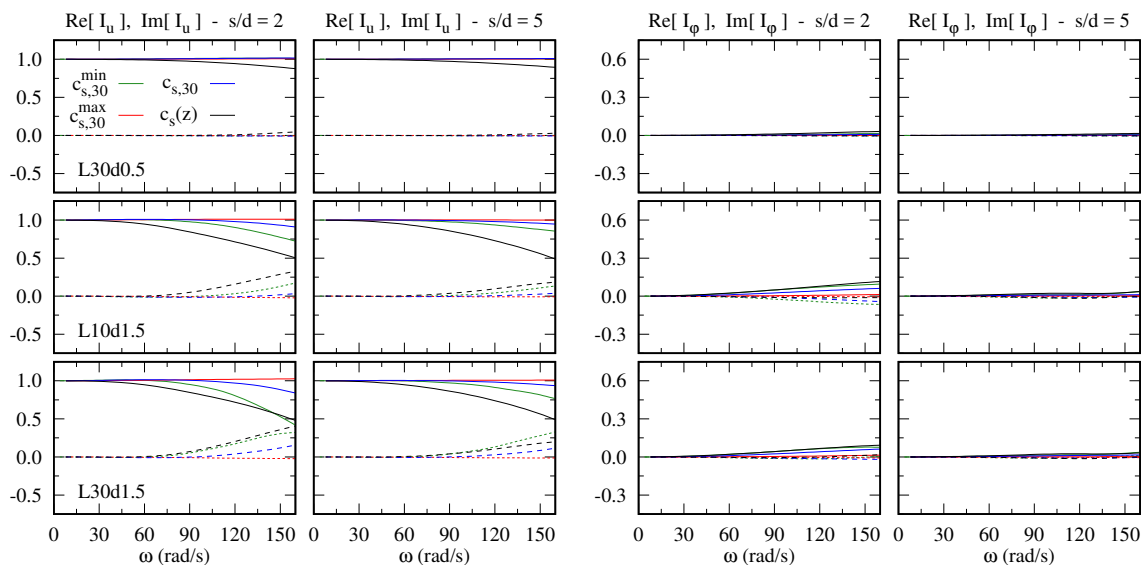


Figure 4.13: Kinematic interaction factors for 3×3 pile groups embedded in soil type C. (Imaginary components presented by dashed lines).

3×3 groups are similar to the ones of the 2×2 groups. The only aspect that is worthy of mention is the fact that for the $L30d1.5$ configuration the oscillations in the absolute value of I_ϕ at large frequencies for the homogeneous profiles disappear and are replaced by an almost linear increase with frequency.

For these pile foundations, also increasing the separation between the piles further reduces the rotation at the centre of the cap. However, the influence of the separation distance is lower than the one of the increment in the number of piles of the group.

4.4.3 Kinematic interaction factors for soil type C

The study of the effects of the soil profile variability has also been carried out for the soil type C. In addition to the results for the single pile configurations presented before in Figs. 4.5 and 4.6, Fig. 4.13 displays the translational and rotational kinematic interaction factors for the representative configurations of the 3×3 pile groups. Only the real and imaginary components are shown and the results of the two different separation distances are presented in different columns.

Regarding the translational interaction factors, the results have practically a static behaviour ($I_u \approx 1$) along the studied frequency range, so virtually no differences are found between the results of the variable and homogeneous profiles. Only for the group configurations with large diameters ($d = 1.5$), the filtering effect of the foundation is perceived at high frequencies for the non-homogeneous and softest homogeneous profiles.

On the other hand, the magnitude of the rotational kinematic interaction factors of the non-homogeneous soil significantly overtakes the one of the homogeneous profiles for all the frequency range. Those differences between the varying and constant profiles are produced only by the contribution of the real component of the interaction factors, as their imaginary



component is almost negligible. Note that, as this soil type is stiffer than the ones studied in the previous section, only the behaviour of the low-frequency zone is seen for the considered frequency range.

4.5 Structural maximum accelerations

In order to illustrate the effects that the differences in the kinematic interaction factors previously studied could have on the response of the supported structure, results are also presented in terms of pseudo-spectral accelerations (PSA) along this section.

The structural time response is obtained from the kinematic interaction factors following the standard frequency-domain method [67] and using the accelerograms presented in Section 4.3. These acceleration signals are assumed to be located at the free-surface level. In order to include the contribution of the rotational kinematic interaction factors in the spectra of maximum response, different structural height ratios h/b are considered going from $h/b = 0$ (neglecting the contribution of the cap rotation) to $h/b = 10$.

The results are presented not only in terms of the elastic response spectra for both the variable ($PSA_{c_s(z)}(T)$) and equivalent homogeneous ($PSA_{c_{s,30}}(T)$) soil profiles, but also in terms of the difference between them which is computed as:

$$\Delta_{PSA}(T) = PSA_{c_{s,30}}(T) - PSA_{c_s(z)}(T) \quad (4.3)$$

where T is the structural period in seconds. The difference Δ_{PSA} is defined in order to ease the analysis of the influence of the soil profile on the structural response. A positive value of Δ_{PSA} indicates that the homogeneous assumption is conservative; while a negative value implies that higher structural accelerations are obtained if the actual variable profile is considered. The response spectra and their differences are expressed in terms of the maximum ground acceleration of the excitation signal a_g .

Fig. 4.14 presents the elastic response spectra for the variable (black lines) and equivalent homogeneous (blue lines) profiles for the representative configuration $L30d1.5$ of a free-head single pile embedded in soils D and E. Also the corresponding differences Δ_{PSA} for each soil type are shown. The results of the different accelerograms are indicated by different line styles according to Fig. 4.4.

Attending to the PSA obtained for soil type D, the results of both profiles practically coincide if the contribution of the rotation of the cap is neglected ($h/b = 0$). However, as the height of the structure is increased, the differences between the non-homogeneous and the constant profile augment. These differences are especially relevant for periods around 0.25 s, but are extended to almost all the studied range for the extreme scenario of $h/b = 10$. This effect of the h/b parameter is also found for the soil type E. Moreover, even for the case of $h/b = 0$ some differences between the results of the varying and equivalent homogeneous profiles can be seen for all the structural period range. For this soil type and for low periods ($T \approx 0.1$ s) the accelerations of the homogeneous profile surpass the ones of the variable profile. Also, for soil E, the effects of the structural height on the magnitude of the PSA are more important than for soil D (note the change of the ordinate-axis scale).

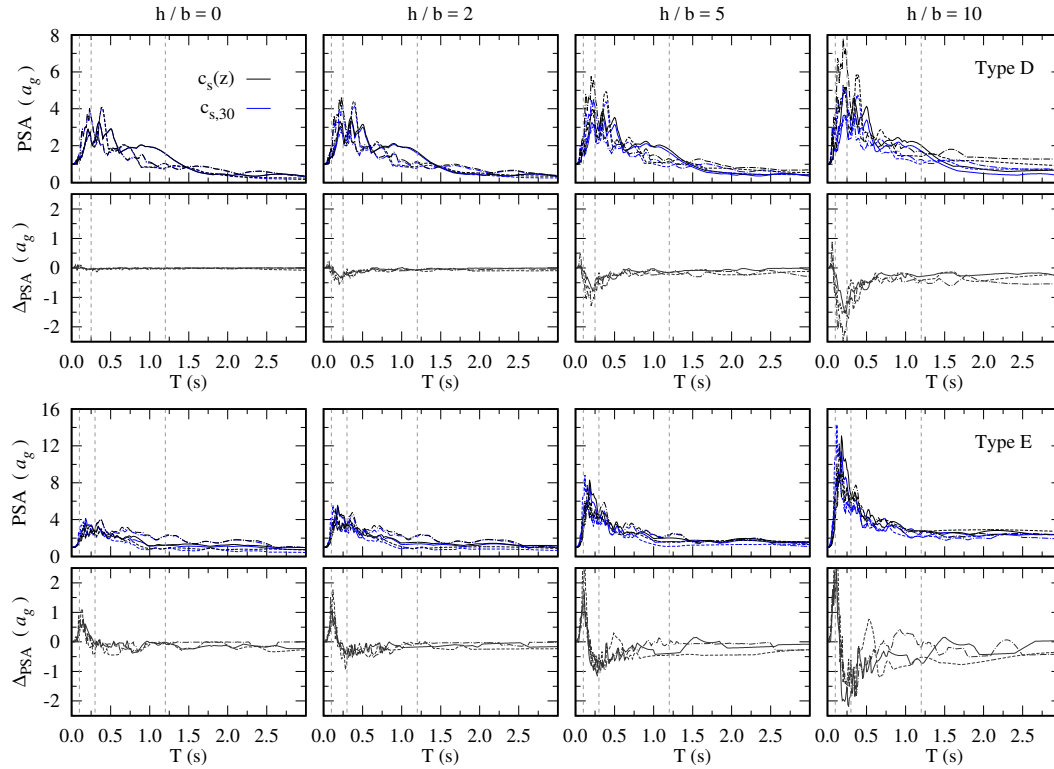


Figure 4.14: Elastic response spectra (PSA) and differences between results of the equivalent homogeneous and non-homogeneous profiles (Δ_{PSA}). Single pile, configuration $L30d1.5$.

These effects of the soil profile on the structural maximum accelerations are also seen and in a clearer way attending to the results of Δ_{PSA} . The homogeneous assumption tends to under-predict the structural maximum accelerations except for systems with very low periods. The highest differences between the two profiles are found around $T = 0.25$ s, for which the equivalent homogeneous soil produces a maximum response that can be up to two times the ground peak acceleration lower than the one of the actual profile.

Fig. 4.15 displays the differences between the pseudo-spectral accelerations Δ_{PSA} now for a group configuration of 3×3 piles with $L30d1.5$. For this pile group, and because the rotational kinematic interaction factor (I_ϕ) is drastically reduced when the number of piles increases, the effects of the structural height are almost negligible, being only appreciable for the largest height ratio ($h/b = 10$). The differences between the two profiles are more evident for the softer soil type (E), and for the groups with closer piles ($s/d = 2$). In general terms, for this configuration the equivalent homogeneous profiles produce higher acceleration values than the variable soils for low periods. However, negative values of Δ_{PSA} exist for soil type E along the whole period range which can be significant.

The results presented in Figs. 4.14 and 4.15 illustrate the general trends that are obtained for all studied configurations. However, more detailed information is given in Tables 4.3 (soil type D) and 4.4 (soil type E). Those tables contain the minimum value of Δ_{PSA} that is obtained for all the representative configurations separated into different period intervals. The

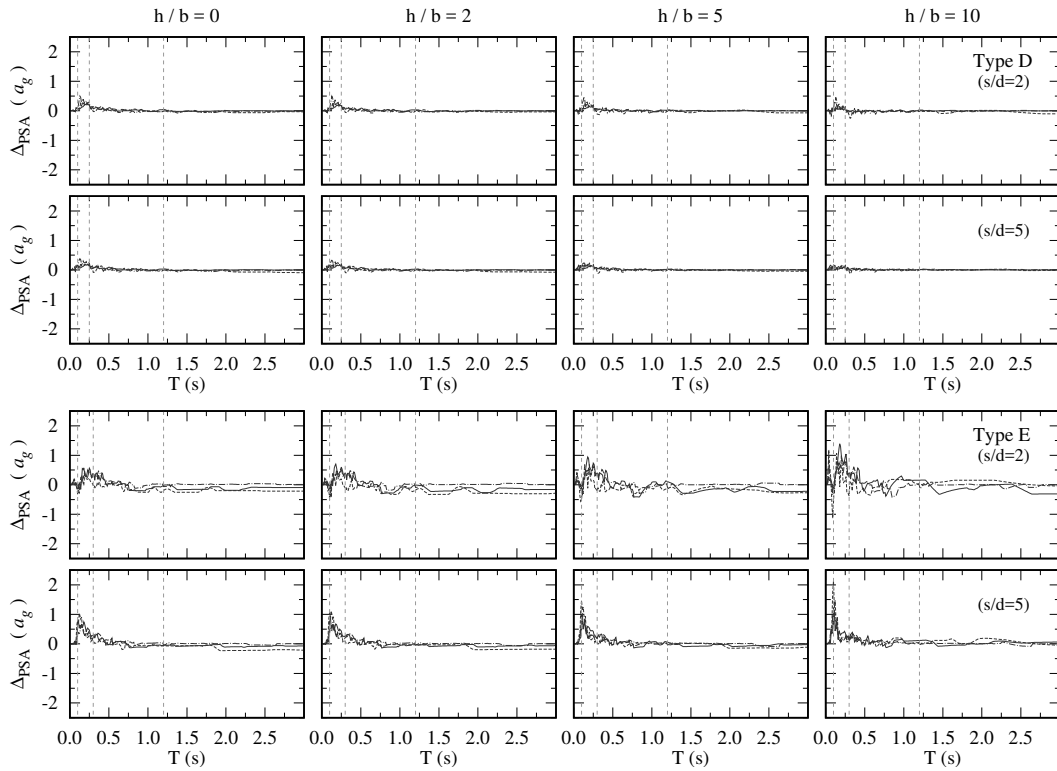


Figure 4.15: Differences between the elastic response spectra of the equivalent homogeneous and non-homogeneous profiles (Δ_{PSA}). 3×3 pile group, configuration $L30d1.5$.

period division is done according to the one proposed in the Eurocode [68] for the definition of the Type 2 spectra for each ground type (note that although the letters of the different soil types do not coincide between the Eurocode and ASCE definitions, the intervals of $c_{s,30}$ that delimit each type are nearly the same). The information presented in Tables 4.3 and 4.4 allow the estimation of the importance of considering the variability of the soil profile when studying the structural maximum acceleration response under different scenarios. The minimum values for each row and column are indicated by bold and italic fonts, respectively. The former indicates for which structural properties neglecting the actual evolution of the profile leads to the most unsafe scenario, while the latter indicates the foundation configuration which is most sensitive (with unfavourable effects) to the variability of the soil profile.

Attending to the results, and summarizing all the previous discussion, the soil type E presents higher differences between the non-homogeneous and equivalent homogeneous profiles. These differences are magnified as the structural height ratio augments due to the higher contribution of the rotational kinematic interaction factors to the structural response. Thus, including the I_φ of the foundation is found to increase the accelerations of the variable profile with respect to the constant one. This effect is explained attending to the rotational kinematic interaction factors presented above: in the low-frequency zone (which is the one that usually contains more energy of the seismic excitation) the variable profiles present higher rotations than their homogeneous equivalent ones. This effect is especially relevant for the single pile



Configuration	$h/b = 0$				$h/b = 2$				$h/b = 5$				$h/b = 10$				
	T_1	T_2	T_3	T_4	T_1	T_2	T_3	T_4	T_1	T_2	T_3	T_4	T_1	T_2	T_3	T_4	
L30d0.5	single	-0.0	-0.1	-0.0	-0.0	<u>-0.2</u>	-0.2	-0.1	-0.0	<u>-0.4</u>	-0.5	-0.3	-0.1	-0.8	-1.0	-0.6	-0.3
	$2\times 2, s/d = 2$	-0.0	+0.0	-0.0	-0.0	-0.0	-0.0	-0.0	-0.0	-0.1	-0.1	-0.1	-0.0	-0.1	-0.3	-0.2	-0.1
	$2\times 2, s/d = 5$	-0.0	+0.0	-0.0	-0.0	-0.0	+0.0	-0.0	-0.0	-0.0	-0.0	-0.0	-0.0	-0.1	-0.1	-0.1	-0.0
	$3\times 3, s/d = 2$	-0.0	+0.0	-0.0	-0.0	-0.0	+0.0	-0.0	-0.0	-0.0	-0.0	-0.0	-0.0	-0.1	-0.1	-0.1	-0.0
	$3\times 3, s/d = 5$	-0.0	+0.0	-0.0	-0.0	-0.0	+0.0	-0.0	-0.0	-0.0	+0.0	-0.0	-0.0	-0.0	-0.0	-0.0	-0.0
L10d1.5	single	-0.1	<u>-0.1</u>	-0.1	-0.1	-0.2	-0.5	<u>-0.3</u>	-0.1	-0.3	-1.3	-0.7	-0.3	<u>-0.8</u>	-2.5	-1.7	-0.6
	$2\times 2, s/d = 2$	-0.1	+0.1	-0.1	-0.1	-0.1	+0.0	-0.1	-0.1	-0.1	-0.2	-0.2	-0.1	-0.1	-0.6	-0.5	-0.2
	$2\times 2, s/d = 5$	<u>-0.1</u>	+0.1	-0.1	-0.1	-0.1	+0.0	-0.1	-0.1	-0.0	-0.0	-0.1	-0.0	-0.1	-0.3	-0.2	-0.1
	$3\times 3, s/d = 2$	-0.1	+0.0	-0.1	-0.1	-0.0	+0.0	-0.1	-0.0	-0.0	-0.0	-0.1	-0.0	-0.1	-0.3	-0.3	-0.1
	$3\times 3, s/d = 5$	-0.1	+0.1	-0.1	<u>-0.1</u>	-0.1	+0.0	-0.1	-0.1	-0.1	+0.0	-0.1	-0.1	-0.0	-0.1	-0.1	-0.0
L30d1.5	single	-0.1	-0.1	<u>-0.1</u>	-0.1	-0.2	<u>-0.6</u>	-0.3	<u>-0.1</u>	-0.4	<u>-1.3</u>	<u>-0.8</u>	<u>-0.3</u>	-0.8	-2.5	<u>-1.7</u>	<u>-0.6</u>
	$2\times 2, s/d = 2$	-0.1	+0.0	-0.1	-0.1	-0.1	+0.0	-0.1	-0.1	-0.1	-0.0	-0.2	-0.1	-0.1	-0.3	-0.4	-0.1
	$2\times 2, s/d = 5$	-0.1	+0.1	-0.1	-0.1	-0.1	+0.0	-0.1	-0.1	-0.1	+0.0	-0.1	-0.0	-0.0	-0.1	-0.1	-0.0
	$3\times 3, s/d = 2$	-0.0	-0.0	-0.1	-0.1	-0.1	-0.0	-0.1	-0.1	-0.1	-0.0	-0.1	-0.1	-0.2	-0.0	-0.2	-0.1
	$3\times 3, s/d = 5$	-0.1	+0.1	-0.1	-0.1	-0.1	+0.0	-0.1	-0.1	-0.1	+0.0	-0.1	-0.0	-0.0	+0.0	-0.1	-0.0

[†] **Bolded** items correspond to the minimum value of the row. Underlined items correspond to the minimum value of the column.

^{††} Definition of the period ranges: $T_1 \equiv T \in [0, 0.1]$ s; $T_2 \equiv T \in [0.1, 0.25]$ s; $T_3 \equiv T \in [0.25, 1.2]$ s; $T_4 \equiv T \in [1.2, 3]$ s.

Table 4.3: Differences between the PSA of the equivalent homogeneous and non-homogeneous profiles Δ_{PSA} (units in a_g). Minimum values (unsafe homogeneous assumption) for different period ranges. Soil type D.

Configuration	$h/b = 0$				$h/b = 2$				$h/b = 5$				$h/b = 10$			
	T_1	T_2	T_3	T_4	T_1	T_2	T_3	T_4	T_1	T_2	T_3	T_4	T_1	T_2	T_3	T_4
L30d0.5																
single	-0.2	-0.4	-0.2	-0.2	-0.9	-0.9	-0.4	-0.3	-1.8	-2.2	-0.8	-0.5	-3.3	-4.3	-1.4	-0.8
2x2, $s/d = 2$	-0.2	-0.3	-0.3	-0.2	-0.2	-0.3	-0.3	-0.2	-0.2	-0.5	-0.3	-0.2	-0.3	-0.8	-0.4	-0.3
2x2, $s/d = 5$	-0.1	-0.2	-0.3	-0.2	-0.1	-0.2	-0.2	-0.2	-0.1	-0.3	-0.3	-0.2	-0.2	-0.4	-0.2	-0.2
3x3, $s/d = 2$	-0.1	-0.2	-0.3	-0.2	-0.2	-0.3	-0.3	-0.2	-0.2	-0.4	-0.3	-0.2	-0.2	-0.5	-0.4	-0.3
3x3, $s/d = 5$	-0.0	-0.2	-0.2	-0.2	-0.0	-0.2	-0.2	-0.1	-0.1	-0.2	-0.2	-0.1	-0.0	-0.2	-0.2	-0.1
L10d1.5																
single	-0.1	-0.4	-0.6	-0.3	-0.1	-0.9	-0.6	-0.2	-0.1	-1.1	-1.1	-0.4	-0.1	-2.5	-1.8	-0.6
2x2, $s/d = 2$	-0.0	-0.1	-0.3	-0.3	-0.1	-0.5	-0.5	-0.3	-0.0	-0.8	-0.5	-0.1	-0.0	-0.9	-0.9	-0.2
2x2, $s/d = 5$	-0.1	-0.1	-0.4	-0.4	-0.0	-0.4	-0.4	-0.2	-0.0	-0.4	-0.3	-0.2	-0.0	-0.5	-0.4	-0.2
3x3, $s/d = 2$	-0.1	-0.1	-0.3	-0.3	-0.0	-0.4	-0.5	-0.3	-0.0	-0.5	-0.5	-0.1	-0.0	-0.5	-0.6	-0.1
3x3, $s/d = 5$	-0.1	-0.1	-0.3	-0.4	-0.0	-0.3	-0.4	-0.3	-0.0	-0.3	-0.4	-0.3	-0.0	-0.5	-0.4	-0.2
L30d1.5																
single	-0.0	-0.4	-0.4	-0.3	-0.0	-0.9	-0.6	-0.3	-0.0	-1.2	-1.0	-0.5	-0.0	-2.2	-1.9	-0.8
2x2, $s/d = 2$	-0.2	-0.3	-0.3	-0.3	-0.2	-0.3	-0.4	-0.5	-0.2	-0.4	-0.5	-0.3	-0.4	-0.7	-0.6	-0.3
2x2, $s/d = 5$	-0.1	+0.0	-0.2	-0.3	-0.0	-0.0	-0.2	-0.3	-0.1	-0.2	-0.3	-0.2	-0.0	-0.2	-0.2	-0.1
3x3, $s/d = 2$	-0.1	-0.3	-0.3	-0.3	-0.2	-0.5	-0.3	-0.3	-0.6	-0.5	-0.4	-0.3	-1.1	-0.6	-0.4	-0.3
3x3, $s/d = 5$	-0.0	+0.1	-0.2	-0.2	-0.0	+0.1	-0.2	-0.2	-0.0	+0.1	-0.1	-0.1	-0.0	+0.1	-0.1	-0.1

[†] **Bolded** items correspond to the minimum value of the row. Underlined items correspond to the minimum value of the column.

^{††} Definition of the period ranges: $T_1 \equiv T \in [0, 0.1)$ s; $T_2 \equiv T \in [0.1, 0.3)$ s; $T_3 \equiv T \in [0.3, 1.2)$ s; $T_4 \equiv T \in [1.2, 3]$ s.

Table 4.4: Differences between the PSA of the equivalent homogeneous and non-homogeneous profiles Δ_{PSA} (units in a_g). Minimum values (unsafe homogeneous assumption) for different period ranges. Soil type E.

configuration, for which assuming the homogeneous profile can lead to a difference in the structural maximum accelerations with respect to the ones of the variable profile that can be over four times the peak ground acceleration. On the other hand, for pile groups these differences are generally not important (specially for soil type D), being the homogeneous assumption on the side of safety. However, for group configurations that present non-negligible cap rotations (i.e., closely spaced and small number of piles) founding slender structures, the variable profile can present maximum accelerations up to $1 a_g$ larger than the ones obtained by considering the equivalent homogeneous profile. Configurations with short piles ($L10d1.5$) are found to be the ones that present the highest negative differences among the pile groups under study.

4.6 Influence of the pile head condition on the foundation seismic input factors

The boundary conditions at the head of the piles assumed in the previous section (free-head for the single pile and fixed union to the rigid cap for the pile groups) are the ones normally found in constructive solutions. However, after unexpected events, such as earthquakes, the pile head can fail due to the excessive stresses that act over this point. In that situation, the material at the pile head will plastify and can be treated as a hinged union between the rigid cap and the rest of the embedded pile. In this section, the influence of the condition at the pile head on both the foundation filtering effect of the seismic motion, and on the spectral response of the supported structure is analysed.

The configuration of a single pile is used as starting point as it corresponds to the simplest scenario. The two head conditions will correspond to a completely free-head (no forces

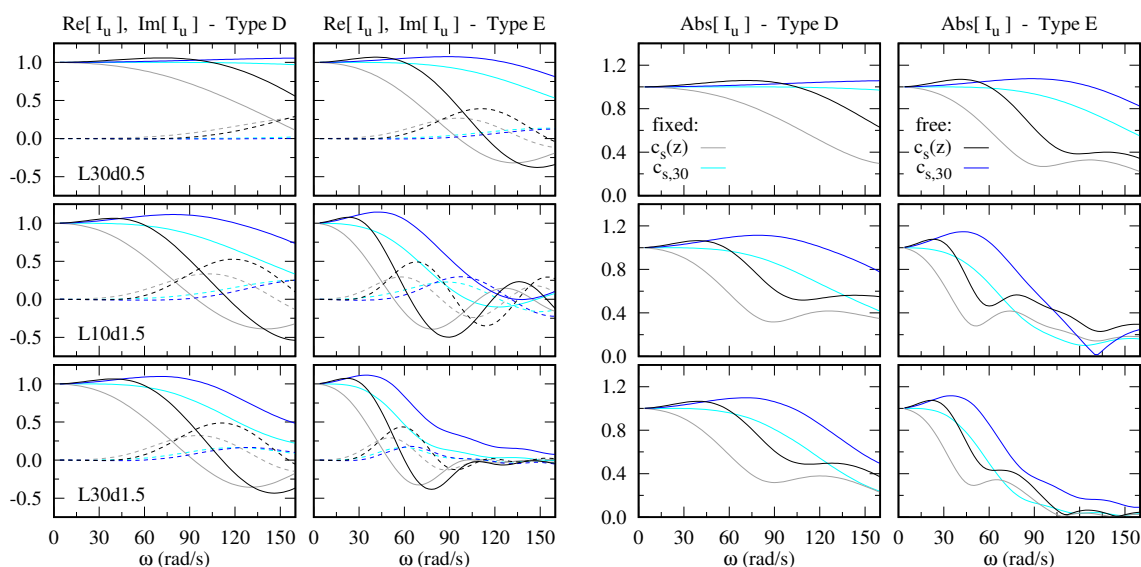


Figure 4.16: Influence of head condition on the translational kinematic interaction factors of single piles. (Imaginary components presented by dashed lines).



acting over it) and a fixed-rotation condition in which the rotation of the pile at head level is imposed to be zero. Fig. 4.16 presents the translational kinematic interaction factors for the representative single pile configurations considering the two studied profiles for each soil types D and E. The results corresponding to the fixed and free head conditions are shown with the light and dark versions of each colour, respectively (see figure key). Restricting the rotation of the pile head results in a reduction in the lateral displacements of the foundation for all the scenarios. This reduction can be explained considering that the fixed condition increases the pile stiffness (as a cantilever beam) and, thus, reduces the response at the pile head. Another approach to explain this phenomenon is the fact that part of the energy transmitted to the pile by the soil is absorbed by the rotation restriction and cannot be transformed into motion.

One aspect to highlight is the fact that there is no frequency range for which the foundation amplifies the ground response if the fixed condition is assumed for the single pile. This absence of amplification is comparable to the behaviour of the fixed-to-the-cap pile groups studied in Section 4.4. On the contrary, for the free-head single piles the amplification of the ground motion can be up to a 20% depending on the pile and soil properties.

Regarding the influence of the variability of the soil profile, its effects are the same regardless the pile head boundary condition. Thus, all the discussion presented in the previous section is valid for both the fixed and free head piles. Also, the frequency dependence of the translational kinematic interaction factors is similar between the two head conditions, with a slight shift of the curves toward smaller frequencies for the fixed-rotation condition.

Fig. 4.17 presents the translational kinematic interaction factors for the representative 3×3 pile groups assuming either a fixed (light colours) or hinged (dark colours) union to the rigid cap. As found for the single pile, the hinged condition at the pile head increases the displacements of the foundation, reaching values of the translational kinematic interaction factor that correspond to amplifications of the ground motion at certain frequencies. As commented in the results of the single pile, there is no change in the importance of the variability of the soil profile with the head condition, and the evolution with frequency of the group displacements moves toward higher frequencies if the piles are hinged.

Fig. 4.18 now shows the rotational kinematic interaction factors for the same 3×3 configurations and head conditions. Note that the trivial comparison between the rotational factors for the single pile was omitted as there is no rotation of the pile head if the fixed condition is assumed. The rotational kinematic interaction factors of the pile groups are strongly affected by the pile-cap union condition. If a hinged union is assumed, the rotation of the pile cap is significantly reduced. Depending on the configuration, reductions over 4 times in the group rotation can be found along wide frequency ranges. This decrement in the rotation of the cap is produced because the rotation induced by the incident field in the piles is no longer transmitted to the cap. Thus, despite from a pile point of view the hinged condition implies larger rotations, articulating the pile-cap union drastically reduces the rotational kinematic interaction factors of the foundation. Note that in Fig. 4.18 the ordinate scale has been amplified in order to see the differences.

Following the same procedure as done for studying the effects of the variability of the soil profile, the influence of the pile head condition over the supported structure is analysed in terms of the differences between the PSA corresponding to the two configurations. For this

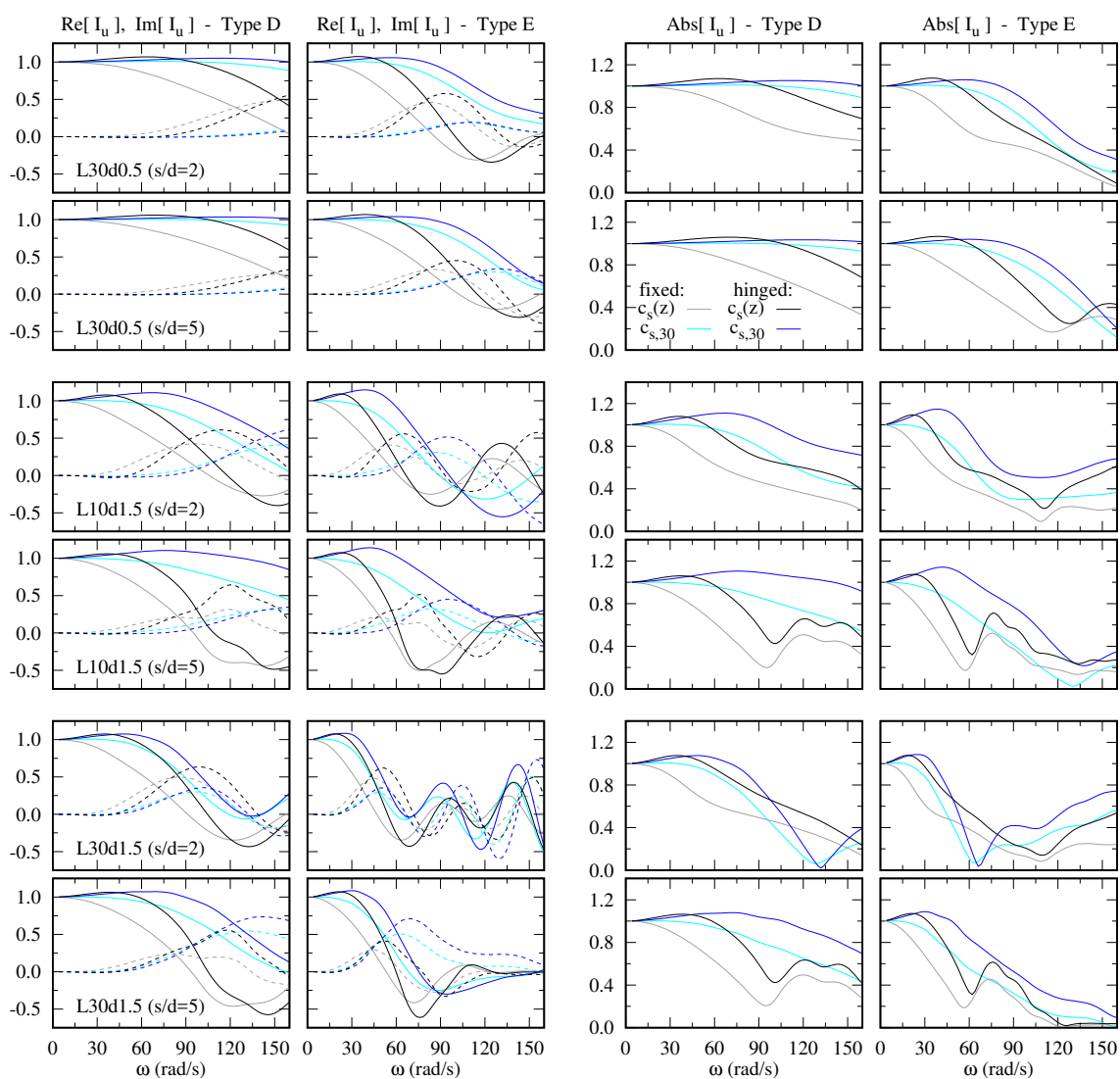


Figure 4.17: Influence of head condition on the translational kinematic interaction factors of 3×3 pile groups. (Imaginary components presented by dashed lines).

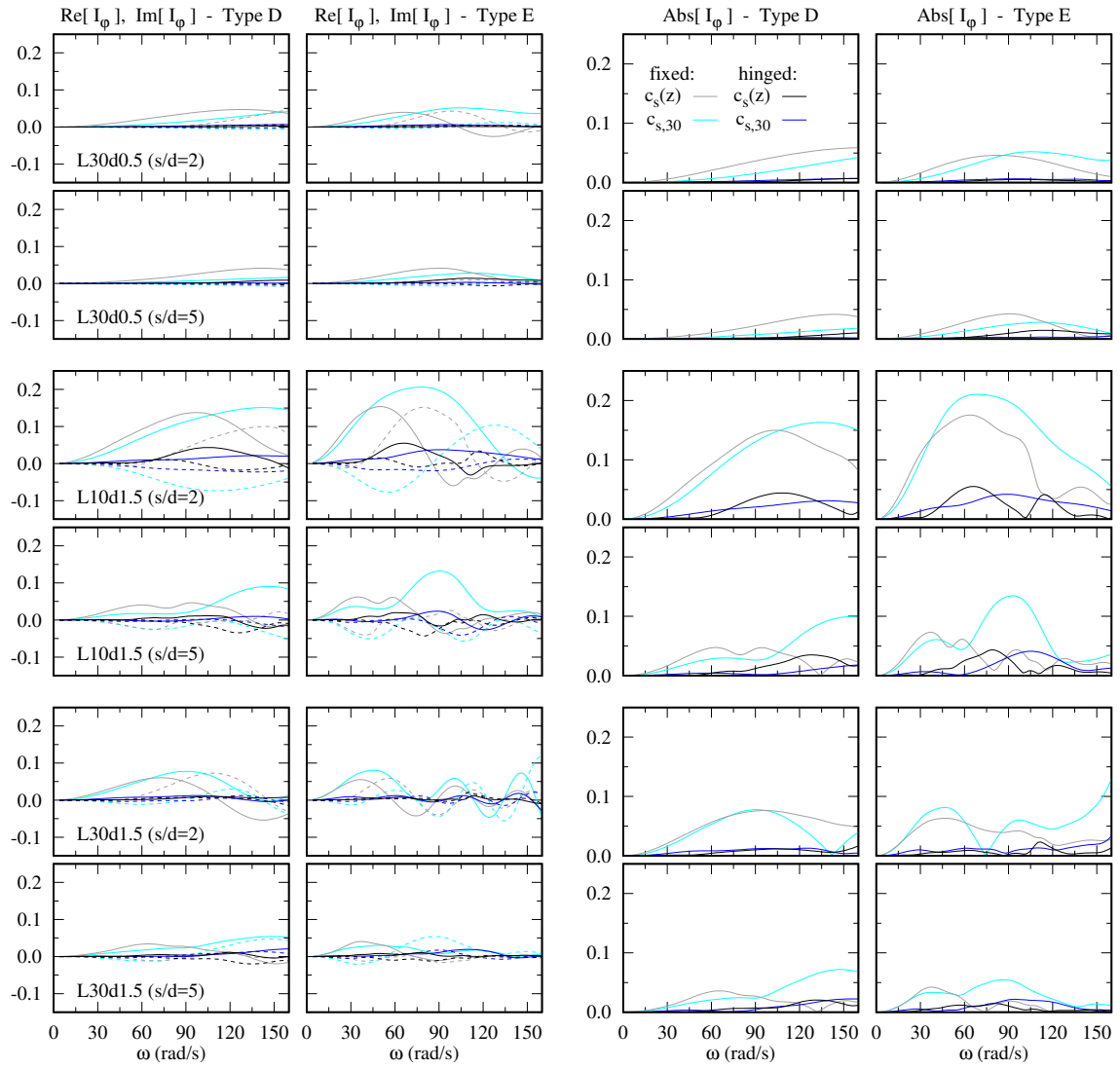


Figure 4.18: Influence of head condition on the rotational kinematic interaction factors of 3×3 pile groups. (Imaginary components presented by dashed lines).

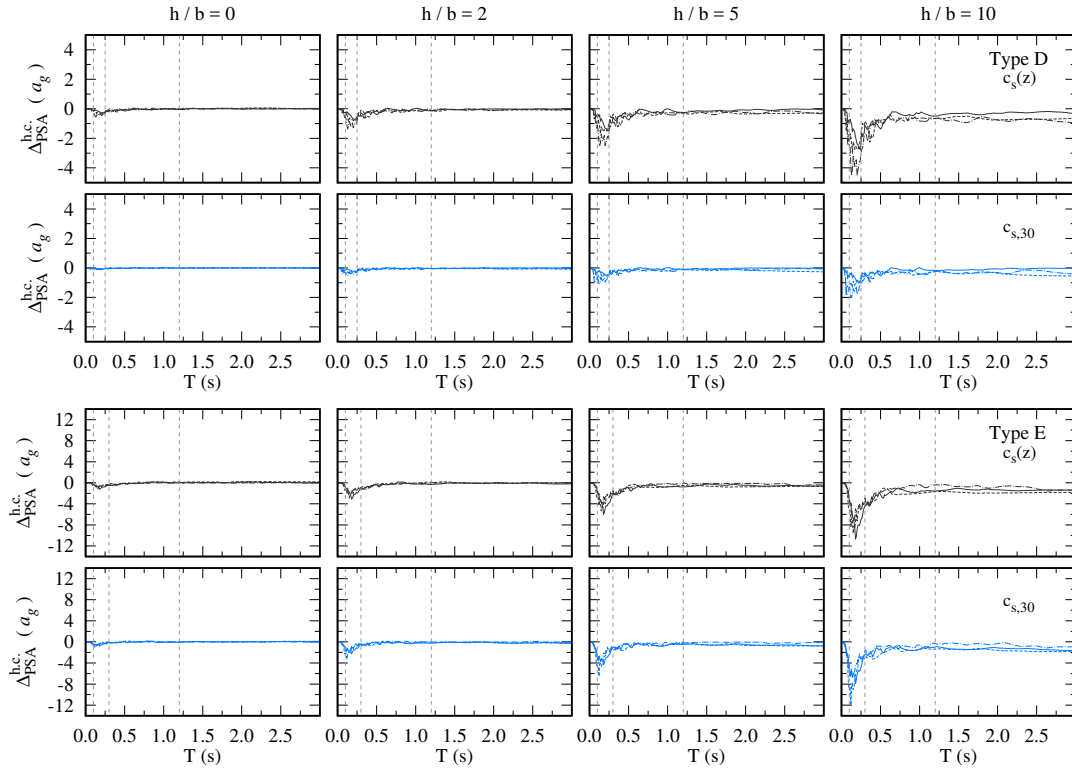


Figure 4.19: Differences between the elastic response spectra of the free and fixed-rotation pile head condition ($\Delta_{PSA}^{h.c.}$). Single pile, configuration *L30d1.5*.

purpose, the magnitude $\Delta_{PSA}^{h.c.}$ is defined as:

$$\Delta_{PSA}^{h.c.}(T) = PSA_{\text{fixed condition}}(T) - PSA_{\text{hinged condition}}(T) \quad (4.4)$$

A positive value of $\Delta_{PSA}^{h.c.}$ implies that the maximum response of the structure is larger when assuming a fixed-head configuration, while a negative value means that the articulation of the pile head leads to higher structural accelerations.

Fig. 4.19 presents the values of $\Delta_{PSA}^{h.c.}$ for the configuration labelled as *L30d1.5* of a single pile embedded in a soil type D or E and considering both the variable (dark grey) and equivalent homogeneous (blue) profile. For the single pile foundation, the effect of the pile head condition is the same for all the scenarios: the free-head foundation leads to a higher structural response in terms of maximum accelerations. Note that the magnitude of the translational and rotational kinematic interaction factors is larger for the free-head condition than for the fixed-rotation one. The difference between the two head types increases for slender structures due to the contribution of the foundation rotation (which is zero for the fixed-head). As found for the differences associated to the variability of the soil profile, the effects of the pile head conditions are amplified for the softest soil type and the maximum values are found for structural periods near 0.15 s. Note that the scale of the ordinate axes has been increased for Fig. 4.19.

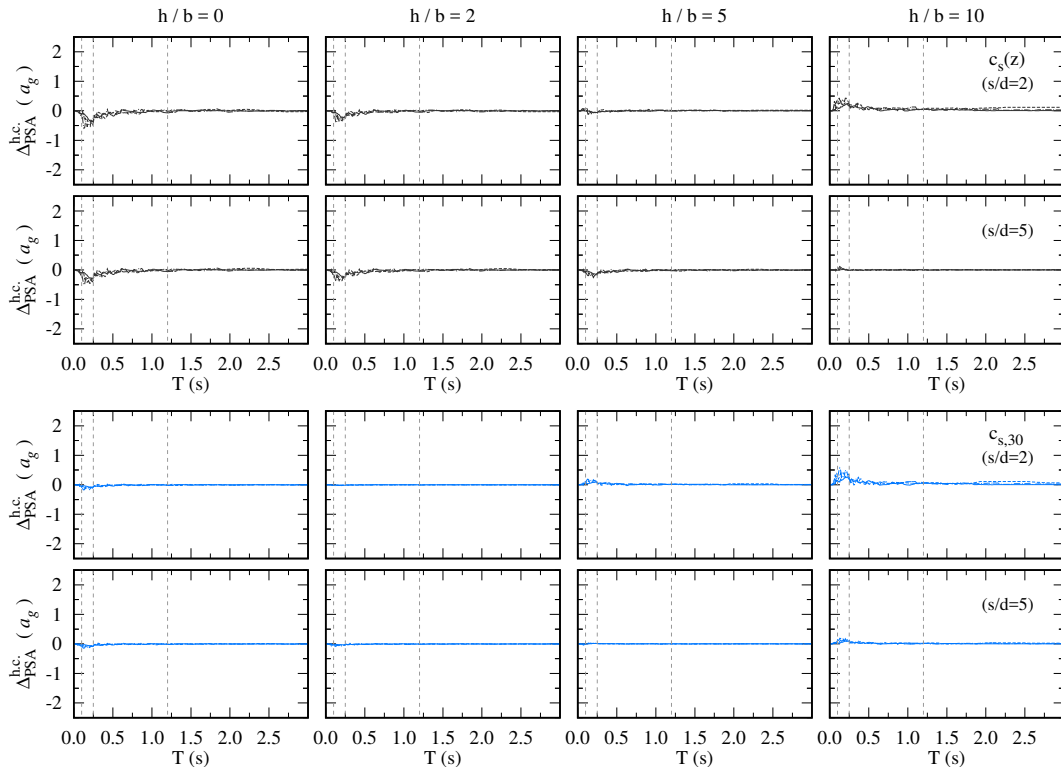


Figure 4.20: Differences between the elastic response spectra of the hinged and fixed pile-cap union condition ($\Delta_{PSA}^{h.c.}$). 3×3 pile group, configuration $L30d1.5$. Soil Type D.

The differences in the structural acceleration spectra associated to the pile-cap union condition for the representative configuration $L30d1.5$ of 3×3 pile groups are shown in Fig. 4.20 for soil type D and in Fig. 4.21 for soil type E. For the group configuration two different effects are found depending on the slenderness of the supported structure. For short buildings, assuming a hinged pile-cap union leads to higher accelerations as the response of these configurations are governed by the translational kinematic interaction factors (which are larger for the hinged piles). On the other hand, for slender structures the opposite effect is found due to the reduction in the rotational kinematic interaction factors that is produced by the articulation of the pile heads. Thus, for slender buildings the fixed pile-cap union produces a higher structural response. This effect is more important for configurations with larger rotations (i.e., small number of piles and close separation distances).

In order to complete the information for all of the representative configurations, Tables 4.5 and 4.6 (soil type D) and Tables 4.7 and 4.8 (soil type E) present the values of $\Delta_{PSA}^{h.c.}$ that correspond to the largest differences associated to the pile head condition. Tables 4.5 and 4.7 display the values for which the fixed condition leads to the maximum structural response, while Tables 4.6 and 4.8 show the highest differences for which the hinged assumption is more unfavourable. Furthermore, the text colour of each value indicates if the maximum difference is produced for the variable (black) or equivalent homogeneous (blue) soil profile.

As commented before, it can be found that for short structures the pile group configu-

Configuration	$h/b = 0$				$h/b = 2$				$h/b = 5$				$h/b = 10$			
	T_1	T_2	T_3	T_4	T_1	T_2	T_3	T_4	T_1	T_2	T_3	T_4	T_1	T_2	T_3	T_4
L30d0.5																
single	-0.1	-0.2	-0.1	-0.0	-0.3	-0.4	-0.3	-0.0	-0.6	-0.8	-0.5	-0.1	-1.2	-1.3	-0.8	-0.3
2x2sd2	-0.1	-0.2	-0.1	-0.0	-0.1	-0.1	-0.0	-0.0	-0.0	+0.0	-0.0	-0.0	-0.0	+0.0	-0.0	-0.0
2x2sd5	-0.1	-0.2	-0.1	-0.0	-0.1	-0.1	-0.1	-0.0	-0.0	-0.1	-0.0	-0.0	-0.0	+0.0	-0.0	-0.0
3x3sd2	-0.1	-0.2	-0.1	-0.0	-0.1	-0.2	-0.1	-0.0	-0.0	-0.1	-0.0	-0.0	-0.0	+0.0	-0.0	-0.0
3x3sd5	-0.1	-0.2	-0.1	-0.0	-0.1	-0.2	-0.1	-0.0	-0.1	-0.1	-0.1	-0.0	-0.0	-0.0	-0.0	-0.0
L10d1.5																
single	-0.2	-0.5	-0.3	-0.1	-0.6	-1.3	<u>-0.8</u>	-0.2	-1.3	-2.5	<u>-1.6</u>	<u>-0.4</u>	-2.5	-4.5	<u>-3.0</u>	-0.9
2x2sd2	-0.1	-0.5	-0.3	-0.1	-0.0	-0.1	-0.1	-0.0	-0.0	+0.1	-0.0	+0.0	-0.0	+0.2	-0.0	+0.0
2x2sd5	-0.2	-0.5	-0.3	-0.1	-0.1	-0.2	-0.2	-0.0	-0.0	+0.0	-0.0	-0.0	-0.0	+0.1	-0.0	+0.0
3x3sd2	-0.1	-0.5	-0.4	-0.1	-0.0	-0.2	-0.2	-0.0	-0.0	+0.1	-0.0	-0.0	-0.0	+0.1	-0.0	+0.0
3x3sd5	-0.2	-0.5	-0.3	-0.1	-0.1	-0.3	-0.2	-0.1	-0.1	-0.1	-0.1	-0.0	-0.1	+0.0	-0.0	-0.0
L30d1.5																
single	<u>-0.2</u>	-0.5	-0.3	-0.1	<u>-0.6</u>	<u>-1.3</u>	-0.8	<u>-0.2</u>	<u>-1.3</u>	<u>-2.5</u>	-1.6	-0.4	<u>-2.5</u>	-4.6	-3.0	<u>-0.9</u>
2x2sd2	-0.1	-0.5	-0.3	-0.1	-0.0	-0.3	-0.2	-0.0	-0.0	+0.0	-0.0	-0.0	-0.0	+0.1	-0.0	+0.0
2x2sd5	-0.2	-0.5	-0.3	-0.1	-0.1	-0.3	-0.2	-0.0	-0.0	-0.1	-0.1	-0.0	-0.0	+0.1	-0.0	-0.0
3x3sd2	-0.2	-0.6	<u>-0.4</u>	<u>-0.1</u>	-0.1	-0.4	-0.3	-0.1	-0.0	-0.1	-0.1	-0.0	-0.0	+0.1	-0.0	+0.0
3x3sd5	-0.2	-0.5	-0.3	-0.1	-0.1	-0.4	-0.3	-0.1	-0.1	-0.3	-0.2	-0.0	-0.1	-0.0	-0.0	-0.0

[†] **Bolded** items correspond to the minimum value of the row. Underlined items correspond to the minimum value of the column.

^{††} **Blue** items indicates that the minimum corresponds to the equivalent homogeneous profile, while black items correspond to the variable profile.

^{†††} Definition of the period ranges: $T_1 \equiv T \in [0, 0.1)$ s; $T_2 \equiv T \in [0.1, 0.25)$ s; $T_3 \equiv T \in [0.25, 1.2)$ s; $T_4 \equiv T \in [1.2, 3]$ s.

Table 4.5: Differences between the PSA of the fixed and hinged head conditions $\Delta_{PSA}^{h.c.}$ (units in q_g). Minimum values (higher response for hinged condition) for different period ranges. Soil type D.

Configuration	$h/b = 0$				$h/b = 2$				$h/b = 5$				$h/b = 10$			
	T_1	T_2	T_3	T_4	T_1	T_2	T_3	T_4	T_1	T_2	T_3	T_4	T_1	T_2	T_3	T_4
L30d0.5																
single	+0.0	-0.0	+0.0	+0.0	+0.0	-0.0	+0.0	+0.0	+0.0	-0.0	+0.0	+0.0	+0.0	-0.0	+0.0	+0.0
2x2sd2	+0.0	-0.0	+0.0	+0.0	+0.0	+0.0	+0.0	+0.0	+0.0	+0.1	+0.0	+0.0	+0.2	+0.3	+0.2	+0.1
2x2sd5	+0.0	-0.0	+0.0	+0.0	+0.0	-0.0	+0.0	+0.0	+0.0	+0.0	+0.0	+0.0	+0.1	+0.1	+0.1	+0.0
3x3sd2	+0.0	-0.0	+0.0	+0.0	+0.0	-0.0	+0.0	+0.0	+0.0	+0.0	+0.0	+0.0	+0.1	+0.1	+0.1	+0.0
3x3sd5	+0.0	-0.0	+0.0	+0.0	+0.0	-0.0	+0.0	+0.0	+0.0	+0.0	+0.0	+0.0	+0.0	+0.0	+0.0	+0.0
L10d1.5																
single	+0.0	-0.0	+0.1	+0.1	+0.0	-0.1	+0.1	+0.0	+0.0	-0.2	+0.0	-0.0	-0.0	-0.3	+0.0	-0.0
2x2sd2	+0.0	-0.0	+0.0	+0.1	<u>+0.1</u>	<u>+0.1</u>	+0.1	+0.0	+0.4	<u>+0.5</u>	<u>+0.3</u>	<u>+0.1</u>	<u>+0.8</u>	+1.5	<u>+0.9</u>	<u>+0.3</u>
2x2sd5	+0.0	-0.0	+0.0	+0.1	+0.0	+0.0	+0.0	+0.0	+0.1	+0.3	+0.1	+0.0	+0.5	+0.9	+0.5	+0.1
3x3sd2	+0.0	-0.0	+0.0	+0.1	+0.0	+0.1	+0.0	+0.0	+0.3	+0.4	+0.2	+0.1	<u>+0.8</u>	+1.1	+0.7	+0.2
3x3sd5	+0.0	-0.0	+0.1	+0.1	+0.0	-0.0	+0.0	+0.0	+0.0	+0.1	+0.1	+0.0	+0.1	+0.4	+0.2	+0.1
L30d1.5																
single	+0.0	-0.0	<u>+0.1</u>	+0.1	+0.0	-0.1	+0.1	+0.0	+0.0	-0.2	+0.0	-0.0	+0.0	-0.3	+0.0	-0.0
2x2sd2	+0.0	-0.0	+0.0	+0.1	+0.0	+0.0	+0.0	+0.0	+0.2	+0.3	+0.2	+0.1	+0.6	+0.9	+0.5	+0.2
2x2sd5	+0.0	-0.0	+0.1	+0.1	+0.0	-0.0	+0.0	+0.0	+0.1	+0.1	+0.1	+0.0	+0.3	+0.4	+0.2	+0.1
3x3sd2	+0.0	-0.0	+0.0	<u>+0.1</u>	+0.0	+0.0	+0.0	+0.0	+0.1	+0.2	+0.1	+0.0	+0.4	+0.6	+0.3	+0.1
3x3sd5	+0.0	-0.0	+0.1	+0.1	+0.0	-0.0	+0.0	+0.0	+0.0	+0.0	+0.0	+0.0	+0.1	+0.2	+0.1	+0.0

[†] **Bolded** items correspond to the maximum value of the row. Underlined items correspond to the maximum value of the column.

^{††} **Blue** items indicates that the maximum corresponds to the equivalent homogeneous profile, while black items correspond to the variable profile.

^{†††} Definition of the period ranges: $T_1 \equiv T \in [0, 0.1)$ s; $T_2 \equiv T \in [0.1, 0.25)$ s; $T_3 \equiv T \in [0.25, 1.2)$ s; $T_4 \equiv T \in [1.2, 3]$ s.

Table 4.6: Differences between the PSA of the fixed and hinged head conditions $\Delta_{PSA}^{\text{h.c.}}$ (units in a_g). Maximum values (higher response for fixed condition) for different period ranges. Soil type D.

Configuration	$h/b=0$				$h/b=2$				$h/b=5$				$h/b=10$				
	T_1	T_2	T_3	T_4	T_1	T_2	T_3	T_4	T_1	T_2	T_3	T_4	T_1	T_2	T_3	T_4	
L30d0.5	single	<u>-0.9</u>	-1.1	-0.2	-0.0	-2.0	-2.3	-0.6	-0.2	-3.7	-4.1	-1.1	-0.6	-6.6	-7.1	-2.2	-1.4
	2x2sd2	-0.8	-1.0	-0.2	-0.1	-0.4	-0.5	-0.1	-0.0	-0.0	-0.1	-0.0	-0.0	-0.0	-0.0	-0.0	-0.0
	2x2sd5	-0.8	-1.0	-0.2	-0.1	-0.6	-0.7	-0.2	-0.1	-0.1	-0.3	-0.1	-0.0	-0.0	-0.0	-0.0	-0.0
	3x3sd2	-0.8	-1.0	-0.3	-0.1	-0.5	-0.8	-0.2	-0.1	-0.1	-0.3	-0.1	-0.0	-0.0	-0.0	-0.0	-0.0
	3x3sd5	-0.9	-1.0	-0.2	-0.1	-0.7	-0.8	-0.2	-0.1	-0.4	-0.5	-0.2	-0.1	-0.1	-0.1	-0.1	-0.0
L10d1.5	single	-0.9	-1.2	-0.6	-0.1	<u>-2.6</u>	<u>-3.3</u>	<u>-1.4</u>	<u>-0.4</u>	<u>-5.4</u>	<u>-6.7</u>	<u>-2.5</u>	<u>-1.2</u>	<u>-10.5</u>	<u>-12.3</u>	<u>-4.5</u>	<u>-2.5</u>
	2x2sd2	-0.6	-0.8	-0.5	-0.1	-0.1	-0.0	-0.0	-0.0	-0.0	+0.5	+0.0	+0.0	-0.0	+1.5	+0.3	+0.2
	2x2sd5	-0.8	-1.0	-0.6	-0.1	-0.3	-0.4	-0.2	-0.1	-0.0	+0.2	-0.2	-0.0	-0.0	+0.9	-0.0	-0.0
	3x3sd2	-0.8	-1.0	-0.7	-0.1	-0.2	-0.2	-0.2	-0.1	-0.1	+0.5	-0.0	-0.0	-0.0	+1.5	+0.2	+0.1
	3x3sd5	-0.8	-1.0	-0.6	-0.1	-0.4	-0.8	-0.3	-0.1	-0.1	-0.3	-0.1	-0.1	-0.0	+0.2	-0.2	-0.0
L30d1.5	single	-0.8	<u>-1.2</u>	-0.6	-0.1	-2.2	-3.3	-1.4	-0.3	-4.4	-6.5	-2.5	-0.8	-8.2	-12.0	-4.4	-2.0
	2x2sd2	-0.5	-1.0	-0.6	-0.1	-0.1	-0.4	-0.3	-0.0	+0.0	+0.1	-0.1	-0.1	+0.0	+0.8	-0.1	+0.0
	2x2sd5	-0.6	-1.1	-0.6	-0.1	-0.2	-0.7	-0.4	-0.0	-0.1	-0.2	-0.1	-0.1	+0.0	+0.2	-0.1	-0.0
	3x3sd2	-0.3	-1.0	<u>-0.7</u>	-0.1	-0.2	-0.6	-0.5	-0.0	-0.1	-0.1	-0.2	-0.0	-0.0	+0.4	-0.0	-0.0
	3x3sd5	-0.7	-1.1	-0.6	<u>-0.1</u>	-0.5	-0.9	-0.5	-0.1	-0.2	-0.6	-0.3	-0.1	-0.1	-0.1	-0.1	-0.1

[†] **Bolded** items correspond to the minimum value of the row. Underlined items correspond to the minimum value of the column.

^{††} **Blue** items indicates that the minimum corresponds to the equivalent homogeneous profile, while black items correspond to the variable profile.

^{†††} Definition of the period ranges: $T_1 \equiv T \in [0, 0.1]$ s; $T_2 \equiv T \in [0.1, 0.3]$ s; $T_3 \equiv T \in [0.3, 1.2]$ s; $T_4 \equiv T \in [1.2, 3]$ s.

Table 4.7: Differences between the PSA of the fixed and hinged head conditions $\Delta_{PSA}^{h,c}$ (units in q_g). Minimum values (higher response for hinged condition) for different period ranges. Soil type E.

Configuration	$h/b = 0$				$h/b = 2$				$h/b = 5$				$h/b = 10$			
	T_1	T_2	T_3	T_4	T_1	T_2	T_3	T_4	T_1	T_2	T_3	T_4	T_1	T_2	T_3	T_4
L30d0.5																
single	+0.0	<u>+0.1</u>	+0.2	+0.2	+0.0	<u>+0.0</u>	+0.2	+0.1	<u>+0.0</u>	<u>+0.0</u>	+0.1	<u>+0.0</u>	<u>+0.0</u>	-0.1	-0.0	-0.0
2x2sd2	<u>+0.0</u>	<u>+0.0</u>	+0.2	+0.1	<u>+0.0</u>	<u>+0.0</u>	+0.1	+0.1	<u>+0.3</u>	<u>+0.4</u>	+0.1	+0.1	+1.3	+1.4	+0.5	+0.4
2x2sd5	+0.0	<u>+0.0</u>	+0.2	+0.1	+0.0	+0.0	+0.1	+0.1	<u>+0.1</u>	<u>+0.2</u>	+0.1	+0.1	+0.6	+0.7	+0.2	+0.2
3x3sd2	<u>+0.0</u>	<u>+0.0</u>	+0.2	+0.2	<u>+0.0</u>	+0.0	+0.2	+0.2	<u>+0.2</u>	<u>+0.2</u>	+0.1	+0.1	+0.7	+0.8	+0.3	+0.2
3x3sd5	+0.0	<u>+0.0</u>	+0.2	+0.1	+0.0	+0.0	+0.1	+0.1	<u>+0.0</u>	<u>+0.0</u>	+0.1	+0.1	<u>+0.2</u>	+0.3	<u>+0.1</u>	<u>+0.1</u>
L10d1.5																
single	+0.0	<u>+0.0</u>	<u>+0.2</u>	+0.2	+0.0	-0.1	+0.2	+0.2	+0.0	-1.0	-0.1	-0.0	-0.0	-2.4	-0.5	-0.5
2x2sd2	<u>+0.0</u>	-0.0	+0.1	+0.1	<u>+0.7</u>	<u>+0.9</u>	<u>+0.3</u>	<u>+0.2</u>	<u>+2.9</u>	<u>+3.4</u>	<u>+1.1</u>	<u>+0.9</u>	<u>+6.6</u>	<u>+7.6</u>	<u>+2.6</u>	<u>+2.0</u>
2x2sd5	+0.0	<u>+0.0</u>	<u>+0.2</u>	+0.2	+0.0	<u>+0.3</u>	+0.1	+0.1	+1.3	+2.2	+0.7	+0.3	+4.1	+5.8	+1.8	+1.1
3x3sd2	<u>+0.0</u>	-0.1	+0.2	+0.2	+0.4	+0.6	+0.2	+0.1	+2.3	+3.1	+1.0	+0.6	+5.7	+7.5	<u>+2.5</u>	+1.7
3x3sd5	+0.0	<u>+0.0</u>	<u>+0.2</u>	+0.2	<u>+0.0</u>	<u>+0.0</u>	+0.1	+0.1	+0.4	+0.4	+0.3	+0.1	+1.3	+1.7	+0.8	+0.5
L30d1.5																
single	+0.0	<u>+0.0</u>	<u>+0.2</u>	+0.2	+0.0	-0.2	+0.1	<u>+0.2</u>	+0.0	-1.0	-0.1	+0.0	-0.0	-2.4	-0.2	-0.1
2x2sd2	-0.0	-0.1	+0.1	+0.1	<u>+0.1</u>	<u>+0.2</u>	+0.1	+0.1	<u>+0.7</u>	<u>+1.5</u>	<u>+0.5</u>	<u>+0.3</u>	+1.6	+3.8	+1.2	+0.7
2x2sd5	+0.0	-0.1	+0.1	+0.2	+0.0	-0.0	+0.1	+0.1	<u>+0.4</u>	<u>+0.6</u>	<u>+0.2</u>	<u>+0.1</u>	+1.5	+2.4	+0.7	+0.4
3x3sd2	-0.0	-0.1	+0.2	+0.1	<u>+0.0</u>	-0.0	+0.1	+0.1	+0.4	<u>+0.8</u>	<u>+0.3</u>	<u>+0.2</u>	+1.3	+2.5	+1.0	+0.6
3x3sd5	+0.0	-0.1	+0.1	+0.2	+0.0	-0.0	+0.1	+0.1	<u>+0.0</u>	<u>+0.1</u>	<u>+0.1</u>	<u>+0.1</u>	<u>+0.4</u>	+0.5	<u>+0.3</u>	<u>+0.2</u>

[†] **Bolded** items correspond to the maximum value of the row. Underlined items correspond to the maximum value of the column.

^{††} **Blue** items indicates that the maximum corresponds to the equivalent homogeneous profile, while black items correspond to the variable profile.

^{†††} Definition of the period ranges: $T_1 \equiv T \in [0, 0.1)$ s; $T_2 \equiv T \in [0.1, 0.3)$ s; $T_3 \equiv T \in [0.3, 1.2)$ s; $T_4 \equiv T \in [1.2, 3]$ s.

Table 4.8: Differences between the PSA of the fixed and hinged head conditions $\Delta_{PSA}^{h.c.}$ (units in a_g). Maximum values (higher response for fixed condition) for different period ranges. Soil type E.

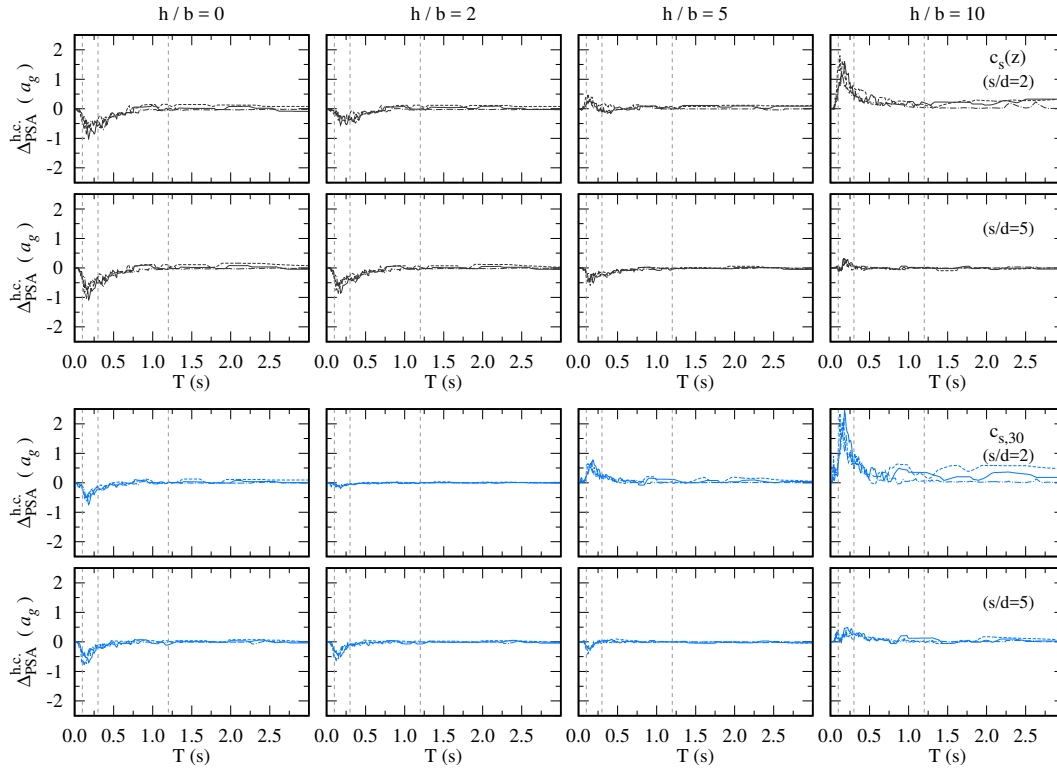


Figure 4.21: Differences between the elastic response spectra of the hinged and fixed pile-cap union condition ($\Delta_{PSA}^{h.c.}$). 3×3 pile group, configuration $L30d1.5$. Soil Type E.

rations with hinged piles produce a higher structural response. For slender buildings, on the contrary, the fixed pile-cap union leads to larger maximum acceleration of the supported structure. The influence of the pile head condition is more important for the softer soil type, specially to the period range corresponding to the constant zone of the normalized spectrum ($T_1 < T < T_2$). The configuration most sensitive to the pile head condition is again the one labelled as $L10d1.5$, corresponding to the foundation with the shortest piles. Attending to the text colour of the results, it is found that the scenarios in which the hinged condition leads to higher structural responses are produced for the variable profile, while the cases with higher accelerations for the hinged piles generally correspond to the homogeneous profile. However, attending to the results presented in Figs. 4.20 and 4.21, the magnitude of the differences due to the pile head condition is found to be similar regardless the variation of the soil profile.

4.7 Pile kinematic bending moments

The seismic analysis of the pile foundations is completed by studying how the kinematic bending moments of the piles are affected by the variability of the soil profile and the pile head condition. For this purpose, envelopes of maximum bending moments are obtained for the six studied pile geometries (diameters and lengths). As stated for the PSA analyses, the standard frequency domain method [67] is followed in order to obtain the time response of

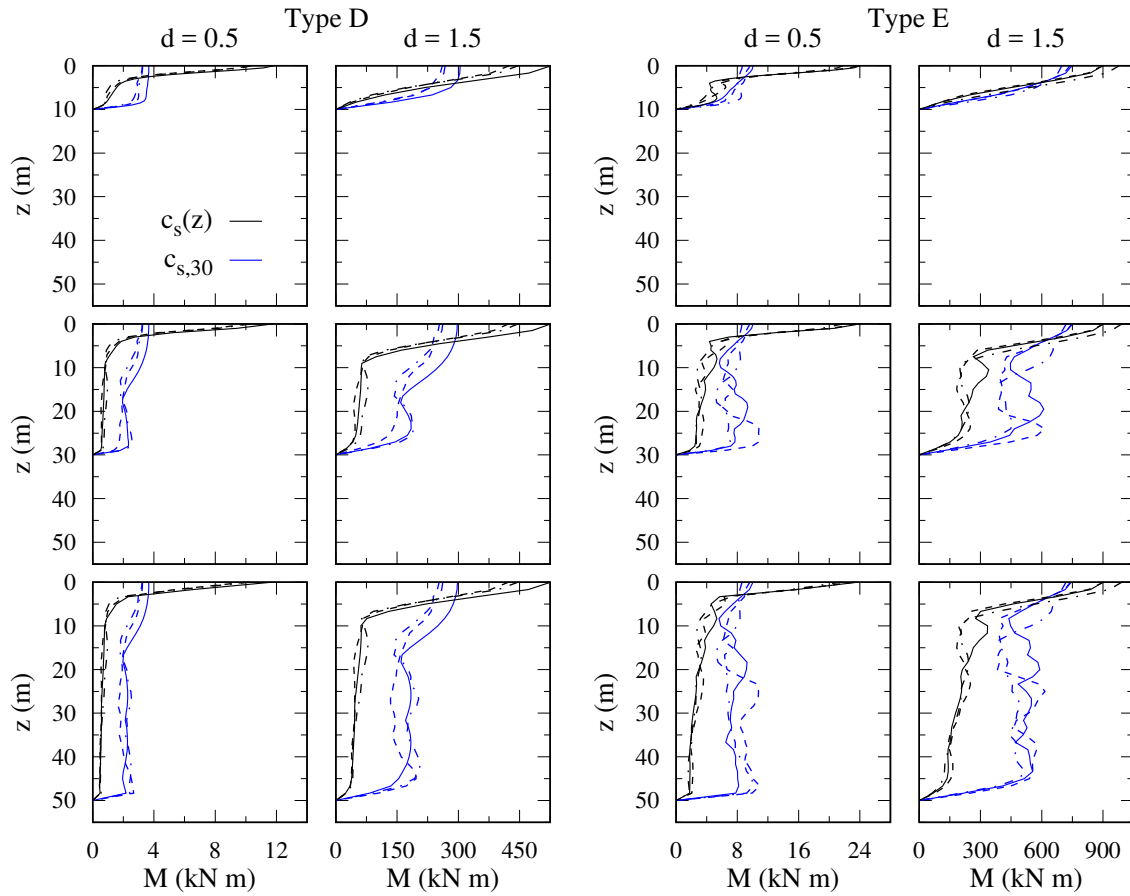


Figure 4.22: Influence of the variability of the soil profile on the pile envelope of maximum bending moments. Fixed-rotation at head single piles.

the piles. In order to present the bending moments in physical units, a maximum ground acceleration $a_g = 0.25g$ is assumed.

Fig. 4.22 shows the envelopes of maximum bending moments for the fixed-head single piles embedded in soil types D and E. The results for each diameter value are shown in different columns, while the envelopes of the different pile lengths are displayed in different rows. As done in the previous sections, the results corresponding to the variable profile are shown with black lines, while the ones of the homogeneous equivalent profile are displayed by blue lines. The different line types correspond to the three studied accelerograms per soil type following Fig. 4.4.

The results show that the maximum bending moments at the pile head that are obtained for the variable profile are significantly larger than the ones obtained by assuming an equivalent homogeneous profile with identical $c_{s,30}$. For configurations with small diameter, the value of the head bending moments considering the variable profile can be more than three times larger than the ones of the homogeneous media. The differences in the head bending moment are significant for both soil types, being the relative difference slightly higher for soil type D. This increase in the value of the bending moment is produced due to the softer superficial

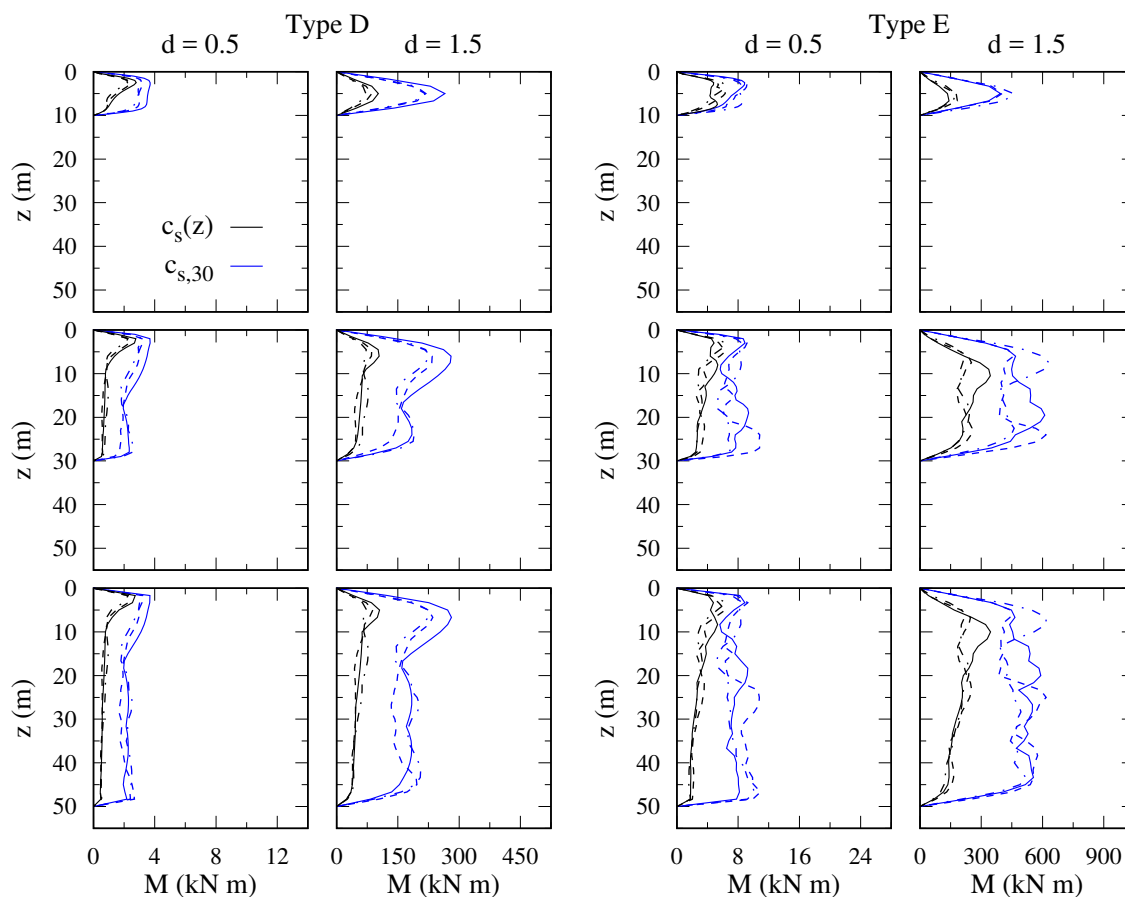


Figure 4.23: Influence of the variability of the soil profile on the pile envelope of maximum bending moments. Free-head single pile.

layers that constitute the variable profile. On the other hand, for the rest of the pile length (approximately below 5 m), the maximum bending moments obtained by the homogeneous assumption significantly overtake the ones of the variable profile.

The over-estimation of the envelope of bending moments by the homogeneous profile can be found along all the pile length for the free-head pile configurations, as illustrated by Fig. 4.23. Note that the envelopes obtained by the homogeneous profile can be over three times larger than the ones produced by the actual variable profile along all the pile. Thus, for estimating the pile maximum bending moments the homogeneous assumption is not accurate.

To verify that the conclusions obtained for the single pile can be extrapolated to pile group configurations, Figs. 4.24 (fixed condition) and 4.25 (hinged condition) show the envelopes of maximum bending moments obtained for the different studied pile groups together with the results of the corresponding single pile. For clarity's sake, only the results obtained for one of the three used accelerograms per soil type are shown (Coalinga-01 and Imperial Valley-06). This choice of input signals does not alter the conclusions of the analysis. For the 3×3 pile group only the envelopes corresponding to the central pile are shown, but the effect of the pile position on the maximum bending moments is discussed later in this section.

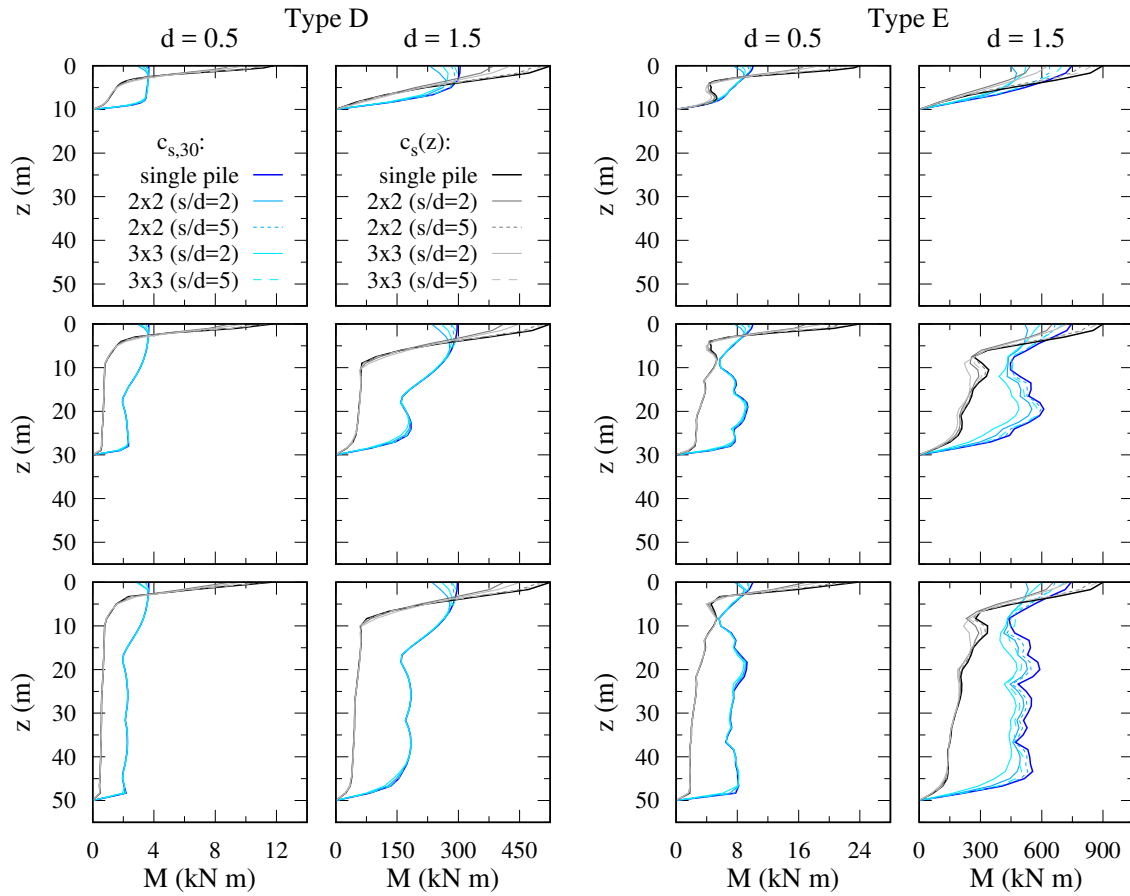


Figure 4.24: Influence of the group configuration on the pile envelope of maximum bending moments. Fixed pile-cap union condition.

Attending to the obtained results, it is found that the envelopes of the single pile configurations accurately estimate the maximum bending moments of the piles within the groups. Pile-to-pile interaction effects play a minor role in the envelopes, being noticeable only for the configurations with closer piles ($s/d = 2$) and large diameters ($d = 1.5$ m). The pile-to-pile interaction is more important for soft soils. Thus, greater differences are appreciated for the soil type E and the superficial layers of the variable profile. Also, the pile-to-pile interaction effects can be observed at the maximum bending moments at pile head level for the configurations with restricted rotation. As consequence of the interaction between piles, the maximum bending moments obtained for the piles within the group are slightly smaller than the ones corresponding to the single pile configurations, being this effect more important as the number of piles increases or the separation distance decreases.

The influence of the position of the pile within the group is analysed through Fig. 4.26, which presents the envelopes corresponding to the four different pile positions (due symmetry) in the 3×3 group by using different line styles. It is found that the variations between the different piles in the group are almost negligible, being observable only for the configurations of large diameters in soft soils and specially at the pile head level. For this reason, the

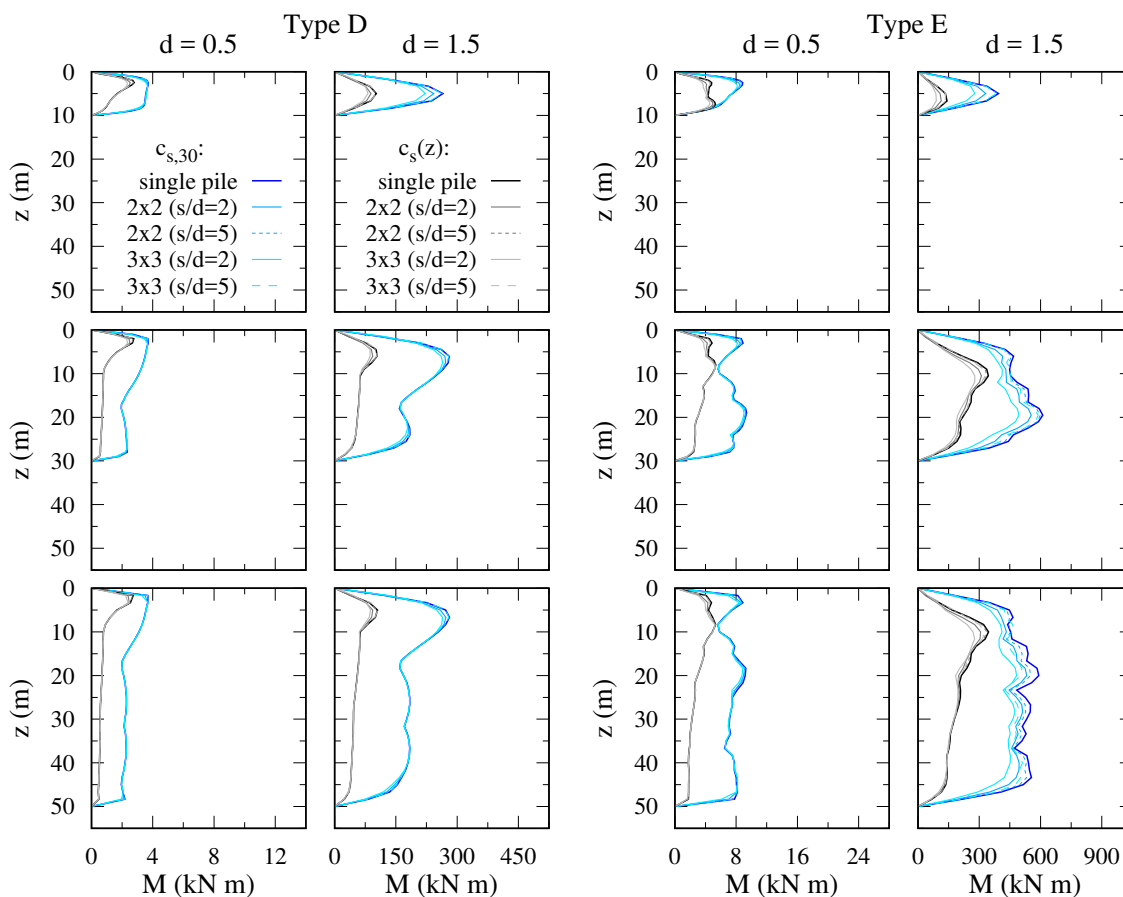


Figure 4.25: Influence of the group configuration on the pile envelope of maximum bending moments. Hinged pile-cap union condition.

comparison for the hinged head configurations are not shown. Note that the results presented in Fig. 4.23 correspond to the configuration with closest piles ($s/d = 2$) and, therefore, with larger pile-to-pile interaction effects.

In order to finish this study, Fig. 4.27 presents the envelopes of maximum bending moments for a large configuration based on one of the buildings studied in [124]. The pile group is composed by a regular 13×4 distribution of piles with a separation $s/d = 11$. The pile diameter and length values are assumed to be 0.5 m and 10 m, respectively. Also, the rest of the pile material properties are considered to be equal to the ones used along this chapter.

Fig. 4.27 presents the envelopes obtained by assuming the two profile variations per soil type. As the pile distribution is not symmetric, the two scenarios for which the incident field acts parallel (label 13×4) or perpendicular (label 4×13) to the direction of alignment of the 13 piles are considered. The envelopes of all the piles of the group are plotted superimposed by using the same line type (light colour) and are compared to the results of the corresponding single pile (dark colour) configuration. It is verified that the results of the single pile accurately estimate the envelopes of maximum bending moments of the piles in the large group. Due to the large separation value, the interaction between piles is virtually negligible in this

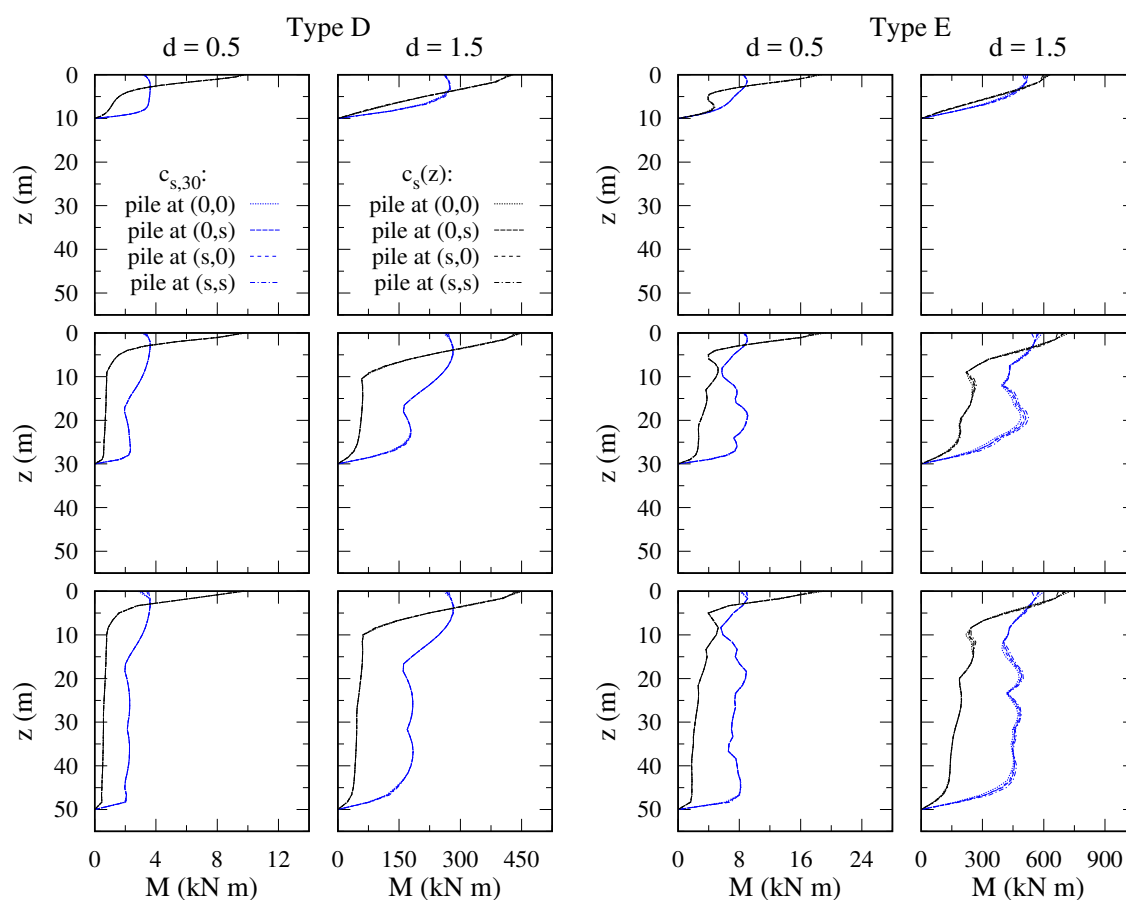


Figure 4.26: Influence of the pile position in the group on the envelope of maximum bending moments. 3×3 pile group ($s/d = 2$) with fixed pile-cap union condition.

configuration, being the only differences observable at the pile head moments.

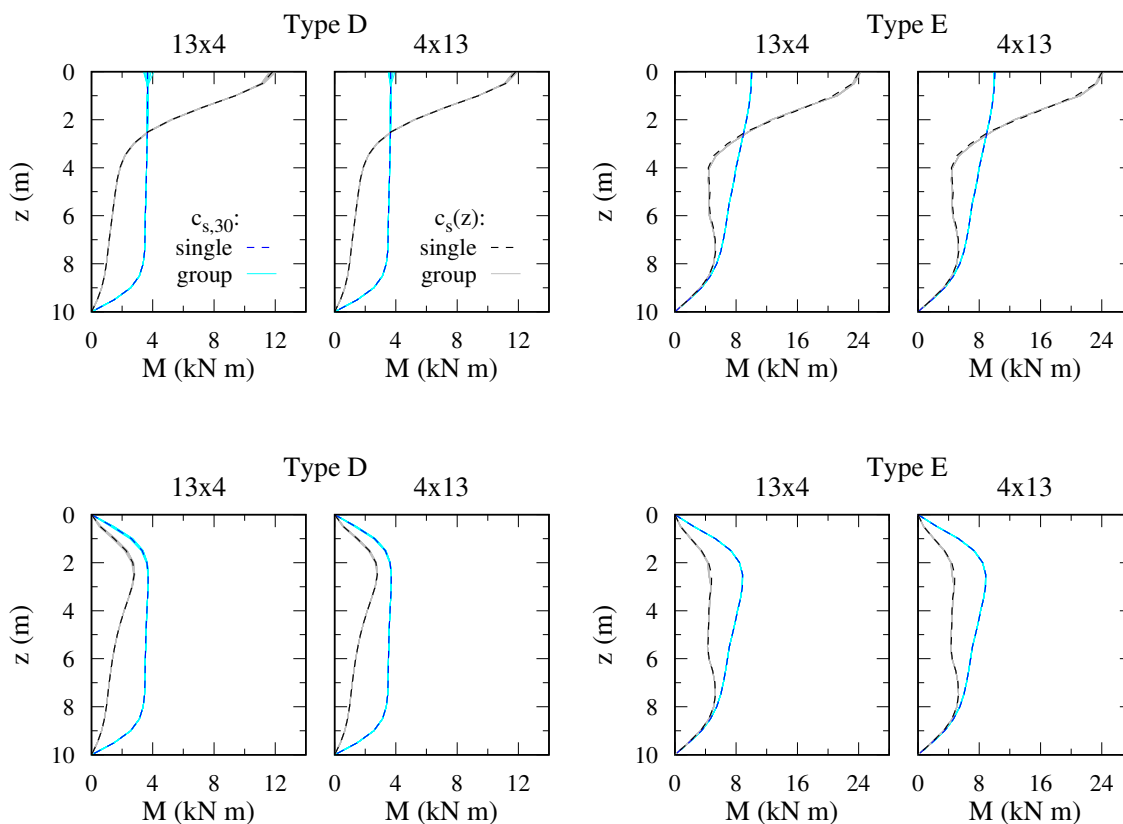


Figure 4.27: Envelopes of maximum bending moments for a large pile foundation.

4.8 Conclusions

In this chapter, the developed integral model is used for the analysis of the seismic response of pile foundations. Special attention is given to the effects of considering the variability with depth of the soil profile. For this purpose, variable profiles representative of different soil types are compared with homogeneous half spaces that are equivalent in terms of the mean shear wave velocity $c_{s,30}$. The main conclusions drawn from this study are:

- Regarding the translational kinematic interaction factors I_u , the pile foundation filters to a great extent the soil seismic motion if the variable-with-depth profile is assumed. However, as the excitation frequency increases, there can be some ranges for which the opposite effect is found.
- On the contrary, the rotational kinematic interaction factors I_ϕ increase their values in the low-frequency range if the variability of the soil profile is considered. In the high-frequency range, the rotations obtained for the equivalent homogeneous profile tend to be higher than those of the variable profile.
- These effects can be explained attending to the fact that the first layers of the variable profile are softer with respect to the ones of its equivalent homogeneous soil. Note



that all the non-homogeneous profiles considered in this study have zero shear wave velocity at the free-surface level.

- Those differences between the two profiles in their kinematic interaction factors produce that higher elastic response spectra are obtained for the homogeneous profile in the low period range ($T < 0.15$ s). Thus, for that range, the homogeneous assumption is generally conservative in terms of the structural maximum accelerations.
- For larger structural periods, and specially in soft soils, the relevance of assuming the correct soil profile becomes more important. Appreciable differences between studied profiles are found for the whole range, being the highest pseudo-spectral accelerations obtained when the variability of the soil profile is considered.
- The importance of including the soil variability further increases for those systems in which the foundation rotation has a high contribution to the structural response (i.e., slender structures and foundations with few near piles). The differences between the variable and homogeneous profiles can reach over 4 times the peak ground acceleration in the case of single piles or up to one time for pile groups and the softest soil type.

The influence of the assumed pile head condition (pile-cap union type) on the seismic motions of the pile foundations is also studied:

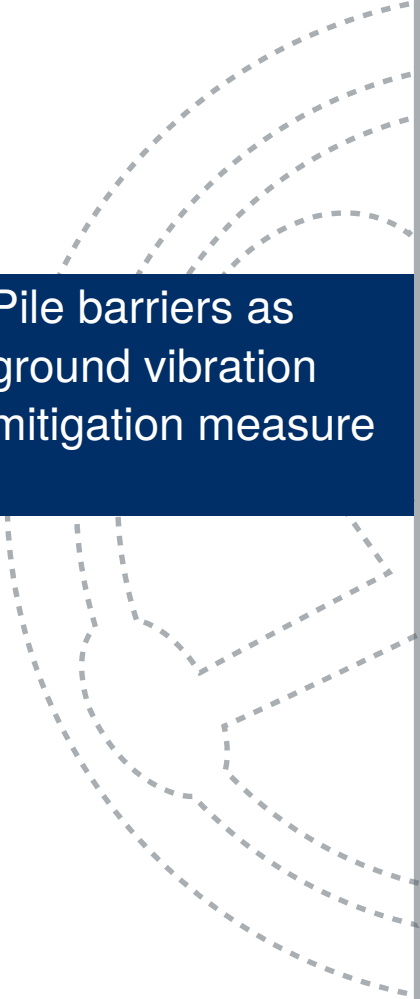
- Foundations with piles with hinged condition at their heads present higher translational kinematic interaction factors I_u than those with piles with restrained head rotations (either externally imposed or due to the influence of the pile cap).
- Despite the differences in the filtering of the seismic lateral motion, the frequency behaviour and effects of the variability of the soil profile on the obtained curves is nearly the same regardless the head condition, being the only difference a shift toward lower frequencies for the fixed-head assumption.
- For pile groups, the cap rotation is significantly reduced by articulating the pile-cap union. Under this condition, the pile rotation produced by the incident field is not transmitted to the rigid cap.
- In terms of the structural response, the effects of the pile head condition depend on the slenderness of the supported system.
- For short structures, foundations with hinged piles produce larger structural accelerations than configurations with fixed-head piles. On the other hand, for slender structures, the articulation of the pile-cap union leads to a reduction in the structural kinematic response.

The pile response in terms of envelopes of maximum bending moments is also analysed:

- The use of single pile configurations for estimating the kinematic bending moments is verified due to the small contribution of the interaction effects between piles.



- Pile-to-pile interaction is only observable for very soft soils and configurations with close piles. As consequence of this interaction, the maximum bending moments are reduced for piles in a group.
- Regarding the influence of the variability of the soil profile, the envelopes of maximum bending moments are highly sensitive to the assumed profile. The equivalent homogeneous profile in terms of mean shear wave velocity is not suitable for reproducing the bending moments of piles in a variable profile under any scenario.
- For configurations of hinged-head piles, the envelopes obtained for the homogeneous media significantly overtake the ones of the variable profiles. On the other hand, for fixed-head pile foundations, and because of the low stiffness of the superficial layers in the variable profile, the maximum bending moments produced at the pile head can reach values over three times higher than the ones of the equivalent homogeneous soil if the variability of the soil profile is considered in the analyses.

A series of concentric dashed lines on the left side of the slide, partially obscured by the title box.

5. Pile barriers as ground vibration mitigation measure

- 5.1 Introduction
- 5.2 Problem definition
- 5.3 Validation of the proposed model
- 5.4 Results
- 5.5 Conclusions





5.1 Introduction

The environmental vibration produced by nearby traffic, machines or construction operations can lead to annoyance for residents or damage for sensitive equipment. Different types of isolation systems can be used to attenuate these ground vibrations, located either at the source point or at the receiver structure. In addition to these, wave barriers can be used along the transmission path to reduce the propagation of vibrations in the ground.

Several types of wave barriers have been used and studied along the last decades. The simplest system consists of an open or in-filled trench situated between the vibration source and the receiver point. The surface disturbance imposed by the trench diffracts the elastic waves resulting in a vibration amplitude reduction [125]. The efficiency of trenches is closely related to their depth and the soil wavelength [125–127] and, for open or in-filled, has been the object of study of a large variety of research works through experimental [127–129] or numerical [130–135] approaches. Depending on the dimensions of the trench or the characteristics of the soil, sometimes it is necessary to include structural elements, such as thin shell walls [39] or sheet-pile walls [136], to guarantee its stability. Systems composed by double wall barriers have been also recently considered [137, 138]. Some of these works [135, 138] have employed optimization techniques in order to improve the performance of the barriers.

On the other hand, wave barriers formed by piles can be also used to mitigate the ground vibrations when large barrier depths are required. The pioneering experimental works of Woods et al. [139] and Liao and Sangrey [140], and the analyses based on the equations of the problem of Avilés and Sánchez-Sesma [141, 142] studied the use of piles as isolation systems. Kattis et al. [143] used a BE formulation to analyse the performance of a row of piles to mitigate the ground surface vibrations produced by an external vertical load. In a later work, they addressed the problem by modelling the pile barrier through an effective trench [144]. A BE model was also used by Tsai et al. [145] to study the effectiveness of barriers formed by different types of hollow and solid piles. Regarding configurations that differ from the single row of piles, Gao et al. [146] studied the performance of three pile rows to mitigate Rayleigh waves; while Xia et al. [147] proposed a formulation to analysis the scattering effects of an arbitrary configuration of piles. Also, periodic pile barriers have been analysed in several research works [148–150]. Some authors have also addressed the problem of pile barriers embedded in poroelastic soils [151–153].

At this point, it should be mentioned other novel systems that have been proposed recently in order to mitigate the vibrations received by structures. One example is the application of structure-soil-structure interaction effects [154, 155] to use an auxiliary system that absorbs part of the energy transmitted through the ground. Also, different kinds of metabarriers or metamaterials [156–162], some of them based on optical principles, can be used to properly channel or filter the elastic waves and, consequently, reduce the ground vibrations at the desired locations.

In most of the previous works, the piles were assumed to be in a homogeneous half space. More studies about how the profile of the soil affects the performance of the pile barrier are demanded. In order to fill this gap, and to take advantage of the characteristics of the developed model, in this chapter this problem is addressed.

This chapter is aimed at studying the performance of pile barriers as ground vibration



mitigation measure, and how it is affected by the characteristics of the soil site. First, the problem under study is defined in Section 5.2. Then, the ability of the integral model to simulate the effects that are involved in the pile barrier problem is validated by comparing with a boundary element model in Section 5.3. After setting the scope of applicability of the numerical tool, results are presented in Section 5.4, followed by the main conclusions drawn from them in Section 5.5.

5.2 Problem definition

The wave barrier is composed by a row (or several rows) of identical piles. A point load in vertical direction, centrally placed at one side of the pile barrier, is assumed as the source of vibrations. On the other side of the barrier, the response at a set of observation (receiver) points distributed along a rectangular surface behind the barrier is measured. A sketch of the problem is shown in Fig. 5.1.

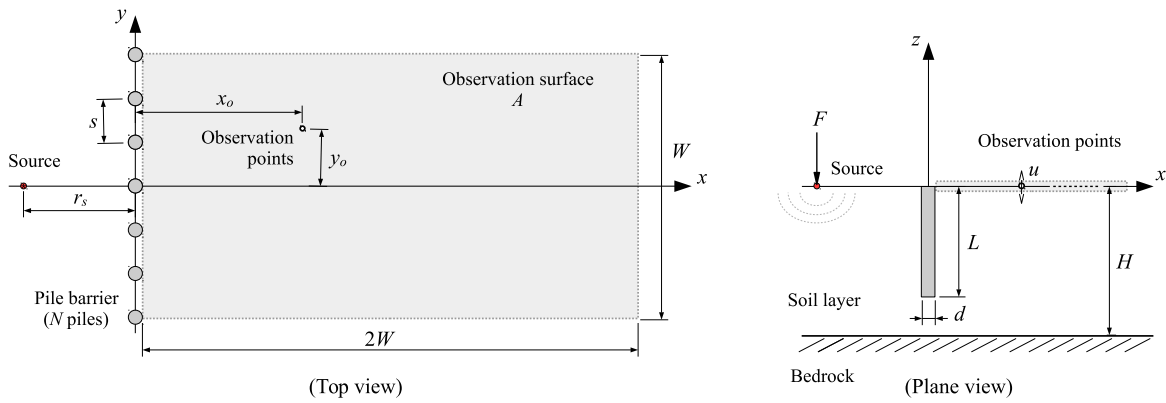


Figure 5.1: Sketch of the pile barrier problem.

In order to present results that can be applied to a wide set of scenarios, the problem is defined in terms of dimensionless parameters. The pile geometry is determined by the pile aspect ratio L/d ; while the barrier geometry is given by the number of piles N and centre-to-centre pile separation s/d . The width of the barrier is denoted as $W/d = (N - 1)(s/d)$.

The source is placed at the central line of the barrier at a distance r_s/d in the x direction. On the other hand, the position of each observation point is defined through the magnitudes x_o/d and y_o/d , corresponding to the distances in directions x and y , respectively, from the observation point to the centre of the barrier.

This chapter aims to study how the performance of the pile barrier is affected by the presence of a stiff bedrock at the soil site. Therefore, two soil profiles are assumed in order to compare their results: a half space and a single soil layer over a bedrock. The relative stiffness between the soil (half space or upper layer) and the pile is given by the pile-soil Young's modulus ratio E_p/E_s . For the soil deposit profile, the thickness of the layer is given by the ratio H/d , and the relative stiffness between bedrock and the upper layer is determined by the ratio E_b/E_s . The rest of soil properties are set to be equal for the layer, bedrock and half



space domains and are: soil-pile density ratio ρ_s/ρ_p , soil Poisson's ratio ν_s and soil hysteretic damping ratio β_s , which gives complex valued elastic properties as: $E^* = \text{Real}[E](1 + 2i\beta_s)$, being i the imaginary unit.

The rest of dimensionless material properties corresponding to the piles are: pile Poisson's ratio ν_p and pile hysteretic damping ratio β_p .

Results are presented in terms of the dimensionless frequency $a_o = fd/c_s$, being f the excitation frequency in hertz and c_s the shear wave propagation velocity of the soil (half space or upper layer). The dimensionless frequency represents the ratio between the pile diameter and the shear wave wavelength in the soil, i.e., $a_o = d/\lambda_s$.

The reduction of surface displacements produced by the pile barrier is measured in terms of the amplitude reduction ratio:

$$A_r = \left| \frac{u}{u_{\text{ref}}} \right| \quad (5.1)$$

where u and u_{ref} are the vertical displacements produced at each observation point by the vertical load with or without the presence of the pile barrier, respectively.

Then, the effectiveness of the pile barrier is measured through the average amplitude reduction factor in the observation surface, which is obtained as:

$$\bar{A}_r = \frac{1}{A} \int_A A_r \, dA \quad (5.2)$$

being $A = 2(W/d)^2$ the dimensionless area of the rectangular observation surface located behind the pile barrier.

5.3 Validation of the proposed model

The aim of this section is to validate the capability of the developed model to handle the pile barrier problem. The presence of the barrier mitigates the ground vibration due to the stiffening of the soil between the receiver and the source points and due to the diffraction of the travelling waves that transmit the energy introduced by the external force. Part of these diffraction effects corresponds to geometrical reflections and transmissions that are produced at the soil-pile interface. However, as the proposed formulation treats the piles as dimensionless load lines, these phenomena cannot be completely captured by the developed model. The importance of the geometrical diffraction is expected to increase as the frequency of the excitation augments, when the soil wavelengths are comparable to the pile cross-section dimensions.

Therefore, in order to test the range of applicability of the proposed model, a reduced set of problems is considered and the results of the integral model are compared with the ones of the previously developed boundary element formulation [16,41] within the Research Group. As stated in the introduction, BE models are often used in the literature to rigorously handle the pile barrier mitigation problem. However, this kind of models demands high computational resources (both in time and memory) and also presents, in their standard formulations,



the uncertainties intrinsically related to the surface and pile meshing. Those inconveniences are avoided by the proposed integral model, which makes it a suitable tool for carrying out parametric analyses if the validation process is satisfactorily completed.

For the validation analysis, several configurations of pile barriers embedded in a homogeneous half space domain are considered by combining the following dimensionless parameters:

- pile aspect ratio $L/d = 10$ and 20
- pile separation distance $s/d = 1.5, 2, 3, 4$ and 5
- pile-soil Young's modulus ratio $E_p/E_s = 65$ and 250
- soil Poisson's ratio $\nu_s = 0.3$ and 0.485

All other dimensionless parameters are kept constant: number of piles $N = 7$, pile Poisson's ratio $\nu_p = 0.25$, pile hysteretic damping ratio $\beta_p = 0\%$, soil hysteretic damping ratio $\beta_s = 2.5\%$, soil-pile density ratio $\rho_s/\rho_p = 0.7$. The source load is located at $r_s/d = 10$ and the response at receivers situated at $x_o/d = 6, 10, 15$ and 20 and at $y_o/d = 0$ and $1.5s/d$ from the centre of the pile barrier are considered. Values of the amplitude reduction ratio A_r at these observation points are obtained for a frequency range from $a_o = 0$ to 0.25 .

It is important to highlight that the validation is made in terms of the amplitude reduction ratio at specific points instead of using its average value along the whole observation surface. This way, the ability of the proposed model to represent the physical behaviour of each point of the soil surface (and not only the average trend) can be validated. Obviously, if the integral model is able to reproduce the point-by-point response of the soil obtained by the BE model, the average values computed by the two methodologies will also coincide.

For illustration purposes, Fig. 5.2 shows the meshes required for solving one of the studied configurations by the BE and integral models. Note that, as the BE formulation exploits the geometrical symmetry of the problem, only one-quarter of it is discretized. However, this makes it necessary to divide the loading problem into its symmetric and antisymmetric components. On the other hand, the integral model does not impose any symmetry conditions, thus, the whole configuration is directly considered (as shown in Fig. 5.2).

The combination of the aforementioned parameters results in 320 curves of the evolution of the A_r with the dimensionless frequency that can be used to compare the two different methodologies. In order to measure the discrepancies between the two models at any point $\mathbf{x}_o = \{x_o/d, y_o/d, 0\}^T$ of the soil surface, the following frequency-dependent relative error is defined:

$$\Delta_{A_r}(a_o, \mathbf{x}_o) = \left| \frac{A_r(a_o, \mathbf{x}_o) - A_r^{\text{BE}}(a_o, \mathbf{x}_o)}{\max_{a_o} (A_r^{\text{BE}}(a_o, \mathbf{x}_o)) - \min_{a_o} (A_r^{\text{BE}}(a_o, \mathbf{x}_o))} \right| \quad (5.3)$$

which represents the importance of the difference between the amplitude reduction ratio obtained by the integral and BE models with respect to the range within which lies the reference (BE) results. This definition of the relative difference is chosen over the classic relative error

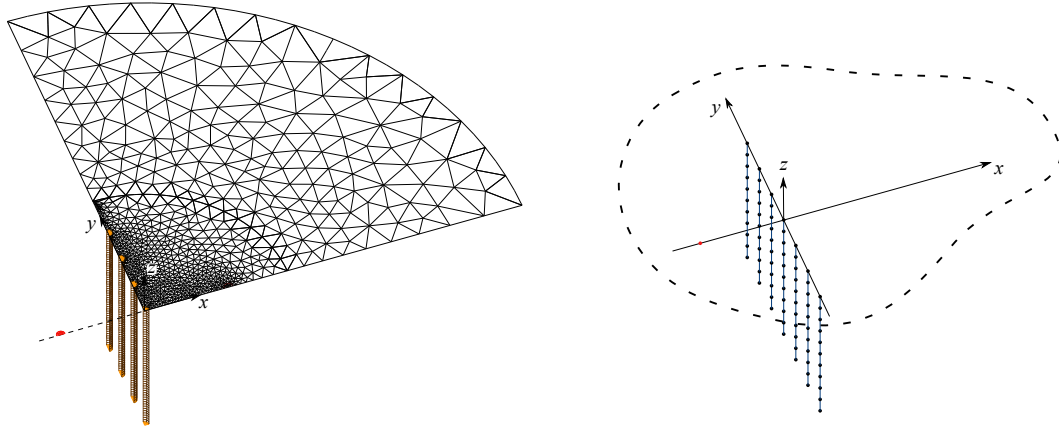


Figure 5.2: Examples of the meshes used for the BE (left) and integral (right) models.

in order to avoid excessive values at frequencies in which the reference value of A_r^{BE} is close to zero.

After computing the Pearson's correlation coefficient (R) between Δ_{A_r} and the variable dimensionless parameters, the only ones that are found to be significantly related to the differences between the two models are the dimensionless frequency a_o ($R = 0.614$) and the separation distance s/d ($R = -0.183$). As expected, as the frequency increases and, consequently, the soil wavelength decreases, the geometrical effects of the pile dimensions are more important and, therefore, the simplified model cannot reproduce the results of the BE formulation. Related to this, as the piles in the barrier are located at closer distances, the quantity of soil situated in between the piles differs more from one model to another. Note that, in the limit scenario of $s/d = 1$, the BE model would have no soil between the line that connects the pile centres, while the integral formulation will consider the propagation of waves through that soil medium. In other words, it is found that as the real problem (BE) presents a geometry closer to the hypotheses of the integral model (one-dimensional load lines, i.e., slender separated piles), the results of the two methodologies converge.

In order to represent the relation between Δ_{A_r} and the aforementioned parameters, the distribution of the differences between the integral and BE model are presented for each separation distance and dimensionless frequency in Fig. 5.3 through box and whiskers diagrams. In coherence with the correlation analysis, it is found that the mean values of the differences are larger for the smallest pile separation distances, and that the magnitude of these differences significantly increases with the frequency. Also, the results presented in Fig. 5.3 indicate the high dispersion that exists for the differences between the models, which led to the statistical treatment of the data instead of a direct evaluation from the graphical results.

Finally, in order to fix the range of applicability of the integral model, the expected difference $\Delta_{A_r}^*$ is obtained for each separation distance s/d through a linear regression of the available data and is shown as a solid line in each graphical area of Fig. 5.3. The comparison between the evolution with frequency of this expected difference for the different separation distances can be easily analysed in Fig. 5.4(a). Once these expected differences are obtained, the integral model is assumed to be valid if the expected value of the difference $\Delta_{A_r}^*$ remains

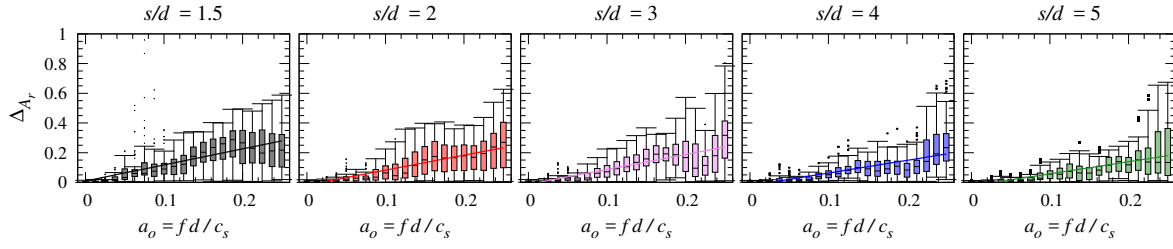


Figure 5.3: Distribution of the differences Δ_{A_r} between the integral and BE models.

below a certain threshold. For this study, a threshold value of 0.1 (ten percent of the A_r^{BE} range) is assumed in order to accept the results of the integral model, yielding the maximum values of the dimensionless frequencies a_o^{lim} that can be reached for each separation distance that are shown in Fig. 5.4(b). Note that a near-linear relation between the separation distance s/d and the maximum dimensionless frequency a_o^{lim} is obtained. Therefore, it is assumed that for separation distances larger than the ones studied herein, the maximum dimensionless frequency of application of the integral model will be, at least, $a_o^{\text{lim}} = 0.15$.

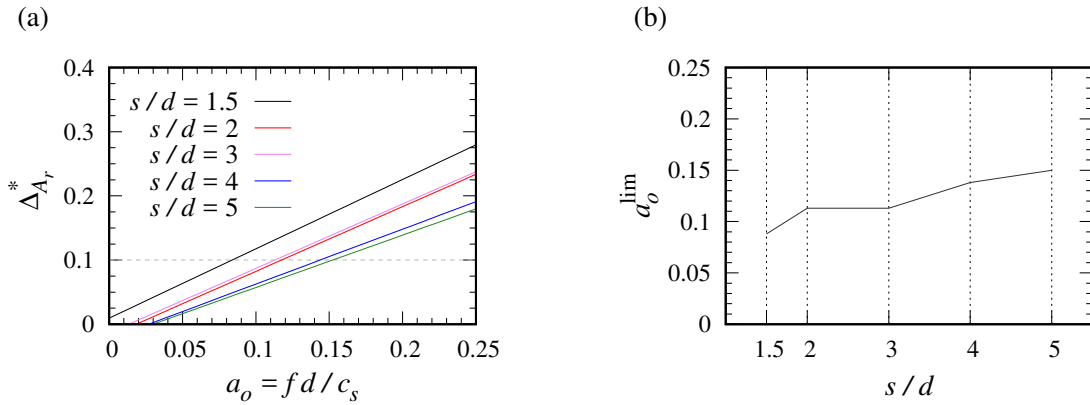


Figure 5.4: Range of applicability of the integral model. (a): Expected difference $\Delta_{A_r}^*$ between the integral and BE models. (b): Maximum dimensionless frequency in which $\Delta_{A_r}^* < 0.1$ as function of the pile separation distance s/d .

To illustrate the validation study, Fig. 5.5 shows the A_r obtained by the integral (lines) and the BE (crosses) models for the configurations of $L/d = 20$ and $\nu_s = 0.485$ at certain observation points. The results corresponding to the different pile separation distances are shown in different rows, while the ones corresponding to the two soil stiffness ratios are plotted in different colours. The observation points are located at the centre of the pile barrier ($y_o/d = 0$) and at a distance indicated by the value of x_o/d at the top of each column. In addition to this, a vertical dashed line shows the value of the limit frequency according to the results presented in this section. It can be seen that a good match between the two models is obtained for low frequencies up to the a_o^{lim} . Also, for configurations with large pile separation distances, the integral model follows the main trend of the BE results for frequencies larger than a_o^{lim} , although their values do not perfectly coincide.

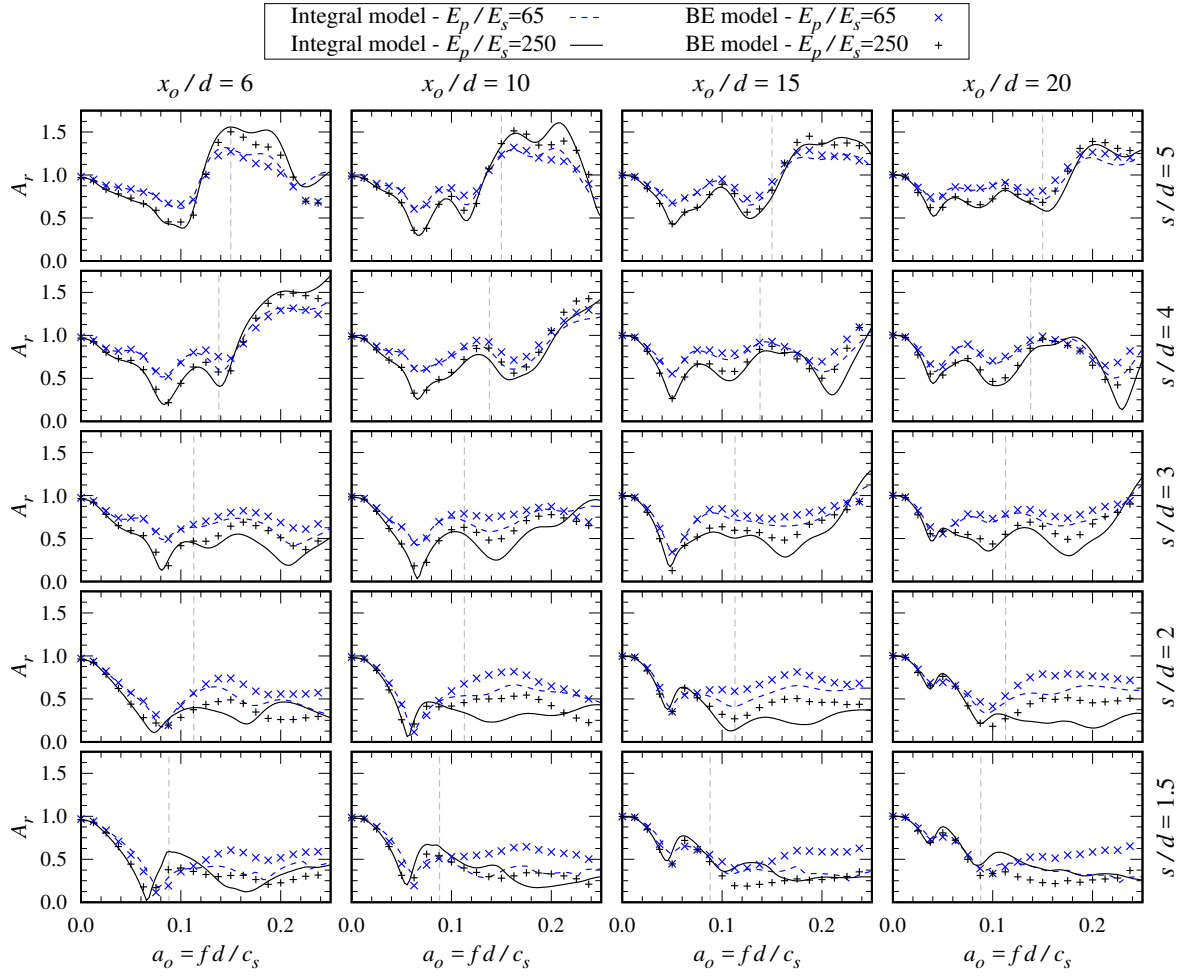


Figure 5.5: Comparison between amplitude reduction ratios obtained by the integral and BE models. $\nu_s = 0.485$, $L/d = 20$. Observation points located at the centre of the barrier ($y_o/d = 0$).

Finally, in order to demonstrate that the scope of applicability of the model obtained from the results of the half space profile are also valid for the layer over bedrock site, results for this profile are presented in Fig. 5.6. The studied geometries and properties coincide with the ones used for Fig. 5.5, but an infinitely rigid bedrock is placed at a depth equal to the pile length. Fixed tip conditions are considered for the piles. The results show that the integral model can also reproduce the results of the BE model up to the limit frequency value a_o^{lim} for the bedrock profile. As commented at the beginning of this section, the discrepancies between the models are produced due to the lack of geometrical diffraction effects in the integral formulation and these phenomena were expected to behave in a similar way regardless the existence of the rigid bedrock.

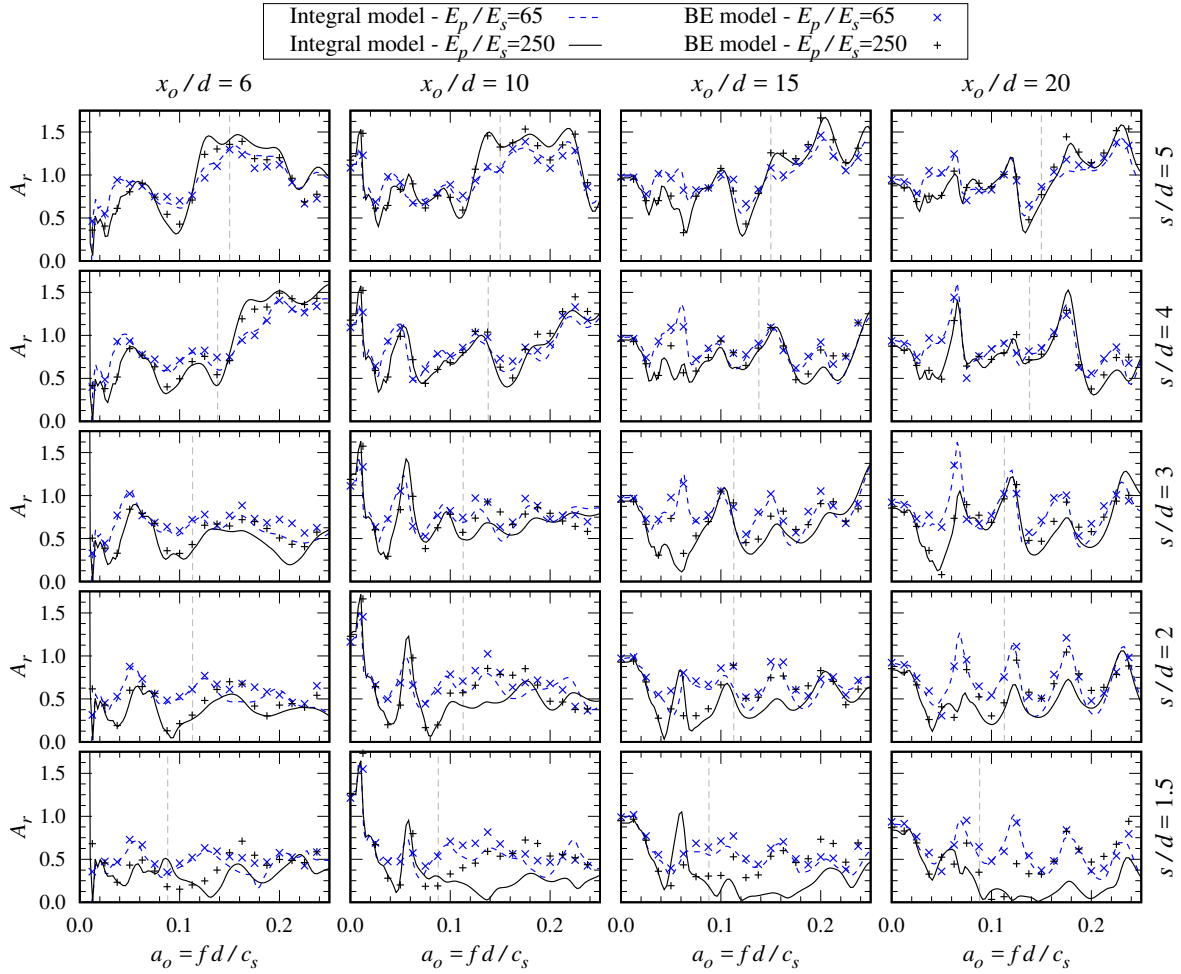


Figure 5.6: Comparison between amplitude reduction ratios obtained by the integral and BE models. $\nu_s = 0.485$, $L/d = 20$. Observation points located at the centre of the barrier ($y_o/d = 0$). Rigid bedrock located at the pile tip depth.

5.4 Results

As previously stated, the objective of the present chapter is to study how the performance of the pile barrier is altered when it is embedded in a soil layer over a stiff bedrock. For that purpose, the results corresponding to this profile (henceforth referred to as *Bedrock* profile) are compared with the ones obtained by assuming the soil as an unbounded semi-infinite medium (*Half space* profile).

Several cases of study are defined in order to analyse the effects of some of the dimensionless parameters that define the problem. Table 5.1 presents each scenario together with the values that are assumed for the different dimensionless parameters and contact conditions at the pile tip-bedrock union. On the other hand, Table 5.2 shows the values for the rest of the dimensionless properties that are kept constant along the different cases.

The study starts with Case A, which compares the vibration mitigation performance of



Case	N (s/d)	L/d	H/d	r_s/d	E_p/E_s	E_b/E_s	tip condition [†]
A	7 (4)	5,10,20	20	24	100,250,500	∞	free
B	7 (4)	10,20	L/d	24	250	∞	free,hinged,fixed
C	7 (4)	10,20	L/d	0-6 (r_s/λ_s)	250	∞	fixed
D	7 (4)	10,20	L/d	24	250	1,2,5,10, ∞	free
E	7 (4)	10,20	L/d	24	250 (Gibson)	∞	fixed
F	^{††}	10,20	L/d	24	250	∞	fixed

[†] only for the Bedrock scenario. Free tip is always assumed for half space profile.

^{††} single barrier configurations: 13(2),7(4),4(8); double barrier configurations: 6&7(4),3&4(8).

Table 5.1: Definition of the cases of study.

ρ_p/ρ_s	ν_s	β_s	ν_p	β_p	a_o
0.7	0.485	2.5%	0.25	0.0%	0-0.15

Table 5.2: Dimensionless properties assumed for all of the cases of study.

pile barriers embedded in the soil layer over a rigid bedrock with the results obtained assuming the half space profile. A constant layer thickness is considered together with three pile aspect ratios for the elements of the barrier. Two of these aspect ratios correspond to piles that are shorter than the layer thickness, while the last ratio corresponds to the situation in which the piles reach the bedrock. For this case of study, the influence of the pile-soil stiffness ratio on the obtained results is also analysed. It is found that only when the piles reach the rigid bedrock a significant variation of the barrier reduction ratio is obtained with respect to the half space scenario. After this finding, only configurations with piles presenting a length equal to the layer thickness are further considered. The influence of the layer thickness on the barrier behaviour is studied in Case B, together with the effects of changing the pile tip boundary condition that represents the union between the piles and the rigid bedrock. Then, Case C studies the influence of the position of the external source with respect to the barrier on its performance, comparing the scenarios of the bedrock and half space soil profiles. In Cases D and E, the academic assumption of the single homogeneous layer over an infinitely rigid bedrock profile is generalized into two more realistic soil profiles: a homogeneous layer overlying a flexible bedrock (Case D), and a variable-with-depth soil layer over a rigid bedrock (Case E). Finally, several barrier configurations are analysed in Case F by changing the pile spacing or adding extra pile rows in order to confirm that the obtained results can be extrapolated to other dispositions of the piles in the barrier. In the following, detailed comments of the different cases of study are presented.

First, Fig. 5.7 presents the average reduction ratio produced by the pile barrier as a function of the dimensionless frequency for the half space and bedrock profiles. Different pile aspect ratios are considered for the piles of the barrier as indicated by the labels atop each column. For the bedrock profile, a layer thickness $H/d = 20$ is assumed regardless of the pile

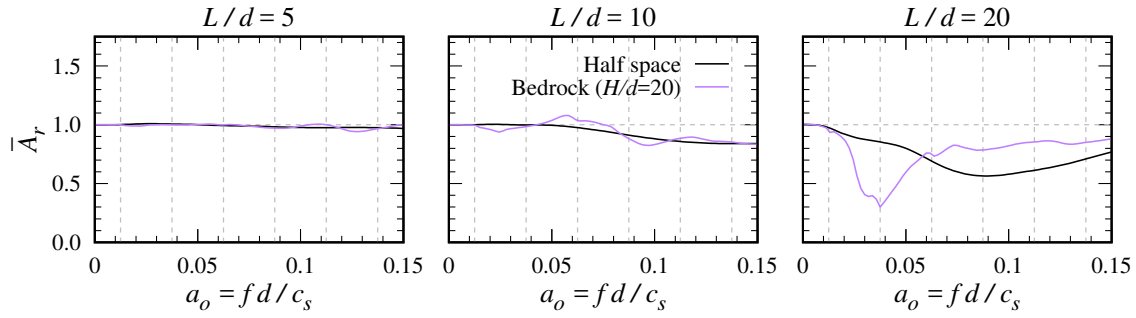


Figure 5.7: Case A. Average amplitude reduction factor. Influence of the pile aspect ratio and presence of a rigid bedrock. $E_p/E_s = 250$.

aspect ratio. The frequencies coinciding with the natural frequencies of the layer are marked with vertical dashed lines (corresponding to $H = n\lambda_s/4$ with $n = 1, 3, 5, \dots$). Two different situations are found depending on whether or not the piles reach the rigid bedrock. When the piles are shorter than the thickness of the soil layer, the average amplitude reduction ratio obtained for the bedrock profile practically coincides with the one for the half space scenario, showing a slight oscillation around it. For the studied frequency range, the barrier with the shortest piles ($L/d = 5$) produces virtually no reduction of the soil displacements; while the one formed by piles with $L/d = 10$ only presents a small attenuation of the soil vibration for high frequencies. For this last configuration in the bedrock profile, there is a frequency range ($a_0 = 0.04 - 0.08$) in which the presence of the piles amplifies the average vertical displacements at the points located behind the barrier. On the other hand, for the case of the piles with a slenderness ratio equal to the layer thickness, a considerable change in the behaviour of the barrier is found between the bedrock and half space profiles. For the single layer over the rigid bedrock, the reduction of the pile barrier starts to increase from frequencies above the fundamental frequency of the soil layer, reaching the maximum reduction, i.e. minimum \bar{A}_r value, around the second natural frequency of the soil layer ($H = 3\lambda_s/4$). For higher frequencies, the barrier loses efficiency but continues to reduce the ground vibration at the points behind it ($\bar{A}_r < 1$). For the half space profile, the average amplitude reduction ratio of the barrier smoothly reduces its value as the frequency increases, reaching a minimum around $a_0 = 0.09$, and then starts to lose efficiency for higher frequencies but at a lower rate than the bedrock profile. Comparing the \bar{A}_r ratios of the two soil types, it can be found that the largest reductions are produced for the bedrock site around its second natural frequency, but for higher frequencies the barrier becomes less effective in this medium compared with the half space scenario.

In order to explain why the performance of the pile barrier at high frequencies is reduced to a larger extent in the bedrock profile than in the half space domain for the $L/d = 20$ piles, Fig. 5.8 shows, for the two studied profiles, the absolute value of the vertical displacements that the external force produces at certain observation points with and without considering the presence of the pile barriers. These observation points are located at the central line of the barrier ($y_o/d = 0$) and at a distance of $1/8$ ($x_o/d = 6$), $1/4$ ($x_o/d = 12$) and $1/2$ ($x_o/d = 24$) of the width of the observation surface ($2W/d$). The results in terms of displacements show

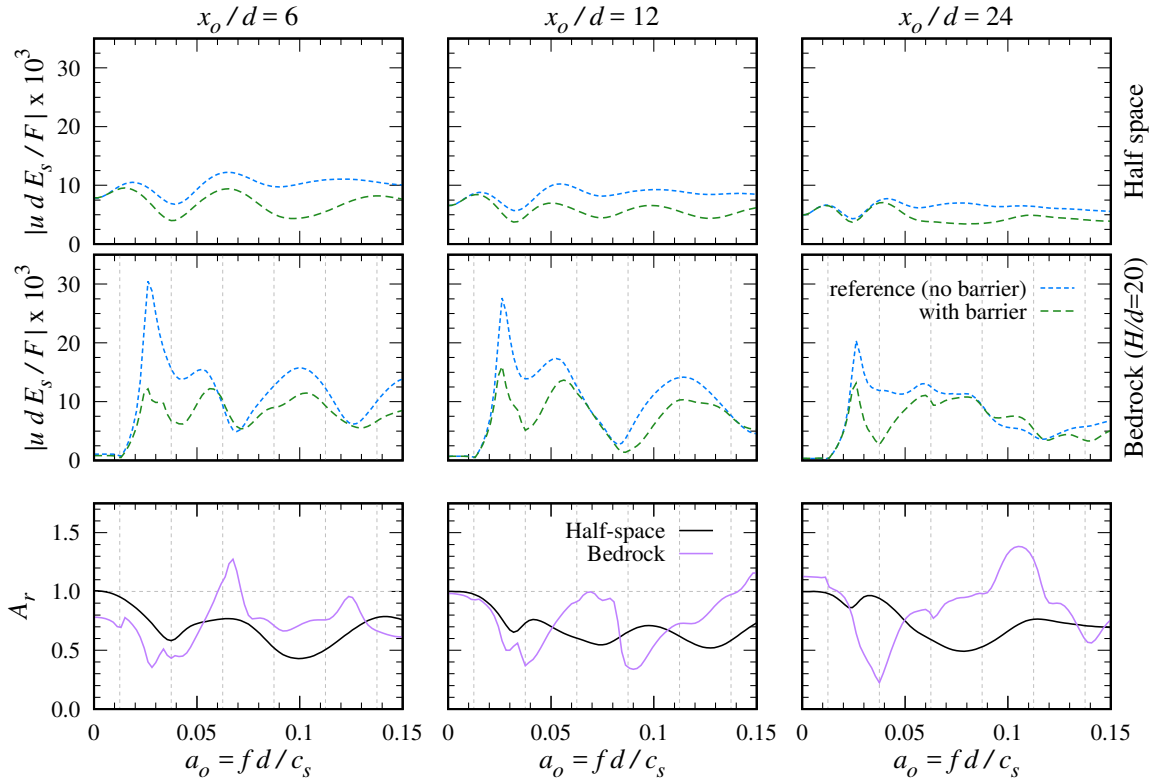


Figure 5.8: Case A. Vertical displacements and amplitude reduction ratio at specific observation points located at the central line ($y_o/d = 0$) behind the barrier. Pile aspect ratio $L/d = 20$. $E_p/E_s = 250$.

the different behaviour corresponding to the two soil profiles: for the half space domain, the displacements present an oscillatory but smooth behaviour with frequency, and the presence of the barrier only scales their value. On the contrary, for the bedrock profile, the influence of the frequency on the soil displacements is more important. Below the fundamental frequency of the soil, the energy introduced by the external force cannot propagate through the layer so the displacements at the points of the soil surface are limited. However, once this cut-off frequency is reached, the displacements of the soil rapidly increase, reaching values that can be three times greater than the ones produced at the half space site. For larger frequencies, a highly frequency-dependent behaviour of the soil displacements is found. At these values of a_o , the presence of the pile barrier in the bedrock profile not only scale the value of the soil displacements, but also slightly modifies their evolution with frequency, shifting the curves toward higher frequencies. This shift is more evident for points more distant to the barrier: e.g., the minimum displacement for the point at $x_o/d = 6$ is moved from $a_o = 0.065$ to $a_o = 0.07$ when the piles are included; but the shift of minimum value for $x_o/d = 24$ goes from $a_o = 0.12$ to $a_o = 0.14$ if the barrier is present. These shifts in frequency between the displacements with and without the barrier produce that, at high frequencies, the amplitude reduction factors for the bedrock profile fluctuate from small to high values, as illustrated by the bottom row of Fig. 5.8. Therefore, the average reduction produced by the barrier in the

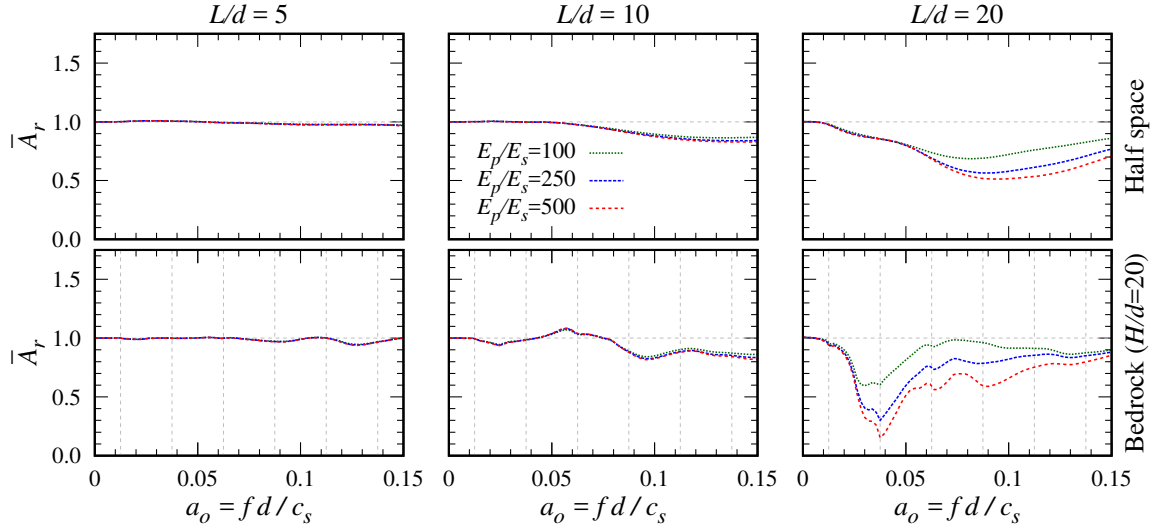


Figure 5.9: Case A. Average amplitude reduction ratio. Influence of the pile-soil stiffness ratio.

bedrock profile loses efficiency for frequencies in which these shifts occur ($a_o > 0.06$ for the studied configuration).

Fig. 5.9 shows the results for Case A that are obtained by assuming different values of the pile-soil stiffness ratio. The initial value $E_p/E_s = 250$ was considered as representative of concrete piles ($E_p \approx 30$ MPa) embedded in a medium-soft soil ($c_s = 150$ m/s). However, scenarios where the soil presents different properties or the piles are made by other materials should also be considered, and are simulated by changing the value of the E_p/E_s ratio. The obtained results show that the main behaviour of the barrier is the same regardless of the pile-soil stiffness ratio. Furthermore, for configurations with $L/d \leq 10$ the average reduction ratios virtually coincide for $E_p/E_s = 100 - 500$. On the other hand, for the barrier with the most slender piles, the higher the pile-soil stiffness ratio, the larger the attenuation produced by the barrier. The influence of the E_p/E_s ratio increases at high frequencies for the half space domain, while it is slightly more significant around the second fundamental frequency for the bedrock profile.

From the results presented in Figs. 5.7 and 5.9 it can be concluded that the behaviour of the pile barrier is only significantly altered by the presence of the rigid bedrock if the piles reach it. For this reason, and in order to study the effects of the layer thickness, Fig. 5.10 compares the average amplitude reduction factor obtained for the half space profile with the one obtained assuming a bedrock profile in which the layer thickness coincides with the pile aspect ratio. The configuration with short piles $L/d = 5$ is omitted as it would imply unrealistic short layers for typical pile dimensions. Note that, as the layer thickness changes, the natural frequencies of the soil profile (indicated by the vertical dashed lines) do not coincide in terms of a_o for the cases of $L/d = 10$ and 20. Also, for the bedrock profile, different pile-bedrock union conditions are assumed in order to check their influence upon the barrier reduction ratios. Free, hinged, and fixed tip conditions are considered. However, the importance of the pile tip condition is found to be negligible. The results for free and hinged

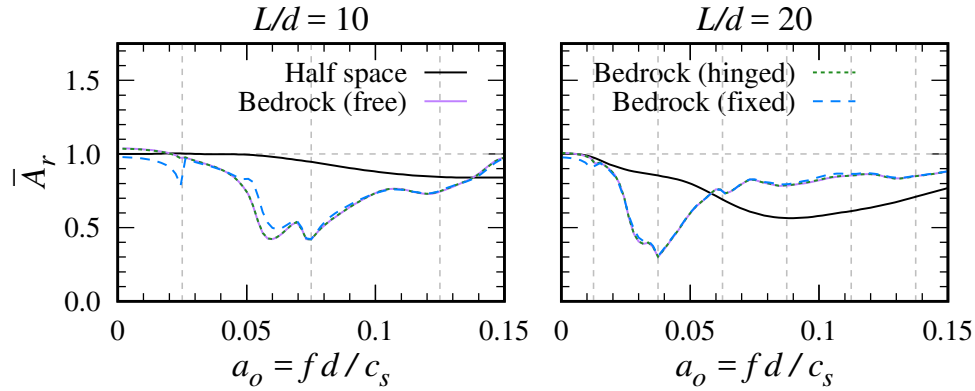


Figure 5.10: Case B. Average amplitude reduction ratio. Influence of the layer thickness and pile tip boundary condition.

tips practically coincide, while the differences between these and the fixed condition only can be seen for low frequencies, especially for the shortest piles. If the rotation of the pile tip is perfectly restrained by the rigid bedrock, a local minimum of the amplitude reduction factor is obtained at the layer fundamental frequency as the pile deformation shape for the fixed tip condition is not compatible to the layer fundamental mode. However, this effect is not really important as for the bedrock profile the displacements on the surface produced by the external force are quite small at these frequencies, as shown in Fig. 5.8. Regarding the influence of the layer thickness, the same trend can be seen for the two studied configurations: the maximum reduction takes place around the second fundamental frequency of the soil layer, and the value of the \bar{A}_r ratio increases for larger excitation frequencies. However, it is important to highlight that, in the studied range, the difference in the minimum value of the average reduction factor depending on the soil profile is higher for the shortest piles: which goes from $\bar{A}_r = 0.8$ for the half space to $\bar{A}_r = 0.4$ for the bedrock profile (for the $L/d = 20$ configuration, these minimum values are 0.55 and 0.3 respectively).

Regarding the influence of the position of the external source upon the barrier performance, Fig. 5.11 presents the average amplitude reduction ratio for the half space and bedrock profiles as functions of this parameter. Note that the distance of the source with respect to the barrier is presented in terms of r_s/λ_s instead of r_s/d in order to obtain similar trends for the three studied frequencies. These frequencies correspond to the second and third natural frequencies of the soil layer, plus the intermediate value. The point marker indicates the results corresponding to the default value ($r_s/d = 24$) assumed in the rest of cases of study. Two different behaviours are found depending on the soil profile. For the half space, great reductions are obtained when the load is placed near the barrier ($r_s/\lambda_s < 1$). For larger separations, the average attenuation ratio of the barrier increases up to a limit value which remains constant regardless the source separation distance. On the contrary, for the bedrock profile, the efficiency of the pile barrier is maintained for all of the studied positions of the external load. The pile effectiveness oscillates depending on r_s/λ_s , but does not decrease as the source moves away from the barrier. For $H/\lambda_s = 5/4$ these effects produce that, depending on the position of the source, the efficiency of the pile barrier can be larger in the half space domain

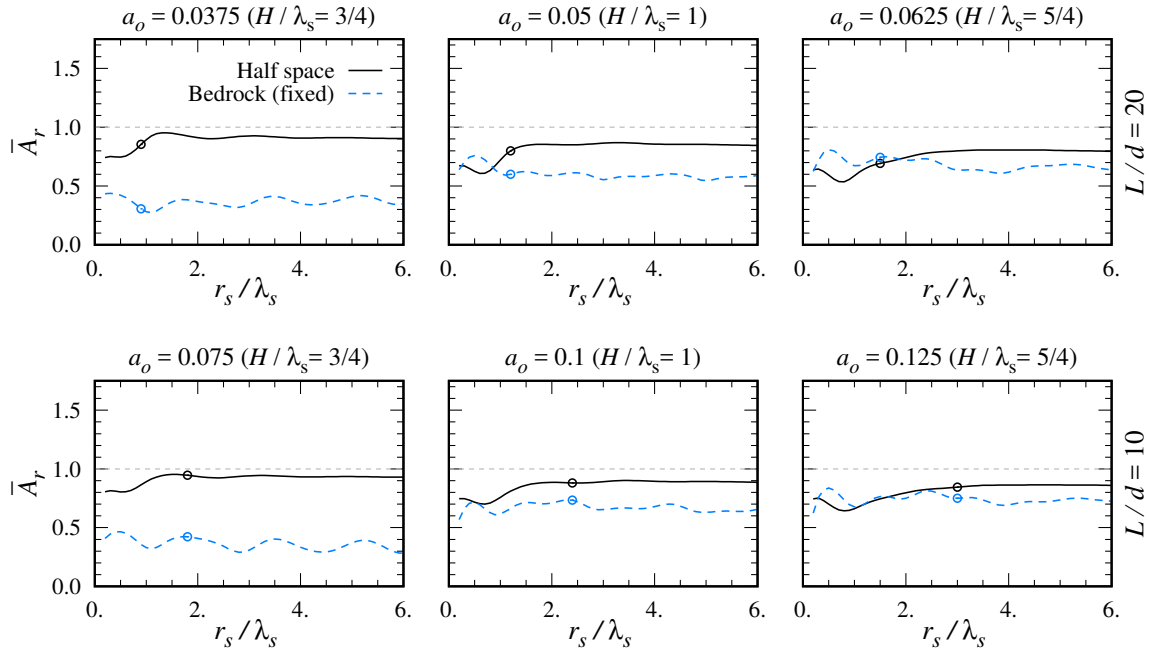


Figure 5.11: Case C. Average amplitude reduction ratio. Influence of the position of the source.

(close loads) or in the bedrock site (distant loads). The two different behaviours of the average reduction ratio depending on the position of the source can be explained considering the different ways in which the energy is transmitted inside the two studied soil media. In the case of the bedrock profile, the propagation of the energy is channelled through the soft layer. On the other hand, for the half space domain, part of the energy introduced by the external load is transmitted through surface waves and the rest is radiated to the unbounded media. In this case, as the source moves away from the barrier, only the portion of the motion transmitted through the surface waves reaches the barrier and, therefore, can be attenuated.

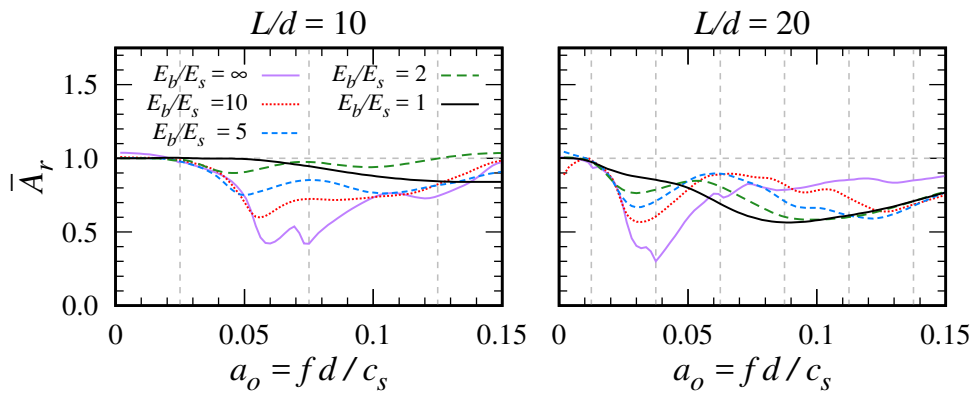


Figure 5.12: Case D. Average amplitude reduction ratio. Influence of the flexibility of the bedrock.

In the previous analyses, the case of an infinitely rigid bedrock has been considered. However, in reality, the lower medium presents a finite flexibility. To study the influence of the stiffness of the bedrock upon the barrier performance, Fig. 5.12 presents the average amplitude reduction ratios obtained by assuming different E_b/E_s values. Free-tip conditions are assumed for all of the soil profiles. The obtained results show that the largest reductions are still found for the rigid bedrock case. However, appreciable differences with respect to the half space profile ($E_b/E_s = 1$) can be seen for the rest of the studied two-layered media. When the lower layer is assumed to be flexible, the minimum value of the average reduction ratio is shifted from the second natural frequency of the soil towards the frequency in which $H = \lambda_s/2$. After this minimum point, the \bar{A}_r of all layer profiles increases, reaching values above the one corresponding to the half space scenario, as well as above the infinitely rigid bedrock profile. For the $L/d = 20$ configuration, the values of the attenuation ratios produced in the flexible bedrock profiles are again reduced at high frequencies, obtaining greater barrier efficiencies than for the rigid bedrock scenario. This improvement takes place at lower frequencies as the E_b/E_s ratio decreases.

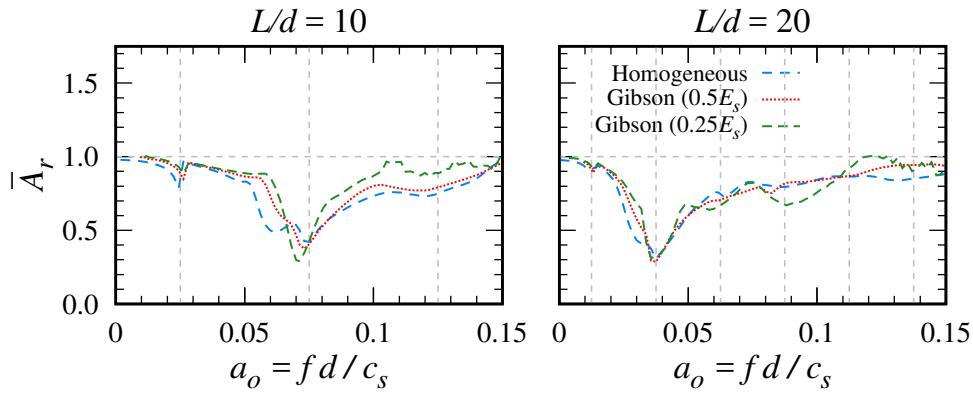


Figure 5.13: Case E. Average amplitude reduction ratio. Influence of the profile of the soil layer.

On the other hand, actual soil profiles can present properties that continuously vary with depth. Normally, the shear wave velocity increases for higher depths due to the soil consolidation process. In order to check how the assumption of a variable profile for the soft layer changes the obtained results, Fig. 5.13 presents the average amplitude attenuation ratio for three different scenarios. First, the previous case of a homogeneous layer over an infinitely rigid bedrock is considered. Then, two profiles in which the soil Young's modulus linearly increases with depth (Gibson soil) are assumed. These profiles are determined by the value of the Young's modulus at the free-surface level (either $0.5E_s$ or $0.25E_s$), and are defined in order to present the same average E_p/E_s ratio along the pile length than the homogeneous layer:

$$\begin{cases} 0.25E_s : & E_s(z) = [0.25 + 1.75(z/L)] (E_p/250) \\ 0.5E_s : & E_s(z) = [0.5 + 1.5(z/L)] (E_p/250) \end{cases} \quad (5.4)$$



The shear wave velocity used to compute the dimensionless frequency is the one that corresponds to the average value of $E_s = E_p/250$. Note that the rest of soil parameters (ρ_s , v_s , β_s) are kept the same for the whole profile. It is found that, despite increasing the frequency variability of the average amplitude reduction ratio, the two variable profiles follow the main trend obtained for the homogeneous layer.

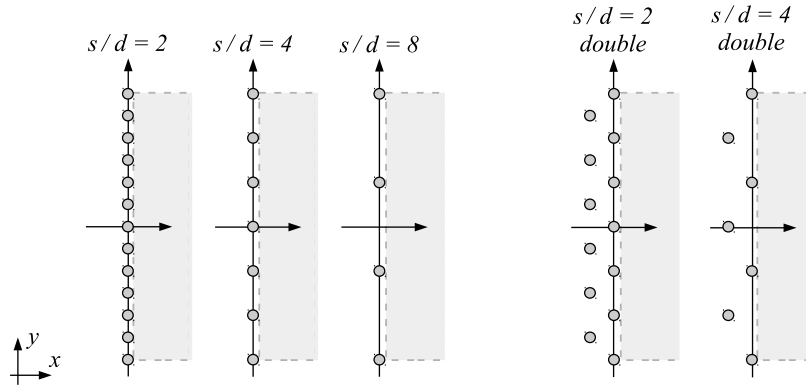


Figure 5.14: Pile barrier configurations analysed in Case F.

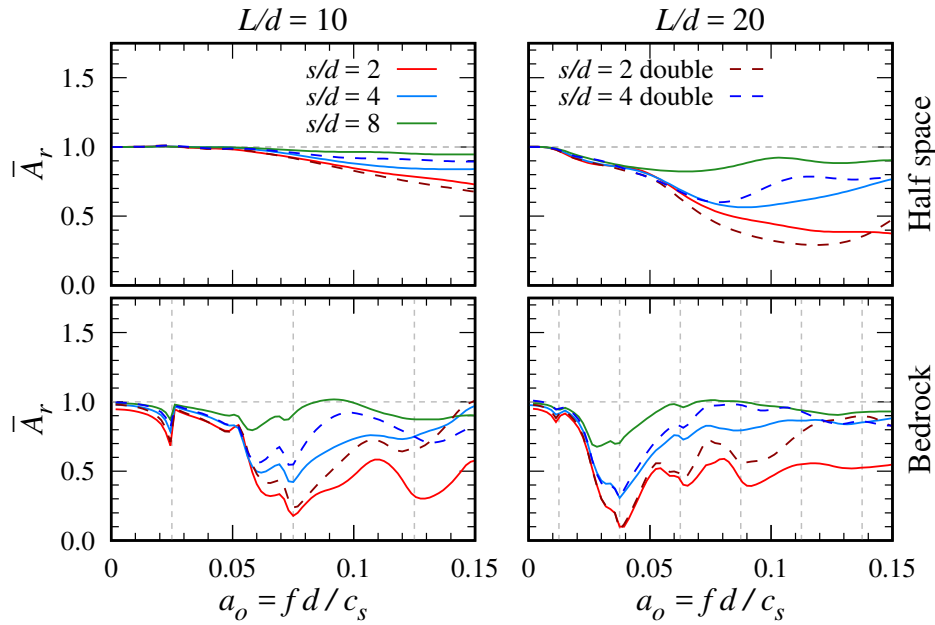


Figure 5.15: Case F. Average amplitude reduction ratio. Influence of the pile separation and pile disposition.

Finally, in order to check if the previous results can be extrapolated to other pile barrier configurations, the pile dispositions presented in Fig. 5.14 are considered. The same barrier width is kept for all of the configurations to preserve the same observation surface. Thus, the pile separation is changed by introducing or removing some piles. Also, two configurations



formed by a double pile barrier are considered. In those configurations, labelled as *double*, the s/d ratio represents the distance between the projections over the y axis of two consecutive piles, and a fixed separation between the two rows $s_x/d = 2$ is assumed. The average amplitude reduction ratios for the half space and bedrock profiles for these configurations are presented in Fig. 5.15. As expected, the closer the piles, the larger the reduction produced by the barrier. This decrement in the \bar{A}_r is found from medium-high frequencies ($a_o > 0.05$) for the half space profile, and above the fundamental frequency of the soil layer for the bedrock site. For the latter soil type, the importance of the pile separation is the same regardless the pile aspect ratio; while for the half space domain the magnitude of the influence of the s/d ratio is significantly higher for slender piles. Regarding the configurations with double pile rows, their results coincide with the ones of the line configurations with the same s/d for $a_o < 0.05$. For higher frequencies, different behaviours are found depending on the problem: For the half space profile, larger reductions are obtained if the piles are distributed into two rows for the configurations $s/d = 2$, but the opposite effect is seen for the $s/d = 4$ barriers. On the other hand, for the bedrock profile the barriers in which the piles are aligned present always higher efficiencies than the corresponding configurations with two rows. Despite these differences, it can be concluded that the main trends of the average amplitude reduction ratios for the half space and bedrock profile are kept for all of the studied pile configurations.

5.5 Conclusions

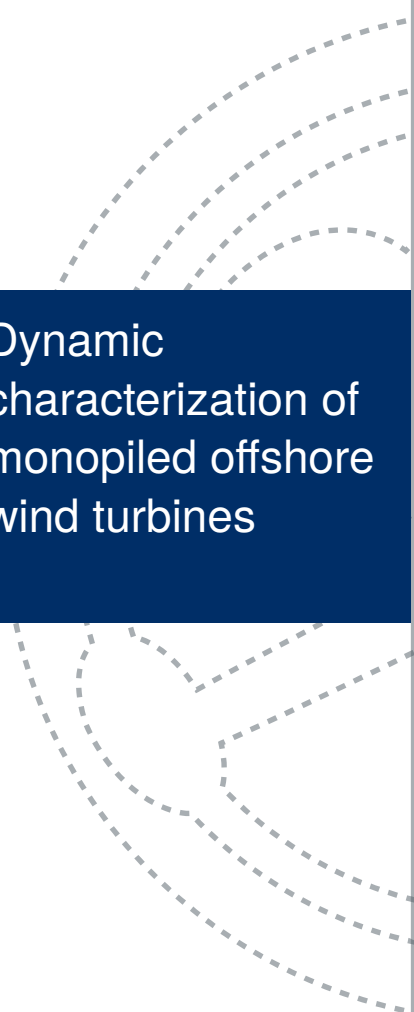
In this chapter, the performance of a pile barrier as ground vibration mitigation measure is analysed. The range of validity of the integral model to handle the wave propagation problem of the pile barrier is tested against a boundary element formulation. After the validation process, the proposed tool is used in order to study how the efficiency of the pile barrier, measured in terms of the average amplitude reduction ratio, changes depending on the considered soil profile. For this purpose, the results for the half space are compared to the ones of a single layer over a rigid bedrock profile. The main conclusions obtained from the analyses are:

- Appreciable differences are found between the half space and bedrock profiles only if the piles reach the rigid stratum. Otherwise, the results of the bedrock site closely oscillate around the ones of the half space domain. For the configurations in which the piles get to the rigid bedrock, the influence of the pile-bedrock union condition is almost negligible.
- The highest reduction due to the presence of the barrier in the bedrock profile is produced at the second natural frequency of the soil layer ($H = 3\lambda_s/4$). For higher frequencies, a decrement in the barrier efficiency is produced due to the shifts in the frequency curves of the soil displacements with and without the barrier.
- The performance of the pile barrier in the half space is highly reduced if the excitation load is placed at a distance $r_s/\lambda_s > 1$ from the pile barrier. On the contrary, the average



amplitude reduction produced by the barrier in the bedrock profile oscillates around the same mean value regardless the position of the source.

- The effects of the presence of the infinitely rigid bedrock are attenuated if the actual flexibility of the stiffer layer is considered. However, the trend in the barrier performance is maintained for the flexible bedrock profiles. Also, considering the variability-with-depth of the properties of the upper layer does not alter the main effects produced by the presence of the rigid bedrock.
- Pile barrier configurations with closer piles produce, as expected, larger attenuations of the vertical ground motion. The influence of the pile spacing is higher for the bedrock profile or for configurations with slender piles embedded in a half space domain. Regarding the pile disposition, a better performance of the pile barrier in the bedrock profile is obtained if the piles are distributed along one single row.



6. Dynamic characterization of monopiled offshore wind turbines

- 6.1 Introduction
- 6.2 Problem definition
- 6.3 Reduced substructuring methodology
- 6.4 Analysis of the properties of the set of OWTs
- 6.5 Dynamic characterization of OWT including SSI
- 6.6 Conclusions





6.1 Introduction

In the last years, the use of Offshore Wind Turbines (OWT) has experienced a great increment owing to the reduction in cost and the increase in the generators size and power. However, further research is demanded in order to better understand the dynamic behaviour of their supporting structure and so that design and lifespan can be improved.

The principal foundation type for OWTs is the monopile (81% of the OWT installed in Europe are founded on monopiles according to WindEurope [163]). Monopile foundations consist of a short hollow pile with large diameter that is driven into the seabed, and are commonly used for water depths of 20-40 meters. The simplicity of the construction and assembly is the principal advantage of this foundation type. However, the pile is a very slender structure and, consequently, more flexible than other foundation configurations (e.g. gravity based or jackets). The soil-structure interaction (SSI) effects have to be carefully considered when studying the dynamical behaviour of the OWT, being these effects highly dependent of the foundation typology used.

One of the principal effects of the SSI is the change of dynamic properties, i.e. fundamental frequency and damping, of the foundation-structure system with respect to the fixed-base structure. The variation in the eigenfrequency has to be carefully considered when designing the OWT structure in order to avoid resonance with the excitation frequencies and the corresponding increase in fatigue damage. Besides the wind and wave loads that present a frequency content below 0.1 Hz, the principal frequencies to avoid are the rotor frequency (1P) and the blade-passing frequency (3P or 2P depending on the number of blades). The first corresponds to rotor or aerodynamic unbalance loads, while the latter is produced by the shadowing effect from the wind of the blades passing the tower. The DNV [164] recommendation is to keep the tower frequency outside the $\pm 10\%$ range of these frequencies. Additionally, depending on the relation between the tower fundamental frequency and the aforementioned frequencies, three classical designs are distinguished [165, 166]: soft-soft if the tower frequency is below the 1P, soft-stiff if it is between 1P and 3P, and stiff-stiff when the structural eigenfrequency is higher than 3P. The soft-soft design is usually avoided as it corresponds to very flexible structures and shows the eigenfrequency near to the wind and wave loads. On the other hand, the stiff-stiff design is not a common choice owing to the high material requirements in order to reach the desired frequencies. Thus, the soft-stiff design is the one that is usually adopted. This design causes the OWT natural frequency to be within a very narrow range, highlighting the importance of an accurate estimation. The dynamic characterization, i.e. computation of the modified fundamental frequency and damping, of OWT structures including the SSI effects has been the object of study for numerous recent works [167–187].

In his early work, Zaaier [167] compared different methodologies used to estimate the structural fundamental frequency taking into account the soil effects. A Finite Element Method (FEM) model including the American Petroleum Institute (API) p-y, t-z, Q-z curves was taken as reference method and different foundation systems, such as monopiles, gravity footings and jackets, were assumed. The best results were obtained by using impedance matrices, as inertia effects in the foundation and non-linear soil-structure interaction were negligible. Thus, stiffness matrix models are applicable for pile foundations under loading conditions relevant



for the fatigue analysis. The obtained numerical results were compared with measures from two wind farms, resulting in acceptable predictions of the fundamental frequencies. However, Zaaier found that, as known from offshore practice, the models tend to underpredict the foundation stiffness and, therefore, the system fundamental frequency. In the same work, Zaaier also studied the sensitivity of the system fundamental frequency to variations in different parameters of soil, structure, foundation and environment, obtaining that soil parameters dominate the uncertainty of the natural frequency. The effect of the uncertainties in the soil profile was also studied by Carswell et al. [172] through probabilistic methods focusing on the Serviceability Limit State (SLS). They concluded that the system reliability shows the same sensibility to load as to soil uncertainty.

Adhikari and Bhattacharya [168] enhanced the Bernoulli model developed by Tempel and Molenaar [188] in order to include the effects of a flexible foundation and the tower axial load. The pile foundation was represented by two frequency-independent springs simulating the lateral and rotational stiffness. They illustrated the analytical results with numerical examples and applied their model to real turbines. Later Bhattacharya and Adhikari [173] evaluated the lateral and rotational foundation stiffness by direct measurement and compared their results with those obtained from a small-scale prototype and from a FEM model. They observed that analytical and FEM results overestimated, in general, the system natural frequency. More recently, Arany et al. [169] further developed their model by including the cross-coupling term in the foundation stiffness and using the Timoshenko theory to model the tower. They concluded that the cross-coupling spring term has a significant effect on the natural frequency, while the Timoshenko beam model does not significantly improve the results, being the slender beam assumption accurate enough. The effect of including the cross-coupling term was also studied by Zania [174]. She presented an analytical iterative method to obtain the equivalent modified period and damping due to SSI effects based on the pile impedance functions from Novak and Nogami [189]. She concluded that disregarding the off-diagonal terms and the frequency dependency of the impedance matrix is inappropriate, since it results in a non-conservative overestimation of the fundamental frequency and underestimation of damping. This effect was more evident as the height of the system increases. This conclusion might explain why Bhattacharya and Adhikari [173] find that natural frequencies tend to be overestimated, disagreeing with what was previously exposed by Zaaier [167].

One of the drawbacks of using the impedance functions is that they are intrinsically defined in the frequency-domain. Implementation into time-domain models allowing non-linear analysis can be done by adopting methodologies such as lumped-parameter models (LPM) [190], as done by Damgaard et al. [175, 176]. They developed different LPM to represent the impedance functions of gravity [175] and monopile [176] foundations and implemented such models in the aeroelastic code HAWC2. By studying the reference NREL 5MW OWT [191], they concluded that the side-side response is more affected by the SSI than the fore-aft vibration for gravity foundations; and that the SSI effects are critical in the design of OWT on monopiles as they have a great impact on the fatigue damage equivalent moment at seabed. Their LPM was used in a later work [177] to study the effect of changes in the soil properties on the system fundamental frequency, damping and fatigue loads in parked conditions. The changes of soil stiffness, soil damping and the presence of sediment transportation at seabed were shown to be critical.



Bisoi and Haldar [170] made use of the p-y curves to represent the soil-pile interaction in a FEM model that included wind and wave loads. They compared three soil profiles (homogeneous, linear and parabolic) obtaining that the natural frequency marginally changes between them. The three profiles presented the same properties at a depth equal to the pile diameter. They also found that the effect of soil non-linearity increases for higher wind speeds. Damgaard et al. [178] obtained the OWT fundamental frequency and damping by using both experimental data from rotor-stop tests and a Winkler approach based on the p-y curves. The Winkler approach together with a hysteresis loop method reasonably estimated the modal soil material damping.

Bhattacharya et al. [179] carried out small scale tests of OWT founded on monopiles and tripods. They illustrated that the natural frequency of the overall system shifts with the number of cycles of loading due to the softening or stiffening of the foundation. Lombardi et al. [171] further studied this relation for monopiles on clay soils, obtaining that the fundamental frequency decreases while the damping increases with the number of cycles of repeated loading. The drop in the natural frequency is higher when the forcing frequency is close to the system natural frequency.

Damgaard et al. [180] studied the influence of the water pore pressure on the estimation of the tower fundamental frequency by combining a Kelvin and a bi-dimensional FEM models. They compared the numerical results with experimental free-vibration tests, obtaining a better agreement when the permeability of the soil was considered. Yu et al. [181] also investigated the effect of the presence of water in the soil on the dynamic behaviour of OWT founded on monopiles and gravity foundations by executing earthquake centrifuge tests. They demonstrated that the SSI plays a significant role in the seismic behaviour of OWT, affecting the structural settlement, foundation response and fundamental frequency of the system. They remarked the difficulty of the observation and analysis, especially if soil liquefaction is produced.

Bisoi and Haldar [182] addressed the optimization of the structural mass for 2 and 5 MW OWT founded on monopiles in clay. The SLS, fatigue life and resonance avoidance criteria were checked and p-y curves were used to model the soil-pile interaction. They found that the rotor and nacelle mass and the tower height play a crucial role on design, while the embedded depth of the monopile beyond the critical length has a marginal impact. Myers et al. [183] analysed when the strength (resistance in operational and extreme conditions) or stiffness (resonance avoidance) criteria govern the design of monopiles for OWT, and presented optimum pile sections that satisfied these demands. If a fixed base was assumed, the strength criterion controlled the design; but when the soil flexibility was included, the stiffness criterion became important in two of the three studied sites, corresponding to deeper water depths.

Despite most of the studies focus on the tower lateral vibrations, there are several works related to other vibration modes. Kjølraug and Kaynia [184] studied the vertical seismic response of the NREL 5MW OWT, showing that the tower could amplify up to two times the vertical accelerations at the seabed. On the other hand, Tibaldi et al. [185] showed that, in addition to the structural modes, the blade and additional aeroelastic modes can play a significant role in the structural response during operational conditions.

An interesting associated phenomenon is highlighted, for instance, by Hu et al. [186], who

showed the tendency of the system to easily get stuck in resonance, exposing the necessity of a good estimation of the system fundamental frequency in generators with variable rotor speed.

In this chapter, the dynamic characterization of structures for offshore wind turbines founded on monopiles is addressed through a simplified substructuring procedure based on modal parameters. The problem under study is defined in Section 6.2, where data of real OWT structures and typical soil profiles are used as starting points. Then, the proposed substructuring approach is detailed in Section 6.3. In Section 6.4 the modal properties of the considered structures are further analysed in order to obtain characteristic trends representative of this type of systems. Section 6.5 presents different parametric analyses that reflect the influence of several properties, such as the soil profile or the dimensions of the monopile, on the dynamic characteristics of the OWT structures. Finally, Section 6.6 summarizes the main conclusions obtained from the previous results.

6.2 Problem definition

As mentioned before, this chapter addresses the dynamic characterization of OWT structures founded on monopiles. The system is assumed to be composed by a conical hollow tower, rotor and generator nacelle located at the tower top, and a monopile acting as foundation (see Fig. 6.1). The tower is connected to the monopile through a transition piece, which is a cylindrical hollow beam presenting some working platforms that give access to the OWT structure for maintenance or repair activities. The monopile is assumed to be a cylindrical hollow beam that is driven into the seabed and that is composed by two different parts: the above-soil portion and the embedded portion, both presenting the same cross-section. The tower and pile are assumed to be made of the same material.

The system geometrical and material properties are: tower length H_t , tower top and bottom external diameters D_{top} and D_{bot} , ratio between the tower cross-section inner and outer diameters δ_t (henceforth, thickness ratio), mass of the blades and generator nacelle M_{RNA} , above-soil pile length H_p , pile embedded length L_p , pile external diameter D_p , pile thickness ratio δ_p , Young's modulus E and density ρ . Owing to the small aspect ratios that the embedded pile can present in this type of constructions, the Timoshenko's beam theory is used to model it. Thus, additional geometrical and material properties are required for the embedded pile: Poisson's ratio ν_p , shear coefficient α , and material hysteretic damping ratio ξ_p .

Finally, the problem is completely defined by knowing the water depth H_w and density ρ_w , and the soil profile. The soil profile is defined by the shear wave velocity c_s , which can change depending on the depth; and the soil Poisson's ratio ν_s , soil density ρ_s , and soil hysteretic damping ratio ξ_s , which are assumed to keep the same value for the whole profile.

The OWT system can be divided into two different parts: the superstructure (above soil) and foundation (under soil). By considering an infinite rigid base, the superstructure dynamic behaviour can be easily characterized by its fundamental frequency f_n and damping ratio ξ . However, if the foundation flexibility is included in the analysis, the SSI effects produce a reduction in the system fundamental frequency and changes in the damping ratio. The aims of this chapter are computing these changes by obtaining the flexible-base fundamen-

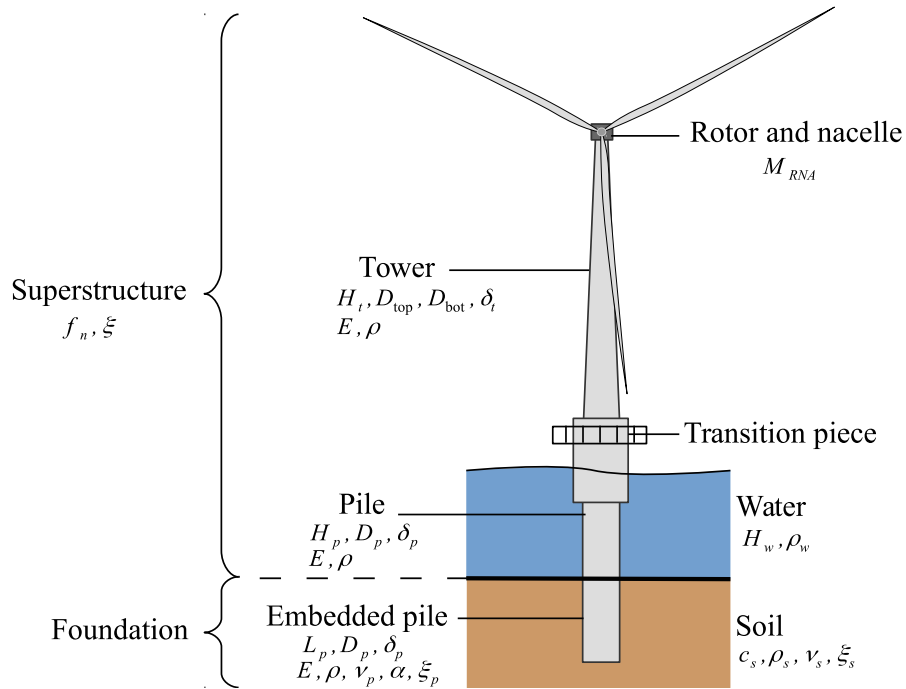


Figure 6.1: Representation of a generic OWT and identification of geometrical and material parameters.

tal frequency \tilde{f}_n and equivalent damping ratio $\tilde{\xi}$, and studying how the superstructure, the foundation and the soil profile characteristics affect them.

Set of existent OWTs taken as starting point

In order to define the properties of the OWT structures, different systems that can be found in the literature are taken as reference data. Their properties and details are presented in Table 6.1. OWTs 1-12 were extracted from the work of Lombardi [192], and correspond to wind turbines from different wind farms already built in the UK. For each farm, a range of hub heights was indicated, so the maximum and minimum values are considered. Only information about diameters and thickness of the Vestas towers was available, so these dimensions are assumed for the Siemens towers too. On the other hand, OWTs 13 and 14 correspond to systems that have been widely studied in different works, e.g. [168–171]. Thus, more detailed information about them was accessible.

However, for the selected cases, there are very few details available about the dimensions of the transition piece and the length of the pile outside the seabed. For this reason, the transition from pile to tower is assumed to be produced at water level, so the pile length is equal to the water depth ($H_p = H_w$). On the other hand, some structures present a constant wall thickness, while others have a thickness that varies along the height. In order to define all the studied OWT systems in a coherent way, the thickness ratio is kept constant for the whole length of the tower. By doing so, thicker walls are presented at the tower base, where



OWT	1-2	3-4	5-6	7-8	9-10	11-12	13	14
	Vestas	Vestas	Vestas	Siemens	Vestas	Siemens	North Hoyle	Walney S 1
	2MW-V66	3MW-V90	2MW-V80	SWT-3.6-107	2MW-V80	SWT-3.6-107	2MW-V80	3.6MW
M_{RNA} (t)	80	111	94	220	94	220	100	234
H_t (m)	60-78	80-105	60-100	80-96	60-100	80-96	70	83.5
H_w (m)	11	10	20	19	21	25	11	20
L_p (m)	15	28	31	11	33	30	33	31
D_{top} (m)	2.3	2.3	2.3	2.3	2.3	2.3	2.3	3.0
D_{bot} (m)	4.2	4.2	4.2	4.2	4.2	4.2	4.0	5.0
δ_t (%)	98.0	98.0	98.0	98.0	98.0	98.0	97.6	97.9
D_p (m)	3.5	4.3	4.2	4.7	4.0	4.7	4.0	4.2
δ_p (%)	97.4	97.9	97.6	97.7	98.2	97.7	97.5	97.6

Table 6.1.: Definition of the set of existent OWTs used in the study.

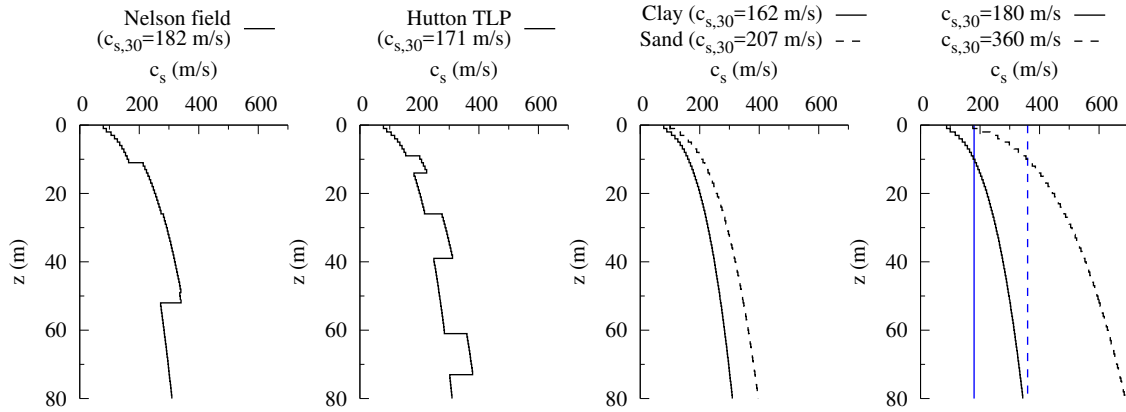


Figure 6.2: Soil profiles used in the study. Evolution of the shear wave velocity with depth.

the largest diameter is located. The values of δ_t presented in Table 6.1 are obtained as the mean value of the ones corresponding to the tower top and bottom sections.

For all the structures, the towers and piles are assumed to be made of steel. Thus, a Young's modulus $E = 210$ GPa, a Poisson's ratio $\nu_p = 0.25$ and a density $\rho = 7850$ kg/m³ are assumed. In addition, for the embedded piles, the hysteretic damping coefficient is set to $\xi_p = 2\%$ and the shear coefficient of a hollow circular cross-section $\alpha = 0.5$ is used. For the water density, $\rho_w = 1000$ kg/m³ is considered.

Soil profiles

The soil profiles assumed for the sites in the analyses are presented in terms of the shear wave velocity c_s in Fig. 6.2. The value of the average shear wave velocity [68], $c_{s,30}$, for each profile is also displayed above each plot as it is widely used to characterize the soil. Following the Eurocode 8 [68] nomenclature, the selected profiles corresponds to C ($180 < c_{s,30} < 360$ m/s) or D soil types ($c_{s,30} < 180$ m/s) which are the ones where OWT systems are usually founded on.

The principal profiles are two typical boreholes (Nelson Field and Hutton TLP) of the North Sea (see [193]) which consist of different layers of clay and sand. The values of the shear wave velocity depend on the soil material and depth, and are estimated through Eq. (6.1), proposed by Ohta and Goto [194] and where $P = 1.000, 1.260$ or 1.286 for clay, fine sand and medium sand, respectively.

$$c_s = 78.98 z^{0.312} P \quad [\text{m/s}] \quad (6.1)$$

Additionally, two soils formed only by clay or medium sand are studied as limit scenarios. Finally, two homogeneous and two variable profiles with identical values of $c_{s,30} = 180$ and 360 m/s are selected in order to present results for a wider range of soils and being able to analyse the effects of the soil non-homogeneity. These variable profiles follow the same evolution with depth as the one presented in Eq. (6.1).

As depicted in Fig. 6.2, the studied profiles are discretized by piece-wise homogeneous layers of 1 m thickness as requirement of the Green's functions used by the proposed model. For depths greater than 80 m, the shear velocity is assumed to be constant with depth (half space domain). These values are obtained after a convergence study. The rest of the soil properties are kept constant for the whole profile and are: soil density $\rho_s = 1800 \text{ kg/m}^3$, Poisson's ratio $\nu_s = 0.35$ and hysteretic damping ratio $\xi_s = 5\%$. In addition to this, the influence of the soil Poisson's ratio on the obtained results is also analysed by assuming different values, going from $\nu_s = 0.35$ to $\nu_s = 0.49$.

6.3 Reduced substructuring methodology

The dynamic characterization of the OWT-monopile system is handled through a three-step substructuring methodology. Following this procedure, one obtains a simplified model that eases the study of the variation of the fundamental frequency and damping due to the foundation stiffness. Fig. 6.3 sketches out the three steps of the proposed substructuring methodology: First of all, the fixed-base superstructure system is reduced to a single-degree-of-freedom system in terms of its shear effective modal mass and height (b). Then, the foundation stiffness is modelled through the corresponding impedance functions (c). Finally, both parts are coupled together into a three degrees-of-freedom substructuring model (d). In the following sections, each step is further detailed.

6.3.1 Foundation modelling

The foundation stiffness is represented by a set of impedance functions (K_{ij}) which relates the force (moment) in direction i with the displacement (rotation) in direction j . As studied in

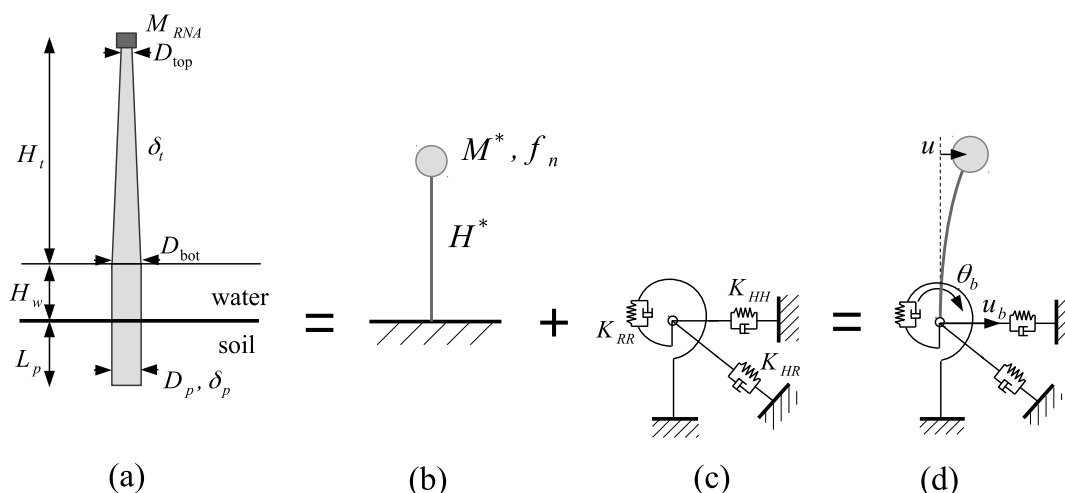


Figure 6.3: Stages of the substructuring methodology. (a): System real geometry. (b): Superstructure representation through modal parameters. (c): Foundation stiffness representation through impedance functions. (d): Simplified substructuring model.



Chapter 3, the impedance functions are frequency-dependent and complex-valued, with real and imaginary terms representing the stiffness and damping components, respectively. As the lateral response of the structure is studied, only the horizontal $K_{HH}(\omega)$, rocking $K_{RR}(\omega)$, and coupled horizontal-rocking $K_{HR}(\omega)$, impedances are considered (Fig. 6.3c).

The developed integral model is used for the computation of the different impedance functions that are needed along this chapter. Due to the high number of combinations of soil profiles and monopile geometries considered in the analyses, and because in Chapter 3 the effects of the soil variability on the impedance functions of pile foundations are thoroughly studied, no results in terms of impedance functions are presented in this chapter.

6.3.2 FE model for the dynamic characterization of the superstructure on fixed base

The application of the simplified three-step procedure implies the need of defining effective masses and heights for every configuration. These are often obtained through explicit expressions derived for simplified geometries. In the present case, the realistic geometrical properties assumed herein for the problem under study do not allow following the same strategy. For this reason, the mass and height that will be used below for the characterization of the superstructure are obtained through a modal analysis based on a finite elements representation of the system, which will also allow the assumption of different properties for each structural section. At this step, fixed-base conditions will be assumed.

The superstructure, composed by the conical tower and the above-soil portion of the slender pile, is modelled as Bernoulli beams. For this type of structures, differences with respect to a more elaborated Timoshenko theory are negligible [169]. Constant-section two-noded four-degrees-of-freedom Hermitian beam elements are used for the discretization of both the cylindrical (pile) and conical (tower) lengths. A high enough number of elements, set by proper convergence studies, is used to correctly represent the conical tower stiffness.

The generator and rotor masses are added as a punctual mass at the tower tip node. The hydrodynamic water added mass plus the mass of the internal water are also considered for the submerged elements. This additional mass is included by using a modified density $\bar{\rho} = \rho + \rho_w(C_m + \delta^2)/(1 - \delta^2)$ for the computation of the translational mass matrix of the submerged beam elements. An added mass coefficient $C_m = 1$ is assumed in this study. This consideration, despite significantly increasing the system total mass, does not affect the obtained results for the fundamental mode of vibration, as observed by Zania [174].

Considering harmonic displacements and forces, the fundamental frequency and its modal shape are obtained by solving the eigenvalues problem:

$$[\mathbf{K} - \omega^2 \mathbf{M}] = 0 \quad (6.2)$$

where \mathbf{K} and \mathbf{M} are the superstructure stiffness and mass matrices obtained by the assembly of the elemental ones. As this equation is used to obtain the system modes of vibration, no damping is considered.

The fundamental frequency $\omega_n = 2\pi f_n$ and its modal shape ϕ_n are obtained as the smallest eigenvalue (frequency) and its eigenvector (shape). Once the modal shape is known, the



base shear effective modal mass M^* and height H^* of the system to a base acceleration excitation can be obtained through, e.g. [67]:

$$M^* = \frac{(\phi_n^T \mathbf{M} \mathbf{l})^2}{\phi_n^T \mathbf{M} \phi_n}; \quad H^* = \frac{\mathbf{h}^T \mathbf{M} \phi_n}{\phi_n^T \mathbf{M} \mathbf{l}} \quad (6.3)$$

where \mathbf{l} is the influence vector presenting unitary values in the terms that correspond to lateral displacements and zeros in the components corresponding to rotations; and \mathbf{h} is the vector containing the height of each node in the terms that correspond to its lateral displacements and unitary values in the components corresponding to rotations.

The base shear effective modal mass (henceforth modal mass) coincides with the mass of a single-degree-of-freedom system that produces the same base shear force as the complete system vibrating at the corresponding modal frequency. On the other hand, the base-moment effective modal height (henceforth modal height) is the height of the aforementioned modal mass at which its inertia force produces the same base overturning moment as the distributed masses of the system at the modal frequency. The modal mass and height can also be obtained for all the modes of vibration by using expression (6.3) with the corresponding modal shapes. For higher modes negative modal heights can be obtained, implying that the base shear force and moment have opposite algebraic signs. The choice of these parameters to represent the system is made as the base shear force and moment are the reactions that interact with the foundation impedance functions.

6.3.3 Reduced substructuring model

Once the modal parameters of the OWT in fixed-base conditions and the impedance functions representing the soil-foundation system are obtained, they are coupled together reducing the problem to a three degrees-of-freedom model representing the complete system as depicted in Fig. 6.3d, where u is the mass lateral displacement relative to the base and u_b and θ_b are the base displacement and rotation. In coherence with the model used for the computation of the fixed-base modal parameters, a given harmonic free-field ground lateral acceleration \ddot{u}_g is defined as system excitation. The equations of motion of the simplified problem can then be expressed in matrix form as:

$$\left(\begin{bmatrix} K^* & 0 & 0 \\ 0 & K_{HH}(\omega) & K_{HR}(\omega) \\ 0 & K_{HR}(\omega) & K_{RR}(\omega) \end{bmatrix} - M^* \omega^2 \begin{bmatrix} 1 & 1 & H^* \\ 1 & 1 & H^* \\ H^* & H^* & (H^*)^2 \end{bmatrix} \right) \begin{Bmatrix} u \\ u_b \\ \theta_b \end{Bmatrix} = -M^* \ddot{u}_g \begin{Bmatrix} 1 \\ 1 \\ H^* \end{Bmatrix} \quad (6.4)$$

where $K^* = (2\pi f_n)^2 M^* (1 + 2i\xi)$ is the lateral structural stiffness associated with the first mode that also includes the structural damping through the modal damping factor ξ .

In order to obtain the flexible-base fundamental frequency and damping ratio, the methodology of finding an equivalent single-degree-of-freedom oscillator that reproduces the system response is used (see e.g., [26, 195]). In this study, a hysteretically damped oscillator with



natural frequency $\tilde{\omega}_n$ and damping ratio $\tilde{\xi}$ is assumed and the equivalence is established in terms of the transfer function:

$$Q(\omega) = \left| \frac{\omega_n^2 u}{\ddot{u}_g} \right| = \left| \frac{1}{\left(1 - \frac{\omega^2}{\tilde{\omega}_n^2}\right) + 2i\tilde{\xi}} \right| \quad (6.5)$$

which represents the shear force at the base of the structure per effective seismic force [67]. As the single-degree-of-freedom system cannot reproduce the response of the substructuring model in all the frequency range, the maximum value Q_m of the transfer function is chosen as common point between both models. This maximum value is obtained by iteratively solving Eq. (6.4). The flexible-base fundamental frequency corresponds to the frequency at which this maximum value takes place, while the equivalent damping ratio is computed as:

$$\tilde{\xi} = \frac{1}{2Q_m} \quad (6.6)$$

Validation of the reduced substructuring model

In order to validate the ability of the proposed formulation to correctly capture the flexible-base fundamental frequency, an enhanced FEM model where the presence of the soil-pile system is included through the corresponding impedance functions is used. For that purpose, the displacement of the superstructure due to the ground horizontal acceleration and considering the foundation stiffness and damping is obtained by solving the equation:

$$(\mathbf{K}'(\omega) - \omega^2 \mathbf{M}) \mathbf{U} = -\mathbf{M} \mathbf{I} \ddot{u}_g \quad (6.7)$$

being $\mathbf{K}'(\omega)$ the superstructure stiffness matrix including the foundation dynamic stiffness and damping functions in the terms that correspond to the ground node and \mathbf{U} the vector containing the nodal lateral displacements and rotations relative to the ground displacement. The flexible-base fundamental frequency is then obtained as the one at which the maximum response, in terms of $Q(\omega)$, takes place.

The flexible-base fundamental frequencies of the OWTs defined in Table 6.1 are computed through both the proposed three-step and the enhanced FEM formulations. Table 6.2 shows the computed modified eigenfrequencies together with the errors with respect to the enhanced FEM model, considering the Nelson Field soil profile. The results show negligible differences between both methodologies, revealing the ability of the proposed strategy to correctly represent the effects of the foundation on the system fundamental frequency. Results for harder soils were also obtained producing smaller differences, but are not presented for simplicity's sake.

It is important to notice that both the three-step and the FEM approaches are substructuring methodologies, as they incorporate the soil-foundation interaction effects through the impedance functions. The principal difference between them is that the three-step formulation makes use of the fundamental modal mass and height concepts (and therefore considers



OWT	1	2	3	4	5	6	7	8	9	10	11	12	13	14
\tilde{f}_n (Hz)	0.44	0.32	0.31	0.21	0.42	0.22	0.23	0.18	0.37	0.20	0.22	0.17	0.37	0.22
error (%)	0.38	0.25	0.12	0.07	0.53	0.16	0.19	0.12	0.34	0.12	0.16	0.09	0.24	0.19

Table 6.2: Validation of the proposed three-step formulation against the FEM model. Flexible-base fundamental frequency for the OWT systems. Results for the Nelson Field soil profile.

the fundamental mode only), while the FEM model does not, and takes all modes into account. The validation results show that the flexible-base fundamental frequency can be accurately estimated by using the three-step approach owing to the fact that the first mode of the soil-structure system is principally influenced by the first mode of the fixed-base structure. However, the three-step methodology does not guarantee a correct estimation of the modified natural frequencies for higher modes. The principal advantage of the proposed three-step methodology lies in its efficiency and suitability for undertaking parametric studies.

6.4 Analysis of the properties of the set of OWTs

In this section, the modal parameters and monopile geometries of the set of real offshore wind turbines presented in Section 6.2 are analysed. The purpose of this study is to delimit the typical range in which the values of those parameters lie in order to adequately define the parametric study of the influence of the SSI effects. As a result of the analyses, characteristic relations between the modal parameters of medium-sized monopiled OWT structures are found.

Analysis of the modal properties

The results of the modal analysis following the methodology presented in Section 6.3.2 for the studied OWT systems are shown in Table 6.3. The fixed-base fundamental frequencies of the superstructures are found to be between 0.2-0.55 Hz, agreeing with the typical range for OWT constructions. On the other hand, the values of the modal mass and height are closely related to the structural dimensions. The modal mass is found to be 25-35% of the system total mass (including water added mass), while the modal height coincides with 85-90% of the system total height.

The obtained modal parameters for the studied OWT systems are plotted against each other in Fig. 6.4. A strong correlation is found for all the three possible combinations. A par-

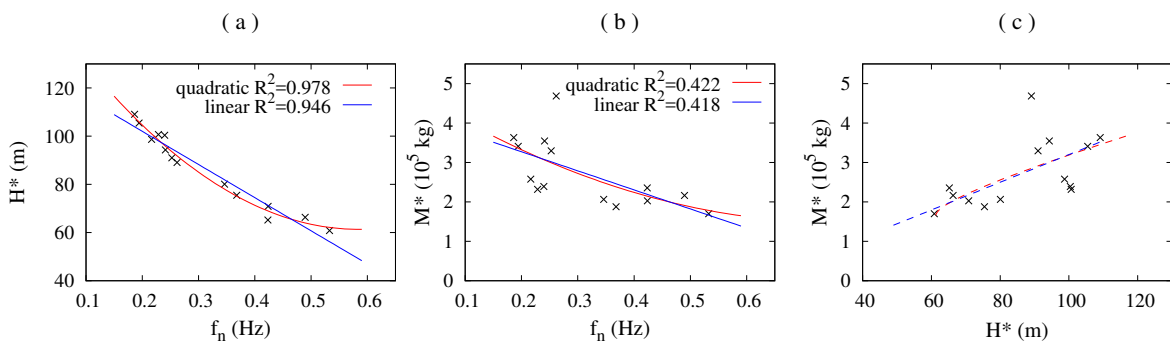


Figure 6.4: Modal parameters for the studied set of OWT (crosses). Polynomial regressions of the modal height (a, solid lines) or mass (b, solid lines) as a function of the fixed-base fundamental frequency. Relation between the modal mass and modal height obtained by using the regressed expressions (c, dashed lines).



OWT	1	2	3	4	5	6	7	8	9	10	11	12	13	14
f_n (Hz)	0.53	0.37	0.35	0.23	0.49	0.24	0.25	0.19	0.42	0.22	0.24	0.19	0.42	0.26
H^* (m)	60.8	75.4	80.1	100	66.3	100	91.0	105	65.2	98.7	94.3	109	70.8	89.1
H^*/H_{total}	0.86	0.85	0.89	0.88	0.83	0.84	0.92	0.92	0.81	0.82	0.90	0.90	0.87	0.86
M^* (t)	170	188	206	232	216	239	329	341	236	258	355	363	203	469
M^*/M_{total}	0.34	0.35	0.31	0.32	0.24	0.24	0.27	0.27	0.28	0.27	0.24	0.24	0.32	0.38

Table 6.3: Modal parameters for the studied OWT systems.



ticularly high dependence between the modal height and fixed-base fundamental frequency is found. In order to derive an expression that relates the modal parameters, the computed modal mass and height values are fitted by first and second order polynomials as functions of the superstructure fixed-base eigenfrequency, yielding the following expressions:

$$H^*(f_n) = 130 - 138f_n \quad [\text{m}] \quad (6.8a)$$

$$M^*(f_n) = 4.24 - 4.84f_n \quad [10^5 \text{ kg}] \quad (6.8b)$$

$$H^*(f_n) = 161 - 341f_n + 292f_n^2 \quad [\text{m}] \quad (6.9a)$$

$$M^*(f_n) = 5.92 - 8.97f_n + 4.89f_n^2 \quad [10^5 \text{ kg}] \quad (6.9b)$$

The proposed polynomials are also plotted in Figs. 6.4a,b as solid lines, showing that the modal height and mass can be fitted without significant errors by both the linear and quadratic expressions. Dispersion is higher for modal mass than for modal height. The modal mass corresponding to OWT number 14 is the only one that does not adequately fit in the obtained mass-frequency relations. This structure has a higher modal mass owing to its thick tower and pile walls when compared to the rest of the studied systems. Finally, Fig. 6.4c shows the relations between modal mass and height obtained by using the proposed polynomials. Eqs. (6.8) or (6.9) correctly represent the relation between both parameters. The use of these expressions is not recommended outside the frequency range 0.15-0.60 Hz shown in Figs 6.4a,b.

Now, and once the fixed-base fundamental frequency is set, the modal mass and modal height can be accurately estimated through Eqs. (6.8) or (6.9), reducing the number of parameters needed to represent the superstructure from three to one. With the aid of those expressions, instead of a discrete number of structures, a continuous set of OWT systems representing the typical dimensions for this type of constructions can be included in the results presented in the following sections. Both the quadratic and linear expressions are used: the first fits the data better, while the constant slope of the latter allows to easily understand the contribution of each parameter to the obtained results.

Analysis of the monopile dimensions

Now that the superstructure is completely defined, it is necessary to establish the dimensions of the monopile foundations. Following the same procedure conducted for the modal parameters, Fig. 6.5 presents the relation between the pile diameter (a) or pile embedded length (b) and the modal parameters for the OWT systems defined in Table 6.1. The data are fitted again by first and second order polynomials as functions of the system fixed-base fundamental frequency.

A high correlation is found between the pile diameter and the superstructure fixed-base fundamental frequency, showing that smaller pile diameters tend to correspond to shorter

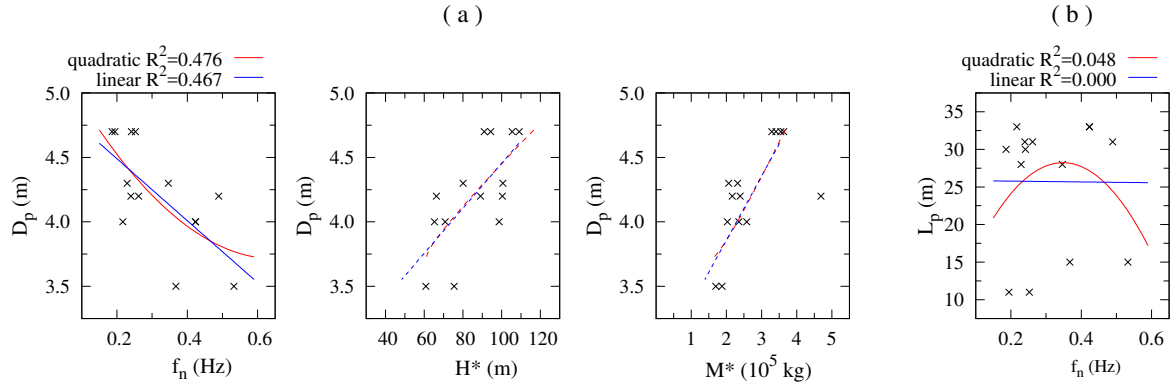


Figure 6.5: Pile diameter (a) and pile length (b) with respect to superstructure modal parameters for the studied OWT systems (crosses). Polynomial regressions of the pile diameter as a function of the fixed-base fundamental frequency (a, solid lines). Relations between the pile diameter and modal height or mass obtained by using the regressed expressions (a, dashed lines). Polynomial regressions of the pile embedded length as a functions of the fixed-base fundamental frequency (b, solid lines).

and more rigid structures. The fitting procedure yields to the following expressions, plotted as solid lines in Fig. 6.5a:

$$D_p(f_n) = 4.97 - 2.40f_n \quad [\text{m}] \quad (6.10)$$

$$D_p(f_n) = 5.40 - 5.15f_n + 3.93f_n^2 \quad [\text{m}] \quad (6.11)$$

The use of these expressions together with Eqs. (6.8) and (6.9) adequately represents the relations between the pile diameter and superstructure modal mass and height too, as shown by the dashed lines in Fig. 6.5a.

On the other hand, the pile length cannot be correctly adjusted by the polynomial fitting as a function of the fixed-base fundamental frequency. In this type of constructions, the pile embedded length is more dependent on the soil properties than on the superstructural dimensions. Thus, different values of the pile length can be found independently of the fixed-base fundamental frequency.

Finally, the pile wall thickness value is established following the API [196] recommendation as a function of the pile diameter:

$$t_p \approx 6.37 + \frac{D_p}{100} \quad [\text{mm}] \quad (6.12)$$

Note that $\delta_p = (D_p - 2t_p)/D_p$.

6.5 Dynamic characterization of OWT including SSI

As commented in the previous section, if Eqs. (6.8) or (6.9) are used, the superstructure is completely defined by setting the fixed-base fundamental frequency and the structural modal

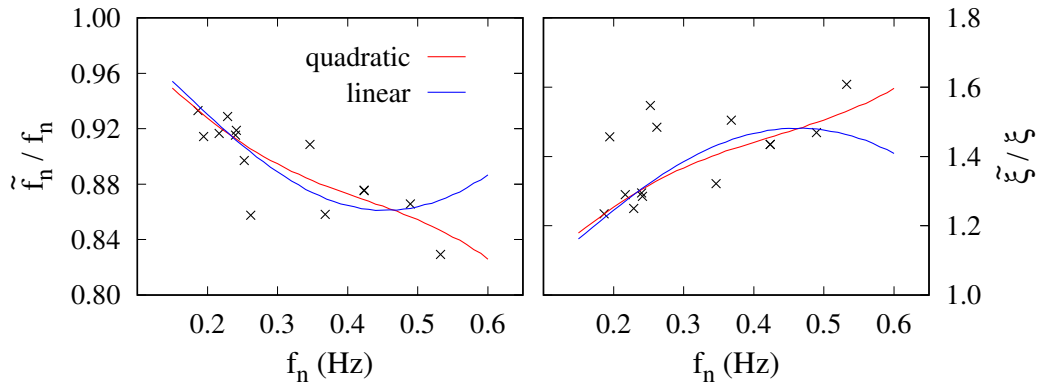


Figure 6.6: Effective-to-fixed-base natural frequency and effective-to-structural damping ratios. Comparison between the results of the regressed (lines) and real (crosses) modal parameters and pile dimensions. Results for the Nelson Field soil profile. Pile length $L_p = 25$ m for the regressed dimensions.

damping. Values between 0.15-0.60 Hz are used as a common range within which the OWT fixed-base eigenfrequency is found and coinciding with the range within the studied set of OWT structures lies. On the other hand, for the fixed-base modal damping ratio a value of $\xi = 1\%$ is chosen following the recommendation of the GL Guideline [197].

The pile diameter and wall thickness are also determined once the fixed-base fundamental frequency is set by using Eqs. (6.10) or (6.11) and (6.12), respectively. On the other hand, and aiming at studying different foundation geometries, three values of pile embedded length $L_p = 15, 25$ and 35 m are considered.

In the following, the effects of the structural properties, soil profile and monopile dimensions on the dynamic characterization of offshore wind turbines are analysed.

6.5.1 Influence of the superstructure properties

In order to explore the influence of the OWT fixed-base fundamental frequency and damping on the magnitude of the SSI phenomena, Fig. 6.6 presents the ratios \tilde{f}_n/f_n (effective-to-fixed-base natural frequency ratio) and $\tilde{\xi}/\xi$ (effective-to-structural damping ratio) as functions of the fixed-base fundamental frequency of the superstructure. Their values are obtained following the simplified procedure detailed in section 6.3.3. The results are obtained assuming the Nelson Field soil profile. The crosses represent the results obtained assuming the properties of each one of the initial OWT systems (modal properties listed in Table 6.3 and pile dimensions in Table 6.1). On the other hand, the lines present the results that are obtained by using the regressions from (6.8) to (6.12) and assuming a pile embedded length $L_p = 25$ m.

Attending to Fig. 6.6, the curves from the fitted polynomials follow the overall trends of the points representing the actual OWT systems, both in the frequency and damping variations. Thus, the use of the fitting expressions for the structural modal mass and height and for the monopile diameter is justified for the general study of the SSI effects on the dynamic properties of OWT structures.



At low frequencies ($f_n < 0.45$ Hz), virtually the same results are obtained from the use of both the linear or quadratic fitting. However, at higher frequencies ($f_n > 0.45$ Hz), the curves diverge owing to the differences that are produced at these frequencies in the regression polynomials, especially the ones of the modal mass and height (see Fig. 6.4). The quadratic expressions are found to better adjust the real points, but, as only two points are available within this frequency range, it is not possible to discern whereas the quadratic polynomials represent the real trend or if this effect is produced due to overfitting.

In order to explain the shapes of the curves and the differences observed between the results of the real and fitted data, one has to consider the influence of each modal parameter (fixed-base frequency, modal mass and height) on the magnitude of the SSI phenomena. All of these parameters have the same effect: increasing its value amplifies the magnitude of the SSI (i.e. increases the reduction of the fundamental frequency and the damping gain). This can be easily explained for the modal mass and fixed-base fundamental frequency: when one of these parameters augments while keeping the other constant, an increment of the system stiffness is produced. Thus, the foundation becomes relatively softer compared to the superstructure, resulting in more significant SSI phenomena taking place. On the other hand, the increasing importance of SSI effects for higher wind turbines is in line with the results of Zania [174], and also agrees with the conclusions of classical works [195, 198] showing that the SSI effects becomes more evident as the wave parameter ($\sigma = c_s/H f_n$) decreases. Those effects are further illustrated by Fig. 6.7, which presents the changes in the fundamental frequency and structural damping ratio that are produced when one of the three modal parameters varies keeping the other two constant. Several values within the considered ranges are used, and the diameter of the monopile is kept independent of the fundamental frequency in order to isolate the effects of the modal properties.

Attending to the commented effects, the shape of the curves in Fig. 6.6 can be explained considering that, in their first part ($f_n < 0.45$ Hz) the magnitude of the SSI phenomena increases with the fixed-base natural frequency; while in the second part ($f_n > 0.45$ Hz) the effect of the reduction in the modal mass and height (Fig. 6.4) overtakes the effect of the increment in the eigenfrequency if the linear expressions are used. On the other hand, if the quadratic relations are considered, only the frequency effect is present as the modal mass and height remain practically the same in the high frequency range, explaining why the magnitude of the SSI phenomena continues increasing with the fixed-base natural frequency. It is important to note that the influence of the variation of the pile diameter due to the changes in the fixed-base fundamental frequency has been omitted in the previous discussion in order to focus on the effects of the modal properties. As the monopile diameter decreases as the fixed-based fundamental frequency increases (see Fig. 6.5), the SSI effects are further magnified due to the higher flexibility of the foundation. In any case, the influence of the pile diameter is thoroughly analysed in Section 6.5.3.

The results presented by Fig. 6.6 also prove the importance of including the SSI effects in the preliminary design stages of OWT structures. For $f_n < 0.25$ Hz, the \tilde{f}_n/f_n ratio is found to be around 0.92 (8% reduction) while for $f_n > 0.25$, this reduction can be greater than 15%, with one data point at $f_n \approx 0.25$ yielding a \tilde{f}_n/f_n ratio much smaller than the one obtained from the fitted expressions, and with the effects of SSI growing with the fixed-base fundamental frequency of the superstructure.

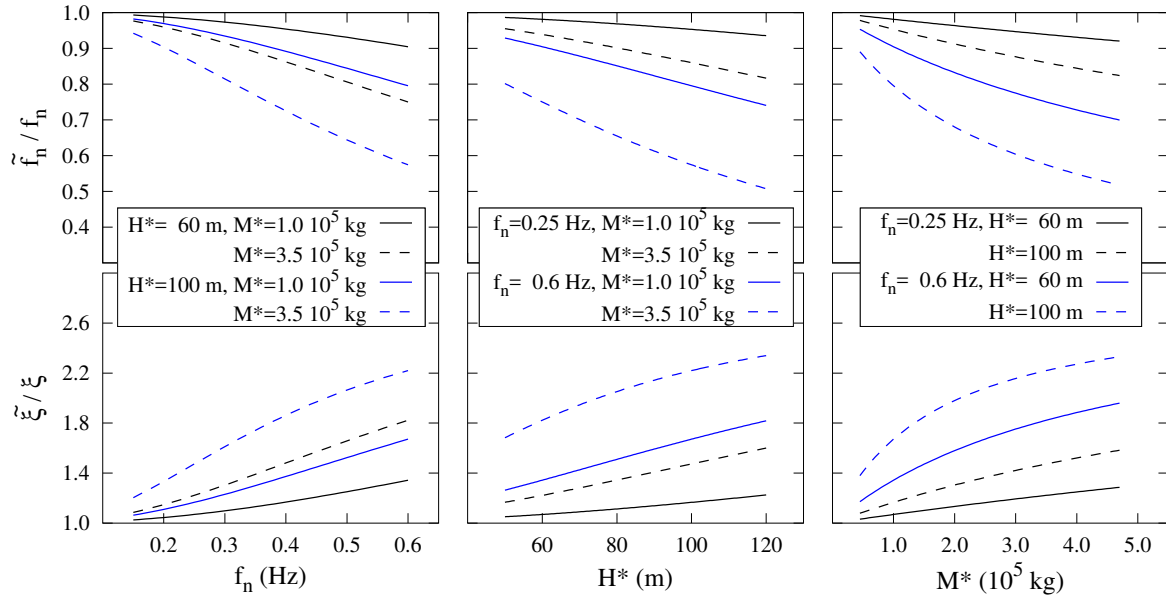


Figure 6.7: Influence of the modal parameters on the fundamental frequency and damping variations. Pile diameter $D_p = 4$ m and length $L_p = 25$ m. Results for the Nelson Field soil profile.

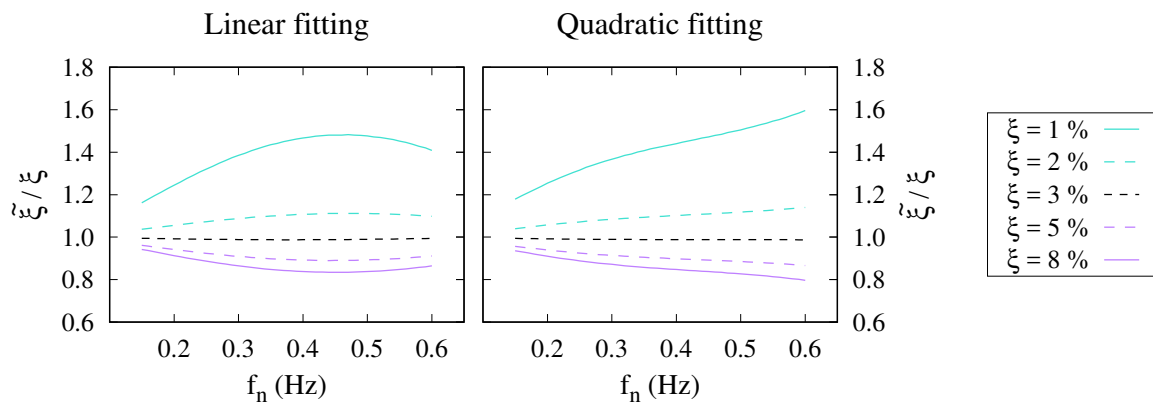


Figure 6.8: Influence of the fixed-base structural modal damping on the damping variations. Pile length $L_p = 25$ m. Results for the Nelson Field soil profile.

Despite for all of the studied systems a structural modal damping $\xi = 1\%$ is assumed, Fig. 6.8 illustrates that depending on the considered fixed-base modal damping coefficient, the SSI effects change its value in a different manner. Fig. 6.8 shows the relation between the flexible and fixed-base damping ratios that is obtained by assuming different modal damping ratios ($\xi = 1-8\%$) and considering the same pile length and soil profile as for Fig. 6.6. For a modal damping $\xi = 3\%$ virtually no variations are seen. As the modal damping goes away from this value, the variations become stronger: increasing the flexible-base damping ratio for $\xi < 3\%$ and decreasing it otherwise. Nevertheless, the frequency range at which the system is more sensitive to the SSI effects, i.e. stronger variations, is almost the same. These conclusions are equally valid both for the linear and quadratic fittings.

6.5.2 Influence of the soil profile

Figs. 6.9 and 6.10 present the effective-to-fixed-base natural frequency ratio and the effective-to-structural damping ratio as a function of the fixed-base fundamental frequency of the superstructure for the continuous set of configurations obtained from the fitting expressions obtained in Section 6.4 and assuming a pile length $L_p = 25$ m. The results are grouped according to the use of the linear or the quadratic fitting. First, Fig. 6.9 shows the results for the two typical North Sea's profiles (Nelson Field and Hutton TLP), the sand and clay profiles, and the homogeneous soil with $c_{s,30} = 180$ m/s as its value is the closest to the one of the Nelson Field profile. Then, Fig. 6.10 compares the results obtained for the homogeneous and variable profiles with $c_{s,30} = 180$ and 360 m/s in order to study the effects of harder soils and the influence of the variable-with-depth profile.

The soil properties and profile evolution with depth have a direct influence on the magnitude of the SSI effects, producing higher variations as the soil becomes softer. However, the obtained results show the necessity of using a good measure to characterize the soil flexibility. Using the $c_{s,30}$ as a value to define the soil seems not to be a feasible option: profiles with close (e.g. Nelson Field and Homogeneous in Fig. 6.9) or even the same (Fig. 6.10) value of this mean shear wave velocity produce different frequency and damping variations depending on the evolution with depth of the profile. Moreover, the homogeneous assumption is a non-conservative hypothesis as those profiles produce smaller variations in both the fundamental frequency and equivalent damping than variable profiles with similar or higher values of $c_{s,30}$.

The superficial layers are the ones that govern the effects of the SSI on the dynamic properties of the studied structures. Fig. 6.9 shows that Nelson Field, Hutton TLP and clay profiles (which present identical properties along the first ~ 10 meters) produce virtually the same variations in the system fundamental frequency and damping. This is related to the fact that the horizontal impedance of piles in non-homogeneous soils is principally determined by the superficial layers [84, 85], being this impedance term of crucial importance to the studied problem.

As expected, the magnitude of the SSI phenomena is less significant in harder soils (Fig. 6.10). However, variations over 10% in the system fundamental frequency and over 30% in the structural damping can be produced even for these hard soils. Fig. 6.10 shows again the importance of accurately knowing the actual soil profile. Results for the variable-with-depth

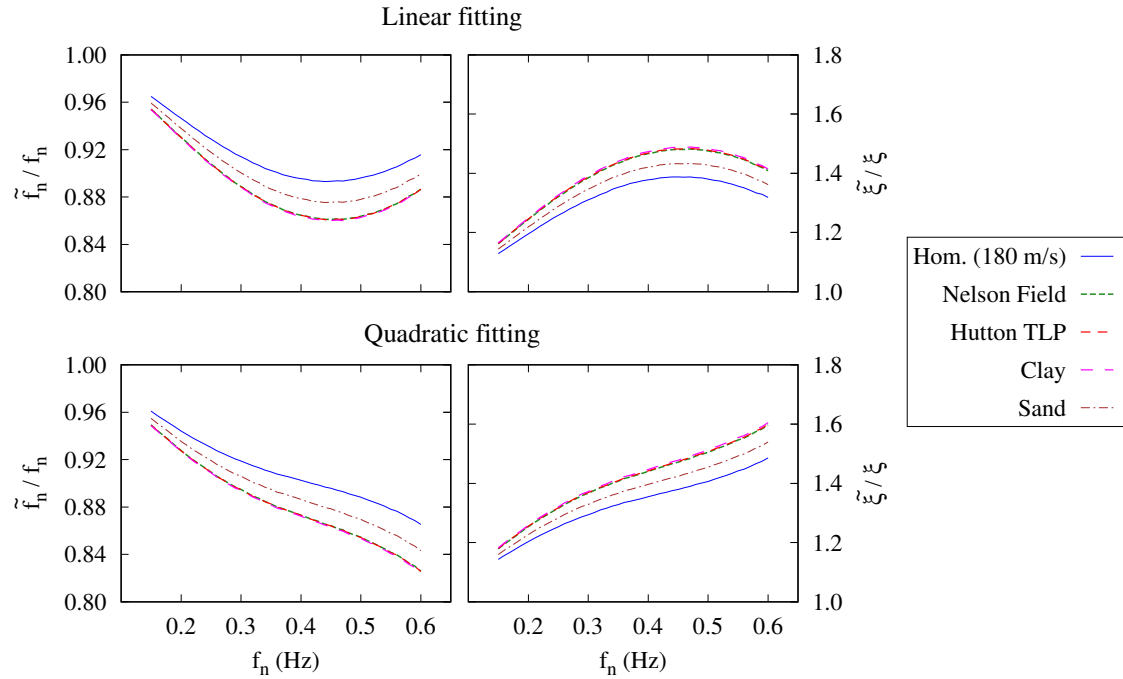


Figure 6.9: Influence of the soil profile on the effective-to-fixed-base natural frequency ratio and effective-to-structural damping ratio. Pile length $L_p = 25$ m.

soil with $c_{s,30} = 360$ m/s are closer to the ones for the $c_{s,30} = 180$ m/s homogeneous profile rather than to the homogeneous soil with the same mean velocity.

Influence of the soil Poisson's ratio

Fig. 6.11 presents the variations in the fundamental frequency and damping of the OWT systems for the Nelson Field profile and considering different values of the soil Poisson's ratio. This analysis is made in order to show the influence of this parameter on the SSI effects, as high Poisson's ratios are commonly used to represent saturated soils (through equivalent elastic media). Values of ν_s between 0.35-0.49 are considered, while the rest of soil properties have the same values introduced in Section 6.2.

The results of Fig. 6.11 show that increasing the soil Poisson's ratio has almost no influence on the SSI effects, agreeing with the findings of Daamgard et al. [177]. The soil profile is defined in terms of the shear wave velocity. Thus, as the Poisson's ratio augments, the soil becomes slightly more rigid and, therefore, the variations in the system fundamental frequency and damping are marginally reduced. However, practically the same results are obtained for the extreme cases of $\nu_s = 0.35$ and 0.49. This effect is seen for all the studied profiles, but only the ones corresponding to the Nelson Field profile are presented for brevity's sake.

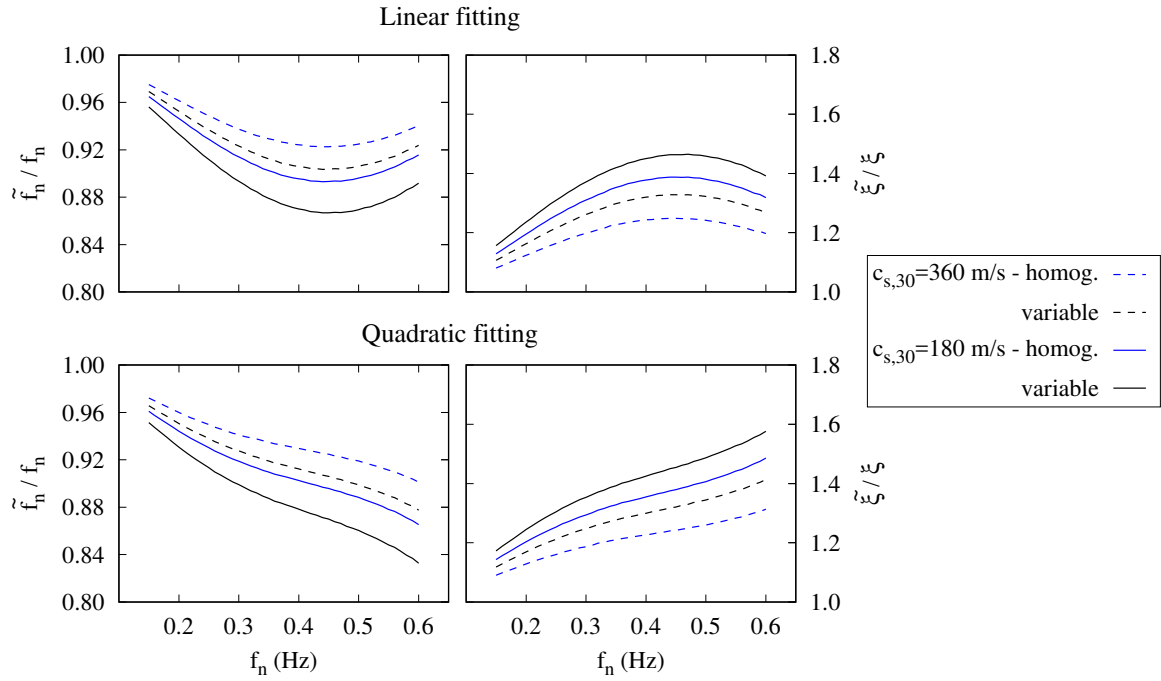


Figure 6.10: Influence of the soil profile on the effective-to-fixed-base natural frequency ratio and effective-to-structural damping ratio. Comparison between soft (solid) and hard (dashed) soils and between homogeneous (blue) and variable-with-depth (black) profiles with identical $c_{s,30}$. Pile length $L_p = 25$ m.

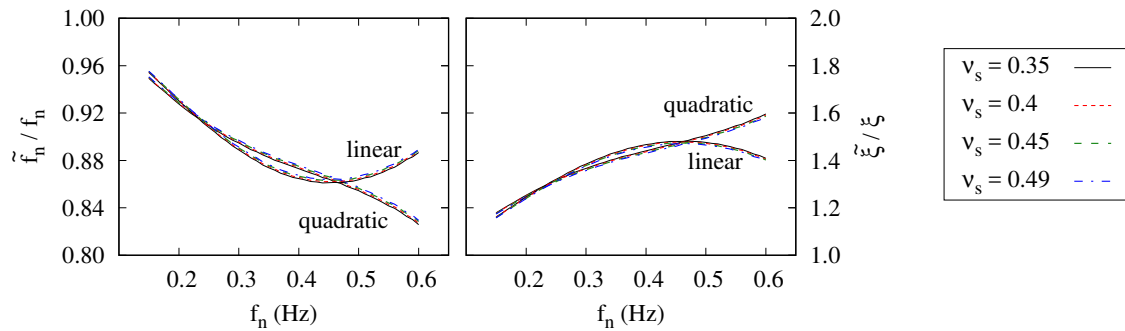


Figure 6.11: Influence of the soil Poisson's ratio on the effective-to-fixed-base natural frequency ratio and effective-to-structural damping ratio. Pile length $L_p = 25$ m. Results for the Nelson Field soil profile.

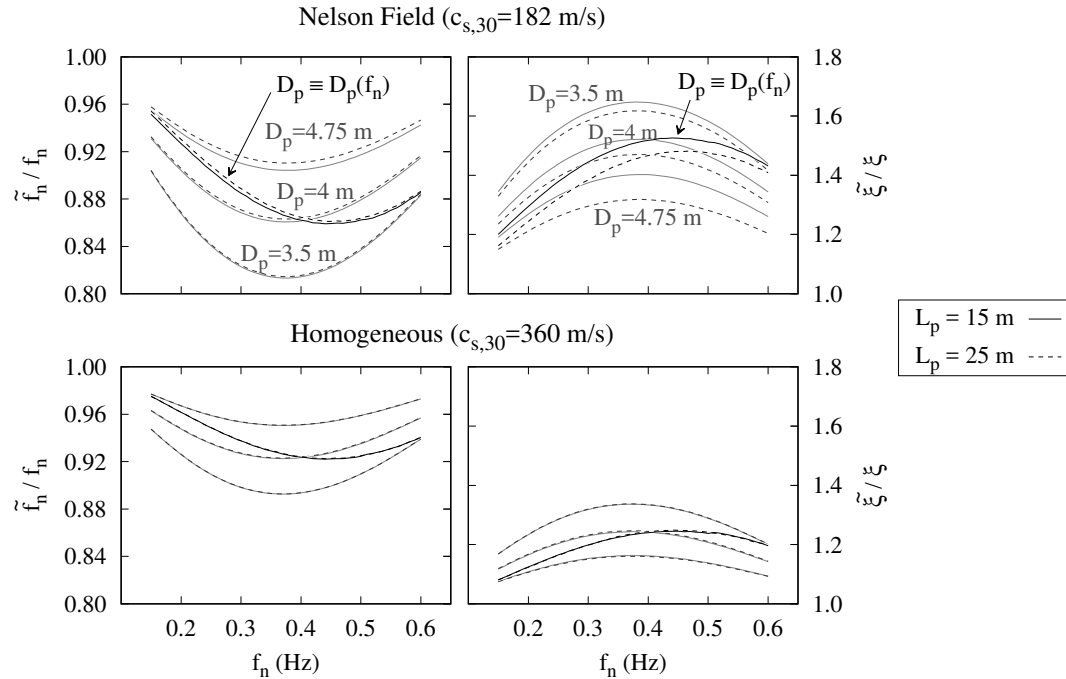


Figure 6.12: Influence of pile diameter and pile length on the effective-to-fixed-base natural frequency ratio and effective-to-structural damping ratio. Linear fitting. $L_p = 15$ m (solid lines) and $L_p = 25$ m (dashed lines).

6.5.3 Influence of the monopile dimensions

Influence of the pile diameter

The pile diameter has a decisive role in the variations in the fundamental frequency and damping of the superstructure produced due to SSI effects. As the foundation stiffness strongly depends on the pile diameter, increasing its value results in a great reduction of the shifts in both the system eigenfrequency and damping. However, this role is not clearly seen in the previous results, as the diameter is implicitly defined as a function of the fixed-base fundamental frequency. Fig. 6.12 presents the effective-to-fixed-base natural frequency ratio and the effective-to-structural damping ratio obtained by assuming three frequency-independent pile diameters in addition to the results corresponding to the use of the diameter linear regression (eq. 6.10). As the same effects are found for all the studied cases, only the results corresponding to the linear expressions and for two soils profiles: Nelson Field and Homogeneous ($c_{s,30} = 360$ m/s) representing soft and hard soils, respectively, are shown.

The curves obtained through the regressed pile diameter present an increment in the magnitude of the SSI phenomena as the fixed-base frequency augments, due to the reduction in the pile diameter (see Fig. 6.5). The effect of the pile diameter is almost independent of the pile length or the soil profile. However, for the softest soil profile, the differences between the results of the higher and lower diameters increase: e.g., for Nelson Field, the highest variation in the system fundamental frequency goes from 0.81 to 0.91 depending on the diameter,

while for the Homogeneous ($c_{s,30} = 360$ m/s) this variation goes from 0.89 to 0.95.

Influence of the pile length

Fig. 6.12 also presents the results obtained assuming two different pile embedded lengths: $L_p = 15$ m and $L_p = 25$ m.

Contrary to the diameter, the pile length has little importance on the effects of the foundation on the system fundamental frequency. Only for the highest diameter and softest soil profile, some differences can be seen between the 15 m piles and the longer one. This is produced because of the fact that for higher diameters (smaller L/D ratios) the active length of the pile increases. Moreover, the differences between the 15 and 25 m lengths increase for the variable-with-depth profiles, where longer piles can reach stiffer layers. The above-mentioned effects are also manifested for the damping variations in a greater extent. $L_p = 25$ m is found to be larger than the active pile length in all cases, as results obtained for $L_p = 35$ m are completely coincident with those of $L_p = 25$ m (not shown for the sake of clarity).

On the other hand, for harder soils (Homogeneous $c_{s,30} = 360$ m/s), the active length for all diameters is below the 15 meters. Thus, no differences are observed between the studied lengths in both the frequency and damping variations.

6.6 Conclusions

In this chapter, the developed model is used together with a simplified substructuring methodology for the dynamic characterization of monopiled offshore wind turbines. The integral model is used to compute the impedance functions of different variable-with-depth soil profiles based on real boreholes of the North Sea. On the other hand, the superstructure is represented by its fixed-base fundamental frequency and the first-mode base shear effective modal mass and height in the substructuring model.

Data from different medium-sized existent OWT systems that are found in the literature are used to obtain relations between the modal properties that are characteristics of this type of constructions. These relations are then employed to study the changes in the fundamental frequency and damping ratio of general OWT structures founded on different monopiles and soil profiles:

- The results confirm the importance of considering the foundation stiffness in the design stage of OWT systems in order to keep its fundamental frequency within the allowed range and to estimate the equivalent damping ratio of the structure.
- The influence of the flexibility of the foundation is especially relevant for small diameter monopiles on soft soils.
- The magnitude of the SSI phenomenon is significant for $f_n > 0.25$ Hz, and specially for $f_n \approx 0.45$ Hz. This frequency range usually corresponds to a soft-stiff design, so special attention is required for those systems whose fundamental frequency is close to the 1P frequency.



- The recommendation of keeping the structural fundamental frequency $\pm 10\%$ away from the 1P and 3P (or 2P for two-bladed rotors) frequencies may not be enough if the foundation-structure fundamental frequency is not adequately computed, as the SSI effects can reduce the fixed-base fundamental frequency more than a 15%.
- An accurate knowledge of the soil properties and their evolution with depth is required when evaluating the foundation effects. Mean values, such as $c_{s,30}$, are insufficient for characterizing the soil stiffness.
- The superficial soil layers are found to be the ones that govern the changes in the fundamental frequency and damping ratio due to SSI effects.

A vertical grey line runs down the page. To its left, several sets of concentric dashed grey arcs are visible, some above and some below a dark blue rectangular box.

7. Summary, conclusions and future research directions

- 7.1 Summary and conclusions
- 7.2 Future research directions





7.1 Summary and conclusions

The present dissertation formulates and implements a numerical model for the dynamic analysis of pile foundations. The formulation is based on the integral expression of the reciprocity theorem in elastodynamics and the use of specific Green's functions for the layered half space. On the other hand, piles are treated as load lines acting inside the soil domain, introducing their additional stiffness effects through the equilibrium finite element equations. The soil and piles equations are coupled together by imposing compatibility and equilibrium conditions in terms of displacements and soil-pile interaction tractions, respectively.

The use of the advanced fundamental solution, that already satisfies the boundary conditions of the layered half space, removes the need of meshing any of the soil contours (free-surface or layer interfaces). In addition to this, the treatment of piles as dimensionless load lines avoids any discretization of the soil-pile interfaces, with the corresponding reduction in the number of degrees of freedom of the problem, especially at the pile shaft. Thus, a simplified (yet still rigorous) model is obtained where all the formulation is written only in terms of the pile variables: displacements and interaction tractions. The proposed numerical tool allows the study of the dynamic behaviour of pile foundations in a highly efficient way, even in soil profiles that present a high variability of their properties with depth.

The computational performance of the developed code is further optimized through a numerical strategy that significantly reduces the number of times that the advance fundamental solution has to be computed. As the evaluation of the fundamental solution is the most time-consuming process of the model, the implementation of this strategy leads to important savings in the running times of the code, especially when dealing with regular pile configurations.

The developed model can assume different excitation types in order to tackle a variety of engineering problems. The incidence of seismic wavefronts propagating through the layered media, the presence of external loads acting over some regions of the free-surface, and boundary conditions directly imposed at the pile caps or pile heads in terms of displacements or forces are the possible excitations sources. After validating the proposed integral model, in the present dissertation the following problems involving piles in non-homogeneous media have been considered:

- *Impedances of inclined piles in non-homogeneous soil profiles.* The stiffness and damping functions of single piles and pile groups with inclined elements have been obtained in the frequency domain. The influence of the soil profile on the impedance functions has been demonstrated by comparing the results of different soils with several levels of non-homogeneity.
- *Seismic response of piles in non-homogeneous soil profiles.* Kinematic interaction factors and maximum bending moments for piles embedded in continuously-variable soil profiles have been obtained. The importance of the soil profile and the inability of the recommended mean soil properties to estimate the foundation response have been highlighted by the obtained results.



- *Piles as ground vibration mitigation measure.* The proposed model is able to simulate the use of piles as a measure to limit the transmission through the soil of vibrations produced by a point load in the vertical direction. The performance of pile barriers embedded in different soil profiles has been discussed in terms of the average amplitude reduction factor over a surface behind the piles.
- *Dynamic characterization of monopiled offshore wind turbines including SSI effects.* The importance of considering the flexibility of the monopile in the estimation of the dynamic properties of the foundation-structure system for offshore wind turbines has been confirmed through the use of a substructuring methodology and impedance functions obtained by the integral model. It has been found that the reductions in the system fundamental frequency due to the soil-structure interaction effects can be larger than the 10% value given by the recommended design guides, especially in soil profiles with a high variability.

A thorough analysis of each one of these problems and more detailed conclusions are presented at the end of their corresponding chapters.

7.2 Future research directions

In this section several future research directions are proposed accordingly with the experience gained from the present work. They are separated into three main directions. The first focuses on the use and enhancement of the developed model for the analysis of pile foundations and piled structures in layered soils. The second group is related to the implementation of the advanced fundamental solution into other boundary-element-based codes developed by the Research Group. The last direction is aimed at extracting technical knowledge from the results obtained by the integral model. These proposed lines of research are detailed in the following:

Integral model:

- *Dynamic analysis of pile foundations.* In its present form, the developed numerical tool can be used to address a wide variety of problems involving piles in layered media. Some of these problems are:
 - From the impedance functions and kinematic interaction factors obtained by the integral model, and making use of substructuring techniques [26], study the influence of the soil profile on the soil-structure interaction phenomena (variations in structural period and damping).
 - Study of the seismic response of pile foundations embedded in layered soils subjected to incident waves with an arbitrary angle of propagation. Analysis of the influence of the soil profile on kinematic displacements and bending moments.
 - Application of the integral model to study more complex pile configurations. Several examples are the analysis of pile groups formed by a large number of elements or the study of the performance of “metabarriers” [159, 160] as ground vibration

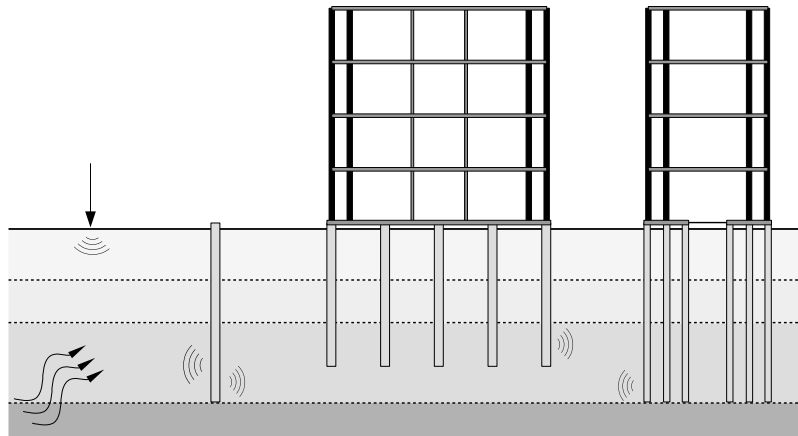


Figure 7.1: Sketch of the enhanced integral model with finite element structures.

mitigation measure. In this direction, analysis of optimal pile configurations by using any optimization techniques.

- *Implementation of superstructures.* Following the previous BE-FE model, it would be possible to introduce the presence of superstructures supported by the pile foundations. This way, the enhanced model would allow the direct solving of problems that are complex to handle through substructuring approaches.
 - Generic structural types could be implemented by combining beam and shell finite elements. The coupling between these structures and the piles could be done through the rigid caps or directly by imposing compatibility and equilibrium conditions at the corresponding nodes. This approach would allow the simulation of flexible foundations, as well as structures supported by several pile groups.
 - This enhanced code could also consider several structures that only interact between each other through the energy propagation in the soil. By doing so, the influence of the soil profile in the structure-soil-structure interaction effects could be analysed.
 - Other application of the enhanced model with structures is the analysis of site-city interactions [199–203]. For this study, each building could be modelled as a single beam (complex beam elements could be used in order to consider eccentricity between the elastic and mass centres) connected to a single pile (which could have equivalent properties that represent other foundation types).
- *Study of moving-load problems.* The developed formulation could be adapted to analyse problems involving a point load that moves with a certain velocity over the free-surface. The tuning of this type of formulation would allow analysing study cases in which the excitation of the system is the passing of near vehicles, such as railway traffic.

In its most developed form, the developed numerical model could be used to simulate systems involving generic sources of excitation (seismic waves, traffic loads, etc.), several piled

structures and the presence of pile barriers to mitigate the ground vibrations, as represented in Fig. 7.1. The problem would be tackled through a direct approach, and a high variability of the soil profile could be considered.

Use of the advanced fundamental solution in other codes:

- *Regularization of the fundamental solution.* An adequate regularization process of the fundamental solution should be implemented in order to accurately integrate it inside two-dimensional elements without using any special collocation strategy. Once this problem is solved, it would be possible to introduce the fundamental solution for the layered half space in the previous boundary element codes. This way, different foundation types (e.g. surface or embedded foundations) could be analysed without meshing the free-surface and layer interfaces. The Research Group has started working in this direction. As a first approach, Mindlin's solution for the homogeneous half space has

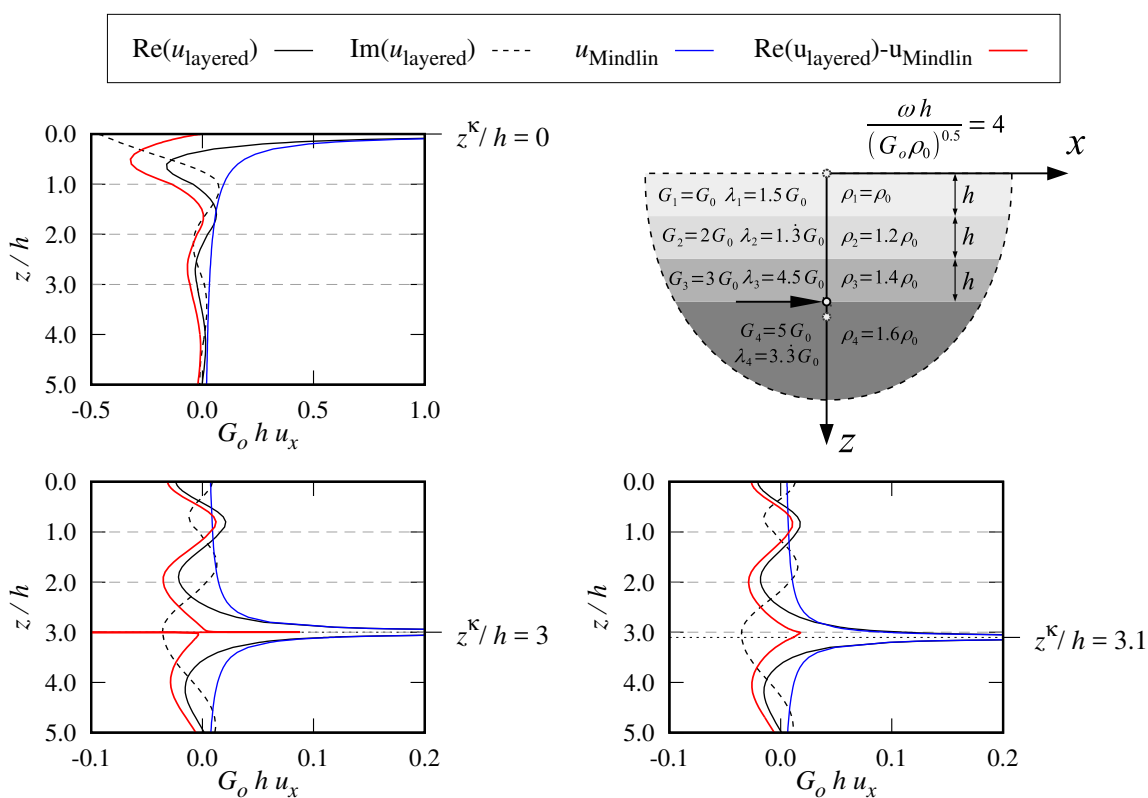


Figure 7.2: Regularization of the fundamental solution for the layered half space. Problem adapted from [62]. Collocation point at the free surface ($z^k/h = 0$), at a layer interface ($z^k/h = 3$) and inside a layer close to an interface ($z^k/h = 3.1$). Regularization of the layered fundamental solution by using Mindlin's solution assuming the properties of the layer (collocation inside a layer or at free-surface) or the average properties of the two layers connected by the interface (collocation at layer interface).



been used to subtract the singularity of the layered fundamental solution. This technique has led to satisfactory results when the collocation point is located at the free-surface or inside a soil layer, but not when the collocation point coincides with a layer interface, as illustrated by Fig. 7.2. This first approach could be used to analyse soils with low non-homogeneity. For a more general solution, in a further step, the regularization through the static bi-material solution [64] would be considered.

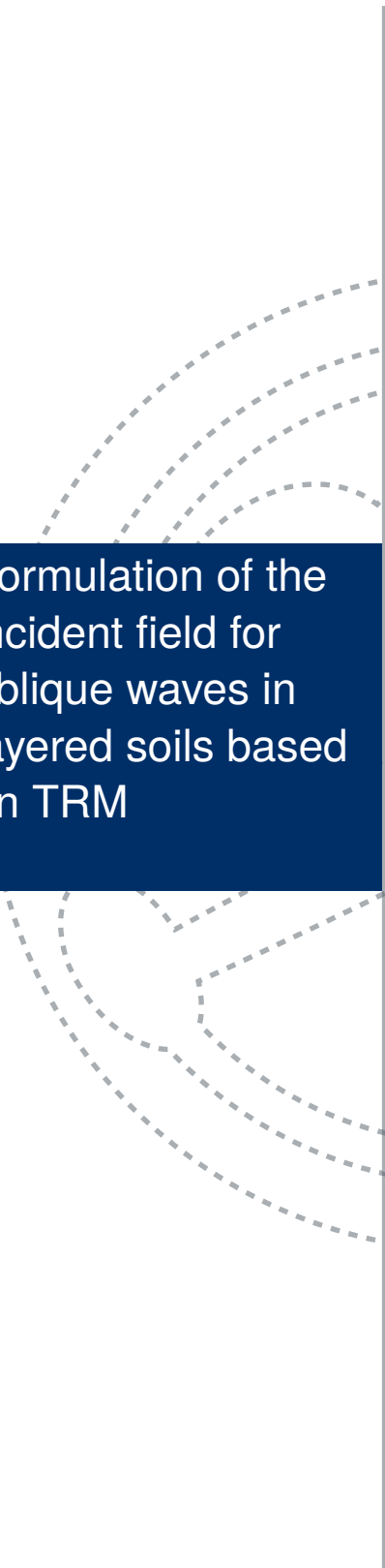
- *Numerical strategies for an efficient use of the fundamental solution.* In order to efficiently use the advanced fundamental solution in a boundary element code (which generally implies a larger number of degrees of freedom) it would be necessary to develop some techniques that speed up the evaluation process of the fundamental solution. These techniques could be considered in the sense of reusing values for pairs of collocation-observation points, either by exploiting geometrical symmetries or setting some kind of databases; but also more elaborated approaches such as the use of appropriate interpolation functions or surrogate models could be contemplated.

By completing these tasks, the numerical models could efficiently simulate the dynamic behaviour of a huge number of structural and foundations types founded in soils with a high non-homogeneity level. The structural design could even be made by combining continuous elements with simplified beam or shell elements.

Knowledge transfer:

- *Open access software.* The models and numerical tools developed from the present research work could be released in the future. This could be in form of open source libraries or executable files. It is worthy to highlight that owing to the benefits of the used fundamental solution, these codes could be run in a standard-performance computer.
- *Extraction of recommendations through Machine Learning.* The versatility and efficiency of the proposed model could be used to obtain large sets of results for problems with high interest in engineering. By using those large databases together with machine learning techniques [204–209], it would be possible to obtain expressions and recommendations of direct practical applicability. Security factors for including soil-structure interaction effects, expressions for equivalent properties that allow the study of variable profiles through homogeneous models or corrector coefficients that incorporate the effects of the soil profile are some examples of possible applications. This new line of research has several common points with some of the work done by other Divisions of the SIANI Institute. Thus, it could open new collaborations and synergies between the different Research Groups.

These last future research directions are aimed at giving practical value and utility to the results obtained by the developed model. They try to take advantage of the efficiency of this model in order to produce scientific knowledge that could be useful for the scientific and technical communities in the field of civil engineering.

A vertical grey line runs down the center of the slide. To its left, several concentric dashed grey arcs are visible, some above and some below the main text box.

A. Formulation of the incident field for oblique waves in layered soils based on TRM

- A.1 Problem definition
- A.2 Incident SH waves (out-of-plane problem)
- A.3 Incident SV-P waves (in-plane problem)
- A.4 Generic incident waves
- A.5 Numerical aspects



This appendix contains the formulation of the displacements and stresses at any point of the layered soil domain produced by the incidence of body waves with a generic angle of propagation. The proposed formulation starts with the expressions proposed by Wolf [210] to define the displacements and stress tensor for each layer of the soil. Then, a procedure based on Transmission and Reflection Matrices (TRM), similar to the one employed to obtain the used Green's functions [62], is used in order to relate the amplitudes of the upwards and downwards waves that propagates inside each layer to the ones that defines the seismic excitation. Following the presented methodology, it is possible to directly obtain the displacements and stresses at any depth of the layered half space domain without having to solve any system of equations.

First, Section A.2 details the procedure for incident SH waves. Then, the obtained expressions are generalized to the SV-P wave problem in Section A.3. Section A.4 couples together both formulations into a single set of equations. The appendix is ended by Section A.5 which highlights some numerical aspects that should be considered for the implementation of the proposed methodology.

A.1 Problem definition

The seismic excitation is modelled as a wavefront of body waves originated by an infinitely-distant source. At the studied site, this wavefront is assumed to propagate through the half space layer inside the $x-z$ plane with a known (yet arbitrary) angle of propagation. Once this incident wavefront reaches the first layer interface, reflection and transmission phenomena take places, producing different waves that either propagates upwards to the free-surface or are reflected back to the unbounded media.

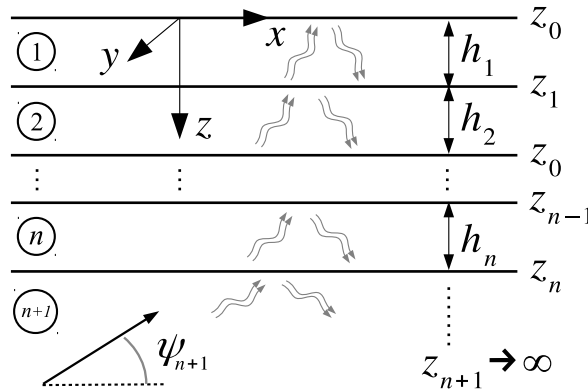


Figure A.1: Definition of the soil stratification.

Fig. A.1 shows a sketch of the problem, together with the layer numbering and coordinate system of reference that is used along this appendix. The nomenclature of the properties for each layer j of the soil is:

- Layer thickness: h_j

- Position of the lower interface with respect to the free-surface: z_j
- Angle of propagation of each body wave: ψ_{SH_j} , ψ_{SV_j} and ψ_{P_j}
- Shear and Primary wave propagation velocity: c_{s_j} and c_{p_j}
- Shear and Lamé's elastic constants: G_j and λ_j
- Displacement vector at any point inside the layer:

$$\mathbf{u}^j = \begin{Bmatrix} u_x^j \\ u_y^j \\ u_z^j \end{Bmatrix} \quad (\text{A.1})$$

- Stress tensor at any point inside the layer:

$$\boldsymbol{\sigma}^j = \begin{pmatrix} \sigma_{xx}^j & \tau_{xy}^j & \tau_{xz}^j \\ \tau_{xy}^j & \sigma_{yy}^j & \tau_{yz}^j \\ \tau_{xz}^j & \tau_{yz}^j & \sigma_{zz}^j \end{pmatrix} \quad (\text{A.2})$$

Together with the aforementioned properties, the following layer-independent parameters are also used: excitation angular frequency ω , imaginary unit $i = \sqrt{-1}$, apparent velocity c and its corresponding wavenumber $k = \omega/c$.

A.2 Incident SH waves (out-of-plane problem)

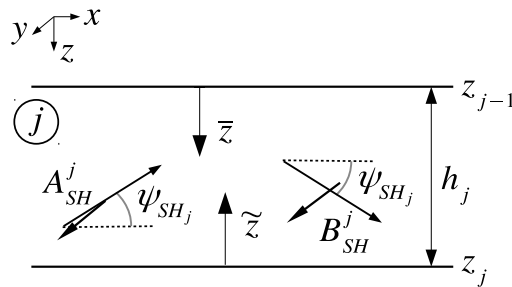


Figure A.2: Definition of the waves travelling through each layer. Incident SH waves.

First, the out-of-plane problem of incident SH waves is considered. The waves that propagate through each layer of the soil are depicted in Fig. A.2. For this excitation, the waves propagate in the $x - z$ plane imposing displacements in the y direction. The compatibility condition in the x direction for each soil interface imposes that:

$$c = \frac{c_{s_j}}{m_j} \quad (\text{A.3a})$$

$$k = \frac{\omega}{c} = \frac{\omega}{c_{s_j}} m_j \quad (\text{A.3b})$$

where, for simplicity:

$$m_j = \cos \psi_{SH_j} \quad (\text{A.4a})$$

$$t_j = -i \sqrt{1 - \frac{1}{m_j^2}} \equiv \tan \psi_{SH_j} \quad (\text{A.4b})$$

$$m_j t_j = \sin \psi_{SH_j} \quad (\text{A.4c})$$

As defined before, c is the apparent propagation velocity of the waves inside the soil. It indicates the speed at which the wave front travels along the horizontal direction and its value is the same for all of the soil layers. Thus, from Eq. (A.3a) it is possible to determine the propagation angles of all layers once one of them is fixed (usually the one corresponding to the bottom unbounded domain). Note that, despite it is not necessary for the SH wave problem, the definition of t_j results in the correct sign for the case of SV waves with an angle of propagation below the critical one [210].

The necessary displacements and components of the stress tensor for the application of the boundary conditions of the problem are:

$$u_y^j(x, z) = \bar{u}_y^j(z) e^{-ikx}; \quad \bar{u}_y^j(z) \equiv \bar{u}_y^j(\bar{z}) = A_{SH}^j e^{ikt_j \bar{z}} + B_{SH}^j e^{-ikt_j \bar{z}} \quad (\text{A.5})$$

$$\tau_{yz}^j(x, z) = G_j \left(\frac{du_y^j}{dz} \right) = \bar{\tau}_{yz}^j(z) e^{-ikx}; \quad \bar{\tau}_{yz}^j(z) \equiv \bar{\tau}_{yz}^j(\bar{z}) = ikt_j G_j \left(A_{SH}^j e^{ikt_j \bar{z}} - B_{SH}^j e^{-ikt_j \bar{z}} \right) \quad (\text{A.6})$$

Expressing these relations in matrix form results in:

$$\begin{bmatrix} \bar{u}_y^j(\bar{z}) \\ \bar{\tau}_{yz}^j(\bar{z}) \end{bmatrix} = \begin{bmatrix} 1 & 1 \\ \beta_j G_j & -\beta_j G_j \end{bmatrix} \begin{bmatrix} e^{ikt_j \bar{z}} & 0 \\ 0 & e^{-ikt_j \bar{z}} \end{bmatrix} \begin{bmatrix} A_{SH}^j \\ B_{SH}^j \end{bmatrix} \quad (\text{A.7})$$

where:

$$\beta_j = ikt_j \quad (\text{A.8})$$

It can be seen that in Eq. (A.7) both positive and negative exponential terms are present. The positive exponentials can lead to numerical instabilities. Therefore, they must be transformed into negative ones by expressing the displacements produced by the upwards waves (A_{SH}^j) in terms of the local variable \bar{z} . This way, each component of the displacement expression results in:

$$u_A = e^{-ikt_j \bar{z}} A_{SH}^j; \quad u_B = e^{-ikt_j \bar{z}} B_{SH}^j \quad (\text{A.9})$$

In order to write all expressions in terms of the same variable, the global depth coordinate z is used. Thus, the two local depth coordinates can be written as:

$$\bar{z} = z - z_{j-1}; \quad \tilde{z} = z_j - z \quad (\text{A.10})$$

With these transformations, Eq. (A.7) results in:

$$\begin{bmatrix} \bar{u}_y^j(\bar{z}) \\ \bar{\tau}_{yz}^j(\bar{z}) \end{bmatrix} = \begin{bmatrix} 1 & 1 \\ \beta_j G_j & -\beta_j G_j \end{bmatrix} \begin{bmatrix} e^{-ikt_j(z_j-z)} & 0 \\ 0 & e^{-ikt_j(z-z_{j-1})} \end{bmatrix} \begin{bmatrix} A_{SH}^j \\ B_{SH}^j \end{bmatrix} \quad (A.11)$$

where, now, all exponential terms are negative because, in any layer j , it is always satisfied that $z_{j-1} \leq z \leq z_j$.

Following the TRM methodology, the next redefinitions are made:

$$\mathcal{E}_j(z) = e^{-\beta_j z} \quad (A.12)$$

$$w_u^j(z) = \mathcal{E}_j(z_j - z) A_{SH}^j \quad (A.13a)$$

$$w_d^j(z) = \mathcal{E}_j(z - z_{j-1}) B_{SH}^j \quad (A.13b)$$

where w_u^j and w_d^j represent the amplitudes of the upwards and downwards waves at any point of the layer.

With this change, the previous relation between the displacements and stresses with the wave amplitudes results in:

$$\begin{bmatrix} \bar{u}_y^j(z) \\ \bar{\tau}_{yz}^j(z) \end{bmatrix} = \begin{bmatrix} 1 & 1 \\ \beta_j G_j & -\beta_j G_j \end{bmatrix} \begin{bmatrix} w_u^j(z) \\ w_d^j(z) \end{bmatrix} \quad (A.14)$$

This expression can be expressed in a generic form as:

$$\begin{bmatrix} \bar{u}_y^j(z) \\ \bar{\tau}_{yz}^j(z) \end{bmatrix} = \begin{bmatrix} H_{11}^j & H_{12}^j \\ H_{21}^j & H_{22}^j \end{bmatrix} \begin{bmatrix} w_u^j(z) \\ w_d^j(z) \end{bmatrix} \quad (A.15)$$

This notation will ease the comparison between the formulations of the SH and SV-P waves.

In order to obtain the values of the amplitudes w_u^j and w_d^j , the boundary conditions of the problem are applied:

Free-surface boundary condition

$$\tau_{yz}^1(z_o, x) = 0 \rightarrow \bar{\tau}_{yz}^1(z_o) = 0 = \beta_1 G_1 w_u^1(z_o) - \beta_1 G_1 w_d^1(z_o) \quad (A.16)$$

$$w_d^1(z_o) = w_u^1(z_o) \quad (A.17)$$

which can be expressed in general form as:

$$w_d^1(z_o) = R_0^u w_u^1(z_o); \quad \text{being: } R_0^u = (H_{22}^1)^{-1} H_{21}^1 = 1 \quad (A.18)$$

Boundary conditions in the infinite

Opposite to the zero amplitude conditions assumed in the work of Pak and Guzina [62] where no waves were reflected back from the unbounded media, for the problem of seismic incidence, these waves constitute, indeed, the source of excitation. Therefore, these conditions for the studied problem impose a known amplitude for the upwards waves in the last (deeper) stratum, which can be written as:

$$w_u^{n+1}(z_n) = 1 \quad (\text{A.19})$$

Boundary conditions at the layer interfaces

In each interface j between the soil layers j and $j + 1$, continuity conditions in terms of displacements and stresses should be satisfied:

$$\begin{cases} \bar{u}_y^j(z_j) = \bar{u}_y^{j+1}(z_j) \\ \bar{\tau}_{yz}^j(z_j) = \bar{\tau}_{yz}^{j+1}(z_j) \end{cases} \quad (\text{A.20})$$

Substituting the expressions from Eq. (A.14):

$$\begin{cases} w_u^j(z_j) + w_d^j(z_j) = w_u^{j+1}(z_j) + w_d^{j+1}(z_j) \\ \beta_j G_j w_u^j(z_j) - \beta_j G_j w_d^j(z_j) = \beta_{j+1} G_{j+1} w_u^{j+1}(z_j) - \beta_{j+1} G_{j+1} w_d^{j+1}(z_j) \end{cases} \quad (\text{A.21})$$

Writing these equations in matrix form, and arranging the terms:

$$\begin{bmatrix} 1 & -1 \\ \beta_{j+1} G_{j+1} & \beta_j G_j \end{bmatrix} \begin{bmatrix} w_d^{j+1}(z_j) \\ w_u^j(z_j) \end{bmatrix} = \begin{bmatrix} 1 & -1 \\ \beta_j G_j & \beta_{j+1} G_{j+1} \end{bmatrix} \begin{bmatrix} w_d^j(z_j) \\ w_u^{j+1}(z_j) \end{bmatrix} \quad (\text{A.22})$$

which can be expressed in general form as:

$$\mathbf{Q}_j^{j+1} \begin{bmatrix} w_d^{j+1}(z_j) \\ w_u^j(z_j) \end{bmatrix} = \mathbf{Q}_{j+1}^j \begin{bmatrix} w_d^j(z_j) \\ w_u^{j+1}(z_j) \end{bmatrix} \quad \text{being: } \mathbf{Q}_q^p = \begin{bmatrix} H_{12}^p & -H_{11}^q \\ H_{22}^p & -H_{21}^q \end{bmatrix} \quad (\text{A.23})$$

By inverting the left matrix, the interface condition can be written in general terms as:

$$\begin{bmatrix} w_d^{j+1}(z_j) \\ w_u^j(z_j) \end{bmatrix} = \begin{bmatrix} T_j^d & R_j^u \\ R_j^d & T_j^u \end{bmatrix} \begin{bmatrix} w_d^j(z_j) \\ w_u^{j+1}(z_j) \end{bmatrix} \quad (\text{A.24})$$

where $T_j^d, T_j^u, R_j^d, R_j^u$ are the transmission (T) and reflection (R) matrices for the upwards (u) and downwards (d) waves corresponding to the interface j . These relations between the different wave amplitudes are depicted in Fig. A.3.

As mentioned before, the terms of the transmission and reflection matrix can be computed as:

$$[\mathbf{TR}_j] = \begin{bmatrix} T_j^d & R_j^u \\ R_j^d & T_j^u \end{bmatrix} = [\mathbf{Q}_j^{j+1}]^{-1} [\mathbf{Q}_{j+1}^j] \quad (\text{A.25})$$

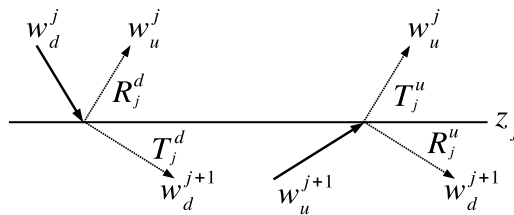


Figure A.3: Interpretation of the transmission and reflection matrices for layer interface j .

being their expressions for the incident SH waves:

$$\begin{bmatrix} T_j^d & R_j^u \\ R_j^d & T_j^u \end{bmatrix} = \frac{1}{\beta_j G_j + \beta_{j+1} G_{j+1}} \begin{bmatrix} 2\beta_j G_j & \beta_j G_j - \beta_{j+1} G_{j+1} \\ \beta_{j+1} G_{j+1} - \beta_j G_j & 2\beta_{j+1} G_{j+1} \end{bmatrix} \quad (\text{A.26})$$

Relations between the amplitudes of each strata

In order to obtain the amplitudes at each soil layer in terms of the incident ones, the aforementioned boundary conditions should be combined. Before continuing with this process, it is important to highlight that, due to their definition, the amplitudes at any point inside the layer j can be expressed in terms of the amplitudes at the top ($j - 1$) and lower (j) interfaces as:

$$w_u^j(z) = \mathcal{E}_j(z_j - z) w_u^j(z_j) \quad (\text{A.27a})$$

$$w_d^j(z) = \mathcal{E}_j(z - z_{j-1}) w_d^j(z_{j-1}) \quad (\text{A.27b})$$

Combining Eq. (A.27a) with the free-surface boundary condition given by Eq. (A.18) leads to:

$$w_d^1(z_0) = R_0^u w_u^1(z_0) = R_0^u \mathcal{E}_1(h_1) w_u^1(z_1) \quad (\text{A.28})$$

On the other hand, by using the equation corresponding to w_u^j in the interface conditions (A.24) applied at the first interface (z_1), and using the relation given by Eq. (A.27b):

$$w_u^1(z_1) = R_1^d w_d^1(z_1) + T_1^u w_u^2(z_1) = R_1^d \mathcal{E}_1(h_1) w_d^1(z_0) + T_1^u w_u^2(z_1) \quad (\text{A.29})$$

Defining the following auxiliary matrices that combine the effects of reflection and transmission together with the propagation inside the layer:

$$R_0^{ue} = R_0^u \mathcal{E}_1(h_1) \quad (\text{A.30})$$

$$\begin{bmatrix} T_j^{de} & R_j^{ue} \\ R_j^{de} & T_j^{ue} \end{bmatrix} = \begin{bmatrix} T_j^d & R_j^u \\ R_j^d & T_j^u \end{bmatrix} \begin{bmatrix} \mathcal{E}_j(h_j) & 0 \\ 0 & \mathcal{E}_{j+1}(h_{j+1}) \end{bmatrix} \quad (\text{A.31})$$

substituting (A.28) into (A.29) and solving for $w_u^1(z_1)$:

$$w_u^1(z_1) = R_1^{de} R_0^{ue} w_u^1(z_1) + T_1^u w_u^2(z_1) \quad (\text{A.32})$$

$$(I - R_1^{de} R_0^{ue}) w_u^1(z_1) = T_1^u w_u^2(z_1) \quad \text{with: } I = 1 \quad (\text{A.33})$$

the expressions that give the amplitudes at the first layer in terms of the ones corresponding to the second soil layer are obtained as:

$$\begin{cases} w_u^1(z_1) = (I - R_1^{de} R_0^{ue})^{-1} T_1^u w_u^2(z_1) \equiv \hat{T}_1^u w_u^2(z_1) \\ w_d^1(z_0) = R_0^{ue} w_u^1(z_1) \equiv \hat{R}_0^{ue} w_u^1(z_1) \end{cases} \quad (\text{A.34})$$

In a similar way, combining the between-layer boundary conditions at z_1 and z_2 , the following relations can be obtained for the second layer ($j = 2$):

$$\begin{cases} w_u^2(z_2) = \hat{T}_2^u w_u^3(z_2) \\ w_d^2(z_1) = \hat{R}_1^{ue} w_u^2(z_2) \end{cases} \quad (\text{A.35})$$

Proof. From the equation corresponding to w_d^{j+1} in the interface conditions (A.24) applied at the first interface (z_1) and using Eqs. (A.27) and (A.34), it can be obtained that:

$$\begin{aligned} w_d^2(z_1) &= T_1^d w_d^1(z_1) + R_1^u w_u^2(z_1) = \\ &= T_1^d \mathcal{E}_1(h_1) w_d^1(z_0) + R_1^u w_u^2(z_1) = \\ &= T_1^{de} \hat{R}_0^{ue} w_u^1(z_1) + R_1^u w_u^2(z_1) = \\ &= T_1^{de} \hat{R}_0^{ue} \hat{T}_1^u w_u^2(z_1) + R_1^u w_u^2(z_1) = \\ &= (T_1^{de} \hat{R}_0^{ue} \hat{T}_1^u + R_1^u) w_u^2(z_1) = \\ &= \hat{R}_1^u \mathcal{E}_2(h_2) w_u^2(z_2) \equiv \hat{R}_1^{ue} w_u^2(z_2) \end{aligned}$$

While from the equation corresponding to w_u^j in the interface conditions (A.24) applied at z_2 , together with Eq. (A.27b) and the previous expression it can be obtained that:

$$\begin{aligned} w_u^2(z_2) &= R_2^d w_d^2(z_2) + T_2^u w_u^3(z_2) = \\ &= R_2^d \mathcal{E}_2(h_2) w_d^2(z_1) + T_2^u w_u^3(z_2) = \\ &= R_2^{de} \hat{R}_1^{ue} w_u^2(z_2) + T_2^u w_u^3(z_2) = \\ &= (I - R_2^{de} \hat{R}_1^{ue})^{-1} T_2^u w_u^3(z_2) \equiv \hat{T}_2^u w_u^3(z_2) \end{aligned}$$

Substituting now Eq. (A.35) into (A.34), and with the aid of Eqs. (A.27), it is possible to express the amplitudes at any point of the first layer in terms of the amplitudes of the third layer as:

$$\begin{aligned} w_u^1(z) &= \mathcal{E}_1(z_1 - z) w_u^1(z_1) = \\ &= \mathcal{E}_1(z_1 - z) \hat{T}_1^u w_u^2(z_1) = \\ &= \mathcal{E}_1(z_1 - z) \hat{T}_1^u \mathcal{E}_2(h_2) w_u^2(z_2) = \\ &= \mathcal{E}_1(z_1 - z) \hat{T}_1^{ue} \hat{T}_2^u w_u^3(z_2) \end{aligned} \quad (\text{A.36})$$

$$\begin{aligned} w_d^1(z) &= \mathcal{E}_1(z - z_0) w_d^1(z_0) = \\ &= \mathcal{E}_1(z - z_0) \hat{R}_0^{ue} w_u^1(z_1) \end{aligned} \quad (\text{A.37})$$

Where:

$$\begin{bmatrix} \hat{T}_j^{de} & \hat{R}_j^{ue} \\ \hat{R}_j^{de} & \hat{T}_j^{ue} \end{bmatrix} = \begin{bmatrix} \hat{T}_j^d & \hat{R}_j^u \\ \hat{R}_j^d & \hat{T}_j^u \end{bmatrix} \begin{bmatrix} \mathcal{E}_j(h_j) & 0 \\ 0 & \mathcal{E}_{j+1}(h_{j+1}) \end{bmatrix} \quad (\text{A.38})$$

and $\hat{T}_j^d, \hat{T}_j^u, \hat{R}_j^d, \hat{R}_j^u$ are referred to as the generalized transmission and reflection matrices.

Repeating the same procedure for all soil layers, it can be obtained for any layer j that:

$$\begin{cases} w_u^j(z_j) = \hat{T}_j^u w_u^{j+1}(z_j) \\ w_d^j(z_{j-1}) = \hat{R}_{j-1}^{ue} w_u^j(z_j) \end{cases} \quad (\text{A.39})$$

The generalized transmission and reflection matrices for each layer are computed recursively from the ones corresponding to the upper stratum as:

$$\hat{R}_0^u = R_0^u \quad (\text{A.40a})$$

$$\hat{T}_j^u = \left(I - R_j^{de} \hat{R}_{j-1}^{ue} \right)^{-1} T_j^u \quad (\text{A.40b})$$

$$\hat{R}_j^u = R_j^u + T_j^{de} \hat{R}_{j-1}^{ue} \hat{T}_j^u \quad (\text{A.40c})$$

In these expressions, the roots of $I - R_j^{de} \hat{R}_{j-1}^{ue} = 0$ correspond to the wavenumbers associated to the generalized Love waves of the layered medium.

This way, the amplitudes of the upwards and downwards waves at any point inside the soil layer j can be expressed in terms of the amplitude of the incident wave as:

$$\begin{cases} w_u^j(z) = \mathcal{E}_j(z_j - z) \prod_{k=j}^{n-1} (\hat{T}_k^{ue}) \hat{T}_n^u w_u^{n+1}(z_n) \\ w_d^j(z) = \mathcal{E}_j(z - z_{j-1}) \hat{R}_{j-1}^{ue} w_u^j(z_j) \end{cases} \quad (\text{A.41})$$

Finally, once these amplitudes are known, the displacements and stresses at the desired point of the soil domain can be obtained from Eq. (A.14), which, including the dependence of x , results in:

$$u_y^j(x, z) = (w_u^j(z) + w_d^j(z)) e^{-ikx} \quad (\text{A.42})$$

$$\tau_{yz}^j(x, z) = \beta_j G_j (w_u^j(z) - w_d^j(z)) e^{-ikx} \quad (\text{A.43})$$

which, again, can be written in general terms as:

$$\begin{bmatrix} u_y^j(x, z) \\ \tau_{yz}^j(x, z) \end{bmatrix} = \mathbf{H}^j \begin{bmatrix} w_u^j(z) \\ w_d^j(z) \end{bmatrix} e^{-ikx} \quad (\text{A.44})$$

A.3 Incident SV-P waves (in-plane problem)

In this section, the expressions presented before for the incident SH waves problem are adapted in order to obtain the displacements and stresses corresponding to the in-plane problem of incident SV and P waves. Fig. A.4 depicts the amplitudes of the waves travelling inside each layer for the studied problem.

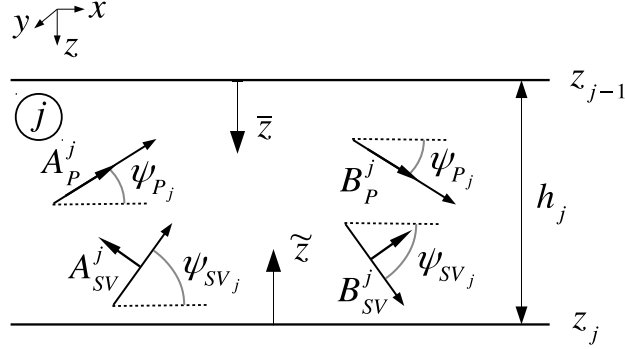


Figure A.4: Definition of the waves travelling through each layer. Incident SV-P waves.

Again, the waves propagate inside the $x - z$ plane but, now, the displacements produced by them are also inside this plane. The compatibility condition in the x direction imposes that:

$$c = \frac{c_{s_j}}{m_j} = \frac{c_{p_j}}{l_j} \quad (\text{A.45a})$$

$$k = \frac{\omega}{c} = \frac{\omega}{c_{s_j}} m_j = \frac{\omega}{c_{p_j}} l_j \quad (\text{A.45b})$$

where

$$m_j = \cos \psi_{SV_j} \quad (\text{A.46a})$$

$$t_j = -i \sqrt{1 - \frac{1}{m_j^2}} \equiv \tan \psi_{SV_j} \quad (\text{A.46b})$$

$$m_j t_j = \sin \psi_{SV_j} \quad (\text{A.46c})$$

$$l_j = \cos \psi_{P_j} \quad (\text{A.47a})$$

$$s_j = -i \sqrt{1 - \frac{1}{l_j^2}} \equiv \tan \psi_{P_j} \quad (\text{A.47b})$$

$$l_j s_j = \sin \psi_{P_j} \quad (\text{A.47c})$$

As commented for the SH waves, the apparent wave velocity c relates all of the propagation angles inside the layered domain. The definition of the tangents s and t ensures the correct sign when the propagation angle is below the critical one [210].

The expressions of the displacements and stresses that are needed for applying boundary conditions in the in-plane problem are:

$$u_x^j(x, z) = \bar{u}_x^j(z) e^{-ikx};$$

$$\bar{u}_x^j(z) \equiv \bar{u}_x^j(\bar{z}) = l_j \left(A_P^j e^{iks_j \bar{z}} + B_P^j e^{-iks_j \bar{z}} \right) - m_j t_j \left(A_{SV}^j e^{ikt_j \bar{z}} - B_{SV}^j e^{-ikt_j \bar{z}} \right) \quad (\text{A.48})$$

$$u_z^j(x, z) = \bar{u}_z^j(z) e^{-ikx};$$

$$\bar{u}_z^j(z) \equiv \bar{u}_z^j(\bar{z}) = -l_j s_j \left(A_P^j e^{iks_j \bar{z}} - B_P^j e^{-iks_j \bar{z}} \right) - m_j \left(A_{SV}^j e^{ikt_j \bar{z}} + B_{SV}^j e^{-ikt_j \bar{z}} \right) \quad (\text{A.49})$$

$$\tau_{xz}^j(x, z) = G_j \left(\frac{du_x^j}{dz} + \frac{du_z^j}{dx} \right) = \bar{\tau}_{xz}^j(z) e^{-ikx};$$

$$\bar{\tau}_{xz}^j(z) \equiv \bar{\tau}_{xz}^j(\bar{z}) = i2kl_j s_j G_j \left(A_P^j e^{iks_j \bar{z}} - B_P^j e^{-iks_j \bar{z}} \right) +$$

$$+ ikm_j (1 - t_j^2) G_j \left(A_{SV}^j e^{ikt_j \bar{z}} + B_{SV}^j e^{-ikt_j \bar{z}} \right) \quad (\text{A.50})$$

$$\sigma_{zz}^j(x, z) = 2G_j \frac{du_z^j}{dz} + \lambda_j \left(\frac{du_x^j}{dx} + \frac{du_z^j}{dz} \right) = \bar{\sigma}_{zz}^j(z) e^{-ikx};$$

$$\bar{\sigma}_{zz}^j(z) \equiv \bar{\sigma}_{zz}^j(\bar{z}) = ikl_j (1 - t_j^2) G_j \left(A_P^j e^{iks_j \bar{z}} + B_P^j e^{-iks_j \bar{z}} \right) +$$

$$- i2km_j t_j G_j \left(A_{SV}^j e^{ikt_j \bar{z}} - B_{SV}^j e^{-ikt_j \bar{z}} \right) \quad (\text{A.51})$$

Note that the Lamé constant can be omitted if the following relation is considered:

$$\frac{2G_j + \lambda_j}{G_j} = \frac{c_{pj}^2}{c_{sj}^2} = \frac{l_j^2}{m_j^2} = \kappa_j^{-2} \quad (\text{A.52})$$

Defining:

$$\alpha_j = iks_j \quad (\text{A.53a})$$

$$\beta_j = ikt_j \quad (\text{A.53b})$$

$$\gamma_j = ikm_j (1 - t_j^2) \quad (\text{A.53c})$$

and transforming the depth coordinates (\bar{z} , \bar{z} , z) as done for the SH wave problem, the depth-dependent displacements and stresses can be obtained as:

$$\begin{bmatrix} \bar{u}_x^j(z) \\ \bar{u}_z^j(z) \\ \bar{\tau}_{xz}^j(z) \\ \bar{\sigma}_{zz}^j(z) \end{bmatrix} = \begin{bmatrix} l_j & -m_j t_j & l_j & m_j t_j \\ -l_j s_j & -m_j & l_j s_j & -m_j \\ 2\alpha_j l_j G_j & \gamma_j G_j & -2\alpha_j l_j G_j & \gamma_j G_j \\ \gamma_j \kappa_j^{-1} G_j & -2\beta_j m_j G_j & \gamma_j \kappa_j^{-1} G_j & 2\beta_j m_j G_j \end{bmatrix} \begin{bmatrix} A_P^j e^{-\alpha_j(z_j - z)} \\ A_{SV}^j e^{-\beta_j(z_j - z)} \\ B_P^j e^{-\alpha_j(z - z_{j-1})} \\ B_{SV}^j e^{-\beta_j(z - z_{j-1})} \end{bmatrix} \quad (\text{A.54})$$

Now, the definitions that are made in order to follow the TRM methodology have a vectorial nature (owing to the two wave types present in the problem) but, in essence, are the

same transformations that were conducted in the previous section. This way, the exponential matrix and the upwards and downwards waves amplitudes are defined as:

$$\mathbf{E}_j(z) = \begin{bmatrix} e^{-\alpha_j z} & 0 \\ 0 & e^{-\beta_j z} \end{bmatrix} \quad (\text{A.55})$$

$$\mathbf{w}_u^j(z) = \mathbf{E}_j(z_j - z) \begin{bmatrix} A_P^j \\ A_{SV}^j \end{bmatrix} \quad (\text{A.56a})$$

$$\mathbf{w}_d^j(z) = \mathbf{E}_j(z - z_{j-1}) \begin{bmatrix} B_P^j \\ B_{SV}^j \end{bmatrix} \quad (\text{A.56b})$$

So, the matrix relation between the displacements and stresses with the transformed amplitudes of the travelling waves results in:

$$\begin{bmatrix} \bar{u}_x^j(z) \\ \bar{u}_z^j(z) \\ \bar{\tau}_{xz}^j(z) \\ \bar{\sigma}_{zz}^j(z) \end{bmatrix} = \begin{bmatrix} \mathbf{H}_{11}^j & \mathbf{H}_{12}^j \\ \mathbf{H}_{21}^j & \mathbf{H}_{22}^j \end{bmatrix} \begin{bmatrix} \mathbf{w}_u^j(z) \\ \mathbf{w}_d^j(z) \end{bmatrix} \quad (\text{A.57})$$

where each sub-matrix \mathbf{H}_{pq}^j is defined following Eq. (A.54).

As done for the SH waves, the next step is to apply boundary conditions:

Free-surface boundary condition

$$\begin{bmatrix} \bar{\tau}_{xz}^1(z_0) \\ \bar{\sigma}_{xz}^1(z_0) \end{bmatrix} = \begin{bmatrix} 0 \\ 0 \end{bmatrix} = \mathbf{H}_{21}^1 \mathbf{w}_u^1(z_0) + \mathbf{H}_{22}^1 \mathbf{w}_d^1(z_0) \quad (\text{A.58})$$

which can be written as:

$$\mathbf{w}_d^1(z_0) = \mathbf{R}_0^u \mathbf{w}_u^1(z_0) \quad (\text{A.59})$$

being:

$$\mathbf{R}_0^u = (\mathbf{H}_{22}^1)^{-1} \mathbf{H}_{21}^1 = \frac{1}{\gamma_j^2 + 4\alpha_j\beta_j m_j^2} \begin{bmatrix} 4\alpha_j\beta_j m_j^2 - \gamma_j^2 & 4\beta_j\gamma_j m_j \kappa_j \\ -4\alpha_j\gamma_j l_j & 4\alpha_j\beta_j m_j^2 - \gamma_j^2 \end{bmatrix} \quad (\text{A.60})$$

The denominator of this expression is associated with the Rayleigh waves of the free-surface.

Boundary conditions in the infinite

As done for the SH waves, the amplitudes of the waves at the bottom layer are known as they constitute the source of energy of the problem. In this case, depending if the incident wave is a SV or P wave, the amplitudes at the lower interface of the layered domain will be:

$$\mathbf{w}_u^{n+1}(z_n) = \begin{bmatrix} 0 \\ 1 \end{bmatrix} \text{ for incident SV waves} \quad \text{o} \quad \mathbf{w}_u^{n+1}(z_n) = \begin{bmatrix} 1 \\ 0 \end{bmatrix} \text{ for incident P waves} \quad (\text{A.61})$$

Boundary conditions at the layer interfaces

The continuity conditions at each layer interface j are:

$$\begin{cases} \bar{u}_x^j(z_j) = \bar{u}_x^{j+1}(z_j) \\ \bar{u}_z^j(z_j) = \bar{u}_z^{j+1}(z_j) \\ \bar{\tau}_{xz}^j(z_j) = \bar{\tau}_{xz}^{j+1}(z_j) \\ \bar{\sigma}_{zz}^j(z_j) = \bar{\sigma}_{zz}^{j+1}(z_j) \end{cases} \quad (\text{A.62})$$

which can be expressed in matrix form and in terms of the wave amplitudes as:

$$\mathbf{Q}_j^{j+1} \begin{bmatrix} \mathbf{w}_d^{j+1}(z_j) \\ \mathbf{w}_u^{j+1}(z_j) \end{bmatrix} = \mathbf{Q}_{j+1}^j \begin{bmatrix} \mathbf{w}_d^j(z_j) \\ \mathbf{w}_u^j(z_j) \end{bmatrix} \quad \text{being: } \mathbf{Q}_q^p = \begin{bmatrix} \mathbf{H}_{11}^p & -\mathbf{H}_{12}^q \\ \mathbf{H}_{22}^p & -\mathbf{H}_{21}^q \end{bmatrix} \quad (\text{A.63})$$

Inverting the first matrix, the transmission and reflection matrices for the SV-P waves are obtained in the form:

$$\begin{bmatrix} \mathbf{w}_d^{j+1}(z_j) \\ \mathbf{w}_u^{j+1}(z_j) \end{bmatrix} = \begin{bmatrix} \mathbf{T}_j^d & \mathbf{R}_j^u \\ \mathbf{R}_j^d & \mathbf{T}_j^u \end{bmatrix} \begin{bmatrix} \mathbf{w}_d^j(z_j) \\ \mathbf{w}_u^j(z_j) \end{bmatrix} \quad \text{being: } \begin{bmatrix} \mathbf{T}_j^d & \mathbf{R}_j^u \\ \mathbf{R}_j^d & \mathbf{T}_j^u \end{bmatrix} = \left(\mathbf{Q}_j^{j+1} \right)^{-1} \mathbf{Q}_{j+1}^j \quad (\text{A.64})$$

Note that now each transmission and reflection matrix is of size 2×2 instead of a scalar value. Their close-form expressions are not detailed owing their complexity, but they share a common denominator which is related to the Stoneley waves of the layered media. For the developed model, the values of these matrices can be obtained numerically from the matrices \mathbf{Q}_q^p .

Relations between the amplitudes of each strata

If the same steps presented for the SH waves are followed (just caring about the change in the dimension of the variables) it is possible to obtain the expressions of the generalized

transmission and reflection matrices for each layer j as:

$$\mathbf{R}_0^u = \mathbf{R}_0^u \quad (\text{A.65a})$$

$$\mathbf{T}_j^u = \left(\mathbf{I} - \mathbf{R}_j^{de} \mathbf{R}_{j-1}^{ue} \right)^{-1} \mathbf{T}_j^u \quad (\text{A.65b})$$

$$\mathbf{R}_j^u = \mathbf{R}_j^u + \mathbf{T}_j^{de} \mathbf{R}_{j-1}^{ue} \mathbf{T}_j^u \quad (\text{A.65c})$$

where \mathbf{I} is now the identity 2×2 matrix, and the matrices that include the exponential terms are defined in the same manner than for the SH waves as:

$$\mathbf{R}_0^{ue} = \mathbf{R}_0^u \mathbf{E}_1(h_1) \quad (\text{A.66})$$

$$\begin{bmatrix} \mathbf{T}_j^{de} & \mathbf{R}_j^{ue} \\ \mathbf{R}_j^{de} & \mathbf{T}_j^{ue} \end{bmatrix} = \begin{bmatrix} \mathbf{T}_j^d & \mathbf{R}_j^u \\ \mathbf{R}_j^d & \mathbf{T}_j^u \end{bmatrix} \begin{bmatrix} \mathbf{E}_j(h_j) & 0 \\ 0 & \mathbf{E}_{j+1}(h_{j+1}) \end{bmatrix} \quad (\text{A.67})$$

$$\begin{bmatrix} \mathbf{T}_j^{de} & \mathbf{R}_j^{ue} \\ \mathbf{R}_j^{de} & \mathbf{T}_j^{ue} \end{bmatrix} = \begin{bmatrix} \mathbf{T}_j^d & \mathbf{R}_j^u \\ \mathbf{R}_j^d & \mathbf{T}_j^u \end{bmatrix} \begin{bmatrix} \mathbf{E}_j(h_j) & 0 \\ 0 & \mathbf{E}_{j+1}(h_{j+1}) \end{bmatrix} \quad (\text{A.68})$$

The amplitudes at the interfaces of each layer can be obtained in terms of the amplitudes corresponding to the bottom layer as:

$$\begin{cases} \mathbf{w}_u^j(z_j) = \mathbf{T}_j^u \mathbf{w}_u^{j+1}(z_j) \\ \mathbf{w}_d^j(z_{j-1}) = \mathbf{R}_{j-1}^{ue} \mathbf{w}_u^j(z_j) \end{cases} \quad (\text{A.69})$$

At any point inside the layer, the amplitudes of the upwards and downwards waves can be obtained from their values at the upper and lower interfaces as:

$$\mathbf{w}_u^j(z) = \mathbf{E}_j(z_j - z) \mathbf{w}_u^j(z_j) \quad (\text{A.70a})$$

$$\mathbf{w}_d^j(z) = \mathbf{E}_j(z - z_{j-1}) \mathbf{w}_d^j(z_{j-1}) \quad (\text{A.70b})$$

and, also, can be obtained in terms of the known amplitude of the incident waves at the last layer as:

$$\begin{cases} \mathbf{w}_u^j(z) = \mathbf{E}_j(z_j - z) \prod_{k=j}^{n-1} (\mathbf{T}_k^{ue}) \mathbf{T}_n^u \mathbf{w}_u^{n+1}(z_n) \\ \mathbf{w}_d^j(z) = \mathbf{E}_j(z - z_{j-1}) \mathbf{R}_{j-1}^{ue} \mathbf{w}_u^j(z_j) \end{cases} \quad (\text{A.71})$$

Finally, once the desired amplitudes are known, the displacements and stresses at that point of the layered domain is obtained from:

$$\begin{bmatrix} u_x^j(x, z) \\ u_z^j(x, z) \\ \tau_{xz}^j(x, z) \\ \sigma_{zz}^j(x, z) \end{bmatrix} = \mathbf{H}^j \begin{bmatrix} \mathbf{w}_u^j(z) \\ \mathbf{w}_d^j(z) \end{bmatrix} e^{-ikx} \quad (\text{A.72})$$

A.4 Generic incident waves

Despite in the two previous sections the in-plane and out-of-plane problems are treated independently, they can be merged into one single formulation if the proper redefinitions of \mathbf{w}_u^j , \mathbf{w}_d^j , \mathbf{E}_j and \mathbf{H}^j are considered:

$$\mathbf{E}_j(z) = \begin{bmatrix} e^{-\alpha_j z} & 0 & 0 \\ 0 & e^{-\beta_j z} & 0 \\ 0 & 0 & e^{-\beta_j^{\text{SH}} z} \end{bmatrix} \quad (\text{A.73})$$

$$\mathbf{w}_u^j(z) = \mathbf{E}_j(z_j - z) \begin{bmatrix} A_P^j \\ A_{\text{SV}}^j \\ A_{\text{SH}}^j \end{bmatrix} \quad (\text{A.74a})$$

$$\mathbf{w}_d^j(z) = \mathbf{E}_j(z - z_{j-1}) \begin{bmatrix} B_P^j \\ B_{\text{SV}}^j \\ B_{\text{SH}}^j \end{bmatrix} \quad (\text{A.74b})$$

$$\begin{bmatrix} \bar{u}_x^j(z) \\ \bar{u}_z^j(z) \\ \bar{u}_y^j(z) \\ \bar{\tau}_{xz}^j(z) \\ \bar{\sigma}_{zz}^j(z) \\ \bar{\tau}_{yz}^j(z) \end{bmatrix} = \mathbf{H}^j \begin{bmatrix} \mathbf{w}_u^j(z) \\ \mathbf{w}_d^j(z) \end{bmatrix} \quad \text{where now: } \mathbf{H}_{pq}^j = \begin{bmatrix} \mathbf{H}_{pq}^{j\text{-P-SV}} & \mathbf{0}_{2 \times 1} \\ \mathbf{0}_{1 \times 2} & \mathbf{H}_{pq}^{j\text{-SH}} \end{bmatrix} \quad (\text{A.75})$$

This way, all the expressions presented in the previous sections are still valid (with the proper dimensions changes), as they have been introduced in terms of these four variables. Obviously, the two wave problems remain uncoupled, so the obtained matrices will be formed by the sub-matrices corresponding to the SV-P and SH problems presented before.

A.5 Numerical aspects

A.5.1 Vertical incidence

The formulation presented in this appendix is also valid for vertically propagating waves. However, it should be carefully handled because for propagation angles equal to 90° the corresponding cosines m_j (for S waves) or l_j (for P waves) are equal to zero. These terms appear

in the denominator of the apparent velocity c (which does not properly exist for the vertical incidence problem), and in the definition of the tangents t_j or s_j (which are infinite for this propagation angle). These aspects can lead to numerical singularities. In order to avoid them, and to obtain a routine that can be used for the vertical incidence problem, the following considerations should be made:

- Define k directly as:

$$k = \frac{\omega}{c_{s_j}} m_j \quad \text{or} \quad k = \frac{\omega}{c_{p_j}} l_j \quad (\text{A.76})$$

instead of $k = \omega/c$. This way, this term will vanish when it appears alone in the expressions.

- Use variables for the sines instead of the ones of the tangents. Note that in the obtained formulation, the terms of the tangents (t_j , s_j) do never appear alone, but always are multiplied by the corresponding cosine (sometimes directly and other times through k). This way, instead of saving variables with the value of t_j or s_j , directly the value of $m_j t_j$ or $l_j s_j$ should be stored. These new variables will present a unitary value for the vertical incidence, and their expressions for an arbitrary propagation angle are:

$$m_j t_j = -i \sqrt{m_j^2 - 1} \quad \text{and} \quad l_j s_j = -i \sqrt{l_j^2 - 1} \quad (\text{A.77})$$

Taking these considerations into account for the definition of the matrices \mathbf{H}^j and the coefficients α_j , β_j , and γ_j , the singularities corresponding to the vertical incidence can be completely avoided.

A.5.2 Routine pseudo-algorithm

In order to compute the displacements produced by the incident field, the process is divided into two stages:

Stage 1: Computation of the amplitudes at each interface

The amplitudes will be stored in two variables $WU(:, j) \equiv \mathbf{w}_u^j(z_j)$ and $WD(:, j) \equiv \mathbf{w}_d^j(z_{j-1})$ which will contain the amplitudes at the interfaces needed to compute the displacements inside the n layers of interest (the bottom unbounded layer is not considered). The process is:

1. define $\mathbf{w}_u^{n+1}(z_n)$ depending on the incident wave
2. compute $WU(:, n)$ and $WD(:, n)$ for the deepest finite layer from Eq. (A.69) and the previous known amplitude:

$$\begin{cases} \mathbf{w}_u^n(z_n) = \mathbf{T}_n^u \mathbf{w}_u^{n+1}(z_n) & \rightarrow & WU(:, n) = \mathbf{T}_n^u \mathbf{w}_u^{n+1}(z_n) \\ \mathbf{w}_d^n(z_{n-1}) = \mathbf{R}_{n-1}^{ue} \mathbf{w}_u^n(z_n) & \rightarrow & WD(:, n) = \mathbf{R}_{n-1}^{ue} WU(:, n) \end{cases} \quad (\text{A.78})$$

3. iteratively for each layer j from $n - 1$ to 1, compute $WU(:, j)$ and $WD(:, j)$ from Eqs. (A.69) and (A.70):

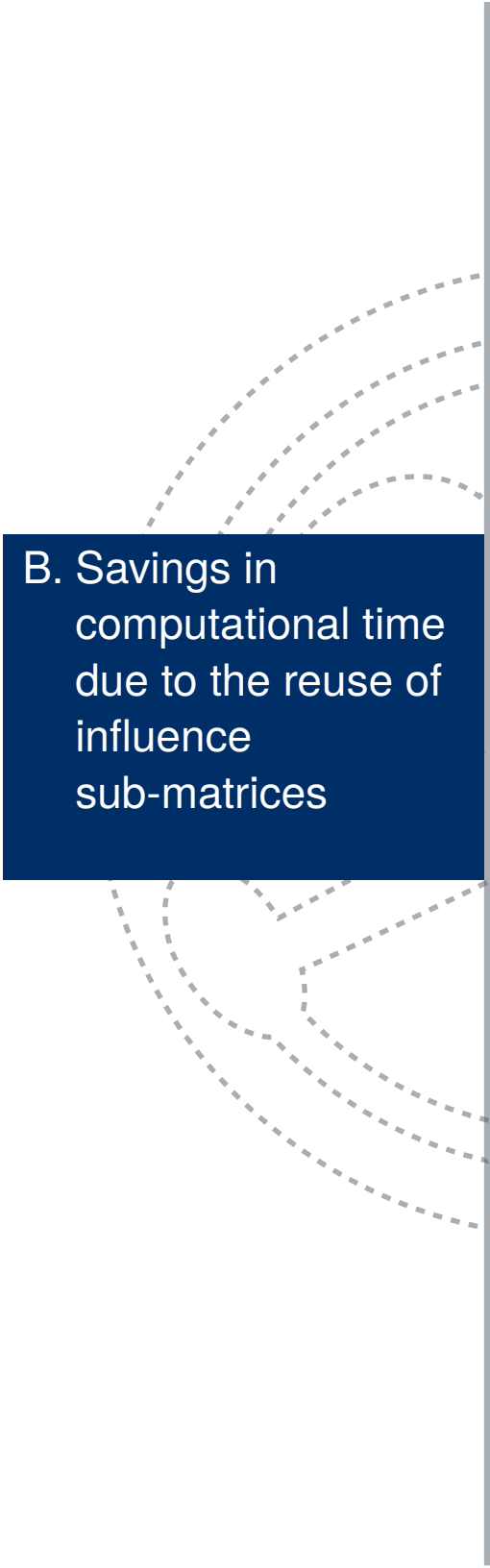
$$\begin{cases} \mathbf{w}_u^j(z_j) = \mathbf{T}_j^{ue} \mathbf{w}_u^{j+1}(z_{j+1}) & \rightarrow & WU(:, j) = \mathbf{T}_j^{ue} WU(:, j+1) \\ \mathbf{w}_d^j(z_{j-1}) = \mathbf{R}_{j-1}^{ue} \mathbf{w}_u^j(z_j) & \rightarrow & WD(:, j) = \mathbf{R}_{j-1}^{ue} WU(:, j) \end{cases} \quad (\text{A.79})$$

Stage 2: Computation of the displacements at the desired point

To obtain the displacements at any point (x, z) belonging to the layer j ($z_{j-1} \leq z < z_j$), first the amplitudes at the desired point are computed through Eq. (A.70):

$$\begin{cases} \mathbf{w}_u^j(z) = \mathbf{E}_j(z_j - z) \mathbf{w}_u^j(z_j) & \rightarrow & \mathbf{w}_u^j(z) = \mathbf{E}_j(z_j - z) WU(:, j) \\ \mathbf{w}_d^j(z) = \mathbf{E}_j(z - z_{j-1}) \mathbf{w}_u^j(z_{j-1}) & \rightarrow & \mathbf{w}_d^j(z) = \mathbf{E}_j(z - z_{j-1}) WD(:, j) \end{cases} \quad (\text{A.80})$$

and then, the displacements are obtained from Eq. (A.72).

A vertical grey line runs down the right side of the slide. To its left, there are several sets of concentric dashed grey arcs, resembling a stylized 'C' or a partial circle, positioned behind the text box.

B. Savings in
computational time
due to the reuse of
influence
sub-matrices



Section 2.3.2.2 presented the procedure that is used in the proposed model to compute the influence matrix \mathbf{G} needed in the soil equations. It is based on the similarities between the sub-matrices corresponding to equivalent collocation-observation pile pairs. In the aforementioned section, the procedure was detailed and the reduction in the number of collocation-observation pile pairs required for different regular configurations of piles was given as an example. In order to complete this information, and to give an insight into the savings in computational time that the proposed methodology implies, in this appendix two different problems are considered. For each scenario, the running times required for obtaining the foundation response both considering or not the reuse of influence sub-matrices are compared. The two problems, referred to as Case A and Case B, are sketched in Fig. B.1 and correspond to situations in which the fundamental solution is easily or slowly computed, respectively.

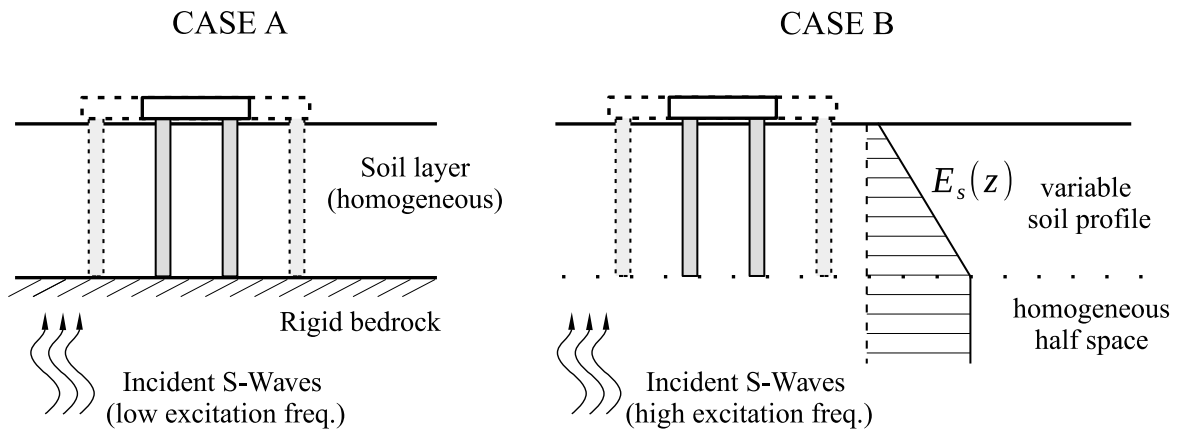


Figure B.1: Cases considered for the analysis of the savings in the computational time due to the reuse of influence sub-matrices.

The two cases correspond to a seismic problem, in which vertically incident shear waves impinge over the studied site. Case A represents a pile foundation embedded in a soil layer over a rigid bedrock. Pile tips are assumed to be hinged to the rigid stratum. The excitation frequency coincides with the fundamental frequency of the soil stratum. The assumed properties for piles and soil lead to a dimensionless frequency $a_o = 0.03$, which is a relatively low value with respect to the typical frequency range used for studying pile foundations.

On the other hand, Case B corresponds to a pile foundation embedded in a variable soil profile in which the soil Young's modulus linearly increases with depth along the piles (from $0.1 E_s$ at the free-surface level to E_s at the pile tip) and remains constant for the underlying half space. The variable profile is discretized by using 60 homogeneous layers with the same thickness. For this problem, a relatively high excitation frequency is assumed ($a_o = 1$, the value of the shear wave velocity at the pile tip level is used to define the dimensionless frequency). The high value of the frequency and the complexity of the soil profile make that, in this situation, the computation of the fundamental solution presents a slow convergence velocity.

Case	Group	single	2×2	3×3	4×4	6×6	10×10
A	Without reuse	0.4 s	0.9 s	2.7 s	6.6 s	30 s	3.5 min
	With reuse	0.4 s	0.5 s	0.7 s	1.0 s	2.5 s	11 s
B	Without reuse	0.6 s	2.1 s	9.3 s	33 s	3.6 min	42 min
	With reuse	0.6 s	1.2 s	2.8 s	5.8 s	15 s	61 s

Table B.1: Times required to obtain the response of the foundation at the considered frequency. Regular pile groups.

In the two studied cases, different regular pile groups with vertical elements are considered. The piles are equally spaced with a centre-to-centre separation ratio $s/d = 5$ and are distributed in squared $N \times N$ groups. For all groups, 10 elements per pile are used in order to obtain the results.

The computational times required to obtain the response of the foundation for the two cases by incorporating or not the reuse of influence sub-matrices are compared in Table B.1. Note that the displayed times include both the assembly and solving of the required system of equations, being the time needed for the assembly process significantly larger. As expected, the times corresponding to Case B are much larger than the ones of Case A. Comparing the times with and without the reuse of influence sub-matrices, it is found that the proposed procedure allows saving a significant amount of time. Of course, for the single pile configuration there is no difference between the computed times as only one possible collocation-observation pair exists, but even for the smallest 2×2 group the computational time is halved if the proposed methodology is followed. As the number of piles in the group grows, the running time is vastly reduced by the proposed strategy, changing even its scale from minutes to seconds for the larger configurations. Note that these times are the ones required to solve the system at the assumed frequency. Normally, a set of 20-40 frequency values is needed in order to adequately determine the behaviour of the foundation in the frequency range of interest. Thus, the savings in time produced by the proposed methodology become even more important.

The computational times are also presented in Fig. B.2 for a clearer comparison. The required time with and without the reuse of influence sub-matrices are presented as functions of the number of piles in the group (which is directly proportional to the number of pile elements). The two studied cases are plotted separately. Attending to the curves, it is found that the order of the computational time falls from $\mathcal{O}(N^2)$ to $\mathcal{O}(N)$ if the reuse of influence sub-matrices is included.

The results presented in this Appendix have been obtained by using a parallel version of the developed integral model run in a 28 cores (Intel® Xeon® CPU E5-2690 v4 @ 2.60GHz), 260 GB RAM computer.

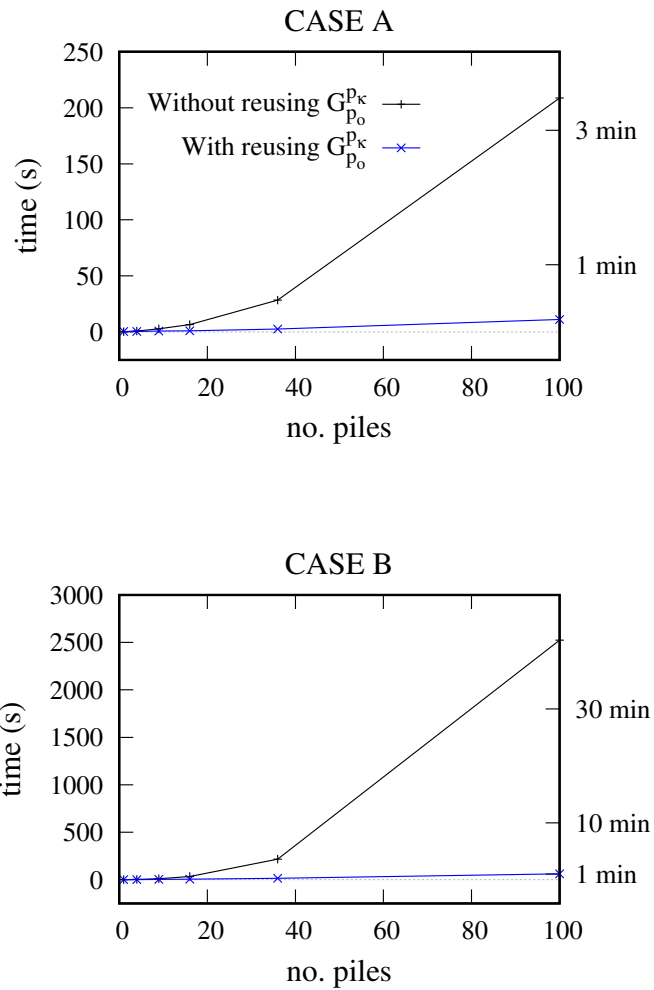
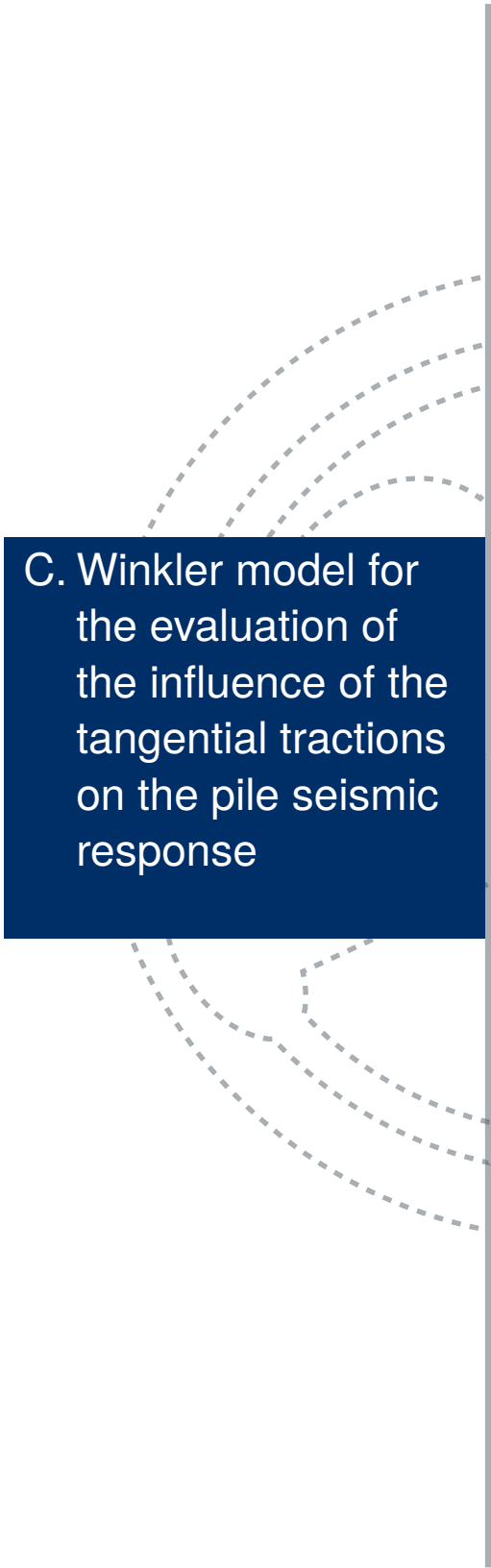


Figure B.2: Computational time required to obtain the response of the foundation at the considered frequency. Regular pile groups.

A vertical grey line runs down the page. To its left, there are several sets of concentric dashed grey arcs, resembling wave fronts or soil layers, some above and some below a dark blue rectangular box.

C. Winkler model for the evaluation of the influence of the tangential tractions on the pile seismic response

- C.1 Introduction
- C.2 Problem definition
- C.3 Loads acting over the soil-pile interface
- C.4 Formulation of the Winkler model



C.1 Introduction

This appendix presents a Beam-on-Dynamic-Winkler-Foundation (BDWF) model that can be used to analyse the influence of the tangential tractions arising in the soil-pile interface on the seismic response of piles. Although the BDWF model was initially designed (and still used) for studying beams resting over the soil [211–213], it also has an important application in the modelling of embedded piles [214–216] and the computation of their seismic response [94, 99, 109, 217–220].

In the Winkler models, the interaction between soil and pile is often reduced to the lateral stiffness of the soil (the soil reaction against the horizontal displacements of the pile). Nevertheless, in addition to the lateral soil reactions, tangential tractions can also arise along the soil-pile interface depending on the terrain characteristics. Regarding the Winkler formulation, the additional loads that those tangential stresses produce into the pile can be represented as distributed moments [221]. This approach is followed in the present work, distinguishing and detailing the different components of the distributed moment: the one related to the rotation of the pile cross-section and the one related to the action of the incident field.

C.2 Problem definition

The problem represented by the BDWF model corresponds to a single pile of length L and diameter d embedded in a (in general) layered half space. Fig. C.1(a) sketches the problem. Along this appendix, the properties that determine the dynamic behaviour of the pile are denoted as: Young's modulus E , density ρ , Poisson's ratio ν , shear modulus G , area A , moment of inertia I and shear coefficient α (Timoshenko's beam theory). No damping is assumed for the pile in the Winkler model.

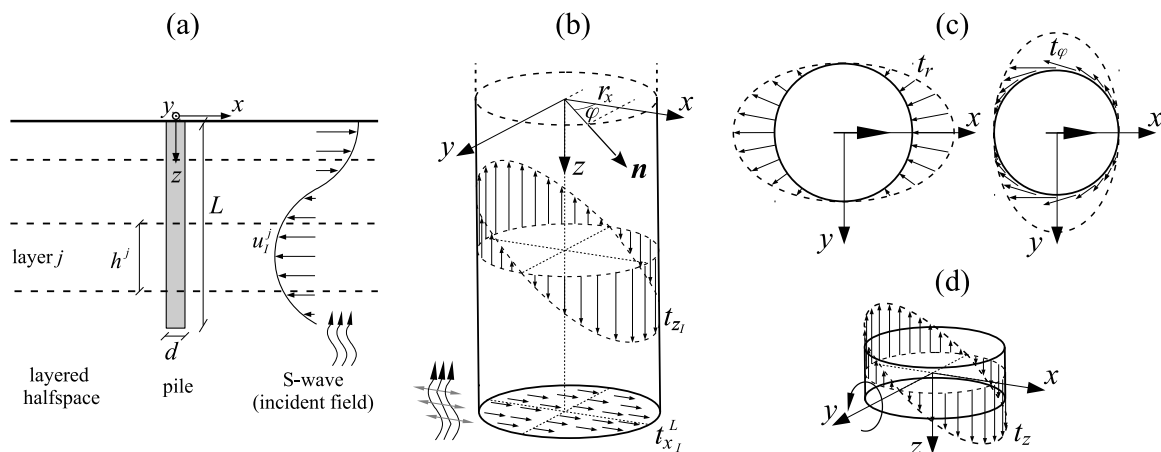


Figure C.1: (a) Problem under study. (b) Tangential tractions due to the incident field. (c) Normal and tangential tractions due to a horizontal displacement of the pile cross-section. (d) Tangential tractions due to a rotation of the pile cross-section.

The soil domain is composed by a finite number of homogeneous viscoelastic layers resting over a half space. Each layer j of the soil profile has the following properties: Young's modulus E_s^j , density ρ_s^j , Poisson's ratio ν_s^j , shear modulus G_s^j , shear wave propagation velocity c_s^j and hysteretic damping coefficient β_s^j . The portion of the pile length that crosses each soil layer is denoted as h^j .

The system is excited by planar shear waves that propagate vertically through the soil acting in the x direction. For each layer, the horizontal displacements that this incident field generates are obtained through the expression:

$$u_I^j(z) = A_I^j e^{ik_I^j z} + B_I^j e^{-ik_I^j z} \quad (C.1)$$

where A_I^j , B_I^j are the amplitudes of the incident and reflected waves for layer j obtained by solving the one-dimensional wave propagation problem; $k_I^j = \omega/c_s^j$ is the wave number; i is the imaginary unit; ω is the angular frequency; and the term $e^{i\omega t}$ is omitted for simplicity's sake as done in the rest of the document.

C.3 Loads acting over the soil-pile interface

The soil-pile interaction along the pile shaft is produced through the horizontal (t_x) and tangential (t_z) tractions acting between them. The firsts, produced by the contribution of the normal tractions (t_r) and the horizontal component of the tangential tractions (t_ϕ), see Fig. C.1(c), are the ones of most importance. Nevertheless, the vertical tangential tractions (henceforth referred to just as tangential tractions), can also have an important role in the seismic response of the pile.

The soil-pile horizontal tractions are modelled in BDWF formulations through the soil lateral stiffness, that will be denoted as K_x . These tractions, proportional to the horizontal relative displacement between pile and soil, constitute the main excitation of the beam. Thus, this component has to be always included into any Winkler model for the analysis of pile foundations.

On the other hand, the effects of the tangential stresses are usually not considered in BDWF models, or only the distributed moment produced by the rotation of the cross-section is included, see Fig. C.1(d). However, it can be found (see Section 2.8) that this component does not represent the whole tangential tractions that participate in the problem of vertically incident S-waves. In order to completely reproduce the response obtained by rigorous continuous models, the effects of the tangential stresses originated by the distortion of the incident field must also be considered.

Loads due to the incident field

Attending to the expression of the incident field (Eq. C.1), and omitting the soil layer super-index j for clarity's sake, the only term that does not vanish from the stress tensor σ_I is:

$$\tau_{xz_I}(z) = 2G_s \varepsilon_{xz_I} = G_s \frac{du_I}{dz} \quad (C.2)$$

At a point of the soil-pile interface defined by the angle φ and with a normal vector $\mathbf{n} = (\cos \varphi, \sin \varphi, 0)$, see Fig. C.1(b), the traction vector \mathbf{t}_I is obtained as:

$$\mathbf{t}_I(z, \varphi) = \sigma_I \mathbf{n} = (0, 0, \tau_{xz_I} \cos \varphi) \quad (\text{C.3})$$

This vertical tangential traction produces a moment m_y around the y axis equal to:

$$m_y(z, \varphi) = -r_x t_{z_I} = -r \tau_{xz_I} \cos^2 \varphi \quad (\text{C.4})$$

where r is the pile radius. Note that the moment is negative according to the sign criteria assumed.

The total distributed moment m_I acting over the pile cross-section can be finally obtained by integrating the punctual moment m_y over the soil-pile interface:

$$m_I(z) = \int_0^{2\pi} m_y r d\varphi = -\pi r^2 \tau_{xz_I} = -\pi r^2 G_s \frac{du_I}{dz} \quad (\text{C.5})$$

By defining $K_I = \pi r^2 G_s$, one can express this distributed moment in a similar way than the Winkler's distributed soil reactions:

$$m_I(z) = -K_I \frac{du_I}{dz} \quad (\text{C.6})$$

On the other hand, considering the pile cross-section at tip level ($z = L$) with a normal defined by $\mathbf{n} = (0, 0, 1)$, the traction vector \mathbf{t}_I^L is equal to:

$$\mathbf{t}_I^L = \sigma_I \mathbf{n} = (\tau_{xz_I}^L, 0, 0) \quad (\text{C.7})$$

where super-index L indicates that the variable is evaluated at the end of the pile.

Integrating this horizontal component of the traction vector over the pile tip surface, the shear force produced at the end of the pile due to action of the incident field results in:

$$V_I^L = \iint_A t_{x_I}^L dA = \pi r^2 \tau_{xz_I}^L = \pi r^2 G_s \frac{du_I}{dz} \Big|_L \quad (\text{C.8})$$

C.4 Formulation of the Winkler model

The general differential equation that describes the dynamic lateral response of the pile subjected to lateral distributed forces and moments due to seismic excitation is obtained in this section. The pile is modelled as a Timoshenko's beam and the different components of those loads are defined in order to include all phenomena that take place in the problem under study. The result of this procedure is a BDWF model that can be used to estimate the pile response (lateral displacements, rotations, shear forces and bending moments), which is sketched in Fig. C.2(b) for each layer of the soil profile.

The forces acting over a differential element of the beam are represented in Fig. C.2(a). The translational and rotatory inertia of the beam are included in the terms q and m together

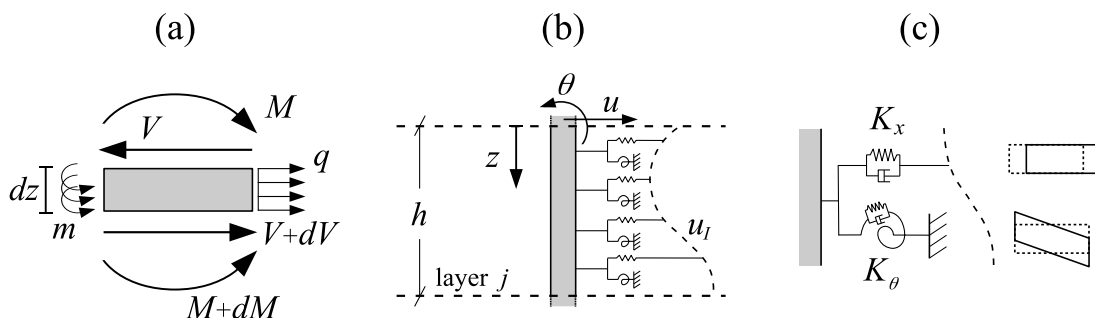


Figure C.2: (a) Forces and moments acting over a differential element of the beam. (b) BDWF model for a pile embedded in a soil layer. (c) Winkler's soil impedance terms for different deformation modes.

with the distributed external forces and moments acting over it. Attending to this, the equilibrium equations of the beam differential element results in:

$$\frac{dV}{dz} + q = 0 \quad (C.9a)$$

$$\frac{dM}{dz} + V + m = 0 \quad (C.9b)$$

The Timoshenko's beam theory includes the effects of the warping of the beam cross-section produced by the shear stresses by assuming a constant value of the beam shear distortion γ_{xz} . The constitutive laws that determine the Timoshenko's beam bending moment (M) and shear force (V) are:

$$M = EI \frac{d\theta}{dz} \quad (C.10a)$$

$$V = \alpha GA \gamma_{xz} = \alpha GA \left(\frac{du}{dz} - \theta \right) \quad (C.10b)$$

where u is the lateral displacement of the beam and θ is the rotation of the beam cross-section produced only by the flexural effects.

Substituting the constitutive laws (C.10) in the equilibrium equations (C.9) and after some simple operations, the differential equation that governs the lateral displacements of the beam results in:

$$\frac{d^4 u}{dz^4} + \frac{1}{\alpha GA} \frac{d^2 q}{dz^2} - \frac{q}{EI} + \frac{1}{EI} \frac{dm}{dz} = 0 \quad (C.11)$$

While the beam rotation can be expressed in terms of the horizontal displacement as:

$$\theta = \frac{EI}{\alpha GA} \left[\frac{d^3 u}{dz^3} + \frac{\alpha GA}{EI} \frac{du}{dz} + \frac{1}{\alpha GA} \frac{dq}{dz} + \frac{1}{EI} m \right] \quad (C.12)$$

Up to this point, the general expressions of the distributed load q and moment m have been used. Considering now the different phenomena that participate in the studied problem,

and omitting the soil layer super-index j for clarity's sake, the components of the distributed lateral force acting over the beam are:

$$q = \rho A \omega^2 u + K_x (u_I - u) \quad (\text{C.13})$$

- $\rho A \omega^2 u$: distributed force due to the translational inertia of the beam.
- $K_x (u_I - u)$: distributed force produced by the soil lateral impedance K_x . This force is produced by the relative lateral displacement between the beam and the soil.

While the different components of the distributed moment are:

$$m = \rho I \omega^2 \theta - K_\theta \theta - K_I \frac{du_I}{dz} \quad (\text{C.14})$$

- $\rho I \omega^2 \theta$: distributed moment due the rotational inertia of the beam cross-section.
- $-K_\theta \theta$: distributed moment associated with the soil rocking impedance K_θ . This moment is produced by the tangential tractions that arise in the soil-pile interface when the cross-section rotates.
- $m_I = -K_I du_I/dz$: distributed moment produced by the tangential tractions that arise in the soil-pile interface due to the action of the incident field.

At this point it is worthy to highlight that the particular feature of the proposed formulation is the approach followed for obtaining this distributed moment produced by the action of the tangential tractions arising due to the incident field. Despite its relevance, this component is not normally considered in the Winkler models used to study the soil-pile seismic problem, or are treated in a completely different way such as the one proposed by Gerolymos and Gazetas [221]. In their work, they included this distributed moment produced by the soil-pile interaction directly by extending the kinematic relation of the horizontal component $K_x(u_I - u)$ to the rocking motion of the pile $K_\theta(du_I/dz - \theta)$. On the other hand, in the proposed formulation, the distributed moment produced by the incident field is obtained in a rigorous approach from the elastodynamic equations of the incident field. This way, the contribution of the incident field distributed moment is separated from the one produced by the soil reaction against the rotation of the pile. Note that this cannot be done for the horizontal component, as there are no resultant forces acting over the pile when the tractions of the incident field are integrated.

Fig. C.2(c) illustrates the different Winkler's soil impedances considered and the deformation modes associated with them. The expressions of the lateral and rocking soil impedances proposed by Novak et al. [222] are used. This set of soil impedances are chosen over other options (e.g., [113, 214, 219, 223]) because they are obtained through an analytical procedure and have explicit expressions that do not depend on heuristic parameters.

Now, including the expressions of the distributed force (C.13) and moment (C.14) in Eqs. (C.11) and (C.12), and after some algebraic operations, the differential equation of the beam

lateral displacement can be expressed in terms of the dimensionless axial coordinate $\xi = z^j/h^j$ as:

$$\frac{d^4 u}{d\xi^4} - (\kappa_1 + \kappa_2) \frac{d^2 u}{d\xi^2} + \kappa_1 (\kappa_2 + \kappa_3) u = \kappa_4 (\kappa_2 + \kappa_3) u_I - (\kappa_4 - \kappa_5) \frac{d^2 u_I}{d\xi^2} \quad (C.15)$$

where κ_{1-4} are a set of dimensionless properties that can be defined in order to write the formulation in a more compact way:

$$\kappa_1 = (h)^2 (K_x - \rho A \omega^2) / \alpha G A \quad (C.16a)$$

$$\kappa_2 = (h)^2 (K_\theta - \rho I \omega^2) / E I \quad (C.16b)$$

$$\kappa_3 = (h)^2 \alpha G A / E I \quad (C.16c)$$

$$\kappa_4 = (h)^2 K_x / \alpha G A \quad (C.16d)$$

$$\kappa_5 = (h)^2 K_I / E I \quad (C.16e)$$

The solution that satisfies this differential equation can be obtained as the sum of the homogeneous and particular terms following the expression:

$$u(\xi) = C_1 e^{\xi s_1} + C_2 e^{\xi s_2} + C_3 e^{\xi s_3} + C_4 e^{\xi s_4} + C_P u_I(\xi) \quad (C.17)$$

where s_{1-4} are the roots of the homogeneous equation:

$$s_{1-4} = \pm \sqrt{\frac{(\kappa_1 + \kappa_2) \pm \sqrt{(\kappa_1 + \kappa_2)^2 - 4\kappa_1(\kappa_2 + \kappa_3)}}{2}} \quad (C.18)$$

C_P is the amplitude of the particular solution related to the dynamic loading (incident field):

$$C_P = \frac{\kappa_4(\kappa_2 + \kappa_3) + (k_I)^2(\kappa_4 - \kappa_5)}{(k_I)^4 + (k_I)^2(\kappa_1 + \kappa_2) + \kappa_1(\kappa_2 + \kappa_3)} \quad (C.19)$$

and C_{1-4} are the amplitudes of the homogeneous solution that are computed by imposing boundary conditions.

Once the pile lateral displacements are known, by including the expressions of the distributed loads (C.13), (C.14) into Eqs. (C.10) and (C.12), the rotation of the cross-section, bending moment and shear force can be obtained as functions of the dimensionless axial coordinate as:

$$\theta(\xi) = \frac{1/h}{\kappa_2 + \kappa_3} \left[\frac{d^3 u}{d\xi^3} - (\kappa_1 - \kappa_3) \frac{du}{d\xi} + (\kappa_4 - \kappa_5) \frac{du_I}{d\xi} \right] \quad (C.20)$$

$$M(\xi) = \frac{EI/(h)^2}{\kappa_2 + \kappa_3} \left[\frac{d^4 u}{d\xi^4} - (\kappa_1 - \kappa_3) \frac{d^2 u}{d\xi^2} + (\kappa_4 - \kappa_5) \frac{d^2 u_I}{d\xi^2} \right] \quad (C.21)$$

$$V(\xi) = \frac{-\alpha G A/h}{\kappa_2 + \kappa_3} \left[\frac{d^3 u}{d\xi^3} - (\kappa_1 + \kappa_2) \frac{du}{d\xi} + (\kappa_4 - \kappa_5) \frac{du_I}{d\xi} \right] \quad (C.22)$$

As mentioned before, in order to obtain the amplitudes of the homogeneous solution C_{1-4} , proper boundary conditions have to be imposed at the pile top and bottom levels. For the comparison presented in Section 2.8, and coinciding with the general assumptions, free displacement and fixed rotation conditions are imposed at pile head: $\theta(0) = 0$, $V(0) = 0$; while free tip conditions are considered at the end of the pile: $M(1) = 0$, $V(1) = 0$. On the other hand, for the model that includes the effects of the loads of the incident field, the free tip conditions are change into loaded tip conditions by imposing that the shear force at the pile tip coincides with the resultant of the horizontal tractions originated by the incident field at this position: $V(1) = V_I^L$, see Eq. (C.8).

For layered soil profiles, Eqs. from (C.15) to (C.22) are applied for each stratum and continuity boundary conditions for pile lateral displacements, rotations, shear forces and bending moments are also imposed at the depth of each layer interface:

$$u^j(1) = u^{j+1}(0) \quad (\text{C.23a})$$

$$\theta^j(1) = \theta^{j+1}(0) \quad (\text{C.23b})$$

$$M^j(1) = M^{j+1}(0) \quad (\text{C.23c})$$

$$V^j(1) = V^{j+1}(0) \quad (\text{C.23d})$$

It is important to notice that the obtained equations include all the phenomena that were described before (soil reaction to pile displacement and rotation, as well as the effects of the incident field). However, simpler formulations that neglect the contribution of some of the components can be directly obtained by nullifying the corresponding terms.



D. Resumen en castellano

- D.1 Objetivos
- D.2 Modelo integral
- D.3 Problemas estudiados
- D.4 Conclusiones y desarrollos futuros



Título de la Tesis Doctoral: Respuesta dinámica de estructuras pilotadas. Implementación de un modelo basado en la formulación integral del problema y el uso de una solución fundamental del semiespacio estratificado¹

D.1 Objetivos

El objetivo último de la disertación que se presenta es la implementación de un código basado en la formulación integral del problema elástico que incorpore una Solución Fundamental para el semiespacio viscoelástico estratificado, así como su aplicación al análisis de la respuesta dinámica de cimentaciones pilotadas y estructuras sobre este tipo de cimentaciones.

El semiespacio (en general estratificado) es modelado haciendo uso de una estrategia numérica de colocación con esta habilidad mientras pilotes y estructura son tratados como elementos finitos de tipo viga. El nuevo software desarrollado con estos principios reducirá notablemente los recursos de computación, permitiendo modelar problemas que, con los programas previamente disponibles por el Grupo, eran inabordables.

En el camino de consecución de este objetivo principal, se establecerán una serie de objetivos parciales:

Formulación e implementación:

- Estudio de las bases teóricas y de la formulación de la solución fundamental del semiespacio viscoelástico estratificado que pretende utilizarse. Familiarización con las rutinas desarrolladas para este tipo de soluciones fundamentales específicas.
- Implementación de dicha solución fundamental en un modelo acoplado para el análisis de la respuesta dinámica de cimentaciones pilotadas. Reformulación de los algoritmos previos de EC-EF en el sentido de incorporar este tipo de soluciones fundamentales.
- Validación con resultados existentes. Estudio de los rangos de validez y aplicación del modelo y de la técnica numérica (dificultades numéricas asociadas a la solución adoptada, número de subcapas necesarias para representar adecuadamente una estratigrafía concreta, etc.) mediante la comparación con resultados correspondientes a distintos problemas y configuraciones.
- Elaboración de estrategias numéricas orientadas a la optimización de la eficiencia y requerimientos computacionales del código desarrollado.

¹En este apéndice se presenta un breve resumen en castellano de la Tesis Doctoral de entre 5 y 20 páginas, de acuerdo con el artículo 10 del Reglamento de Estudios de Doctorado de la ULPGC, aprobado por el Consejo de Gobierno el 17 de diciembre de 2012 (BOULPGC de 9 de enero de 2013) y modificado por el Consejo de Gobierno de 23 de octubre de 2013 (BOULGPC de 4 de noviembre de 2013), de 21 de abril de 2016 (BOULPGC de 11 de mayo de 2016) y de 29 de septiembre de 2016 (BOULPGC de 7 de octubre de 2016).

Aplicación del modelo:

- Aplicación del modelo desarrollado a la caracterización de las propiedades dinámicas de cimentaciones pilotadas mediante la obtención de funciones de rigidez y amortiguamiento en el dominio de la frecuencia. Estudio de la influencia de la variabilidad del perfil en dichas variables.
- Aplicación del modelo desarrollado para la obtención de factores de interacción cinemática de configuraciones de interés. Estudio de la influencia de la variabilidad del perfil.
- Estudio de esfuerzos en pilotes individuales y grupos de pilotes en terrenos estratificados provocados por trenes de ondas sísmicas que inciden sobre el emplazamiento.
- A partir de los resultados obtenidos por el modelo desarrollado y haciendo uso de técnicas de subestructuración, estudio de los efectos de interacción suelo-estructura en la caracterización dinámica de estructuras de aerogeneradores marinos.
- Aplicación del modelo desarrollado para el estudio del uso de barreras de pilotes como medida de mitigación de las vibraciones en el terreno.

Difusión:

- Difusión de los resultados obtenidos en revistas indexadas y ponencias en congresos internacionales.

D.2 Modelo integral

El modelo desarrollado en este documento de tesis se basa en la implementación de una solución fundamental de semiespacio estratificado en un modelo acoplado de Elementos de Contorno - Elementos Finitos (EC-EF) preexistente para el análisis dinámico de cimentaciones y estructuras pilotadas [17]. En este modelo previo, el terreno, considerado como un medio infinito, es discretizado haciendo uso de formulaciones de EC estándares. Los pilotes de la cimentación, por su lado, son modelados haciendo uso de EF tipo viga clásicos. Para la resolución conjunta y directa del problema, se incorporan al sistema ecuaciones de acoplamiento adicionales entre pilotes y terreno y pilotes y encepado. Se trata de ecuaciones de equilibrio y compatibilidad en términos de las variables representativas, con un carácter más o menos directo según sea la metodología (EC ó EF) utilizada para representar el comportamiento de las regiones implicadas.

Las bases del modelo EC-EF previo y, por tanto, también del modelo desarrollado en la presente tesis, nacen del modelo estático presentado por Mendonça et al. [18–20]. En ellos, la interacción entre el suelo y el pilote se reduce a un conjunto de fuerzas distribuidas que actúan sobre una línea de carga, mientras que los efectos de la rigidez adicional aportada por los pilotes se incorporan a través de las ecuaciones de equilibrio de elementos finitos de los mismos. La pérdida de la dimensión de los pilotes evita toda discretización de la interfase

entre ellos y el terreno, con el consiguiente ahorro de grados de libertad respecto a una formulación basada exclusivamente en EC. A pesar de esta simplificación, el modelo EC-EF es capaz de reproducir fielmente la respuesta dinámica de las cimentaciones de pilotes que se obtendría mediante el uso de una formulación completa de medio continuo (EC).

El nuevo modelo desarrollado en esta tesis pretende avanzar en las prestaciones y posibilidades del modelo EC-EF anterior con la implementación de soluciones fundamentales (Funciones de Green) de semiespacio estratificado en el módulo que simula el comportamiento dinámico del terreno. Debido a que esta nueva solución fundamental ya satisface las condiciones de contorno del medio estratificado, se evita la discretización de la superficie libre del mismo y las interfases entre estratos. Este avance permite reducir la dimensión del problema de forma muy notable y elimina, asimismo, una importante fuente de incertidumbre en cuanto a la cantidad de semiespacio a discretizar.

En relación con el modelo que se propone, no es de rigor hablar en términos de Elementos de Contorno en referencia a la técnica numérica que se emplea, ya que:

- La estrategia utilizada para el acoplamiento pilote-suelo (idéntica a la seguida en el modelo previo) no implica variables de contorno del terreno. No se discretiza la interfase suelo-pilote y las fuerzas asociadas a esta interacción pueden tratarse como fuerzas de volumen en el terreno.
- En caso de existir un encepado que conecte las cabezas de los pilotes, se considera que no existe contacto entre este y el terreno
- Las condiciones de contorno entre estratos y en la superficie del suelo del problema real a resolver son verificadas ya por la solución fundamental que pretende utilizarse por lo que no es necesaria la discretización de dichos contornos.

Así, es mejor referirnos al modelo desarrollado en términos de una metodología de colocación basada en la formulación integral del problema para el terreno. Por tanto, en este modelo integral, solo el pilote es discretizado con elementos finitos tipo viga y las variables primarias del problema son los desplazamientos y las fuerzas resultantes que representan la interacción con el suelo, ambas a lo largo del eje de los mismos (ver Fig. D.1).

La formulación del modelo desarrollado permite asumir diferentes fuentes de excitación del sistema suelo-pilotes. Dichas fuentes pueden ser: trenes de ondas sísmicas que imponen un campo incidente en los puntos del terreno estratificado, cargas externas actuando sobre la superficie libre del terreno o acciones directamente impuestas en los encepados o en las cabezas de los pilotes mediante el establecimiento de fuerzas o desplazamientos prescritos.

Por último, cabe destacar que, si bien la nueva solución fundamental empleada en el modelo propuesto supone un considerable ahorro en términos de grados de libertad del problema, el proceso de cálculo de la misma es mucho más costoso (desde el punto de vista computacional) que las soluciones fundamentales empleadas en los modelos clásicos. Por ello, y con el objetivo de disponer de una herramienta eficiente, se ha implementado una estrategia numérica que permite optimizar el uso de la nueva solución fundamental, reduciendo enormemente el tiempo computacional requerido por el código desarrollado.

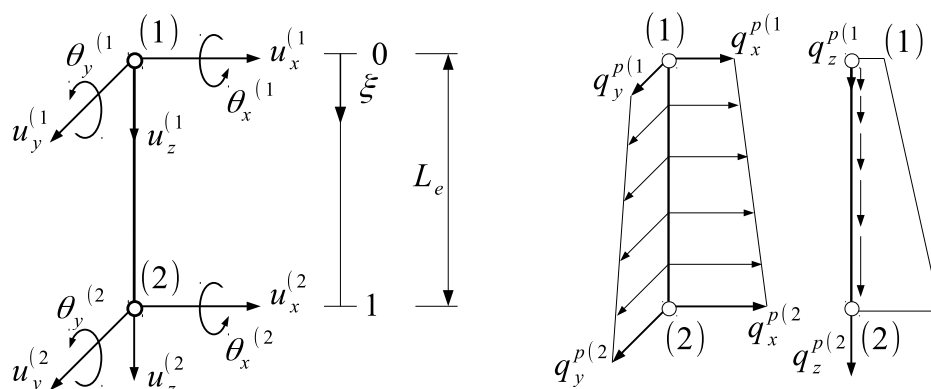


Figura D.1: Grados de libertad de los elementos empleados para los pilotes. Desplazamientos y giros de la sección (izquierda) y fuerzas distribuidas de interacción suelo-pilote (derecha).

D.3 Problemas estudiados

Una vez implementado y validado el nuevo modelo, se han realizado una serie de estudios relacionados con el comportamiento dinámico de cimentaciones de pilotes y estructuras pilotadas. A continuación, se describen brevemente los diferentes problemas considerados. Con la intención de aprovechar al máximo las habilidades del modelo integral desarrollado, todos los estudios se centran en analizar cómo afecta la estratigrafía del terreno a diferentes variables de respuesta de las cimentaciones y estructuras pilotadas.

D.3.1 Efecto de la variabilidad del perfil en las impedancias de pilotes inclinados

En primer lugar, se estudia el problema de las impedancias de grupos reducidos de pilotes inclinados, analizando cómo varían las curvas de impedancia debido a la variabilidad del perfil del terreno. Para ello, se comparan los resultados obtenidos considerando un semiespacio homogéneo con los resultados correspondientes a diferentes perfiles en los que la velocidad de propagación de la onda aumenta con la profundidad de forma continua siguiendo una ley exponencial. Los resultados se presentan de forma totalmente adimensional para una mayor generalidad y utilidad práctica de las curvas obtenidas.

D.3.2 Efecto de la variabilidad del perfil en la respuesta sísmica de cimentaciones pilotadas

A continuación, se estudia la influencia de la variabilidad del perfil sobre la respuesta sísmica de cimentaciones de pilotes. En este caso, se asumen dimensiones usualmente empleadas para dichas cimentaciones y se eligen tipos de suelo representativos de los que se pueden encontrar en la realidad. Estos suelos presentan una variabilidad continua del valor de la velocidad de onda con la profundidad y los resultados obtenidos con dichos perfiles

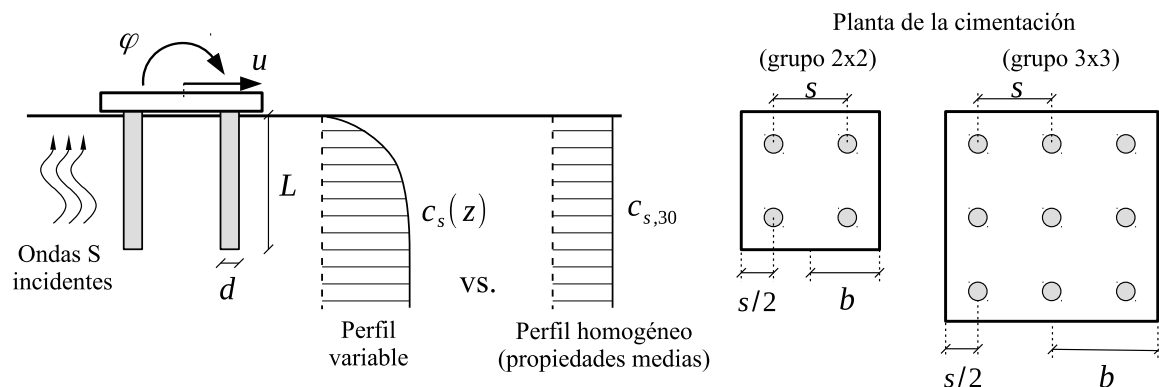


Figura D.2: Representación del problema sísmico.

se comparan con los correspondientes a un medio homogéneo con las propiedades medias según recomienda la norma, ver Fig. D.2.

Se estudia cómo influye esta variabilidad del terreno en los factores de interacción cinemática de la cimentación (dominio de la frecuencia), así como sobre la respuesta de los sistemas que se sitúan sobre ellos mediante la obtención de espectros de aceleración máxima (dominio del tiempo). Para completar el análisis, también se estudia si la suposición del terreno homogéneo equivalente permite estimar, o no, los esfuerzos cinemáticos máximos a los que se ven sometidos los pilotes ante la actuación de ondas sísmicas.

D.3.3 Efecto de la estratigrafía en la eficacia de barreras de pilotes

La versatilidad del modelo desarrollado permite su aplicación para problemas en los que los pilotes no se emplean como cimentación, sino como medida para la mitigación de las vibraciones que se propagan por el terreno. En concreto, y aprovechando las fortalezas del modelo desarrollado, se estudia cómo se ve afectada la eficiencia de la barrera de pilotes debido a la presencia de un estrato rocoso de gran rigidez a una cierta profundidad en el terreno. El problema estudiado se representa en la Fig. D.3.

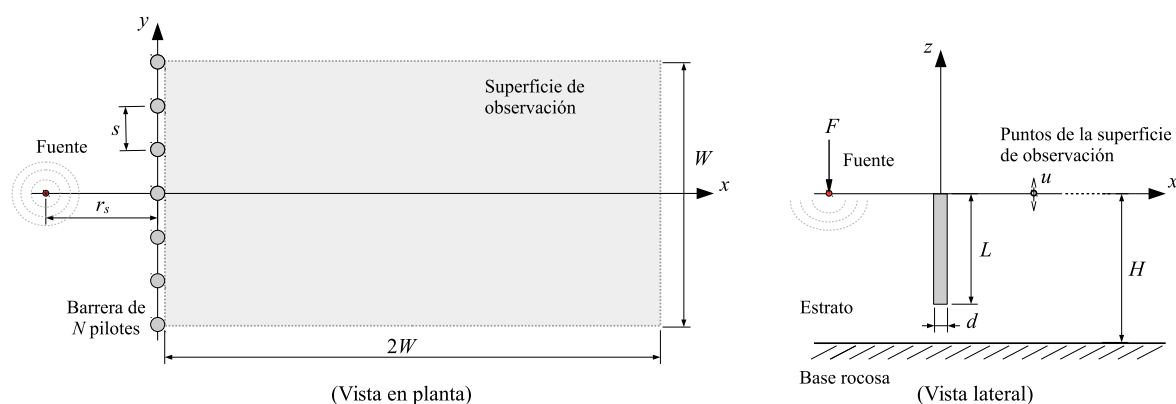


Figura D.3: Representación del problema de barreras de pilotes.

D.3.4 Efecto de la variabilidad del perfil en la caracterización dinámica de estructuras de aerogeneradores monopilotados

El último problema abordado está íntimamente relacionado con el proyecto de investigación en el que se enmarca la tesis. Se analiza el problema de la caracterización dinámica de estructuras de aerogeneradores marinos soportados por monopilotes. El modelo desarrollado se utiliza para obtener las funciones de impedancia de los mismos y, mediante una metodología de subestructuración, se calculan las variaciones en la frecuencia fundamental y amortiguamiento del sistema debidas a la flexibilidad de la cimentación. Para este estudio, se emplean propiedades características de los suelos y de las dimensiones estructurales para este tipo de construcciones que han sido obtenidas a partir de datos reales disponibles en la literatura.

D.4 Conclusiones y desarrollos futuros

En el presente trabajo de tesis se desarrolla e implementa un modelo numérico para el análisis dinámico de cimentaciones de pilotes. La formulación del modelo se basa en la formulación integral del teorema de reciprocidad en el medio viscoelástico y el uso de una solución fundamental avanzada para el semiespacio estratificado. A su vez, los pilotes se tratan como líneas unidimensionales de carga actuando en el interior del terreno, incorporando los efectos derivados de la rigidez de los mismos mediante las ecuaciones de equilibrio características de una representación mediante elementos finitos. Las formulaciones del terreno y pilotes se acoplan imponiendo condiciones de compatibilidad y equilibrio en términos de los desplazamientos y fuerzas distribuidas de interacción suelo-pilote, respectivamente.

El uso de soluciones fundamentales avanzadas que ya satisfacen las condiciones de superficie libre y compatibilidad entre estratos, elimina la necesidad de discretizar dichos contornos del terreno. Mientras que el tratamiento unidimensional de los pilotes elimina la necesidad de discretizar todas las interfases entre el suelo y dichos elementos, ahorrando un número significativo de grados de libertad del problema (especialmente a lo largo del fuste de los pilotes). Con todo esto, se obtiene un modelo simplificado, pero a la vez riguroso, formulado exclusivamente en términos de las variables de los pilotes. Esta herramienta permite el estudio dinámico de cimentaciones pilotadas de una forma muy eficiente, incluso en terrenos cuyas propiedades presenten un alto grado de variabilidad.

El modelo desarrollado ha permitido al Grupo de Investigación en el que se integra la tesis abordar problemas que, con las herramientas previas del grupo, eran computacionalmente inabordables. Algunos de estos problemas se han analizado en el presente documento, poniendo de manifiesto la influencia de la variabilidad del perfil del terreno en la respuesta dinámica de cimentaciones pilotadas (impedancias, factores de interacción cinemática y esfuerzos) y, mediante técnicas de subestructuración, en la caracterización dinámica de estructuras para aerogeneradores marinos monopilotados. También, la versatilidad del modelo desarrollado ha permitido analizar el uso de configuraciones de pilotes como medida de mitigación de las vibraciones del terreno. A partir del modelo y del trabajo desarrollado a lo largo de la duración de la tesis, se proponen las siguientes líneas futuras:

Modelo integral:

- *Estudio del comportamiento dinámico de configuraciones de pilotes.* Uso del modelo en su estado actual para realizar, por ejemplo:
 - Análisis de la influencia del perfil del terreno en los fenómenos de interacción suelo-estructura mediante técnicas de subestructuración y funciones de impedancia y factores de interacción cinemática.
 - Estudio de la respuesta sísmica de cimentaciones de pilotes en medios estratificados o con perfiles de suelo variables ante trenes de ondas con un ángulo de incidencia genérico.
 - Aplicación del modelo desarrollado para el análisis de configuraciones más complejas, tales como cimentaciones con un elevado número de elementos o el estudio de “metabarreras” como medidas de mitigación de vibraciones del terreno. Análisis de configuraciones óptimas mediante cualquier tipo de metodología de optimización.
- *Incorporación de superestructuras.* De este modo, se podrán abordar de forma directa problemas que requieren de una mayor elaboración para poder ser estudiados mediante técnicas de subestructuración.
 - La tipología estructural se propone que sea totalmente genérica mediante el uso de elementos finitos de tipo viga y lámina, con una unión a los pilotes mediante encepado rígido o compatibilización nodal.
 - Así mismo, se podrán considerar varias estructuras pilotadas independientes, cuya interacción sea exclusivamente a través de la propagación de energía por el terreno, permitiendo el estudio de efectos de interacción estructura-suelo-estructura.
 - Otra aplicación de este modelo avanzado con superestructuras es la del estudio de los efectos ciudad (*site-city interactions* en terminología inglesa). Para ello, podrá reducirse cada uno de los edificios a un único elemento viga conectado a un único pilote.
- *Estudio de problemas con carga móvil.* Modificación del modelo desarrollado para el tratamiento de problemas con una carga en movimiento por el semiespacio, pudiendo abordar problemas que incluyan como fuente de excitación el paso de vehículos cercanos (tráfico, trenes, etc.).

En su versión más desarrollada, el modelo numérico permitiría la simulación directa de problemas con excitación genérica (ondas sísmicas con propagación arbitraria, cargas de tráfico, etc.) que incluyan una o varias estructuras pilotadas y con la posibilidad de la existencia de barreras de pilotes para mitigar las vibraciones transmitidas por el terreno, todo esto pudiendo considerar una estratigrafía del suelo altamente variable.

Uso de la solución fundamental:

- *Regularización de la solución fundamental.* Búsqueda de un proceso de regularización adecuado para la solución fundamental del semiespacio estratificado, permitiendo su integración en el interior de elementos bidimensionales sin necesidad de estrategias especiales de colocación. Así, podría utilizarse dicha solución fundamental en los códigos de elementos de contorno disponibles por el grupo, permitiendo el estudio de otras tipologías de cimentaciones (p.ej., superficiales o embebidas) sin la necesidad de discretizar la superficie libre ni las interfaces entre estratos.
- *Estrategias para una uso eficiente de la solución fundamental.* Desarrollo de estrategias computacionales que aceleren el proceso de cálculo de la solución fundamental para su incorporación eficiente a los modelos de elementos de contorno.

De esta forma, los modelos numéricos desarrollados podrían simular de forma directa el comportamiento dinámico de infinidad de tipologías estructurales y de cimentación construidas sobre perfiles con un alto grado de heterogeneidad. El diseño estructural podría incluso realizarse combinando elementos de continuo con elementos reducidos de tipo viga o lámina.

Transferencia de conocimiento:

- *Software en abierto.* El modelo desarrollado en el presente documento podrá ser colgado públicamente en la web, ya sea en forma de código abierto o mediante ejecutables. Cabe destacar que la eficiencia del mismo permitiría su uso, incluso, en ordenadores sin grandes prestaciones.
- *Obtención de recomendaciones mediante Machine Learning.* La versatilidad y eficiencia del modelo desarrollado pueden aprovecharse para obtener un gran volumen de resultados en problemas de interés. A partir de estas grandes bases de datos, y mediante el uso de técnicas de aprendizaje automático, podrían inferirse expresiones y recomendaciones de aplicación práctica directa. Algunos ejemplos pueden ser: factores de seguridad para incorporar efectos de interacción suelo-estructura, o coeficientes correctores que incorporen los efectos de la estratigrafía del terreno. Esta nueva línea propuesta tiene puntos en común con líneas de trabajo seguidas por otras divisiones del Instituto SIANI, por lo que su desarrollo abriría la posibilidad nuevas colaboraciones y sinergias entre los distintos grupos de investigación.

De esta forma, se pretende dar utilidad y valor práctico a los resultados obtenidos con el modelo desarrollado, intentando aprovechar las prestaciones del mismo para proporcionar conocimiento de aplicación directa que puedan ser empleados por la comunidad científica y profesional en el ámbito de la ingeniería civil.

The image features a minimalist design on a light gray background. A solid vertical line runs down the right side of the page. To its left, several curved, dashed lines in a light gray color sweep across the page, creating a sense of movement and depth. These lines are of varying lengths and radii, some starting from the top and others from the bottom, all curving towards the right. A dark blue rectangular box is positioned horizontally, overlapping the vertical line and the dashed curves. Inside this box, the word "BIBLIOGRAPHY" is written in white, uppercase, sans-serif font.

BIBLIOGRAPHY





- [1] R. Abascal and J. Domínguez. Vibrations of footings on zoned viscoelastic soils. *Journal of Engineering Mechanics ASCE*, 112(5):433–447, 1986.
- [2] E. Alarcón, J. J. Cano and J. Domínguez. Boundary element approach to the dynamic stiffness functions of circular foundations. *International Journal for Numerical and Analytical Methods in Geomechanics*, 13(6):645–664, 1989.
- [3] J. Domínguez and E. Alarcón. *Elastodynamics. Progress in Boundary Element Methods*. Pentech Press Ltd., London, UK, 1981.
- [4] F. Medina and J. Domínguez. Boundary elements for the analysis of the seismic response of dams including dam-water-foundation interaction effects. I. *Engineering Analysis with Boundary Elements*, 6(3):152–157, 1989.
- [5] J. Domínguez and F. Medina. Boundary elements for the analysis of the seismic response of dams including dam-water-foundation interaction effects. II. *Engineering Analysis with Boundary Elements*, 6(3):158–163, 1989.
- [6] O. Maeso. *Modelo para el análisis sísmico de presas bóveda incluyendo los efectos de interacción suelo-agua-estructura*. Ph. D. Thesis, Universidad de Las Palmas de Gran Canaria, 1992.
- [7] O. Maeso and J. Domínguez. Earthquake analysis of arch dams. I: dam-foundation interaction. *Journal of Engineering Mechanics ASCE*, 119(3):496–512, 1993.
- [8] J. Domínguez and O. Maeso. Earthquake analysis of arch dams. II: dam-water-foundation interaction. *Journal of Engineering Mechanics ASCE*, 119(3):513–530, 1993.
- [9] J. J. Aznárez. *Efectos de los fenómenos de interacción incluyendo los factores espaciales y sedimentos de fondo en la respuesta sísmica de presas bóveda*. Ph. D. Thesis, Universidad de Las Palmas de Gran Canaria, 2002.
- [10] O. Maeso, J. J. Aznárez and J. Domínguez. Three-dimensional models of reservoir sediment and effects on the seismic response of arch dams. *Earthquake Engineering & Structural Dynamics*, 33(10):1103–1123, 2004.
- [11] J. J. Aznárez, O. Maeso and J. Domínguez. BE analysis of bottom sediments in dynamic fluid-structure interaction problems. *Engineering Analysis with Boundary Elements*, 30(2):124–136, 2006.
- [12] F. García, J. J. Aznárez, H. Cifuentes, F. Medina and O. Maeso. Influence of reservoir geometry and conditions on the seismic response of arch dams. *Soil Dynamics and Earthquake Engineering*, 67:264–272, 2014.
- [13] O. Maeso, J. J. Aznárez and J. Domínguez. Effects of space distribution of excitation on seismic response of arch dams. *Journal of Engineering Mechanics ASCE*, 128(7):759–768, 2002.



- [14] F. García, J. Aznárez, L. Padrón and O. Maeso. Relevance of the incidence angle of the seismic waves on the dynamic response of arch dams. *Soil Dynamics and Earthquake Engineering*, 90:442–453, 2016.
- [15] F. Vinciprova, J. J. Aznárez, O. Maeso and G. Oliveto. *Problems in structural identification and diagnostic: General aspects and applications*, chapter Interaction of BEM analysis and experimental testing on pile-soil systems, 195–227. Springer-Verlag, 2003.
- [16] O. Maeso, J. J. Aznárez and F. García. Dynamic impedances of piles and groups of piles in saturated soils. *Computers and Structures*, 83:769–782, 2005.
- [17] L. A. Padrón. *Numerical model for the dynamic analysis of pile foundations*. Ph. D. Thesis, Universidad de Las Palmas de Gran Canaria, 2009.
- [18] A. V. Mendonça and J. B. de Paiva. A boundary element method for the static analysis of raft foundations on piles. *Engineering Analysis with Boundary Elements*, 24(3):237–247, 2000.
- [19] A. V. Mendonça and J. B. de Paiva. An elastostatic FEM/BEM analysis of vertically loaded raft and piled raft foundation. *Engineering Analysis with Boundary Elements*, 27(9):919–933, 2003.
- [20] R. Matos Filho, A. V. Mendonça and J. B. Paiva. Static boundary element analysis of piles submitted to horizontal and vertical loads. *Engineering Analysis with Boundary Elements*, 29(3):195–203, 2005.
- [21] L. Padrón, J. Aznárez and O. Maeso. BEM–FEM coupling model for the dynamic analysis of piles and pile groups. *Engineering Analysis with Boundary Elements*, 31(6):473–484, 2007.
- [22] L. A. Padrón, J. J. Aznárez and O. Maeso. Dynamic analysis of piled foundations in stratified soils by a BEM-FEM model. *Soil Dynamics and Earthquake Engineering*, 28(5):333–346, 2008.
- [23] L. A. Padrón, J. J. Aznárez, O. Maeso and A. Santana. Dynamic stiffness of deep foundations with inclined piles. *Earthquake Engineering & Structural Dynamics*, 39(12):1343–1367, 2010.
- [24] L. a. Padrón, J. J. Aznárez and O. Maeso. 3-D boundary element-finite element method for the dynamic analysis of piled buildings. *Engineering Analysis with Boundary Elements*, 35(3):465–477, 2011.
- [25] L. A. Padrón, J. J. Aznárez, O. Maeso and M. Saitoh. Impedance functions of end-bearing inclined piles. *Soil Dynamics and Earthquake Engineering*, 38:97–108, 2012.
- [26] C. Medina, J. J. Aznárez, L. A. Padrón and O. Maeso. Effects of soil-structure interaction on the dynamic properties and seismic response of piled structures. *Soil Dynamics and Earthquake Engineering*, 53:160–175, 2013.



- [27] J. M. Zarzalejos, J. J. Aznárez, L. A. Padrón and O. Maeso. Influences of type of wave and angle of incidence on seismic bending moments in pile foundations. *Earthquake Engineering & Structural Dynamics*, 43(1):41–59, 2014.
- [28] C. Medina, L. A. Padrón, J. J. Aznárez, A. Santana and O. Maeso. Kinematic interaction factors of deep foundations with inclined piles. *Earthquake Engineering & Structural Dynamics*, 43(13):2035–2050, 2014.
- [29] L. A. Padrón, A. Suárez, J. J. Aznárez and O. Maeso. Kinematic internal forces in deep foundations with inclined piles. *Earthquake Engineering & Structural Dynamics*, 44(12):2129–2135, 2015.
- [30] C. Medina, L. A. Padrón, J. J. Aznárez and O. Maeso. Influence of pile inclination angle on the dynamic properties and seismic response of piled structures. *Soil Dynamics and Earthquake Engineering*, 69:196–206, 2015.
- [31] G. M. Álamo, A. E. Martínez-Castro, L. A. Padrón, J. J. Aznárez, R. Gallego and O. Maeso. Efficient numerical model for the computation of impedance functions of inclined pile groups in layered soils. *Engineering Structures*, 126:379–390, 2016.
- [32] G. M. Álamo, J. D. R. Bordón, F. García, J. J. Aznárez, L. A. Padrón, F. Chirino and O. Maeso. Review of numerical models for studying the dynamic response of deep foundations for the design and project of wind turbines. In J. L. Ayuso, J. L. Yagüe and S. F. Capuz-Rizo, editors, *Project Management and Engineering Research. AEIPRO 2016, In Press*. Springer International Publishing, 2018.
- [33] B. B. Guzina, R. Y. S. Pak and A. E. Martínez-Castro. Singular boundary elements for three-dimensional elasticity problems. *Engineering Analysis with Boundary Elements*, 30(8):623–639, 2006.
- [34] A. E. Martínez-Castro and R. Gallego. Three-dimensional green’s function for time-harmonic dynamics in a viscoelastic layer. *International Journal of Solids and Structures*, 44(13):4541–4558, 2007.
- [35] R. Toledo, J. J. Aznárez, O. Maeso and D. Greiner. Optimization of thin noise barrier designs using evolutionary algorithms and a dual BEM formulation. *Journal of Sound and Vibration*, 334:219–238, 2015.
- [36] R. Toledo, J. J. Aznárez, O. Maeso and D. Greiner. Un procedimiento basado en el uso de algoritmos genéticos y elementos de contorno para el diseño óptimo de la geometría de pantallas acústicas de pequeño espesor. *Revista de Acústica*, 46(1-2):13–21, 2015.
- [37] R. Toledo, J. J. Aznárez, D. Greiner and O. Maeso. Shape design optimization of road acoustic barriers featuring top-edge devices by using genetic algorithms and boundary elements. *Engineering Analysis with Boundary Elements*, 63:49–60, 2016.



- [38] J. D. R. Bordón, J. J. Aznárez and O. Maeso. A 2D BEM–FEM approach for time harmonic fluid–structure interaction analysis of thin elastic bodies. *Engineering Analysis with Boundary Elements*, 43:19–29, 2014.
- [39] J. D. R. Bordón, J. J. Aznárez and O. Maeso. Two-dimensional numerical approach for the vibration isolation analysis of thin walled wave barriers in poroelastic soils. *Computers and Geotechnics*, 71:168–179, 2016.
- [40] J. D. R. Bordón, J. J. Aznárez and O. Maeso. Dynamic model of open shell structures buried in poroelastic soils. *Computational Mechanics*, 60(2):269–288, 2017.
- [41] J. D. R. Bordón. *Coupled model of finite elements and boundary elements for the dynamic analysis of buried shell structures*. Ph. D. Thesis, Universidad de Las Palmas de Gran Canaria, 2017.
- [42] G. M. Álamó, L. A. Padrón, J. J. Aznárez and O. Maeso. Structure-soil-structure interaction effects on the dynamic response of piled structures under obliquely incident seismic shear waves. *Soil Dynamics and Earthquake Engineering*, 78:142–153, 2015.
- [43] M. Faghihnia Torshizi, M. Saitoh, G. M. Álamó, C. S. Goit and L. A. Padrón. Influence of pile radius on the pile head kinematic bending strains of end-bearing pile groups. *Soil Dynamics and Earthquake Engineering*, 105:184–203, 2018.
- [44] G. M. Álamó, J. D. Bordón, J. J. Aznárez and O. Maeso. Relevance of soil-pile tangential tractions for the estimation of kinematic seismic forces: Formulation and setting of a Winkler approach. *Applied Mathematical Modelling*, 59:1–19, 2018.
- [45] G. M. Álamó, J. J. Aznárez, L. A. Padrón, A. E. Martínez-Castro, R. Gallego and O. Maeso. Dynamic soil-structure interaction in offshore wind turbines on monopiles in layered seabed based on real data. *Ocean Engineering*, 156:14–24, 2018.
- [46] G. M. Álamó, J. J. Aznárez, L. A. Padrón, A. E. Martínez-Castro and O. Maeso. Importance of using accurate soil profiles for the estimation of pile kinematic input factors. *Journal of Geotechnical and Geoenvironmental Engineering*, (under review), submitted on Dec 2017.
- [47] C. Medina, G. M. Álamó, J. J. Aznárez, L. A. Padrón and O. Maeso. Variations in the dynamic properties of structures founded on piles induced by obliquely incident SV waves. *Earthquake Engineering & Structural Dynamics*, (under review), submitted on May 2018.
- [48] F. García, G. M. Álamó, L. A. Padrón, J. J. Aznárez and O. Maeso. Rigidez dinámica de cimentaciones tripilote para aerogeneradores marinos. In *Congress of Numerical Method in Engineering (CMN 2015)*. Lisbon, Portugal, 29 June – 2 July 2015.
- [49] L. A. Padrón, C. Medina, G. M. Álamó, J. J. Aznárez, A. Santana, O. Maeso, F. García and F. Chirino. Pilotes inclinados: situación normativa y ventajas e inconvenientes de



- su uso en proyectos de edificación en zonas con riesgo sísmico. In *19th International Congress on Project Management and Engineering*. Granada, Spain, 15–17 July 2015.
- [50] G. M. Álamo, J. D. R. Bordón, F. García, J. J. Aznárez, L. A. Padrón, F. Chirino and O. Maeso. Revisión de modelos numéricos para el estudio del comportamiento dinámico de cimentaciones profundas para el diseño y proyecto de aerogeneradores. In *20th International Congress on Project Management and Engineering*. Cartagena, Spain, 13–15 July 2016.
 - [51] G. M. Álamo, J. J. Aznárez, L. A. Padrón, A. E. Martínez-Castro, R. Gallego and O. Maeso. Dynamic response of real offshore wind turbines on monopiles in stratified seabed. In *VII European Congress on Computational Methods in Applied Sciences and Engineering (ECCOMAS 2016)*. Crete, Greece, 5–10 June 2016.
 - [52] F. García, G. M. Álamo, L. A. Padrón, J. J. Aznárez and O. Maeso. Influencia del comportamiento poroelástico del fondo marino en la rigidez dinámica de cimentaciones pilotadas para aerogeneradores offshore. In *XXI Congreso Nacional de Ingeniería Mecánica (CNIM)*. Elche, Spain, 9–11 November 2016.
 - [53] G. M. Álamo, M. Saitoh, C. S. Goit, L. A. Padrón, J. J. Aznárez and O. Maeso. Pile-to-pile kinematic interaction factors for vertically-incident shear waves. In *2nd Global Conference on Applied Computing in Science and Engineering (ACSE2)*. Las Palmas de Gran Canaria, Spain, 26–28 July 2017.
 - [54] G. M. Álamo, J. J. Aznárez, L. A. Padrón, A. E. Martínez-Castro, R. Gallego and O. Maeso. Integral model for the analysis of pile foundations in stratified soils. In *2nd Global Conference on Applied Computing in Science and Engineering (ACSE2)*. Las Palmas de Gran Canaria, Spain, 26–28 July 2017.
 - [55] M. Castro, J. D. R. Bordón, G. M. Álamo and J. J. Aznárez. Formulation and calibration of a pasternak model for seismic analysis of pile foundations. In *2nd Global Conference on Applied Computing in Science and Engineering (ACSE2)*. Las Palmas de Gran Canaria, Spain, 26–28 July 2017.
 - [56] R. Quevedo, G. M. Álamo, J. J. Aznárez, L. A. Padrón and O. Maeso. Simplified model to calculate the envelopes of bending moments along offshore wind turbines on monopiles. In *2nd Global Conference on Applied Computing in Science and Engineering (ACSE2)*. Las Palmas de Gran Canaria, Spain, 26–28 July 2017.
 - [57] G. M. Álamo, A. E. Martínez-Castro, L. A. Padrón, J. J. Aznárez, R. Gallego and O. Maeso. A proposal for normalized impedance functions of inclined piles in non-homogeneous media. In *X International Conference on Structural Dynamics (EURO-DYN 2017)*. Rome, Italy, 10–13 September 2017.
 - [58] G. M. Álamo, J. J. Aznárez, L. A. Padrón, A. E. Martínez-Castro, R. Gallego and O. Maeso. Direct model for the dynamic analysis of piled structures on non-homogeneous media. In *1st Conference on Structural Dynamics (DinEst 2018)*. Madrid, Spain, 20–21 June 2018.



- [59] Z. Friedman and J. Kosmatka. An improved two-node Timoshenko beam finite element. *Computers and Structures*, 47(3):473–481, 1993.
- [60] R. W. Clough and J. Penzien. *Dynamic of structures*. McGraw-Hill, 1982.
- [61] L. T. Wheeler and E. Sternberg. Some theorems in classical elastodynamics. *Archive for Rational Mechanics and Analysis*, 31(1):51–90, 1968.
- [62] R. Y. S. Pak and B. B. Guzina. Three-dimensional Green's functions for a multilayered half-space in displacement potentials. *Journal of Engineering Mechanics*, 128(4):449–461, 2002.
- [63] R. Y. S. Pak. Asymmetric wave propagation in an elastic half-space by a method of potentials. *Journal of Applied Mechanics*, 54(1):121–126, 1987.
- [64] B. Guzina and R. Pak. Static fundamental solutions for a bi-material full-space. *International Journal of Solids and Structures*, 36(4):493–516, 1999.
- [65] B. B. Guzina and R. Y. S. Pak. On the analysis of wave motions in a multi-layered solid. *Quarterly Journal of Mechanics and Applied Mathematics*, 54(1):13–37, 2001.
- [66] J. Domínguez. *Boundary elements in dynamics*. Computational Mechanics Publications & Elsevier Applied Science, Southampton, NY, 1993.
- [67] A. K. Chopra. *Dynamic of structures. Theory and applications to earthquake engineering*. NJ: Prentice-Hall, 2001.
- [68] ECS. *Eurocode 8: Design of structures for earthquake resistance. Part 5: Foundations, Retaining Structures and Geotechnical Aspects*. European Committee for Standardization (ECS), Brussels, 2004.
- [69] *Récommandations AFPS 90. Association Française de Génie Parasismique. Presses des Ponts et chaussées, Paris*, 1990.
- [70] G. Gazetas and G. Mylonakis. Seismic soil-structure interaction: new evidence and emerging issues. In *Geotechnical Earthquake Engineering and Soil Dynamics III*, 1119–1174. Geotechnical Special Publication II. ASCE: New York, 1998.
- [71] J. B. Berrill, S. A. Christensen, R. P. Keenan, W. Okada and J. R. Pettinga. Case study of lateral spreading forces on a piled foundation. *Geotechnique*, 51(6):501–517, 2001.
- [72] M. Sadek and S. Isam. Three-dimensional finite element analysis of the seismic behavior of inclined micropiles. *Soil Dynamics and Earthquake Engineering*, 24:473–485, 2004.
- [73] N. Gerolymos, A. Giannakou, I. Anastasopoulos and G. Gazetas. Evidence of beneficial role of inclined piles: observations and summary of numerical analyses. *Bulletin of Earthquake Engineering*, 6(4):705–722, 2008.



- [74] A. Giannakou, N. Gerolymos, G. Gazetas, T. Tazoh and I. Anastasopoulos. Seismic behavior of batter piles: Elastic response. *Journal of Geotechnical and Geoenvironmental Engineering*, 136(9):1187–1199, 2010.
- [75] S. Isam, A. Hassan and S. Mhamed. 3D elastoplastic analysis of the seismic performance of inclined micropiles. *Computers and Geotechnics*, 39:1–7, 2012.
- [76] S. Escoffier. Experimental study of the effect of inclined pile on the seismic behavior of pile group. *Soil Dynamics and Earthquake Engineering*, 42:275–291, 2012.
- [77] S. M. Mamoon, A. M. Kaynia and P. K. Banerjee. Frequency domain dynamic analysis of piles and pile groups. *Journal of Engineering Mechanics*, 116(10):2237–2257, 1990.
- [78] C. S. Goit and M. Saitoh. Model tests and numerical analyses on horizontal impedance functions of inclined single piles embedded in cohesionless soil. *Earthquake Engineering and Engineering Vibration*, 12(1):143–154, 2013.
- [79] C. S. Goit and M. Saitoh. Model tests on horizontal impedance functions of fixed-head inclined pile groups under soil nonlinearity. *Journal of Geotechnical and Geoenvironmental Engineering*, 140(6), 2014.
- [80] S. Carbonari, M. Morici, F. Dezi and G. Leoni. Analytical evaluation of impedances and kinematic response of inclined piles. *Engineering Structures*, 117:384–396, 2016.
- [81] F. Dezi, S. Carbonari and M. Morici. A numerical model for the dynamic analysis of inclined pile groups. *Earthquake Engineering & Structural Dynamics*, 45(1):45–68, 2016.
- [82] A. Giannakou, N. Gerolymos and G. Gazetas. On the dynamics of inclined piles. In *Proc. of the 10th International conference on Piling and Deep Foundations*, 286–295. Amsterdam, The Netherlands, 2006.
- [83] A. Velez, G. Gazetas and R. Krishnan. Lateral dynamic response of constrained head piles. *Journal of Geotechnical Engineering*, 109(8):1063–1081, 1983.
- [84] A. M. Kaynia and E. Kausel. Dynamics of piles and pile groups in layered soil media. *Soil Dynamics and Earthquake Engineering*, 10(8):386–401, 1991.
- [85] K. Miura, A. M. Kaynia, K. Masuda, E. Kitamura and Y. Seto. Dynamic behaviour of pile foundations in homogeneous and non-homogeneous media. *Earthquake Engineering & Structural Dynamics*, 23(2):183–192, 1994.
- [86] G. Mylonakis and G. Gazetas. Vertical vibration and additional distress of grouped piles in layered soil. *Soils and Foundations*, 38(1):1–14, 1998.
- [87] G. Mylonakis and G. Gazetas. Lateral vibration and internal forces of grouped piles in layered soil. *Journal of Geotechnical and Geoenvironmental Engineering*, 125(1):16–25, 1999.



BIBLIOGRAPHY

- [88] H. G. Poulos. Analysis of settlement of pile groups. *Geotechnique*, 18(4):449–471, 1968.
- [89] A. M. Kaynia. Dynamic stiffness and seismic response of pile groups. Research Report R83-03, Massachusetts Institute of Technology, Cambridge, MA, 1982.
- [90] W. T. Thomson. Transmission of elastic waves through a stratified solid medium. *Journal of Applied Physics*, 21(2):89–93, 1950.
- [91] E. Kausel and J. M. Roësset. Stiffness matrices for layered soils. *Bulletin of the Seismological Society of America*, 71(6):1743–1761, 1981.
- [92] W. J. Lei and D. M. Wei. Lateral impedances of single pile and pile groups in layered soils. *Engineering Mechanics*, 21(5):36–40, 2004.
- [93] M. S. Huang, Z. M. Wu and Q. Ren. Lateral vibration of pile groups in layered soil. *Chinese Journal of Geotechnical Engineering*, 29(1):32–38, 2007.
- [94] E. Rovithis, G. Mylonakis and K. Pitilakis. Dynamic stiffness and kinematic response of single piles in inhomogeneous soil. *Bulleting of Earthquake Engineering*, 11(6):1949–1972, 2013.
- [95] E. N. Rovithis, H. Parashakis and G. E. Mylonakis. 1D harmonic response of layered inhomogeneous soil: Analytical investigation. *Soil Dynamics and Earthquake Engineering*, 31(7):879–890, 2011.
- [96] K. Fan, G. Gazetas, A. Kaynia, E. Kausel and S. Ahmad. Kinematic seismic response of single piles and pile groups. *Journal of Geotechnical Engineering*, 117(12):1860–1879, 1991.
- [97] N. Makris and G. Gazetas. Dynamic pile-soil-pile interaction. Part II: Lateral and seismic response. *Earthquake Engineering & Structural Dynamics*, 21(2):145–162, 1992.
- [98] G. Gazetas, K. Fan, T. Tazoh, K. Shimizu, M. Kavvadas and N. Makris. Seismic pile-group-structure interaction. *Geotechnical Special Publication*, 56–93, 1992.
- [99] G. Anoyatis, R. Di Laora, A. Mandolini and G. Mylonakis. Kinematic response of single piles for different boundary conditions: Analytical solutions and normalization schemes. *Soil Dynamics and Earthquake Engineering*, 44:183–195, 2013.
- [100] R. Di Laora, Y. Grossi, L. de Sanctis and G. M. B. Viggiani. An analytical solution for the rotational component of the foundation input motion induced by a pile group. *Soil Dynamics and Earthquake Engineering*, 97:424–438, 2017.
- [101] S. M. Mamoon and P. K. Banerjee. Response of piles and pile groups to travelling SH-waves. *Earthquake Engineering & Structural Dynamics*, 19(4):597–610, 1990.



- [102] S. M. Mamoon and S. Ahmad. Seismic response of piles to obliquely incident SH, SV, and P waves. *Journal of Geotechnical Engineering*, 116(2):186–204, 1990.
- [103] A. M. Kaynia and M. Novak. Response of pile foundations to Rayleigh waves and obliquely incident body waves. *Earthquake Engineering & Structural Dynamics*, 21(4):303–318, 1992.
- [104] N. Makris and D. Badoni. Seismic response of pile groups under oblique-shear and Rayleigh waves. *Earthquake Engineering & Structural Dynamics*, 24(4):517–532, 1995.
- [105] H. Mizuno. Pile damage during earthquake in Japan (1923-1983). In T. Nogami, editor, *Dynamic Response of Pile Foundations - Experiment, Analysis and Observation*, 53–78. Geotechnical Special Publication ASCE, New York, 1987.
- [106] T. Tazoh, K. Shimizu and T. Wakahara. Seismic observations and analysis of grouped piles. In T. Nogami, editor, *Dynamic Response of Pile Foundations - Experiment, Analysis and Observation*, 1–20. Geotechnical Special Publication ASCE, New York, 1987.
- [107] S. Nikolaou, G. Mylonakis, G. Gazetas and T. Tazoh. Kinematic pile bending during earthquakes: analysis and field measurements. *Geotechnique*, 51(5):425–440, 2001.
- [108] M. N. Hussien, T. Tobita, S. Iai and M. Karray. Soil-pile-structure kinematic and inertial interaction observed in geotechnical centrifuge experiments. *Soil Dynamics and Earthquake Engineering*, 89:75–84, 2016.
- [109] F. Dezi, S. Carbonari and G. Leoni. A model for the 3D kinematic interaction analysis of pile groups in layered soils. *Earthquake Engineering & Structural Dynamics*, 38:1281–1305, 2009.
- [110] F. Dezi, S. Carbonari and G. Leoni. Static equivalent method for the kinematic interaction analysis of single piles. *Soil Dynamics and Earthquake Engineering*, 30(8):679–690, 2010.
- [111] S. Sica, G. Mylonakis and A. L. Simonelli. Strain effects on kinematic pile bending in layered soil. *Soil Dynamics and Earthquake Engineering*, 49:231–242, 2013.
- [112] M. Martinelli, A. Burghignoli and L. Callisto. Dynamic response of a pile embedded into a layered soil. *Soil Dynamics and Earthquake Engineering*, 87:16–28, 2016.
- [113] G. Mylonakis. Simplified model for seismic pile bending at soil layer interfaces. *Soils and Foundations*, 41(4):47–58, 2001.
- [114] R. M. S. Maiorano, L. de Sanctis, S. Aversa and A. Mandolini. Kinematic response analysis of piled foundations under seismic excitation. *Canadian Geotechnical Journal*, 46(5):571–584, 2009.



- [115] L. de Sanctis, R. M. S. Maiorano and S. Aversa. A method for assessing kinematic bending moments at the pile head. *Earthquake Engineering and Structural Dynamics*, 39(10):1133–1154, 2010.
- [116] S. Sica, G. Mylonakis and A. L. Simonelli. Transient kinematic pile bending in two-layer soil. *Soil Dynamics and Earthquake Engineering*, 31(7):891–905, 2011.
- [117] R. Di Laora, G. Mylonakis and A. Mandolini. Pile-head kinematic bending in layered soil. *Earthquake Engineering and Structural Dynamics*, 42(3):319–337, 2013.
- [118] F. Dezi and H. Poulos. Kinematic bending moments in square pile groups. *International Journal of Geomechanics*, 17(3):04016066, 2017.
- [119] R. Di Laora and E. Rovithis. Kinematic bending of fixed-head piles in non-homogeneous soil. *Journal of Geotechnical and Geoenvironmental Engineering*, 141(4):04014126, 2015.
- [120] S. Wang and H. Wang. Site-dependent shear-wave velocity equations versus depth in California and Japan. *Soil Dynamics and Earthquake Engineering*, 88:8–14, 2016.
- [121] ASCE. *Minimum Design Loads for Buildings and Other Structures*. ASCE/SEI 7-05. American Society of Civil Engineers (ASCE), Reston, VA, 2006.
- [122] BSSC. *NEHRP recommended provisions for seismic regulations for new buildings and other structures (Report FEMA P-750)*. Building Seismic Safety Council (BSSC), Washington, DC, 2009.
- [123] PEER. NGA-West2 Ground Motion Database. <http://ngawest2.berkeley.edu/> (Accessed on May 2017).
- [124] L. Auersch, A. Romero and P. Galvín. Respuesta dinámica de edificaciones producida por campos de ondas incidentes considerando la interacción suelo-estructura. *Revista Internacional de Métodos Numéricos para Cálculo y Diseño en Ingeniería*, 30(4):256–263, 2014.
- [125] F. E. Richart Jr., J. R. Hall and R. D. Woods. *Vibrations of Soils and Foundations*. Prentice-Hall, Englewood Cliffs, NJ, 1970.
- [126] R. D. Woods. Screening of surface waves in soils. *Journal of the Soil Mechanics and Foundations Division (ASCE)*, 94(4):951–979, 1968.
- [127] A. Alzawi and M. Hesham El Nagggar. Full scale experimental study on vibration scattering using open and in-filled (GeoFoam) wave barriers. *Soil Dynamics and Earthquake Engineering*, 31(3):306–317, 2011.
- [128] P. Coulier and H. E. M. Hunt. Experimental study of a stiff wave barrier in gelatine. *Soil Dynamics and Earthquake Engineering*, 66:459–463, 2014.



- [129] P. Coulier, V. Cuéllar, G. Degrande and G. Lombaert. Experimental and numerical evaluation of the effectiveness of a stiff wave barrier in the soil. *Soil Dynamics and Earthquake Engineering*, 77:238–253, 2015.
- [130] B. Dasgupta, D. Beskos and I. G. Vardoulakis. Vibration isolation using open or filled trenches. Part2: 3D homogeneous soil. *Computational Mechanics*, 6:129–142, 1990.
- [131] K. L. Leung, D. E. Beskos and I. G. Vardoulakis. Vibration isolation using open or filled trenches. Part 3: 2-D non-homogeneous soil. *Computational Mechanics*, 7(2):137–148, 1990.
- [132] L. Andersen and S. R. Nielsen. Reduction of ground vibration by means of barriers or soil improvement along a railway track. *Soil Dynamics and Earthquake Engineering*, 25(7-10):701–716, 2005.
- [133] D. J. Thompson, J. Jiang, M. G. Toward, M. F. Hussein, E. Ntotsios, A. Dijckmans, P. Coulier, G. Lombaert and G. Degrande. Reducing railway-induced ground-borne vibration by using open trenches and soft-filled barriers. *Soil Dynamics and Earthquake Engineering*, 88:45–59, 2016.
- [134] P. Persson, K. Persson and G. Sandberg. Numerical study of reduction in ground vibrations by using barriers. *Engineering Structures*, 115:18–27, 2016.
- [135] C. Van hoorickx, O. Sigmund, M. Schevenels, B. S. Lazarov and G. Lombaert. Topology optimization of two-dimensional elastic wave barriers. *Journal of Sound and Vibration*, 376:95–111, 2016.
- [136] A. Dijckmans, A. Ekblad, A. Smekal, G. Degrande and G. Lombaert. Efficacy of a sheet pile wall as a wave barrier for railway induced ground vibration. *Soil Dynamics and Earthquake Engineering*, 84:55–69, 2016.
- [137] C. Van hoorickx, M. Schevenels and G. Lombaert. Double wall barriers for the reduction of ground vibration transmission. *Soil Dynamics and Earthquake Engineering*, 97:1–13, 2017.
- [138] J. D. R. Bordón, C. Van hoorickx, J. J. Aznárez, M. Schevenels, O. Maeso and G. Lombaert. Shape optimized inclined single and double wall wave barriers for ground vibration mitigation. *Soil Dynamics and Earthquake Engineering*, In Press, 2018.
- [139] R. D. Woods, N. E. Barnett and R. Sagesset. Holography - a new tool for soil dynamics. *Journal of Geotechnical Engineering*, 100(11):1231–1247, 1974.
- [140] S. Liao and D. A. Sangrey. Use of piles as isolation barriers. *Journal of Geotechnical Engineering*, 104(9):1139–1152, 1978.
- [141] J. Avilés and F. J. Sánchez-Sesma. Piles as barriers for elastic waves. *Journal of Geotechnical Engineering*, 109(9):1133–1146, 1983.



- [142] J. Avilés and F. J. Sánchez-Sesma. Foundation isolation from vibrations using piles as barriers. *Journal of Engineering Mechanics*, 114(11):1854–1870, 1988.
- [143] S. E. Kattis, D. Polyzos and D. E. Beskos. Vibration isolation by a row of piles using a 3-D frequency domain BEM. *International Journal for Numerical Methods in Engineering*, 46(5):713–728, 1999.
- [144] S. E. Kattis, D. Polyzos and D. E. Beskos. Modelling of pile wave barriers by effective trenches and their screening effectiveness. *Soil Dynamics and Earthquake Engineering*, 18(1):1–10, 1999.
- [145] P. H. Tsai, Z. Y. Feng and T. I. Jen. Three-dimensional analysis of the screening effectiveness of hollow pile barriers for foundation-induced vertical vibration. *Computers and Geotechnics*, 35(3):489–499, 2008.
- [146] G. Y. Gao, Z. Y. Li, C. Qiu and Z. Q. Yue. Three-dimensional analysis of rows of piles as passive barriers for ground vibration isolation. *Soil Dynamics and Earthquake Engineering*, 26(11):1015–1027, 2006.
- [147] T. D. Xia, M. M. Sun, C. Chen, W. Y. Chen and X. Ping. Analysis on multiple scattering by an arbitrary configuration of piles as barriers for vibration isolation. *Soil Dynamics and Earthquake Engineering*, 31(3):535–545, 2011.
- [148] J. Huang and Z. Shi. Attenuation zones of periodic pile barriers and its application in vibration reduction for plane waves. *Journal of Sound and Vibration*, 332(19):4423–4439, 2013.
- [149] X. Liu, Z. Shi, H. Xiang and Y. L. Mo. Attenuation zones of periodic pile barriers with initial stress. *Soil Dynamics and Earthquake Engineering*, 77:381–390, 2015.
- [150] X. Liu, Z. Shi and Y. L. Mo. Comparison of 2D and 3D models for numerical simulation of vibration reduction by periodic pile barriers. *Soil Dynamics and Earthquake Engineering*, 79:104–107, 2015.
- [151] Y. Q. Cai, G. Y. Ding and C. J. Xu. Amplitude reduction of elastic waves by a row of piles in poroelastic soil. *Computers and Geotechnics*, 36(3):463–473, 2009.
- [152] B. Xu, J. F. Lu and J. H. Wang. Numerical analysis of the isolation of the vibration due to Rayleigh waves by using pile rows in the poroelastic medium. *Archive of Applied Mechanics*, 80(2):123–142, 2010.
- [153] P. Xu. Analysis of isolation effectiveness of shear waves by a row of hollow pipe piles in saturated soils. *Transport in Porous Media*, 120(2):415–432, 2017.
- [154] P. Cacciola, M. G. Espinosa and A. Tombari. Vibration control of piled-structures through structure-soil-structure-interaction. *Soil Dynamics and Earthquake Engineering*, 77:47–57, 2015.



- [155] A. Tombari, M. Garcia Espinosa, N. A. Alexander and P. Cacciola. Vibration control of a cluster of buildings through the Vibrating Barrier. *Mechanical Systems and Signal Processing*, 101:219–236, 2018.
- [156] S. Brûlé, E. H. Javelaud, S. Enoch and S. Guenneau. Experiments on seismic metamaterials: Molding surface waves. *Physical Review Letters*, 112(133901), 2013.
- [157] G. Finocchio, O. Casablanca, G. Ricciardi, U. Alibrandi, F. Garesci, M. Chiappini and B. Azzerboni. Seismic metamaterials based on isochronous mechanical oscillators. *Applied Physics Letters*, 104(191903), 2014.
- [158] S. Krödel, N. Thomé and C. Daraio. Wide band-gap seismic metastructures. *Extreme Mechanics Letters*, 4:111–117, 2015.
- [159] A. Palermo, S. Krödel, A. Marzani and C. Daraio. Engineered metabarrier as shield from seismic surface waves. *Scientific Reports*, 6(39356), 2016.
- [160] A. Colombi, P. Roux, S. Guenneau, P. Gueguen and R. V. Craster. Forests as a natural seismic metamaterial: Rayleigh wave bandgaps induced by local resonances. *Scientific Reports*, 6(19238), 2016.
- [161] A. Colombi, S. Guenneau, P. Roux and R. V. Craster. Transformation seismology: Composite soil lenses for steering surface elastic Rayleigh waves. *Scientific Reports*, 6(25320), 2016.
- [162] A. Colombi, D. Colquitt, P. Roux, S. Guenneau and R. V. Craster. A seismic metamaterial: The resonant metawedge. *Scientific Reports*, 6(27717), 2016.
- [163] WindEurope. *The European offshore wind industry - key trends and statistics 2016. Report*, 2017.
- [164] DNV. *Guidelines for design of Wind Turbines. 2nd ed.* Det Norske Veritas, Copenhagen and Wind Energy Department, Risø National Laboratory, 2002.
- [165] M. Kühn. *Dynamics and design optimisation of offshore wind energy conversion systems*. Ph. D. Thesis, Technical University of Delft, 2001.
- [166] J. van der Tempel. *Design of support structures for offshore wind turbines*. Ph. D. Thesis, Technical University of Delft, 2006.
- [167] M. B. Zaaijer. Foundation modelling to assess dynamic behaviour of offshore wind turbines. *Applied Ocean Research*, 28(1):45–57, 2006.
- [168] S. Adhikari and S. Bhattacharya. Dynamic analysis of wind turbine towers on flexible foundations. *Shock and Vibration*, 19(1):37–56, 2012.
- [169] L. Arany, S. Bhattacharya, S. Adhikari, S. J. Hogan and J. H. G. Macdonald. An analytical model to predict the natural frequency of offshore wind turbines on three-spring flexible foundations using two different beam models. *Soil Dynamics and Earthquake Engineering*, 74:40–45, 2015.



- [170] S. Bisoi and S. Haldar. Dynamic analysis of offshore wind turbine in clay considering soil-monopile-tower interaction. *Soil Dynamics and Earthquake Engineering*, 63:19–35, 2014.
- [171] D. Lombardi, S. Bhattacharya and D. M. Wood. Dynamic soil-structure interaction of monopile supported wind turbines in cohesive soil. *Soil Dynamics and Earthquake Engineering*, 49:165–180, 2013.
- [172] W. Carswell, S. R. Arwade, D. J. DeGroot and M. A. Lackner. Soil-structure reliability of offshore wind turbine monopile foundations. *Wind Energy*, 18(3):483–498, 2015.
- [173] S. Bhattacharya and S. Adhikari. Experimental validation of soil-structure interaction of offshore wind turbines. *Soil Dynamics and Earthquake Engineering*, 31(5-6):805–816, 2011.
- [174] V. Zania. Natural vibration frequency and damping of slender structures founded on monopiles. *Soil Dynamics and Earthquake Engineering*, 59:8–20, 2014.
- [175] M. Damgaard, L. V. Andersen and L. B. Ibsen. Computationally efficient modelling of dynamic soil-structure interaction of offshore wind turbines on gravity footings. *Renewable Energy*, 68:289–303, 2014.
- [176] M. Damgaard, V. Zania, L. V. Andersen and L. B. Ibsen. Effects of soil-structure interaction on real time dynamic response of offshore wind turbines on monopiles. *Engineering Structures*, 75:388–401, 2014.
- [177] M. Damgaard, L. V. Andersen and L. B. Ibsen. Dynamic response sensitivity of an offshore wind turbine for varying subsoil conditions. *Ocean Engineering*, 101:227–234, 2015.
- [178] M. Damgaard, L. B. Ibsen, L. V. Andersen and J. K. F. Andersen. Cross-wind modal properties of offshore wind turbines identified by full scale testing. *Journal of Wind Engineering and Industrial Aerodynamics*, 116:94–108, 2013.
- [179] S. Bhattacharya, N. Nikitas, J. Garnsey, N. A. Alexander, J. Cox, D. Lombardi, D. M. Wood and D. F. T. Nash. Observed dynamic soil-structure interaction in scale testing of offshore wind turbine foundations. *Soil Dynamics and Earthquake Engineering*, 54:47–60, 2013.
- [180] M. Damgaard, M. Bayat, L. V. Andersen and L. B. Ibsen. Assessment of the dynamic behaviour of saturated soil subjected to cyclic loading from offshore monopile wind turbine foundations. *Computers and Geotechnics*, 61:116–126, 2014.
- [181] H. Yu, X. Zeng, B. Li and J. Lian. Centrifuge modeling of offshore wind foundations under earthquake loading. *Soil Dynamics and Earthquake Engineering*, 77:402–415, 2015.



- [182] S. Bisoi and S. Haldar. Design of monopile supported offshore wind turbine in clay considering dynamic soil-structure-interaction. *Soil Dynamics and Earthquake Engineering*, 73:103–117, 2015.
- [183] A. T. Myers, S. R. Arwade, V. Valamanesh, S. Hallowell and W. Carswell. Strength, stiffness, resonance and the design of offshore wind turbine monopiles. *Engineering Structures*, 100:332–341, 2015.
- [184] R. A. Kjølraug and A. M. Kaynia. Vertical earthquake response of megawatt-sized wind turbine with soil-structure interaction effects. *Earthquake Engineering & Structural Dynamics*, 44(13):2341–2358, 2015.
- [185] C. Tibaldi, T. Kim, T. J. Larsen, F. Rasmussen, R. de Rocca Serra and F. Sanz. An investigation on wind turbine resonant vibrations. *Wind Energy*, 2015.
- [186] W.-H. Hu, S. Thöns, S. Said and W. Rücker. Resonance phenomenon in a wind turbine system under operational conditions. In *Proceedings of the 9th International Conference on Structural Dynamics, EUROdyn 2014, Porto*, 3619–3626, 2014.
- [187] P. Galvín, A. Romero, M. Solís and J. Domínguez. Dynamic characterisation of wind turbine towers account for a monopile foundation and different soil conditions. *Structure and Infrastructure Engineering*, 13(7):942–954, 2017.
- [188] J. van der Tempel and D.-P. Molenaar. Wind turbine structural dynamics - A review of the principles for modern power generation, onshore and offshore. *Wind Engineering*, 26(4):211–222, 2002.
- [189] M. Novak and T. Nogami. Soil-pile interaction in horizontal vibration. *Earthquake Engineering & Structural Dynamics*, 5(3):263–281, 1977.
- [190] J. P. Wolf. *Foundation vibration analysis using simple physical models*. Prentice-Hall, Englewood Cliffs NJ, 1994.
- [191] J. Jonkman, S. Butterfield, W. Musial and G. Scott. *Definition of a 5-MW reference wind turbine for offshore system development. Technical Report NREL/TP-500-38060*. National Renewable Energy Laboratory, 2009.
- [192] D. Lombardi. *Dynamics of Offshore Wind Turbines*. MSc Thesis, University of Bristol, 2010.
- [193] HSE, A. J. Bond, D. W. Hight and R. J. Jardine. *Design of Piles in Sand in the UK Sector of the North Sea - Report OTH 94 457*. Health and Safety Executive, London (UK), 1997.
- [194] Y. Ohta and N. Goto. Empirical shear wave velocity equations in terms of characteristic soil indexes. *Earthquake Engineering & Structural Dynamics*, 6(2):167–187, 1978.
- [195] A. S. Veletsos and J. W. Meek. Dynamic behaviour of building-foundation systems. *Earthquake Engineering & Structural Dynamics*, 3(2):121–138, 1974.



- [196] API. *Recommended Practice for Planning, Designing, and Constructing Fixed Offshore Platforms - Working Stress Design, Ver. 21*. American Petroleum Institute, USA, 2000.
- [197] GL. *Guideline for the Certification of Offshore Wind Turbines*. Germanischer Lloyd WindEnergie GmbH, Germany, 2005.
- [198] J. P. Stewart, R. B. Seed and G. L. Fenves. Seismic soil-structure interaction in buildings. II: Empirical findings. *Journal of Geotechnical and Geoenvironmental Engineering*, 125(1):38–48, 1999.
- [199] D. Clouteau and D. Aubry. Modifications of the ground motion in dense urban areas. *Journal of Computational Acoustics*, 9(4):1659–1675, 2001.
- [200] M. Kham, J.-F. Semblat, P.-Y. Bard and P. Dangla. Seismic site-city interaction: Main governing phenomena through simplified numerical models. *Bulletin of the Seismological Society of America*, 96(5):1934–1951, 2006.
- [201] M. Ghergu and I. R. Ionescu. Structure–soil–structure coupling in seismic excitation and “city effect”. *International Journal of Engineering Science*, 47(3):342–354, 2009.
- [202] C. Boutin, J. Soubestre, L. Schwan and M. Dietz. Multi-scale modeling for dynamics of structure-soil-structure interactions. *Acta Geophysica*, 62(5):1005–1024, 2014.
- [203] L. Schwan, C. Boutin, L. A. Padrón, M. S. Dietz, P. Y. Bard and C. Taylor. Site-city interaction: Theoretical, numerical and experimental crossed-analysis. *Geophysical Journal International*, 205(2):1006–1031, 2016.
- [204] P. Samui. Application of statistical learning algorithms to ultimate bearing capacity of shallow foundation on cohesionless soil. *International Journal for Numerical and Analytical Methods in Geomechanics*, 36(1):100–110, 2012.
- [205] A. Behnood, J. Olek and M. A. Glinicki. Predicting modulus elasticity of recycled aggregate concrete using M5 model tree algorithm. *Construction and Building Materials*, 94:137–147, 2015.
- [206] A. H. Gandomi, S. Sajedi, B. Kiani and Q. Huang. Genetic programming for experimental big data mining: A case study on concrete creep formulation. *Automation in Construction*, 70:89–97, 2016.
- [207] J. Wang, X. Yang, Z. Zeng, X. Zhang, X. Zhao and Z. Wang. New methods for prediction of elastic constants based on density functional theory combined with machine learning. *Computational Materials Science*, 138:135–148, 2017.
- [208] E. M. Golafshani and A. Behnood. Automatic regression methods for formulation of elastic modulus of recycled aggregate concrete. *Applied Soft Computing Journal*, 64:377–400, 2018.



- [209] H. Moayedi and S. Hayati. Modelling and optimization of ultimate bearing capacity of strip footing near a slope by soft computing methods. *Applied Soft Computing Journal*, 66:208–219, 2018.
- [210] J. P. Wolf. *Dynamic Soil-Structure Interaction*. Prentice-Hall, NJ, 1985.
- [211] D. Froio and E. Rizzi. Analytical solution for the elastic bending of beams lying on a variable Winkler support. *Acta Mechanica*, 227(4):1157–1179, 2016.
- [212] S. Çatal. Solution of free vibration equations of beam on elastic soil by using differential transform method. *Applied Mathematical Modelling*, 32:1744–1757, 2008.
- [213] Y. Miao, Y. Shi, H. Luo and R. Gao. Closed-form solution considering the tangential effect under harmonic line load for an infinite Euler-Bernoulli beam on elastic foundation. *Applied Mathematical Modelling*, 54:21–33, 2018.
- [214] G. Gazetas and R. Dobry. Horizontal response of piles in layered soils. *J Geotech Eng*, 110(1):20–40, 1984.
- [215] Y. Yesilce and H. H. Catal. Free vibration of piles embedded in soil having different modulus of subgrade reaction. *Applied Mathematical Modelling*, 32:889–900, 2008.
- [216] F. Liang, Y. Li, L. Li and J. Wang. Analytical solution for laterally loaded long piles based on Fourier-Laplace integral. *Applied Mathematical Modelling*, 38:5198–5216, 2014.
- [217] R. Flores-Berrones and R. V. Whitman. Seismic response of end-bearing piles. *Journal of the Geotechnical Engineering Division*, 108(4):554–569, 1982.
- [218] R. Dobry and M. J. O’Rourke. Discussion of ‘seismic response of end-bearing piles’ by R. Flores-Berrones and R. V. Whitman. *Journal of Geotechnical Engineering*, 109(5):778–781, 1983.
- [219] M. Kavvas and G. Gazetas. Kinematic seismic response and bending of free-head piles in layered soil. *Geotechnique*, 43(2):207–222, 1993.
- [220] A. Kampitsis, E. Sapountzakis, S. Giannakos and N. Gerolymos. Seismic soil-pile-structure kinematic and inertial interaction-A new beam approach. *Soil Dynamics and Earthquake Engineering*, 55:211–224, 2013.
- [221] N. Gerolymos and G. Gazetas. Winkler model for lateral response of rigid caisson foundations in linear soil. *Soil Dynamics and Earthquake Engineering*, 26(5):347–361, 2006.
- [222] M. Novak, T. Nogami and F. Aboul-Ella. Dynamic soil reaction for plane-strain case. *Journal of the Engineering Mechanics Division*, 104(4):953–959, 1978.
- [223] J. M. Roesset. The use of simple models in soil-structure interaction. In *Second ASCE Conference on Civil Engineering and Nuclear Power*. Knoxville, 1980.



INSTITUTO UNIVERSITARIO
SIANI
INGENIERIA COMPUTACIONAL

Edificio Central del Parque Tecnológico
Campus Universitario de Tafira
35017 Las Palmas de Gran Canaria
e-mail: info@siani.es · www.siani.es



UNIVERSIDAD DE LAS PALMAS
DE GRAN CANARIA